

**THE UNIVERSITY OF MANCHESTER - APPROVED ELECTRONICALLY
GENERATED THESIS/DISSERTATION COVER-PAGE**

Electronic identifier: 16364

Date of electronic submission: 08/10/2015

The University of Manchester makes unrestricted examined electronic theses and dissertations freely available for download and reading online via Manchester eScholar at <http://www.manchester.ac.uk/escholar>.

This print version of my thesis/dissertation is a TRUE and ACCURATE REPRESENTATION of the electronic version submitted to the University of Manchester's institutional repository, Manchester eScholar.

MICROWAVE TOMOGRAPHY

A thesis submitted to the University of Manchester for the degree of

Doctor of Philosophy

In the Faculty of Engineering and Physical Sciences

2015

AGUNG TJAHJO NUGROHO

School of Electrical and Electronic Engineering

Declaration

that no portion of the work referred to in the thesis has been submitted in support of an application for another degree or qualification of this or any other university or other institute of learning.

Agung Tjahjo Nugroho

Copyright Statement

- I. The author of this thesis (including any appendices and/or schedules to this thesis) owns certain copyright or related rights in it (the “Copyright”) and s/he has given The University of Manchester certain rights to use such Copyright, including for administrative purposes.
- II. Copies of this thesis, either in full or in extracts and whether in hard or electronic copy, may be made only in accordance with the Copyright, Designs and Patents Act 1988 (as amended) and regulations issued under it or, where appropriate, in accordance with licensing agreements which the University has from time to time. This page must form part of any such copies made.
- III. The ownership of certain Copyright, patents, designs, trademarks and other intellectual property (the “Intellectual Property”) and any reproductions of copyright works in the thesis, for example graphs and tables (“Reproductions”), which may be described in this thesis, may not be owned by the author and may be owned by third parties. Such Intellectual Property and Reproductions cannot and must not be made available for use without the prior written permission of the owner(s) of the relevant Intellectual Property and/or Reproductions.
- IV. Further information on the conditions under which disclosure, publication and commercialization of this thesis, the Copyright and any Intellectual Property and/or Reproductions described in it may take place is available in the University IP Policy (see <http://documents.manchester.ac.uk/DocuInfo.aspx?DocID=487>), in any relevant Thesis restriction declarations deposited in the University Library, The University Library’s regulations (see <http://www.manchester.ac.uk/library/aboutus/regulations>) and in The University’s policy on Presentation of Theses

About the Author

Agung Tjahjo Nugroho was born in Magelang, Indonesia, in 1968. He received a Sarjana of Physics degree in Gadjah Mada University and a Master of Philosophy in Electrical and Electronic Engineering from the University of Manchester Institute of Science and Technology (UMIST). Since 1994 he has been appointed as a Lecturer in the Department of Physics, The University of Jember, Indonesia. His research interests are in the areas of Electromagnetics Tomography, Inverse Problem and Instrumentation.

Acknowledgement

The author gratefully thanks his supervisors Professor Zhipeng Wu for his mostly appreciated help, guidance, patience and support during the course of this project.

The author deeply thanks his family, Musli Ariani, Bonanza Vidya Rashmi Nugroho, Givano Kynan Rishi Nugroho and Gavino Barca Diyu Nugroho, and his parents, Abdul Karim Rusdiarto, Muslimin, Sajekti and Sulastri for their moral support throughout the duration of studies.

I would also like to express my appreciation for my colleagues: Anugrah Sabdono Sudarsono and Iman Permana for their support in finishing of this work.

The author would like to thank all the members of staff in the school of Electric and Electronic Engineering, the University of Manchester for providing all the required technical and computing facilities.

Finally, I extend my gratitude to The Ministry of Higher Education, The Republic of Indonesia and The University of Jember, Indonesia for their financial support

To Arein, Boni, Gavin n Givan

Abstract

The University of Manchester; Agung Tjahjo Nugroho;
PhD Electrical and Electronic; Microwave Tomography; 08/10/2015

This thesis reports on the research carried out in the area of Microwave Tomography (MWT) where the study aims to develop inversion algorithms to obtain cheap and stable solutions of MWT inverse scattering problems which are mathematically formulated as nonlinear ill posed problems.

The study develops two algorithms namely Inexact Newton Backtracking Method (INBM) and Newton Iterative-Conjugate Gradient on Normal Equation (NI-CGNE) which are based on Newton method. These algorithms apply implicit solutions of the Newton equations with unspecific manner functioning as the regularized step size of the Newton iterative.

The two developed methods were tested by the use of numerical examples and experimental data gained by the MWT system of the University of Manchester. The numerical experiments were done on samples with dielectric contrast objects containing different kinds of materials and lossy materials. Meanwhile, the quality of the methods is evaluated by comparing them with the Levenberg Marquardt method (LM).

Under the natural assumption that the INBM is a regularized method and the CGNE is a semi regularized method, the results of experiments show that INBM and NI-CGNE improve the speed, the spatial resolutions and the quality of direct regularization method by means of the LM method. The experiments also show that the developed algorithms are more flexible to the effect of noise and lossy materials compared with the LM algorithm..

Contents

Declaration	2
Copyright Statement	3
About the Author	4
Acknowledgement	5
Abstract	7
Contents	8
List of Figures	12
List of Tables	20
List of Algorithms	22
List of Symbols	23
List of Abbreviation	25
1 Introduction	27
1.1 Electromagnetic Tomography	27
1.2 Microwave Tomography Inverse problem	28
1.3 Objectives	31
1.4 Contributions	33
2 Microwave Imaging.....	35
2.1 Brief Overview of Electromagnetic Imaging	35
2.1.1 Diffraction tomography.....	36
2.1.2 Terahertz imaging.....	37
2.1.3 Millimeter-wave imaging	39
2.1.4 Microwave imaging	40
2.2 Microwave Tomography Method	42
2.3 Nonlinear Methods to Solve Microwave Tomography Inverse Problems.....	43
2.3.1 Gradient Method	44
2.3.2 Newton's Method	49
2.3.3 Newton Kantorovich method.....	53
2.3.4 Inexact Newton method.....	55
3 Direct Scattering for Microwave Tomography	58
3.1 Introduction	58
3.2 The Method of Moment Solution for Direct Scattering Problem	60
3.2.1 Direct scattering in two-dimensional.....	60
3.2.2 Solving direct scattering using the method of moment	64
3.3 Numerical Experiment	68
3.3.1 Methods	68

3.3.2	Numerical Result	69
3.4	Conclusion	77
4	Inverse Problem of Microwave Tomography	79
4.1	Introduction	79
4.2	Microwave Tomography System.....	80
4.3	Data and domain equations	82
4.4	Microwave Tomography Inverse Problem.....	84
4.4.1	Objective-function of microwave inverse problem	84
4.4.2	The Least-Squares data misfit cost-functional of microwave tomography	85
4.5	The solution of objective-function MWT inverse problem of contrast inversion	86
4.6	The solution of least square cost function of contrast inversion	89
4.7	Numerical experiment of contrast inversion	90
4.8	Conclusions	93
5	Linearizing MWT Inverse Problem.....	95
5.1	Introduction	95
5.2	Newton Iteration	97
5.3	Linear filtering technique for non-linear Microwave Inverse Problem	99
5.3.1	Linear ill posed problem of microwave tomography inverse problem	99
5.3.2	Linearizing by means of Levenberg Marquardt method.....	100
5.4	Numerical experiment	102
5.4.1	Simulated data.....	103
5.4.1	Object domain and object of interest.....	103
5.4.2	Error definition	106
5.4.3	Numerical results	107
5.5	Conclusion	112
6	Iterative Methods for Solving Microwave Inverse Problem	114
6.1	Introduction	114
6.2	Iterative scheme of MWT inverse problem	116
6.2.1	Regularized solution of linear problem of MWT inverse problem	116
6.2.2	Iterative improvement of linear problem	119
6.3	Inexact Newton Backtracking Method (INBM)	120
6.3.1	Inexact Newton to solve Newton equations of microwave tomography inverse problem	120
6.3.2	Backtracking strategy	123
6.3.3	Forcing term	124
6.3.4	Inexact Newton Backtracking Method (INBM)	125

6.4	Numerical Study of INBM	127
6.4.1	Solving Newton equations using INBM.....	129
6.4.2	Study of regularization techniques on INBM algorithm.....	135
6.4.3	Choice of forcing terms	140
6.5	The application of INBM to Solve MWT- inverse problem of lossy object.....	146
6.5.1	Cylindrical homogeneous lossy object	146
6.5.2	Dielectric tube model for INBM test	152
6.5.3	Human arm model.....	157
6.6	Conclusions	161
7	Newton Iterative – Conjugate Gradient on Normal Equation	163
7.1	Newton Iterative	163
7.2	Conjugate Gradient on Normal Equation.....	166
7.3	Stopping Rule of CGNE	169
7.3.1	Discrepancy principle.....	171
7.3.2	The application of NI-cgne- τ to solveMWT inverse problem	173
7.3.3	L-curve criterion for regularizing linear ill posed problem....	179
7.3.4	Discrete L-curve criterion.....	183
7.4	Numerical experiment	185
7.4.1	Dielectric tube model of NI-cgne test	186
7.4.2	Human Arm model.....	191
7.5	Conclusions	195
8	Microwave Tomography System.....	196
8.1	Introduction	196
8.2	Microwave Tomographic System	197
8.3	Architecture of the University of Manchester MWT System	200
8.4	Antennas Arrangement.....	201
8.5	Object Domain of the University of Manchester-MWT System....	203
8.6	Antenna Multiplexing Using Microwave Switching System	204
8.7	Read and Write Data from VNA	207
8.8	Data Collection and Calibration	209
8.8.1	Data collection	209
8.8.2	Calibration	212
8.9	The Results of Reconstructing Experimental Data	214
8.9.1	The effect of antenna arrangement.....	214
8.9.2	The application of reconstruction algorithms	218
8.9.3	Object of interest variation	222
8.10	Conclusions	228
9	Conclusions and Future works	229
9.1	Conclusions	229

9.2	Future works	232
	Reference	234
Appendix A	Integral Equation of Microwave Tomography Inverse Problem	248
Appendix B	Scattering by a dielectric circular cylinder	252
B.1	Normalized Plane Wave	252
B.2	Electric Line Source	253
Appendix C	Regularization of linear ill posed problem	255
C.1	Truncated Singular Value Decomposition	255
C.2	Tikhonov Regularization	256
C.3	Truncated Landweber method	257
Appendix D	The Application of Born Approximation in MWT-Inverse Problem.....	259
D.1	The solution of MWT inverse problem using Born Approximation.....	259
D.2	Minimising the MWT cost function using Born Approximation ...	260
D.3	Numerical experiment of Born Approximation.....	261
Appendix E	Publications	265
E.1	Newton Method for Solving Microwave Inverse Problem; Nugroho, Agung T and Z Wu; The UoM IEEE Electron Devices Poster Conference; 12 th june 2013.....	265
E.2	Reconstructing Image of Microwave Tomography Using Contrast Source Inversion Method; Nugroho, Agung T and Z Wu; The UoM, EE E PGR Poster Conference; 20th November 2013	266
E.3	Inexact Newton Backtracking Method for Solving Microwave Tomography Inverse Problem; Nugroho, Agung T and Z Wu; 2015 IEEE, International Conference on Imaging Systems and Techniques; Macau, China; September 16-18, 2015	267
E.4	Newton Iterative with Conjugate Gradient on Normal Equations for Reconstruction of Free Space Microwave Imaging ; Nugroho, Agung T and Z Wu; To be submitted to: ; Transactions of the Institute of Measurement and Control Journal.....	273
E.5	Microwave Tomography Image Reconstruction Using Inexact Newton Backtracking Method; Nugroho, Agung T and Z Wu; To be submitted to: iopscience; Measurement Science and Technology Journal.....	281

Pages 289

Words: 53,692

List of Figures

Figure 2-1: The Fourier diffraction projection theorem [3]	37
Figure 2-2: Geometrical model of microwave tomography problem.	42
Figure 2-3: Model object of interest used for modified gradient algorithm test and the result of the reconstruction. Large object had the properties $\epsilon_r = 15.0$ and $\sigma = 0.4 S/m$ and two small objects with radius 4mm with parameters $\epsilon_r = 55.0$ and $\sigma = 1.0 S/m$. The background medium is matching liquid with $\epsilon_r = 12.0$ and $\sigma = 0.32 S/m$. [74].	45
Figure 2-4: Relative error of OI complex permittivity of small object resulted by Modified Gradient method with and without a priori data [74].	46
Figure 2-5: CSI and MR-CSI reconstructions for TM data at single frequency of 10 GHz [88]	48
Figure 2-6: Schematic setup of the simulation for Gauss Newton inversion test [67]. The background constitutive parameter is $\epsilon_r = 30$ and $\sigma_r = 1.163 S/m$. The OI is centered at $x, y = 0, 2cm$. The OI radius and constitutive parameter are $r = 2cm$, $\epsilon_r = 50$ and $\sigma_r = 1.6 S/m$	51
Figure 2-7: Normalized norm for MWT cost function of GNI with Tikhonov regularization $(\eta n, GN - T)$ and GNI with conjugate gradient least squares regularization $(\eta n, GN - C)$ [67].	51
Figure 2-8: Reconstructed values of conductivity and permittivity of simulated OI (Figure 2-6) for $(\eta n, GN - T)$ and $(\eta n, GN - C)$ [67].	52
Figure 2-9: The object model with dielectric contrast $\chi_r \in \Omega = 1$, initial guess and reconstruction results of Newton Kantorovich algorithm for noiseless data and noisy data [71].	54
Figure 2-10: The results of inexact Newton test by Bozza et al. Reconstructed distribution of the contrast of OI χ from noisy data with SNR 20dB [112]	56

Figure 2-11: Reconstructed distribution of the contrast of buried OI χ from noisy data with SNR 20dB and the behaviour of mean squared error on the reconstruction of the contrast function [113]	56
Figure 3-1: Cross section of a dielectric object Ω . Object is placed in object domain \mathcal{O} . The domain \mathcal{O} is divided into N squared cells $n = 1, 2 \dots N$. The \mathcal{O} is surrounded by data domain \mathcal{D} where observation points $m = 1, 2 \dots M$ are placed.	61
Figure 3-2: Imaging configuration for microwave tomography. The properties of MWT system are object domain \mathcal{O} , data domain \mathcal{D} , object of interest (OI) and measurement points.....	69
Figure 3-3: The plot of Scattered fields at 36 observation points in object domain \mathcal{D} $\rho = 5$ cm. The OI has permittivity $\epsilon_r = 4 + j0$ and radius 1 cm. 4.5 GHz Plane Wave and Line source equivalence illuminate the OI. The scattered field is approximated using the MM. The results are compared with analytic solution.	71
Figure 3-4: The plot of the magnitude of scattered fields at three observation points in object domain \mathcal{D} $\rho = 5$ cm, $\phi = 0, \pi/2, \pi$ of MM solutions and analytic solution. 4.5 GHz Plane wave (top) and Line source equivalence (bottom) illuminate $\epsilon_r = 4$ a dielectric cylinder with 1 cm in diameter.....	72
Figure 3-5: The plot of exact solutions and MM solutions of scattering field at a single observation point $\mathcal{D}(\rho = 5$ cm, $\phi = \pi/2)$. Dielectric contrasts of OI are varied. Three different frequencies of (top) plane wave and (bottom) line source equivalence illuminate the OI.	73
Figure 3-6: The pattern of scattered field and total electric field around a dielectric cylinder with radius 1 cm when 4.5 GHz-TMz microwave signal illuminates the object from $+x$ direction, for three different relative permittivity.....	76
Figure 4-1: Total electric field generated by the microwave plane wave that illuminates a dielectric object	81
Figure 4-2: The parameter of the solutions of MWT inverse problem in contrast formulation.....	91
Figure 4-3: Images of four cylindrical cross-section objects. The images are the solution of MWT contrast inversion problem GNI. The MWT inverse problems are presented in three different MWT functions.....	92

Figure 5-1: The simulation of measured scattered fields at data domain without and with noise of various SNR_{dB}	104
Figure 5-2: The $x - y$ plane distribution and $y = 0$ cross section of object of interest which is immersed in the object domain.....	105
Figure 5-3: The parameter of the solutions of noisy MWT inverse problem of Linearization technique test. The regularization technique is Tikhonov regularization. The regularization is descended	108
Figure 5-4: The reconstruction of noisy data with SNR 40dB at four different iterations. The images resulted by LM method with Tikhonov regularization. The regularization parameters are descended.....	109
Figure 5-5: The reconstruction of noisy data with various SNR. The images resulted by LM method with Tikhonov regularization. The regularization parameters are descended.....	110
Figure 5-6: the cross section of the contrast χ distribution at $y = 0$ of the images resulted by LM when the noise is introduced with SNR 40.1 dB (above) and 50.3 dB (below)	111
Figure 6-1: The cross section of the object of interest with complex permittivity $\epsilon_r = 3 - j0$. The background of the MWT system is air where the parameter of the dielectric is $\epsilon_r = 1$	128
Figure 6-2: The parameters of MWT inverse problem solutions using INBM and LM algorithms. The OI is a cylindrical with complex permittivity $\epsilon_r = 3 - j0$ and radius 1.5 cm.	131
Figure 6-3: The real part of reconstructed Images using INBM and LM algorithms. The OI is a cylindrical object with complex permittivity $\epsilon_r = 3 - j0$ and radius 1.5 cm. The data is taken at 4.5 GHz. White Gaussian noise is introduced with signal to noise ratio 28 dB, 34dB and 41 dB.....	132
Figure 6-4: The imaginary part of reconstructed Images using INBM and LM algorithms. The OI is a cylindrical object with complex permittivity $\epsilon_r = 3 - j0$ and radius 1.5 cm. The data is taken at 4.5 GHz. White Gaussian noise is introduced with signal to noise ratio 28 dB, 34dB and 41 dB.	133
Figure 6-5: The parameters of MWT inverse problem solutions using INBM with Tikhonov regularization (Thi), Landweber-Friedman iteration (LF) and Truncated Singular Value Decomposition	

(TSVD). The OI is a cylindrical with complex permittivity $\epsilon_r = 3 - j0$ and radius 1.5 cm.....	137
Figure 6-6: The parameters of INBM solutions with respect to forcing term constant. The parameters are number of iteration k , objective function norm and relative error of χ^2 . The OI is a cylindrical object with complex permittivity $\epsilon_r = 3 - j0$ and radius 1.5 cm. The working frequency is 4.5 GHz.	144
Figure 6-7: a cross sectional view of a homogeneous lossy object of interest. The real part of OI complex permittivity is 3.5. The imaginary part of OI is varied.	146
Figure 6-8: The real part of reconstructed images using INBM and LM algorithms. Four different cylindrical OI with radius 2 cm and permittivity $\epsilon = 3.5 - j1$, $\epsilon = 3.5 - j4.8$, $\epsilon = 3.5 - j5.4$ and $\epsilon = 3.5 - j5.8$ are applied. The data are taken at 2.5 GHz. White Gaussian noise is introduced with signal to noise ratio 40 dB	148
Figure 6-9: The imaginary part of reconstructed images using INBM and LM algorithms. Four different cylindrical OI with radius 2 cm and permittivity $\epsilon = 3.5 - j1$, $\epsilon = 3.5 - j4.8$, $\epsilon = 3.5 - j5.4$ and $\epsilon = 3.5 - j5.8$ are applied. The data are taken at 2.5 GHz. White Gaussian noise is introduced with signal to noise ratio 40 dB	149
Figure 6-10 The parameter of iterative solutions for INBM and LM algorithms for solving the MWT inverse problem of homogeneous lossy object a) relative norm of objective function b) relative error of the dielectric contrast of OI.....	150
Figure 6-11: The effect of the imaginary part of the complex permittivity to the results of INBM and LM algorithms. The parameters of the solutions are a) MWT objective function norm b) the relative error of the dielectric contrast. The parameters are plotted with respects to the imaginary part of the complex permittivity of OI.	151
Figure 6-12: the Architecture of a dielectric tube model for INBM test. A) the Dielectric tube is placed in a free space. B) the dielectric cylinder is placed inside dielectric tube.....	153
Figure:6-13: The reconstructed images of the dielectric tube model A. The OI is presented in the images of $Real(\epsilon)$, $Imag(\epsilon)$ and $Abs(\epsilon)$.. The images are resulted using INBM and LM algorithms.	154
Figure:6-14: the reconstructed images of the dielectric tube model B. The OI is presented in the images of the real part and imaginary	

part of complex permittivity. The images are resulted using INBM and LM algorithms	155
Figure 6-15: The parameter of iterative solutions of INBM and LM algorithm for solving MWT inverse problem of the dielectric tube model a) the relative norm of the objective function b) the relative error of the dielectric contrast of OI.	156
Figure 6-16: Two-dimensional models of human arms a) centered bone (left) b) off center bone (right).....	158
Figure 6-17: The images of a human arm model A (centered bone) resulted using INBM and LM algorithms.....	159
Figure 6-18: the images of a human arm model B (off center bone) resulted using INBM and LM algorithms.....	160
Figure 6-19: The parameter of iterative solutions for INBM and LM algorithms for solving the MWT inverse problem of the human arm model a)the relative norm of the objective function b) the relative error of the dielectric contrast of OI.	161
Figure 7-1: the two dimensional cross section of cylindrical dielectric object with two similar holes.....	173
Figure 7-2: The parameters of MWT inverse problem solutions using NI-cgne and LM algorithm. The problem is a dielectric object with two circular holes. NI-cgne with discrepancy τ is applied. Three different discrepancy values $\tau = 0.05$, $\tau = 0.01$ and $\tau = 0.005$ are applied.....	175
Figure 7-3: The reconstructed images of a dielectric lossy material with two circular holes. The $Real(\epsilon)$, $Imag(\epsilon)$ and $Abs(\epsilon)$.. images are resulted using Ni-cgne- τ and LM algorithms.....	176
Figure 7-4: The graph or the parameters of solution with respect to discrepancy constant. The parameters are objective function norm, relative error of dielectric contrast and number of iteration k of the results of NI-cgne algorithm with scanning discrepancy criteria τk	177
Figure 7-5: L curve criteria for continuous regularization parameter. Top: a discrete L curve for Tikhonov regularization of the linear ill posed problem of the first iteration of the nonlinear MWT inverse. Bottom: the part of the Tikhonov L-curve with noisy data for various SNR.	180
Figure 7-6: L curve criteria for discontinuous regulator parameter by means of CGNE.	182

Figure 7-7: Angles between two vectors which construct the vertex of L-curve regularization	184
Figure 7-8: Architecture of dielectric tube model for NI-cgne. Two cylindrical dielectric materials are placed in three different positions inside dielectric tube.	186
Figure 7-9: The images of $Real(\epsilon)$ of the dielectric tube model for NI-cgne test. The tube contains different materials. The images are resulted using NI-cgne and LM algorithms.....	188
Figure 7-10: The images of $Imag(\epsilon)$ of dielectric tube model for NI-cgne test. The tube contains different materials. The images are resulted using NI-cgne and LM algorithms.....	189
Figure 7-11: The architecture of human arms model for NI-cgne algorithm test.....	192
Figure 7-12: Two dimensional cross section of human arm model for NI-cgne test. The model is presented in a) real part b) imaginary part of complex permittivity	192
Figure 7-13: The parameter of the iterative solutions of NI-cgne and LM for solving the MWT inverse problem of human arm model a) the relative norm of objective function b) the relative error of the dielectric contrast of OI.	193
Figure 7-14: Images of human arm model reconstructed by Ni-cgne and LM methods.....	194
Figure 8-1: The University of Manchester microwave tomography prototype. The 16 ground plane antennas are connected to VNA via Cytec 2x16 matrix switch.	198
Figure 8-2: The architecture of the University of Manchester-MWT system. The system is computer controlled via GPIB IEEE 488.2. NI GPIB-USB-HS interface is used to connect the system to portable computer.	198
Figure 8-3: The array of antennas of MWT system. a) 16 monopole antennas are placed in a single ground plane. b) the antenna connectors are connected using RD 316 coaxial cable.	202
Figure 8-4: s_{11} parameter of the monopole antenna in free space.	203
Figure 8-5: the architecture of ground plane antennas. The antennas are arranged circularly around object domain \mathcal{O} of MWT system.....	204

Figure 8-6: the architecture of the matrix switch of Cytec Microwave Multiplexer	205
Figure 8-7: Undisturbed and disturbed electric fields measured at Rx2 and Rx9 when microwave signal is transmitted from Tx1	210
Figure 8-8: Raw data of measured Electric field at Rx antennas around object domain when three different microwave signals are transmitted from first three Tx antennas.....	211
Figure 8-9: The absolute and phase of calibrated scattered field at 4.5 GHz when a plastic rod is introduced.....	213
Figure 8-10: The arrangement of antennas. Tx1 is set as a transmitting antenna and Rx1 to Rx15 are defined as receiving antennas	215
Figure 8-11: The effect of the architecture of the receiver to the pattern of the objective function norms of INBM-Tikhonov and NI-cgne-LC at 4.5 to 5.0 GHz.....	216
Figure 8-12: The results of antenna arrangement test: Images of plastic rod cross section when receiving antennas are set at five different modes. The working frequency is 4.5 GHz	217
Figure 8-13: The objective functional norm and number of iterations of four different algorithms reconstructing the calibrated scattered field due to the presence of homogeneous dielectric cylinder.....	220
Figure 8-14: Images of plastic rod cross section resulted by various algorithms which are Levenberg Marquardt method, Inexact method and Newton Iterative with conjugate gradient at three different frequencies.	221
Figure 8-15: three different objects of interest used to test the adaptability of the inexact Newton and Newton iterative algorithms.....	223
Figure 8-16: Images of three different objects of interest cross section resulted by INBM and NI-cgne at 4.5 GHz.....	224
Figure 8-17: Two small cylindrical Teflons which are placed at object domain with four different gaps.	225
Figure 8-18: Images of two small cylindrical Teflons with four different gaps resulted by INBM and NI-cgne at 4.6 GHz	227
Figure B-1: A TM_z Uniform plane wave incident on a dielectric circular cylinder.	252

Figure B-2: An infinitely long line source current directed at z is placed near a dielectric cylindrical object	254
Figure D-3: Image of cylindrical cross-section object under Born Approximation using Gauss Newton Inversion. Three different MWT inverse problems which are MWT objective function, MWT cost function A and B, are formulated and solved using GNI method.	262
Figure D-4: The parameter of the solutions of Born approximation MWT inverse problem.	263

List of Tables

Table 2-1 Computational time on a Pentium 2.0 GHz dual processor personal computer [88].....	49
Table 3-1: Observation points of scattered field	64
Table 5-1: parameter of the simulated system for the simple test	105
Table 6-1 the parameter of the simulated system for numerical testing of LM and INBM methods	128
Table 6-2: The comparison of INBM results to solve MWT inverse problem of cylindrical dielectric OI with complex permittivity $\epsilon_r = 3 - j0$ and radius 1.5 cm and that LM algorithm.....	134
Table 6-3:The comparison of regularization technique for inner loops of Newton iterative (INBM) and direct regularization method by means of Levenberg Marquardt method (LM) as a result of the numerical data reconstruction.....	138
Table 6-4: The comparison of three different techniques of choosing the forcing term. The MWT inverse problem is solved using INBM with <i>Tikhonov regularization</i>	142
Table 6-5: The comparison of three different techniques of choosing the forcing term. The MWT inverse problem is solved using INBM- <i>Landweber Friedman</i>	142
Table 6-6: The comparison of three different techniques of choosing the forcing term. The MWT inverse problem is solved using <i>INBM-TSVD</i>	142
Table 6-7:Complex permittivity materials of a synthetic model of a human forearm	158
Table 7-1: the parameter of the simulated system for the numerical testing of Ni-cgne- τ method	174
Table 7-2 the parameter of the simulated system for the numerical testing of the dielectric tube model.....	187

Table 7-3: The results of NI-cgne and LM algorithms in solving the MWT inverse problem of the dielectric tube containing different materials.....	190
Table 7-4 complex permittivity materials of a synthetic model of human forearm	191
Table 8-1: The arrangement of Rx antenna when Tx1 is defined as transmitting antenna.	215
Table 8-2: The number of iterations and objective functional norm of Levenberg Marquardt, Inexact Newton and Newton Iterative algorithms when reconstructing the images of the cross section of cylindrical Teflon	219
Table 8-3: The result of reconstruction of varied objects of interest cross sectioned by Inexact Newton and Newton iterative algorithms	224
Table 8-4: The result of reconstruction of two small cylindrical Teflons with four different gaps by Inexact Newton and Newton iterative algorithms.....	226

List of Algorithms

Algorithm 5-1 GNI: Gauss Newton Inversion for MWT Inverse Problem.....	100
Algorithm 6-1:NM: Newton Method to solve MWT- Inverse Problem.....	121
Algorithm 6-2:INM: inexact Newton to solve Newton equations of MMWT Inverse Problem.....	123
Algorithm 6-3: BK: Backtracking strategy of INM.....	124
Algorithm 6-4: INBM: Inexact Newton Method with Backtracking for Microwave Inverse Problem.....	127
Algorithm 7-1NI-cgne: Newton Iterative with Conjugate gradient on normal equation.....	165
Algorithm 7-2: CG: Conjugate gradient step.....	168
Algorithm 7-3cgne : Conjugate Gradient on Normal Equation.....	169
Algorithm 7-4: cgne- τ : cgne with discrepancy Principle.....	172
Algorithm 7-5: Lcurve : Lcurve regularization for cgne.....	184
Algorithm 8-1 MWT: Microwave Tomography Measurement Sequence.....	200
Algorithm 8-2: setMUL: Setting Multiplexer switch.....	206
Algorithm 8-3: VGvna: VISA-GPIB object of VNA.....	208
Algorithm 8-4: getFreq: Acquire Frequency Parameter of VNA.....	208
Algorithm 8-5: getDat: Acquire s21 signal.....	208

List of Symbols

Symbol	Description
j	Imaginary unit $j^2 = -1$
μ_0	permeability of vacuum
μ_r	Relative complex permeability of the object of interest
ϵ_0	Permittivity of vacuum
ϵ_r	Relative complex permittivity of the object of interest
ϵ_b	Complex permittivity of background medium
χ	Dielectric contrast ($\epsilon_r - 1$)
$e^{-j\omega t}$	Harmonic wave varying in time
ω	Radial frequency
k_b	Wave number in background medium $k_b^2 = \omega^2 \mu_0 \epsilon_0 \epsilon_b$
r and r'	Position vector of the imaging
ρ	$ r - r' $
\hat{x}, \hat{y}	Unit vectors along x and y
$\mathbb{G}(r, r')$	Green's function
$g(r, r')$	Dyadic Green's function
\mathcal{O}	Object domain
\mathcal{D}	Data domain
Ω	Cross section of the object
$E^i(r)$	Incident electric fields
$E(r)$	Total electric fields
$E^s(r)$	Scattered electric fields
$t = 1, 2, \dots, T$	Illumination of incident field
$n = 1, 2, \dots, N$	Index of cells of the object
$m = 1, 2, \dots, M$	Index of observation points
$k = 1, 2, \dots, K$	Index of iteration

I	Matrix identity
$[E^i]$	Incident field for all T
$[E_n^i]_t$	Incident field at t (a $N \times 1$ matrix)
$[E_{n'}]_t$	Total field at t (a $N \times 1$ matrix)
$[E_m^s]_t$	Scattered field at t (a $M(t) \times 1$ matrix)
$[E^s]_t$	Measured Scattered field at t (a $M(t) \times 1$ matrix)
$[Z_{nn'}]$	Integral operator maps $L^2(\mathcal{O})$ into $L^2(\mathcal{O})$
$[Z_{mn'}]$	Integral operator maps $L^2(\mathcal{O})$ into $L^2(\mathcal{D})$
$[\chi]$	Unknown dielectric contrast (a $N \times 1$ matrix)
$F_t([\chi])$	Objective functional
D	Deferential of MWT functional
$[L]_k$	Approximation of Hessian matrix = $[D^*D]_k$
$[\delta\chi]$	Direction of correction of unknown contrast
$c_t^A([\chi])$	Cost functional of MWT type A
$c_t^B([\chi])$	Cost functional of MWT type B
ψ	linearized operator
$[b]_k$	exact functional
$[b^\varepsilon]_k$	The approximation $[b]_k$
x	Unknown variable
x_0	Initial value of x
s_k	Search direction
$s_{t,k}^E$	Search direction for total electric field
s_k^χ	Search direction for dielectric contrast
s_k^\ddagger	approximated direction of search
s_k^\dagger	Exact solution of direction of search
α	Regulator parameter

List of Abbreviation

Acronym	Description
2D	Two Dimensional
3D	Three Dimensional
AMMW	Active Millimeter-Wave Imaging
CG	Conjugate Gradient Method
cgne	Conjugate Gradient On Normal Equation
CSI	Contrast Source Inversion
EFIE	Electric Field Integral Equation
ERT	Electrical Resistance Tomography
ET	Electromagnetic Tomography
FD	Frequency Domain
FDTD	Finite-Difference Time-Domain
FOPEN	Foliage Penetration
FPA	Focal Plane Array
GA	Genetic Algorithm
GMRES	Generalized Minimal Residual Method
GNM	Gauss-Newton Method
INBM	Inexact Newton Backtracking Method
INM	Inexact Newton Method
LF	Landweber Friedman Method
LM	Levenberg Marquardt
MM	The Moment of Methods
MMI	Microwave Imaging
MMW	Millimeter-Wave
MWT	Microwave Tomography
NI	Newton Iterative

NK	Newton–Kantorovich Method
OI	Object Of Interest
PMMW	Passive Millimeter-Wave Imaging
QNM	Quasi Newton Method
RF	Radio Frequency
SAR	Synthetic Aperture Radar
TD	Time Domain
TE	Transverse Electric
Thi	Tikhonov Regularization
THz	Terahertz Radiation
TM	Transverse Magnetic

1

Introduction

The thesis presents the research work on *microwave tomography with an emphasis on microwave image reconstruction algorithms*. The main objective of this research in Microwave Tomography (MWT), which is one form of the electromagnetic inverse scattering problems, is to develop an algorithm for reconstructing dielectric properties of an Object of Interest (OI) from microwave measurements collected outside the OI. The first chapter of the thesis introduces the brief overview of electromagnetic inverse scattering and microwave tomography, followed by statements of objectives and contributions.

1.1 Electromagnetic Tomography

Electromagnetic tomography by means of Radio Frequency, microwave, or optical signals, provides inexpensive non-intrusive imaging systems with low but sufficient resolution of the internal distributions of processes. The technique is intended to solve an electromagnetic inverse problem which is generally a nonlinear one; even so, a linear system can be found in a certain limited tomography cases. In the linear systems, an image is obtained by solving the linear equations which are an approximation of the linear relationship between the measured data and the internal property of the OI. In

diffraction tomography for example, a linear relationship between scattered field data which can be approximated using either Born or Rytov approximation [1], and the OI when the dielectric contrast of the OI is low. The advantages of this approach is that it is straightforward to apply and usually computationally efficient [2]. The disadvantages, however, is that due to the underlying approximation involved, the diffraction tomography becomes less accurate when the inhomogeneities in the OI are strongly scattering [3].

The electromagnetic tomography is a nonlinear inverse problem for objects with high contrasts. The nature of the nonlinear system is much more complex than the nature of the linear system, which presents a great difficulty when computing the image reconstruction algorithms. Examples of the nonlinear tomography in the low frequency are electrical impedance tomography [2], electrical capacitance tomography [4] and magnetic inductance tomography [5]. These techniques have advantages mainly they are fast, and least costly; even though unlike MWT which is a high frequency tomography, the low frequency tomography is limited in spatial resolution [6].

In the high frequency, the microwave frequency range for instance, the dielectric contrast of OI, which is a complex number where the imaginary parts of the number tends to be zero in the low frequency, is nonlinearly related to the scattered field data. Though the complex number raises the complexity of the inverse problem, it brings more information than a scalar in the low frequency. For this reason, the electromagnetic tomography in the microwave frequency range is selected as the topic in this thesis.

1.2 Microwave Tomography Inverse problem

This thesis considers electromagnetic tomography in the microwave frequency range; therefore, the thesis refers to the nonlinear inverse scattering problem

within this frequency range as the Microwave Tomography-inverse problem (MWT-inverse problem).

Potential advantages of the MWT-inverse problem include low cost, portability, and nonionizing radiation. On top of this, its ability to produce quantitative images without a contrast agent has highlighted the great potential of the method being applied in medical applications. At the microwave range, the dielectric properties of living tissues like skin, muscle, fat and bone; and more importantly those between healthy and malignant tissues are different [2]. Nevertheless, the lower resolution of MWT in a biomedical application needs to be improved to become a competitive biomedical imaging modalities, in comparison to the magnetic resonance imaging and x-ray computerized tomography

The aim of solving MWT-inverse problem is reconstructing the image of the OI cross section by determining the distribution of the OI dielectric property from the data of Microwave Tomography (MWT). The data are the measured scattered fields around the OI when the OI is successively irradiated with some known incident electromagnetic waves in the microwave frequency range originating from different source positions. Accordingly, the data are processed using nonlinear image reconstruction algorithms in which the reconstructions can be completed in two steps; firstly, by the use of the forward problem, secondly, by the use of the inverse problems.

The forward problem, also known as the direct scattering process, computes the output of a physical system by giving the internal structure of the OI. In this process, both the incident fields and the dielectric contrast of the OI are assumed to be known and the scattered fields are determined by solving the Maxwell's equations for electromagnetic problems. The general solution of the equations may be obtained along with the constitutive solution. However, the unique solutions must enforce the boundary and interface conditions of the system that makes the Maxwell's equations hard to solve analytically. Hence, the numerical solution for the Maxwell's equations, which are usually referred to as computational electromagnetic, is likely to be an alternative.

The numerical tool to solve the forward problem is the Moment of Method (MM) which is classified as a low frequency method. Low-frequency methods are so-named because they solve Maxwell's equations with no implicit approximations and are typically limited to problems of small electrical size due to limitations of computation time and system memory[7; 8; 9]. Since the MM is a technique used to solve electromagnetic boundary or volume integral equations in the frequency domain and the electromagnetic sources are the MWT quantities of interest, the technique is very useful in solving the forward problem of the MWT. The report which deals with ways of solving electric field integral equation using the MM and the numerical experiment results will be described and discussed in chapter 3.

Contrary to the forward problem, the inverse problem reconstructs the distribution of unknown variables, which is the internal characteristic of physical system from the system output behavior data. In the X-ray tomography or computerized tomography, for example, the X-ray attenuation coefficient of the OI is reconstructed from integral summation of the attenuation experienced by the X-ray as it travels a path crossing the OI. Another example is in the MWT, in which the distribution of the dielectric contrast value of the OI is determined from several projections of the scattered field data around the OI.

The inverse problem tends to be an ill-posed problem in term of Hadamard's criteria where existence, uniqueness and stability are the criteria of a well posed problem. In tomography applications, the existence of a solution is not an issue as the inverse problem tries to find the internal properties of an existing OI from measured data. However, the problem is generally an underdetermined system where there are fewer equations than variables, hence, the uniqueness and stability are the two main challenges of solving the problem.

The MWT-inverse problem is a nonlinear and ill posed problem. The nonlinearity of the problem is solved by applying different optimising methods to minimize an objective function which can be the difference between measured scattered fields and calculated scattered fields from a forward

problem solution. Generally, the methods are iterative where these techniques are computationally complex and expensive because the objective function has to be updated at each iteration. Various nonlinear algorithms have been developed to solve MWT problems. These include Modified Gradient method [10; 11], Newton–Kantorovich [2], Gauss Newton inversion [2], Quasi Newton method [12], Contrast source inversion [13; 14] and Inexact Newton method [2]. The ill posedness of the problem is handled by employing different regularization techniques which set an appropriate constrain to the solution [2]. Tikhonov regulator for example, which facilitates the inversion of ill conditioning matrix, limits the value of the update solution. However, the weight of the regularization is generally determined by one or more regulator parameters so that the techniques can be application dependent.

In this thesis, the algorithm to solve MWT inverse problems via implicit solution is developed in which the algorithm presents an intermediate solution of the problem. Consequently the method offers a tradeoff between the accuracy with which the regularized solution is computed. The algorithm handles the ill posedness of the problem by utilizing a semi regularized method in which regularization techniques can be avoided and replaced with an appropriate criterion. The amount of work for solving MWT inverse problem can be decreased as the computation and regularization do not need to be done at each sequence of the iteration. The stability and robustness of the algorithm is studied under noisy numerical data and experimental data.

1.3 Objectives

With the understanding of microwave scattering by dielectric objects, such a scattering process is described. The mechanism of microwave signal penetrating into a dielectric object and the signal which scatters toward the background is modeled in an electric field integral equation. The MM, hence, is used to solve the integral equation using the Pulse Basis Function.

Consequently, numerical calculation can be carried out; and the results are evaluated in comparison to the analytic solutions.

The MWT inverse problem is stated using a forward problem formulation in the form of nonlinear objective function. Deterministic technique based on optimization solves the problem by minimizing the norm of the function using Newton type minimization. The nonlinearity of the MWT inverse problem is linearized via the Frechet differential, then; it is solved using the Levenberg Marquardt method. The ill posedness is treated by employing different regularization techniques which are truncated singular value decomposition; Tikhonov regularization and iterative Landweber. The stability and robustness of the linearization technique for solving MWT problem are studied using synthetic noiseless and noisy data.

An implicit solution of the linearized MWT-inverse problem is introduced as an alternative to a direct regulative solution by employing the class of Inexact Newton in the form of Inexact Newton Backtracking Method (INBM). A forcing term, which is computed using ratio of linear solution with its corresponding nonlinear solution, defines an appropriate approximation of the solution. The stability and robustness of the INBM is tested using synthetic and experimental data.

The Newton Iterative-conjugate gradient on normal equation (NI-cgne) method which is an iterative method with a semi regulated implicit solution is developed to solve MWT-inverse problem. The method is stated in outer and inner loops. The outer loop is the Newton type method for solving a nonlinear problem and the inner loop is the semi regulated implicit method that is conjugate gradient on normal equation (CGNE). At each Newton iteration step a stopping rule of the CGNE, which is used to control the accuracy and the ill posedness when solving the objective function is required. The stability de accuracy of the NI-cgne are studied using numerical experiment and experimental data.

A Microwave tomography system is developed by using monopole ground plane antennas. The system is computer controlled and automatically switched using Cytec multiplexer. A vector Network Analyzer (VNA) handles

the data acquired from the system. In the meantime, the connection uses 488.2 line and MATLAB code, where the interface of the instrument is addressed as a unique object. The capability of the sensor is, then, tested individually to measure the scattered field of object of interest.

The measured scattering data are reconstructed using developed algorithm. The raw data are calibrated using ratio of the ideal measurement model. The incident field of line source equivalent antenna represents the monopole ground plane antenna. The ratio of incident fields at receiving antennas calibrates the disturbance electric fields, which is used to determine the scattered field. The calibrated data is used to test the robustness and stability of developed algorithms.

1.4 Contributions

This thesis reports the contributions made by the author in the area of microwave tomography. The contributions are listed as follows

- Developing algorithms to solve MWT inverse problems. The algorithms are deterministic approaches based using the Newton type of method. An implicit solution, which is introduced to replace a direct regulative solution of the MWT inverse problem, is determined in an unspecific manner. There are two algorithms developed; namely Inexact Newton Backtracking (INBM) method and Newton Iterative-conjugate gradient on normal equation method (NI-cgne).
- Developing the Inexact Newton Backtracking (INBM) method to solve MWT inverse problem. The INBM is an inexact Newton class method to solve nonlinear problems. The implicit regulative Newton steps are defined in an unspecific manner using a forcing term. The steps are iterative solutions of MWT inverse problem linearization. The forcing terms define the accuracy of the MWT linear solutions. INBM is tested using synthetic and experimental data. The results of INBM are

compared to the results of direct linearization technique (Levenberg Marquardt method). The INBM improves the accuracy of MWT results and the speed of reconstructions.

- Developing a Newton Iterative-conjugate gradient on normal equation method (NI-cgne) to solve MWT problem. NI-cgne is an outer-inner loop technique. The outer loops are the Newton Iterative method to solve the nonlinear system. The steps of the method minimize the objective function of MWT inverse problems. The directions of the steps are the solutions of Newton equations of MWT inverse problems in a normal system. Conjugate gradient method computes the solutions. It is conducted in inner loops. Stopping criteria of conjugate gradient on normal equations conduct semi-regularization of the MWT ill posedness. Two different stopping criteria are modified; which are discrepancy and L-curve techniques. They have been tested using numerical and experimental data in which NI-cgne algorithm produces stable solution of MWT inverse problems.
- Introducing MWT problems in the form of nonlinear objective function. The objective function is the difference between measured output MWT systems with the approximation of the output systems. Comparing two formulations of MWT problems, namely, objective function and least squared cost function of MWT problem.
- Formulating forward problem solutions of MWT using Moment of Method. The formulations are stated in the form of electric fields and equivalent current density. Two pairs of objects and domain equations are resulted which are used to formulate the objective function of MWT problems.
- Setting up a microwave tomography system which consists of 16 ground plane antennas, Vector Network Analyzer and microwave multiplexer which is computer controlled. The mnemonic code is listed in MATLAB code and applying INBM and NI-cgne algorithms to the system

2

Microwave Imaging

An Overview of electromagnetic imaging is introduced. The brief overview of the extensive work in electromagnetic imaging by means of microwave, millimeter wave and terahertz imaging is presented and followed by a critical review of microwave tomography.

2.1 Brief Overview of Electromagnetic Imaging

For the last few decades electromagnetic imaging that ranges from electrical, microwave, millimeter-wave, terahertz, and optical imaging gained intensive attention for its unique features as an attractive non-destructive diagnostic tool. Recently, the scope of electromagnetic imaging application has become more extensive, including non-destructive evaluation[15; 16], breast imaging[17; 18], biological [19], geophysical [20; 21] , military [22], inline industrial process [23; 24], and industrial engineering [25; 26]. Many other possible applications could be listed and developed on the assumption that the electromagnetic signal penetrates the Object of Interest (OI).

The electromagnetic imaging can be categorized based on the working frequency due the fact that the working frequency determines the type of relationship between electromagnetic signal and the OI. One of the important relationships is diffraction because it is applicable for a high contrast OI

tomography. The following section of the review is mainly about diffraction tomography and the diffraction imaging at three different frequency ranges (terahertz, millimeter wave, and microwave ranges).

2.1.1 Diffraction tomography

Diffraction Tomography (DT) is a conventional tomography method which refers to tomographic applications that employ diffraction wave fields in the tomographic reconstruction process. The diffraction effect cannot be neglected, when the cells of the OI become comparable in size to a wavelength. The propagation of the electromagnetic signal is not along the lines or rays, and energy transmission is described in terms of wave fronts and fields scattered by the contrast of the OI. In other words, the DT tries to quantify the contrast value of the OI from the scattered field data.

It has been shown [1] that the Fourier Diffraction Projection Theorem, which is formulated with a Fourier-slice-like theorem and certain approximations, can be used to describe the diffraction tomography. Under the Fourier theorem (Figure 2-1), an electromagnetic signal in the time domain illuminates an OI in many different directions where the scattered fields at each projection are measured. Then, the data are reconstructed using Fourier inversion technique like filtered-back-projection algorithm for reconstruction [27]. This approach is comparatively straightforward to apply and is usually computationally efficient, although, the number of measurements for Fourier diffraction theorem is large [1], besides the technique is only accurate for a low contrast OI problem [3]. Moreover, the resolution of the images generated by DT is limited by the wavelength λ of the signal.

The application of conventional scan configuration as described in Figure 2-1 limits the resolution to $\lambda/2$ [28]. Under realistic measurement noise levels, the Fourier inversion algorithm excludes the possibility of resolving features of a wave scattering object which are less than $\lambda/2$ apart.

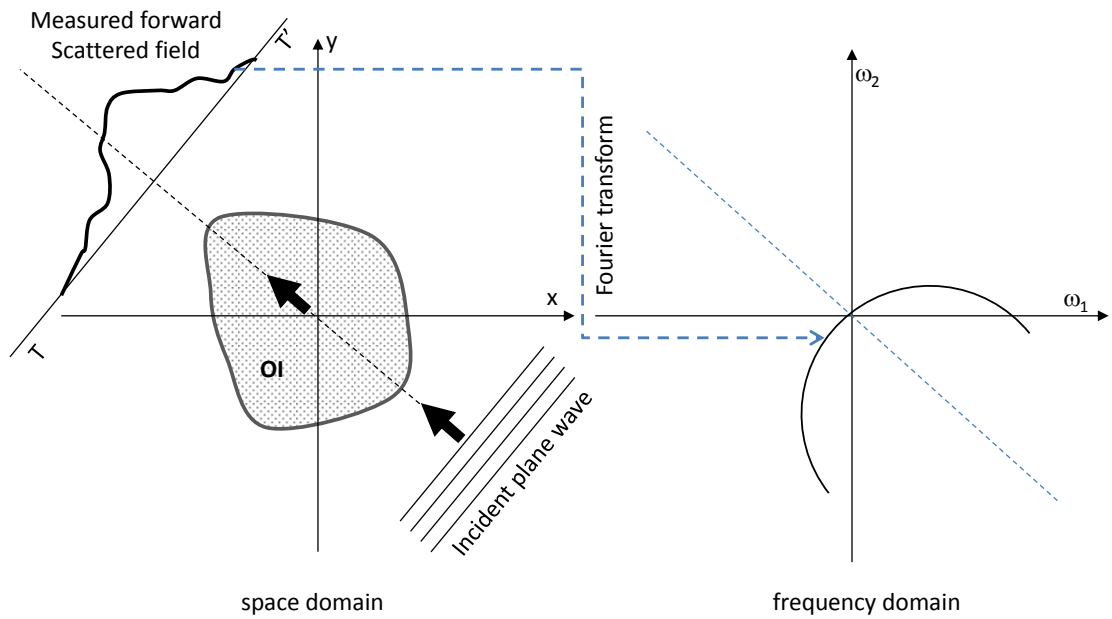


Figure 2-1: The Fourier diffraction projection theorem [3]

The resolution and accuracy of diffraction tomography are also limited due to the underlying approximations that involve the type of objects imaged accurately. Numerical experiment reveals that the first-order Born approximation is only valid for objects when the product of the change in refractive index and the diameter is less than 0.35λ [3].

There are two main problems in conventional diffraction tomography: the number of measurements, and the image resolution. Hence, the diffraction tomography method needs to be developed to decrease the number of measurement, which means reducing data collection time, and also to improve the imaging resolution.

2.1.2 Terahertz imaging

Terahertz radiation (THz), which is electromagnetic radiation ranges from 0.3 to 10 terahertz, has been used as the complementary of ionized X-ray and radioactive signals for non-destructive imaging technique. In addition to nonionizing technique, the THz imaging which penetrates various dielectric

materials, such as plastic, ceramic, and concrete, is advances in noncontact, non-destructive and coherent imaging, therefore, it has been widely used in various imaging modalities, including, spectral imaging, reflection tomography, and computerized tomography.

THz spectral imaging applies tomography technique over terahertz frequency band; typically 0.1-4 terahertz. In this technique, THz pulse is scanned toward an object, then, the reflection and transmission signal are measured. The recorded data are reconstructed using two dimensional image reconstruction algorithms. The advantage of this technique is more on its transient electric field, instead of the radiation intensity measured, where the measured THz field does not only yield a terahertz signal with excellent signal-to-noise ratio and high dynamic range, but also preserves the important phase information. Moreover, the reconstructed 2D image eliminates the need of raster scan and reduces the number of measurements of the conventional spectroscopy technique. This new complementary spectroscopy modal has been developed in various applications [29; 30; 31]. However, commonly, the power level used as THz sources is small, thus, a sensitive and compact THz detector still needs to be developed. Besides that, the large time needed for image reconstruction limits the technique for real time and industrial on line application.

THz reflection tomography makes use of time of flight technique. In this technique, a THz pulse is illuminated to the OI and the reflected signal is measured. The image of the interest is generated from the difference of time of flight in term of phase and amplitude. The technique has been used in various applications, including industrial [32], automotive [33; 34] , pharmaceutical [35; 36] and medical applications [37]. However, the technique is limited due to small dispersion and diffraction properties, weak reflection and uniform refractive indexes within each layer [38].

THz computerized tomography is described in [39; 40]. In this technique, an OI is radiated using THz pulse signal, then, the transmitted amplitude and phase of THz broadband pulses are measured at multiple projection angles. The measured fields which are in complex value are new

alternative of the scalar data of measured X-ray technique. The filtered back projection algorithm is applied to reconstruct the image from the measured data. The technique has been demonstrated for spectral analysis of material, like lactose and glucose [40], turkey bone [41; 42], and vial, and plastic tube [42]. The technique can be used to describe and discriminate the characteristic of the material due to strong absorption lines is present in their terahertz spectra. Nevertheless, the attenuation of THz signal and the cost of high power optical and terahertz sources limit the thickness and transparency of the sample to be imaged[43], besides, THz computerized tomography imaging is affected by different types of noise which can restrict its usefulness [44].

2.1.3 Millimeter-wave imaging

Millimeter-wave imaging (MMW) is a new non-ionizing imaging tool complementary to X-ray and Infrared. The MWT uses operating frequency ranges from 30 to 300 GHz or wavelength ranges from 10 to 1.0 mm, where in those frequencies, the wave penetrates various dielectric materials including plastics, ceramics, living tissues and low visibility objects. In millimeter wave range, an object emits, reflects and diffracts radiation; therefore, the MWT characterized an OI by the distribution of permittivity(ϵ)or dielectric properties.

Generally, Millimeter-wave imaging can be categorized into passive and active imaging. Passive millimeter-wave imaging (PMMW) reconstructs images from ambient radiation and radiation emitted from the objects through passive detection. The rapid development of this passive technique is driven by the ability to form images during the day or night; in clear weather or in low-visibility conditions, such as haze, fog, clouds, smoke, or sandstorms; and even through clothing. There are many applications of the PMMW including restored scene imaging[45], holographic imaging [46], aviation[47]., W-band power detector breakout circuit [48] and concealed hidden weapon detector[49; 50]. The advantages of this system include: high speed imaging [51] compact and analogues to optical camera [52]. However, the system is

limited in having relatively low resolution, small aperture and limited field of views.

Active millimeter-wave imaging (AMMW) directs millimeter wave energy at the subject, and then, reconstructs image by interpreting the reflected energy. The system of AMMW requires transmitting antenna and linear array of receiving antennas. Planar sparse array is used in [53; 54] and holographic linear arrays are applied in [55]. The reflection images may be developed using monostatic system of millimeter wave [56] or applying computer reconstruction methods, like backpropagation algorithm [53], and Synthetic Aperture Radar (SAR) imaging algorithm [54; 57; 58]. The advantages of this system are high speed, high resolution and large aperture.

Millimeter-wave tomography is a type of AMMW procedure. The development of this technique is not as fast as the development of MWT. Subtle interaction between MMW and object of interest which involves diffraction and emission makes the MWT technique and non-diffraction techniques like X-ray and radioactive tomography techniques hard to apply in this band.

2.1.4 Microwave imaging

Microwave imaging using electromagnetic radiation with frequency ranging from 0.3 to 30 GHz, is a promising technique for non-invasive evaluation tools. The technique is an alternative to visible light due to the higher capability in penetrating dielectric object and a better non-ionizing option than X-rays for biomedical investigation. The technique reveals more complete information than electrical imaging which deals with a real value of electric property of an OI, since the physical quantity of the object in microwave domain is stated in complex value of dielectric properties by means of permittivity and conductivity of the material. However, the complex number enhances the description of the interest but increases the difficulty of the problem.

Microwave imaging can mainly be categorized as microwave radar imaging and Microwave Tomography (MWT). The former is commonly known as ultra-wide band radar imaging. The basic principle of this technique is interpreting reflected fields due to strong scatterers. The data by means of the amplitude and phase of the reflection field are collected at a receiver antenna when microwave time domain pulse or swept frequency signal illuminates object domain where an OI takes place. Then, a reconstruction algorithm for example Fourier-based imaging methods like back-projection [59] and synthetic aperture radar algorithm [60] can be used to interpret data or build the image of the OI.

Radar imaging is useful for qualitative imaging that can be used to determine the shape and position of the object. There are many applications for radar imaging, including s through wall imaging [59] and foliage penetration imaging applications [60] which expose the ability of microwave in penetrating concrete and ground. Because it is fast, the technique can also be used to evaluate ground moving targets [61]. Nevertheless, microwave radar imaging is categorized as a qualitative imaging technique which cannot be used to describe the cross section of a complex object. Therefore, radar imaging is not accounted for in this thesis.

The later imaging technique which is the MWT is an active noninvasive imaging technique. The technique reconstructs the image of an OI cross section without a direct contact by solving the non-linear and ill posed MWT problem. The potential advantages of the imaging technique over conventional modalities such as magnetic resonance imaging (MRI) and computed tomography (CT) are: its relatively inexpensive cost and usage of low power, and its non-ionizing radiation. However, the MWT is challenged with nonlinear, ill posed and complex systems. Interestingly a great advantage of having detailed information in data gained in the form of amplitude and phase as well as its safety, mobility, and cost-effective supplement to current imaging modalities for non-invasive assessment has made the MWT urgent to be selected as the topic of this thesis.

2.2 Microwave Tomography Method

The accuracy of reconstructed images by the DT, MMW tomography and THz tomography are limited. These techniques acquire the data acquisition in a time domain. Though the data gathered consist of phase and amplitude of the field, the use of Fourier technique to deal with the swept data disregards the variation of the OI contrast over the working frequency ranges. In contrast, the acquisition of MWT can generally be done a single frequency and the MWT-inverse problem can be formulated in frequency domain with an appropriate electric field integral equation , thus, the artifacts due to ignoring the variation in propagation speed, the multipath effect and loss in the DT, MMW and THz tomography can be avoided.

The architecture of the MWT which works in frequency domain, is presented in Figure 2-2, where the Tx represents the transmitting antenna; and the Rx represents the receiving antennas.

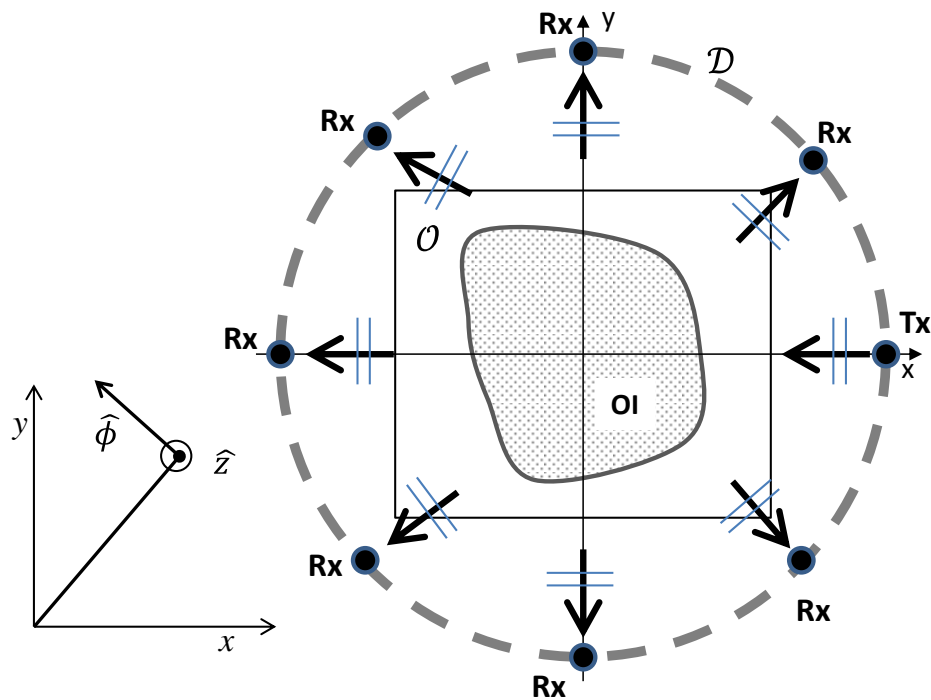


Figure 2-2: Geometrical model of microwave tomography problem.

The domain \mathcal{O} which contains the OI is the imaging domain/object domain. The domain \mathcal{D} which contains antennas is the measurement domain/data domain. It is outside the object domain. These two domains are assumed to be in $x - y$ plane. Practically, the antennas can be used to receive or transmit microwave signal, where the radiation from the Tx can be assumed as a plane wave or electric line source equivalent. At each radiation, the scattered fields are collected at the rest of the antennas which are assigned as the Rx.

Microwave Tomography is the form of active microwave imaging. The goal of the MWT is to estimate unknown attributes distribution of interest from given measurement that only indirectly related to the interaction between the microwave signal and the dielectric property of the interest. Unfortunately, the interaction is nonlinear and a small amount of noise in the data leads to enormous errors in the reconstruction. The nonlinearity of the problem has to be optimized and the instability known as ill condition needs to be regularized. Several methods to solve the nonlinear ill posed problem of the MWT have been developed. The following section overviews the methods to solve the problems.

2.3 Nonlinear Methods to Solve Microwave Tomography Inverse Problems

Nonlinear iterative method for solving MWT-inverse problem can be categorized into two types of algorithms: gradient type method and Newton method. Both types of algorithms with the applications of the algorithms on MWT are described as follows.

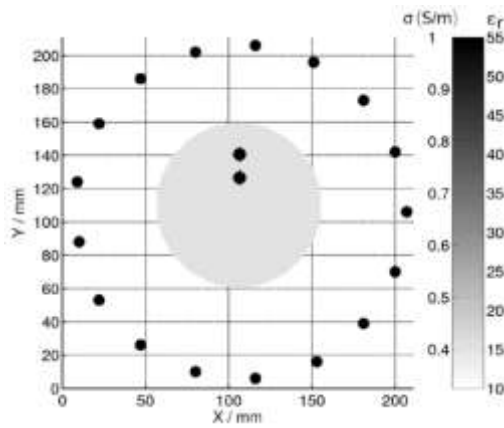
2.3.1 Gradient Method

2.3.1.1 Modified gradient method

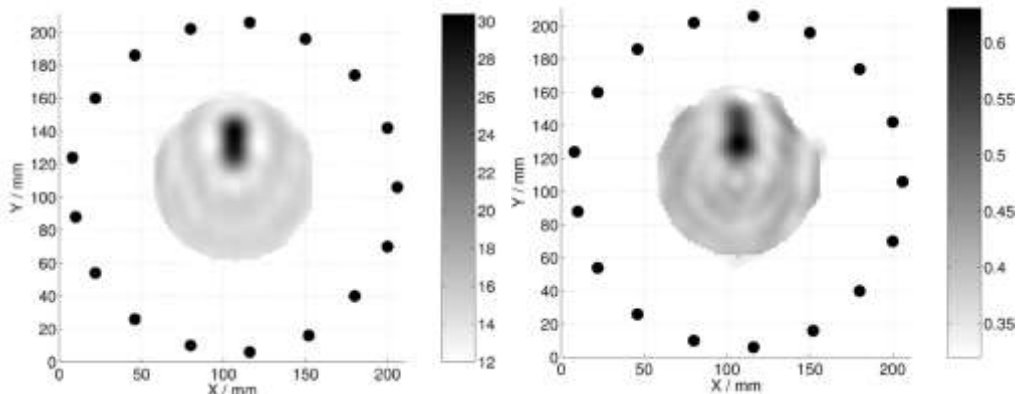
Modified Gradient Method (MG) which is a gradient type algorithm for solving MWT inverse problem, applies a conjugate method on both total electric field and dielectric contrast variables. The iterative sequence of the MG is presented in [11], where both variables are updated simultaneously by minimizing a cost function. The conjugate gradient method determines the search direction of the MG and the Fletcher-Reeves equation [62], Polak and Ribiere [63] or other conjugate techniques with a parameter (β_k) defines the step length of the correction. It can be seen that the MG is basically a conjugate gradient method for minimizing two-terms of MWT cost function.

The MG method has been widely used to solve MWT inverse problem. There are many applications for the MWT inverse problem, including industrial application [64; 65], breast tumor/cancer detection [66; 67; 68], medical/biological reconstruction [69], and geophysical application [70], besides numerical experiments have also been reported in [71; 72; 73]. The MG can be applied to a high contrast OI problem, however the disadvantage of the method is that the initial estimation of the contrast is essential to the quality of the result [66; 74].

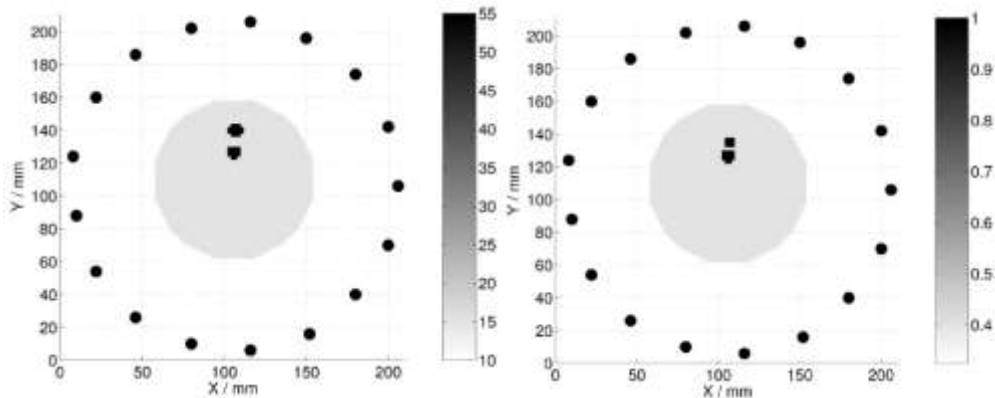
The essential initial guess of MG is described in [74]. The MG is used to reconstruct two small objects in a lossy background medium where the model used for the simulation is a large circular object with properties $\epsilon_r = 15.0$ and $\sigma = 0.4 S/m$ and two small objects with radius 4mm with parameters $\epsilon_r = 55.0$ and $\sigma = 1.0 S/m$. The background medium is matching liquid with $\epsilon_r = 12.0$ and $\sigma = 0.32 S/m$. The results of reconstruction with and without priory information are presented in Figure 2-3 and the relative error of the results is presented in Figure 2-4. It can be seen that when the algorithm has converged, the reconstructions utilizing a priori data have a lower relative error compared to the reconstructions without a priori data. Moreover, the prior information data resolve the reconstructed images while the MG fails to reconstruct the small object without the information.



a) Model used for the simulation



(b) Reconstruction of the two small objects without a priori data



(c) Reconstruction of the two small objects with a priori dielectric data

Figure 2-3: Model object of interest used for modified gradient algorithm test and the result of the reconstruction. Large object had the properties $\epsilon_r = 15.0$ and $\sigma = 0.4 S/m$ and two small objects with radius 4mm with parameters $\epsilon_r = 55.0$ and $\sigma = 1.0 S/m$. The background medium is matching liquid with $\epsilon_r = 12.0$ and $\sigma = 0.32 S/m$. [74].

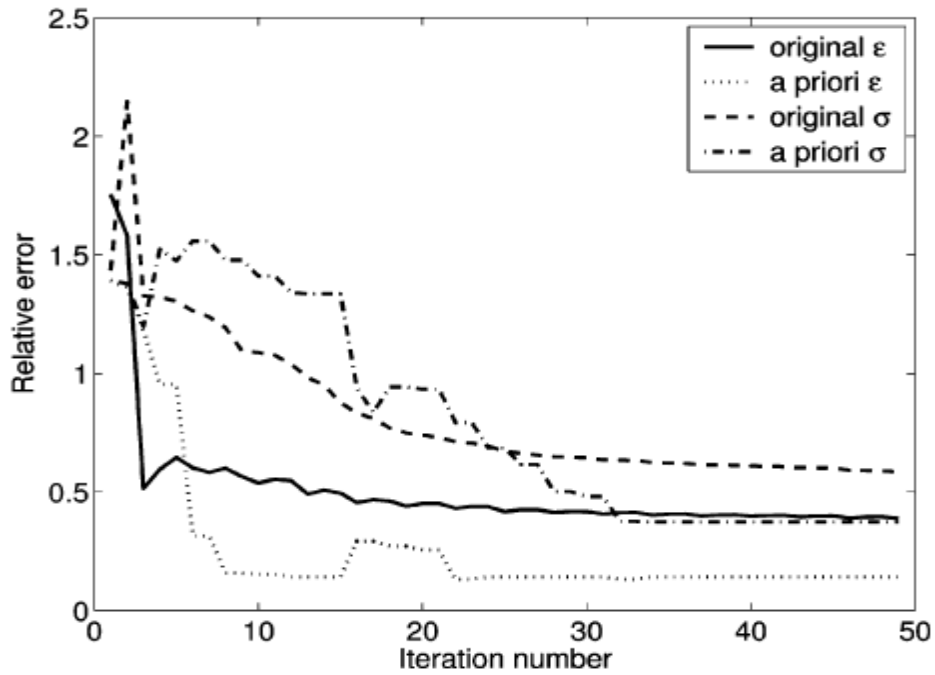


Figure 2-4: Relative error of OI complex permittivity of small object resulted by Modified Gradient method with and without a priori data [74].

The MG method can be categorized as a semi regularized method. The ill conditioning of the problem is regulated by stopping the sequence before the noise starts to govern the inversion [71]. However, the stopping criteria cannot be determined accurately as if the noise level is unknown. An additional procedure to define the stopping position of MG method is needed.

2.3.1.2 Contrast source inversion method

Contrast Source Inversion (CSI) method is a gradient method that combines the unknown total electric field and the dielectric contrast in the imaging domain into a contrast source variable. Basically, this is similar to the application of the volume equivalence principle to the TM polarization of the electric field integral equation where the dielectric contrast of a material and the electric field inside the *OI* is replaced by the equivalent polarization currents variable [9].

The CSI algorithm reconstructs the contrast-source variable and contrast variable iteratively. Different from the MG method which updates

the contrast simultaneously with the total field, the CSI corrects the contrast successively. The contrast is updated by minimizing the second term of a cost function that is constructed from electric field integral equations. However, the contrast is present in the denominator of the cost function. Direct application of a conjugate direction to the cost function may not always reduce the quantity of the functional [13].

Various numerical tests and applications of the CSI have been reported, which include the reconstruction of biological object [75; 76; 77; 78], breast cancer or tumour detection [79] phase less data [80] and other numerical tests [81; 82]. Reconstruction of experimental data in the case of biological object can be found [83; 84], while the capability of the CSI in reconstructing an unknown triangle and other shapes from Ipswich data when the MG fails to build accurate images is demonstrated at [85; 86]. The CSI is also possibly combined with various methods such as, the use of finite element [79] and finite difference solver [77], three dimensional measurement system [87], and application of multi frequency data [88].

The CSI cannot start with zero initial estimates for the contrast, since the cost function of MWT problem is not defined. Therefore, the CSI starts with nonzero initial guess. A priori information is one of the initial input of the method. It has been shown that the use of prior information in cancer detection is better than blind information [79]. Other prior information has been applied like real positive value of the OI contrast [13; 80].

The contrast is updated using second term of the CSI cost function which is formulated by the integral equations of MWT inverse problem. The problem arises is generally over determined, however, a direct calculation which means averaging, may not minimize the cost function due to the presence of the contrast in the denominator. Therefore, minimization functional is constructed to update the contrast. This makes the method rather unpractical and slow.

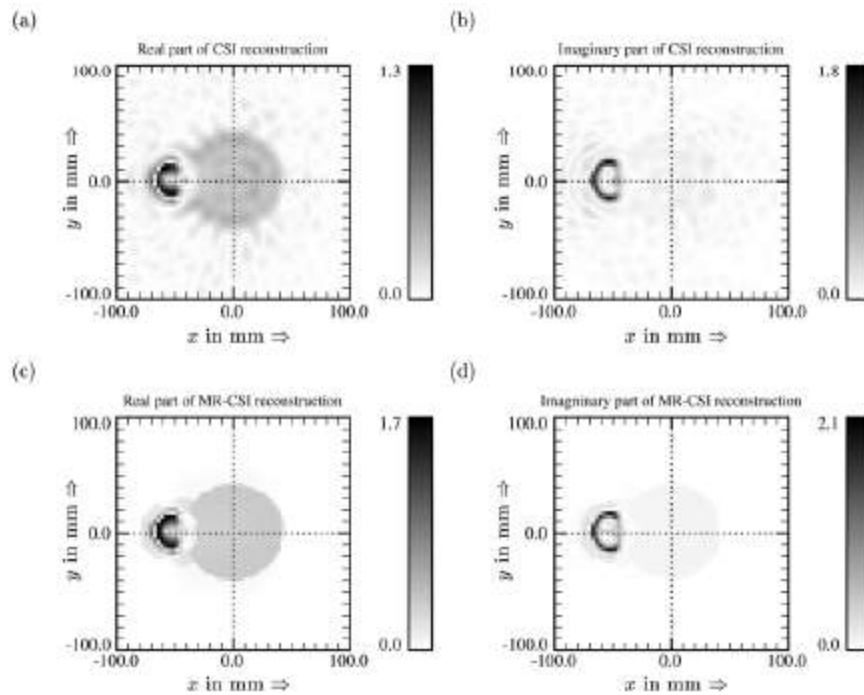


Figure 2-5: CSI and MR-CSI reconstructions for TM data at single frequency of 10 GHz [88]

The advantage of CSI is adaptive to a regularization technique. The application of weighted L2- norm regularization factor named multiplicative regulator to the nonlinear integral equation of the CSI improves the flexibility of the algorithm to the noise. The regularization reformulates the CSI as Multiplicative Regularized CSI (MR-CSI). The MR-CSI seems to handle noise as well as limited data in a robust way, that makes the algorithm suitable to invert experimental data [89; 90; 91].

Jinghong et al compare the CSI with the MR-CSI. The object of interest is a metallic cylinder located outside a large dielectric cylinder with a contrast of 0.45[88]. The source of microwave signal is 10 GHz TM mode. The images resulted by the CSI and the MR-CSI are presented in Figure 2-5. It can be seen that the inversion results achieved by the MR-CSI are better than that obtained by the CSI. The application of regularization improves the quality of the images. Nevertheless, the great limitation of both methods is the speed (see Table 2-1) that they cannot be used in a quasi-real time processing.

Table 2-1 Computational time on a Pentium 2.0 GHz dual processor personal computer [88]

Inversion Schemes	CSI	MR-CSI
<i>Initial Guess</i>	Back Projection	Back Projection
<i>Number of Iteration</i>	500	500
<i>Computational Time</i>	4 hour	4 hour

The gradient methods for solving MWT inverse problem, that are MG and CSI methods, are sensitive to initial guess; but, they are flexible in handling noise. The methods are basically constructed from a conjugate gradient technique. In this thesis, the modification of the CG is used to solve MWT problem. It is used as a part of a Newton iterative method. The CG regulates the ill conditioning and solves the linearization of MWT inverse problem which is constructed along with the Newton Iteration, where the initial guess of the CG is the current nonlinear solution of Newton method.

2.3.2 *Newton's Method*

2.3.2.1 *Gauss-Newton inversion*

Gauss Newton Inversion (GNI) is a well-known Newton's based method for solving MWT problem. Wide area tests and applications have been reported, including testing the GNI to reconstruct synthetic data in the form of inhomogeneous numerical 2D objects [92; 93], 3D objects [94] and synthetic brain and breast models [95]. Furthermore, it has been shown that the method reconstructs experimental data well, like Fresnel experimental data [96; 97], three dimensional experimental objects [98; 99], biomedical experimental data [84; 100], and the applications of breast cancer screening [67].

The GNI is a type of quadratic Newton method optimization which minimizes a non-linear least squares cost function of MWT inverse problem. Consequently, the sequence of the GNI needs a negative gradient of the cost function which can be defined from the first order differential of the cost

function and a Hessian matrix which is constructed from the second order differential of the function. Implicit Jacobian matrix (\mathcal{J}) to approximate both terms, gradient and Hessian matrix, as it has been proved by Mojabi[95], saves memory and computational time [97].

The calculation of the GNI steps involves explicit computation of the inverse of matrix $\mathcal{J}^T \mathcal{J}$ which is ill posed. Therefore, treating the ill posedness via regularization is essential in the GNI procedure. The regularization can be inserted in the pseudo inverse sequence which is done using a singular value decomposition, the examples of this technique include Tikhonov regularization [99], iterative Landweber-Friedman, and Truncated singular value decomposition. An alternative regularization technique is proposed in [101] which regularizes the cost function of MWT inverse problem. Methods for regularizing the cost function include additive [102], multiplicative [93; 97] and additive-multiplicative regularization [96].

The speed of algorithm is mainly governed by two factors. The first factor is the speed of the forward problem solution and the second is the accuracy of the Newton step. The first is done by solving the integral function of direct MWT scattering problem. The function is a well posed system that can be inverted directly. The second are not the issue as they can be controlled by setting the size of the cells [9]. The ideal Newton step of GNI equals to the distance of the parameter of global solution and its current iterative solution. The accuracy of GNI to update parameter of current solution as close as possible to the global solution decreases the number of iteration, therefore, the choice of regularization relates to the number of iteration which has been shown by Rubæk et al[67].

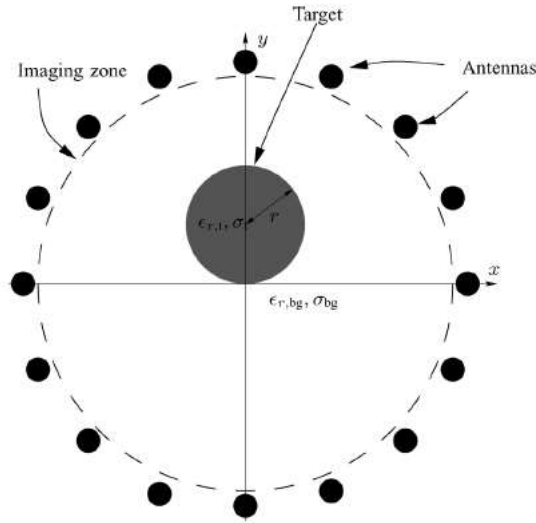


Figure 2-6: Schematic setup of the simulation for Gauss Newton inversion test [67]. The background constitutive parameter is $\epsilon_r = 30$ and $\sigma_r = 1.163 S/m$. The OI is centered at $(x, y) = (0, 2cm)$. The OI radius and constitutive parameter are $r = 2cm$, $\epsilon_r = 50$ and $\sigma_r = 1.6 S/m$.

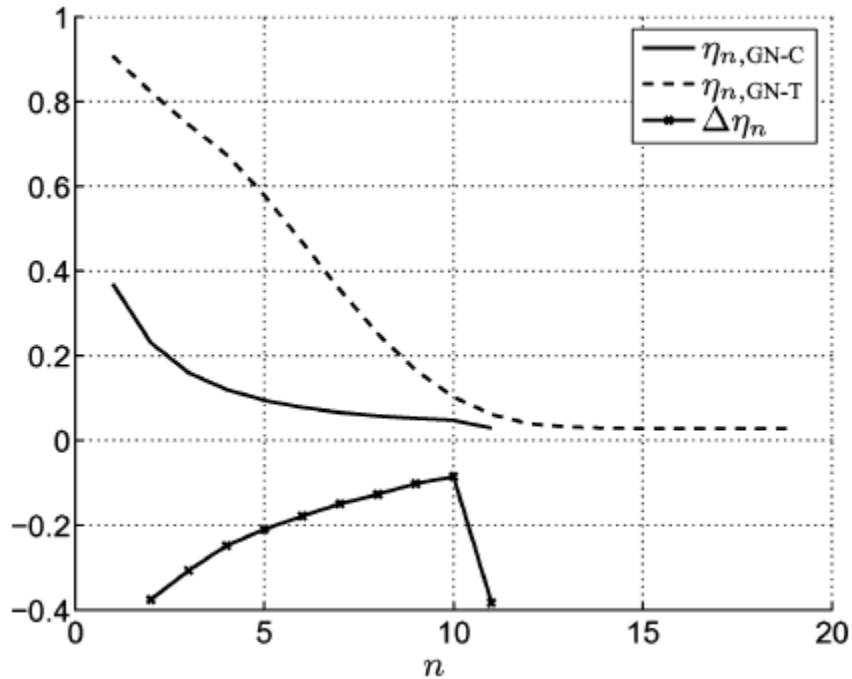


Figure 2-7: Normalized norm for MWT cost function of GNI with Tikhonov regularization ($\eta_n, GN - T$) and GNI with conjugate gradient least squares regularization ($\eta_n, GN - C$) [67].

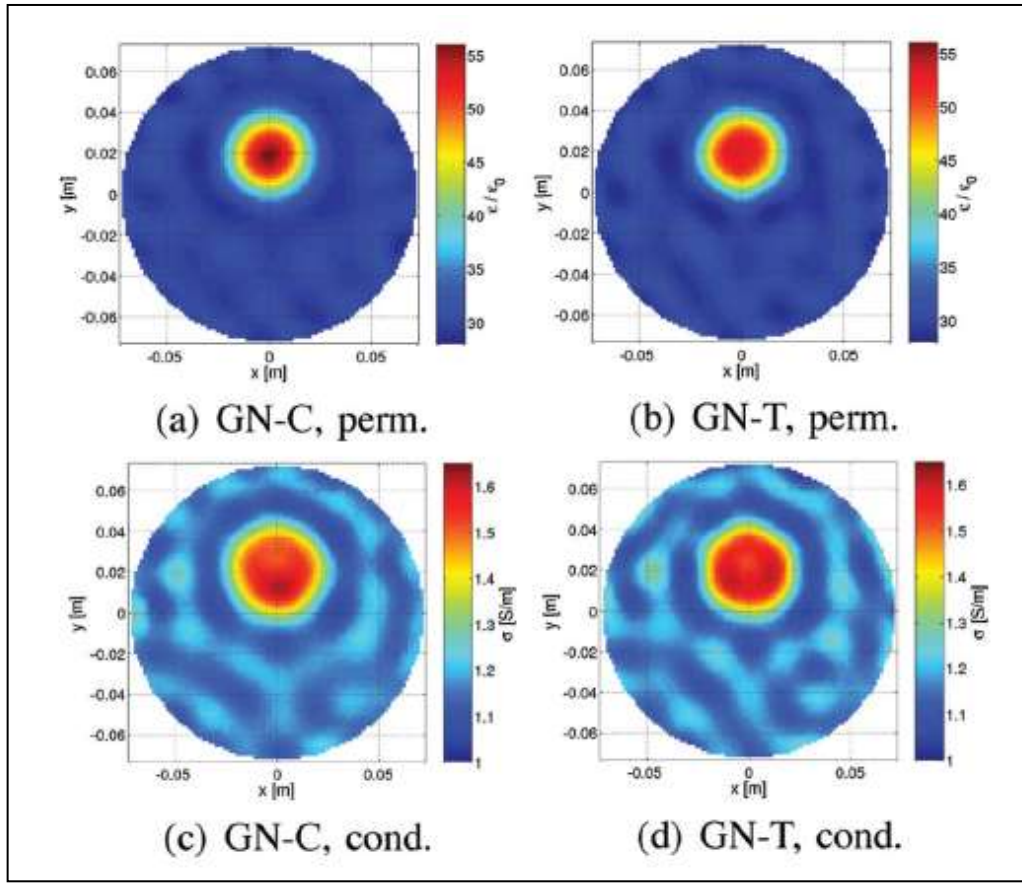


Figure 2-8: Reconstructed values of conductivity and permittivity of simulated OI (Figure 2-6) for $(\eta_n, GN - T)$ and $(\eta_n, GN - C)$ [67]

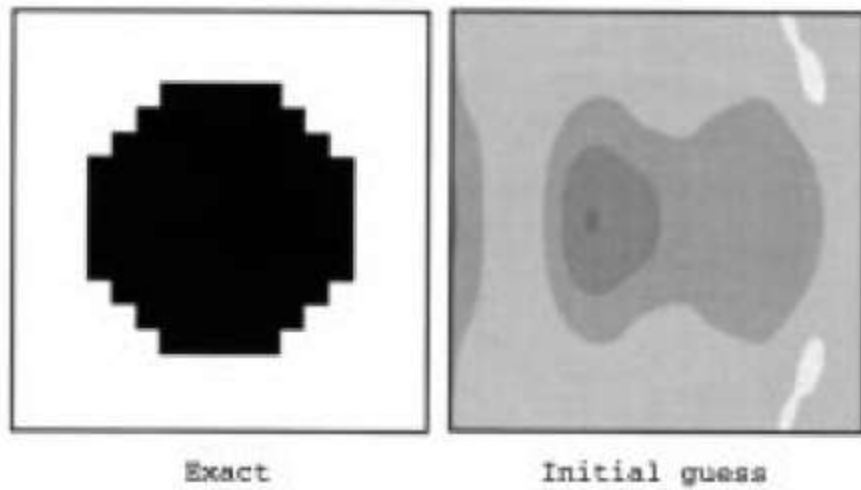
The choice of regularization techniques affects the ability of GNI in solving certain MWT problem [102]. Many researches have been conducted as discussed in previous paragraphs. Moreover, the iterative solution of GNI can be categorized as a one-step exact solution. If the regularization at current iteration fails, then, the general solution will not converge toward global solution. Therefore, the determination of regulator parameter is also an issue; besides, a regulator technique may not be suitable for certain MWT inverse problem. For this reason, a deterministic algorithm based on the GNI to solve MWT inverse problem is selected to be developed in this thesis.

2.3.3 *Newton Kantorovich method*

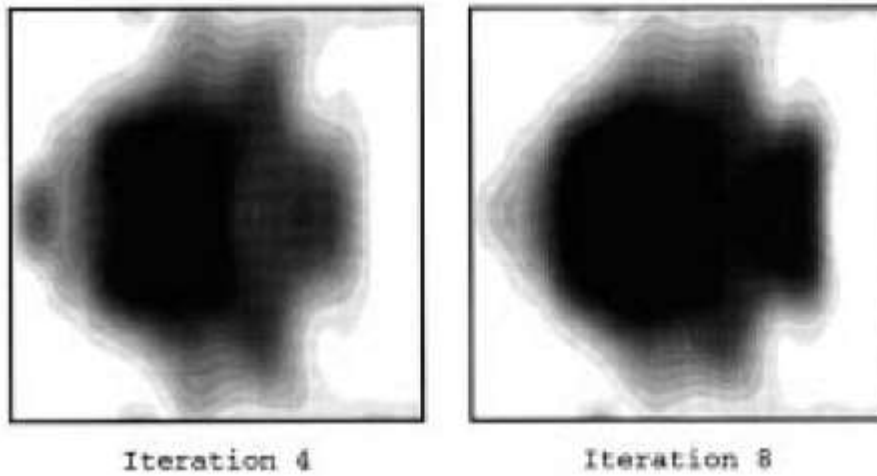
Originally, Roger [103] develops Newton Kantorovich (NK) from the Newton method to reconstruct the inverse scattering of perfect conductive cylinder from TE illumination. The NK is a functional system where the iterative update value is directly proportional to the difference between the parameter value of the output of MWT system and the measured MWT data. The method is constructed from the first two components of Taylor series, where Fréchet derivative defines first order differential of MWT inverse problem. The NK is a linear ill-posed system; however, it is still nonlinear in respect to the solution of the MWT inverse problem which is an ill-posed system, therefore, the NK needs to be regularized. Roger shows that the NK with the Tikhonov-Miller regulator is capable of reconstructing conductive object.

The NK solves MWT inverse problem as linear ill posed problem optimization. The technique, which is introduced by Joachimowich, starts by linearizing the MWT inverse problem, then solves the linear ill posed using a standard Tikhonov regularization with an identity operator being used. Numerical tests show that the NK is reasonably good in reconstructing two and three dimensional inhomogeneous object [104], One dimensional highly contrast object [105], Noise less human arm model [106], and shape and location of an object from noiseless data, but it fails to rebuild a noisy data [69; 71; 107].

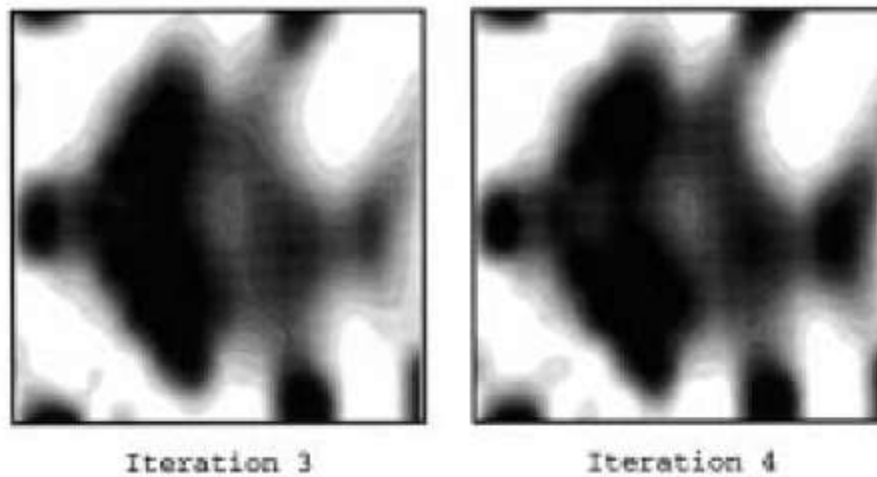
Furthermore, the NK has been reported to be applied to handle experimental data, which include experimental breast cancer imaging using microwave planar camera [108], reconstructing an inhomogeneous lossy dielectric cylinder of Ipswich data [109; 110; 111]. It is reported that NK is flexible in the choice of polarization, and experimental arrangement, but it is sensitive in the initial guess of dielectric contrast.



a) The contrast of OI and its initial guess



b) Reconstruction of contrast from noiseless data



c) Reconstruction of contrast from noisy data with SNR of 30%

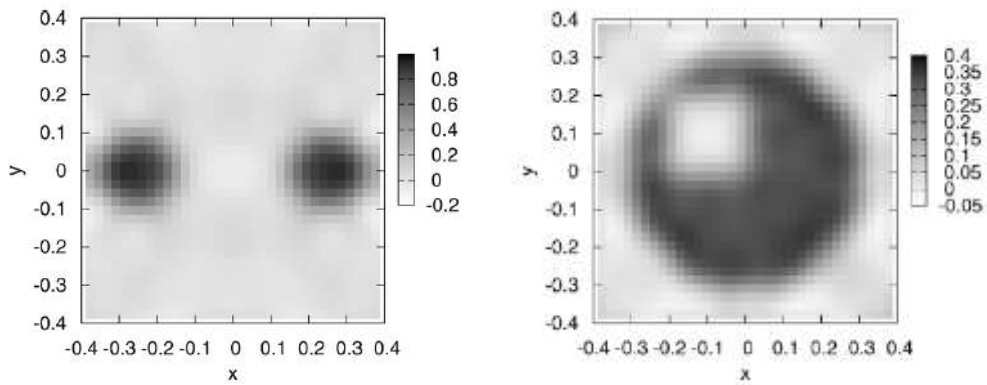
Figure 2-9: The object model with dielectric contrast ($\chi(r \in \Omega) = 1$), initial guess and reconstruction results of Newton Kantorovich algorithm for noiseless data and noisy data [71].

NK reconstructs the linear ill posed problem using the solutions of the direct scattering electric integral equation at each iteration. Then, the problem is directly regulated and solved. It has been shown that the direct and regulated solution is sensitive to the noise level. Therefore, flexibility in determining linear solution is needed to improve the quality of NK. Flexible approximation solution of Inexact Newton class method may replace the rigid solution of NK. For this reason, the thesis focuses on the development of inexact Newton class to solve MWT-inverse problem.

2.3.4 Inexact Newton method

Bozza solves MWT inverse problem in two nested loops [112; 113]. The outer loop is the linearization of MWT problem, while the inner loop determines the regularized solution of the linear ill-posed problem where the iterative Truncated Landweber method is applied. The technique is categorized as Inexact Newton Method (INM)

The INM has been used in several applications, which include reconstructing several different unknown dielectric contrasts of inhomogeneous objects from noisy data [114; 115; 116; 117]. It has been demonstrated that started from an empty scene, the localization and separation of the OI is very good, although the shaping is not very sharp because of the ill-posedness of the problem. The INM has also been used to reconstruct experimental data. The results related to the inversion of far-field data measurement show that the localization of the objects is very good and so are their separation capabilities [116]. Moreover, the INM shows the superiority in conducting noisy data. Satisfying inverting results of noisy data are reported, such as the synthetic two layered dielectric circular [114], three dimensional targets [118], and 3D Breast imaging [119]. The example of the INM in handling noisy data of homogeneous circular cylinder problem as it is reported by Bozza et al in [112] is presented in Figure 2-10



Two identical separate homogeneous circular cylinder ($\chi(r \in \Omega) = 1$)

A circular homogeneous cylinder ($\chi(r \in \Omega) = 0.4$) with a square hole

Figure 2-10: The results of inexact Newton test by Bozza et al. Reconstructed distribution of the contrast of OI (χ) from noisy data with SNR 20dB [112]

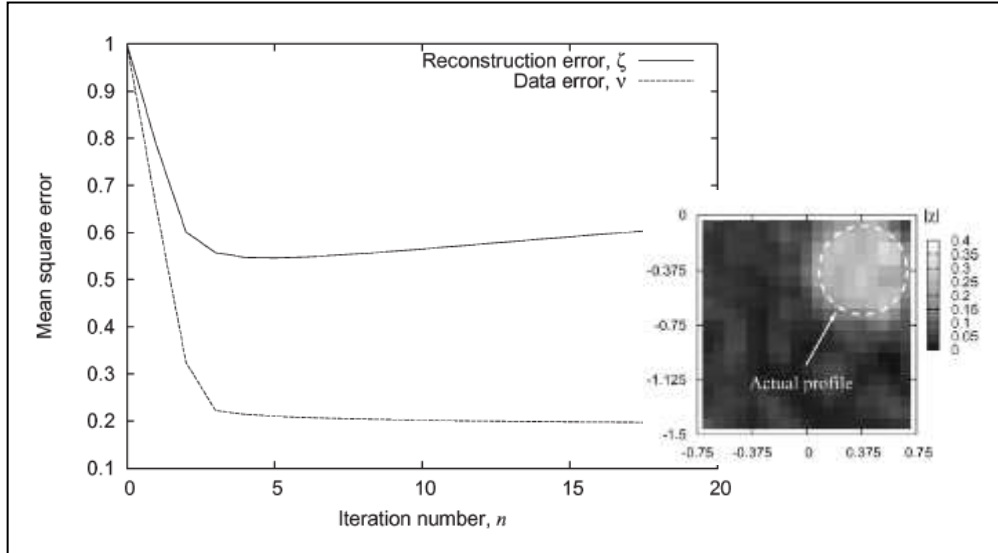


Figure 2-11: Reconstructed distribution of the contrast of buried OI (χ) from noisy data with SNR 20dB and the behaviour of mean squared error on the reconstruction of the contrast function [113]

Bozza et al. exploit the iterative Truncated Landweber method as an inexact solver for MWT linear ill-posed problem which is constructed under first order Newton scheme. It is an alternative to the direct regulative solution as in the NK. It has been shown that the solution is flexible to the introduction of noise and flexible to the initial guess. However, this inner iterative solution is defined in a specific manner which means that the truncated Landweber method finds regularized solution of the linear MWT problem at the inner loop. Then, the solution is directly taken as the update of the Newton solution. The INM sequence is only evaluated in the stopping criteria of the outer loops [112]. The method has to solve the Newton equations at each stage as the inner loop acts as a direct regularization. It can be expensive if the number of unknowns is large and may not be justified if the current solution is far from the target value. Therefore, this thesis develops Inexact Newton Class to solve MWT problems by addressing an implicit solution of the MWT inverse problem. At the inner loop, the first order Newton equation as a result of linearization of MWT problem is solved only approximately and in some unspecified manner. An iterative method solves the Newton equation with a natural stopping rule based on the relative residual linear solution with its corresponding nonlinear solution. The method computes an approximate solution to the Newton equation in some unspecified manner such that a nonnegative forcing sequence controls the level of accuracy.

3

Direct Scattering for Microwave Tomography

The Direct scattering problem is presented in a volume electric field integral equation (VEFIE). The equation which respects to total electric fields (E) and dielectric contrast(χ) is solved using pulse basis function and the Method of Moment (MM). The solution in term of scattered fields (E^s) in data domain is evaluated by comparing it with the analytic solution. The numerical experiment shows that the solution is accurate and flexible to cell size. Perfect solution is generated from a wide range relative permittivity of scatterer. Further extensions of direct scattering problem studies are included: presenting and solving EFIE in term of equivalent current density (J) and ratio of the dielectric contrast; and applying the microwave incident fields under both plane wave and line source equivalent.

3.1 Introduction

The direct scattering problem is essential to develop methods in inverse scattering problems as in the MWT inverse problem. The direct scattering problem is the forward problems of the MWT. The solution of the problem

defines the cost function of the MWT inverse problem; therefore, the accuracy of the direct scattering problem solution directly influences the results of the MWT inverse problem.

A general scattering problem can be solved using an integral equation, like calculating scattering fields due to the illumination of electromagnetic field to an Object of Interest (OI). Richmond [120] introduced the simulation of the integral equation for an electromagnetic scattering problem. The magnetic and the electric field interior and exterior of a cylinder with arbitrary cross-sectional shape are calculated using the integral equation. Furthermore, methods to solve the integral equation have grown since the work of Richmond's. Harrington[8] proposed a numerical solution of the integral equation using the Method of Moment (MM). The MM is a numerical procedure to solve a linear operator equation by transforming it to a system of simultaneous linear algebraic equation which is commonly referred to as matrix equation. The MM quantifies current distribution in the surface of a conducting cylinder which can be used to determine the value of scattering field outside the cylinder. It becomes very popular as a solver for the integral equation of direct scattering problem.

Generally, the MM can be applied to solve two types of integral equations namely surface integral and volume integral. The application of the MM for the surface integral usually involves scattering from a conducting cylinder. The MM has been implemented to simulate scattering fields from various types of conducting materials[121; 122; 123]. The surface integral can be applied to calculate the scattering from a conducting object of homogeneous scatterer, but it is not suitable for an inhomogeneous penetrable object [9]. Therefore, the surface integral is not further discussed in this thesis.

The MM for solving the volume integral equation works in the centre of the cells across the OI slice. This is suitable for MWT application which is aimed to reconstruct the image of the dielectric value of OI cross section. Richmond approach is used to develop the forward problems. Then, it is followed by developing several inverse methods based on the defined forward problems. The results show that the volume integral can be used to develop

microwave imaging. It can be used to reconstruct simple objects [107; 124; 125]. Nevertheless, it is sensitive to noises and initial guess besides gaining big error; thereto, the investigation on the forward problems needs to be done.

The feature of the MM has included a frequency domain prediction technique and taken to the account the entire electromagnetic phenomenon and the polarization effects. The MM, which is based on an integral equation technique, advances in the accuracy of the results as it is essentially exact and provides direct numerical solutions. It is also applicable to complex inhomogeneous(OI). Nevertheless, the MM is classified into low frequency methods. It is typically limited to problems of small electrical size due to limitations of computation time and memory system. Thereto, an investigation of the MM solution for higher frequency is necessary to be done.

3.2 The Method of Moment Solution for Direct Scattering Problem

3.2.1 *Direct scattering in two-dimensional*

The direct scattering problem of an inhomogeneous OI involves the interaction between microwave and a penetrable OI. The interaction can be described in term of a volume electric field integral equation (VEFIE). In the special case in which the OI is composed entirely of dielectric material, the electric field integral equation can be stated as in [9]

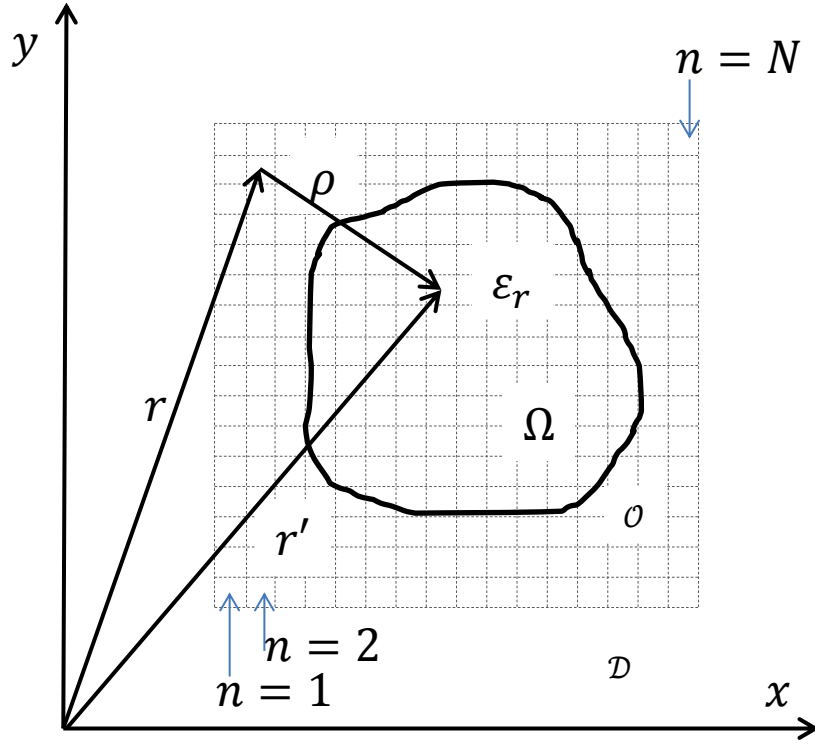


Figure 3-1: Cross section of a dielectric object (Ω). Object is placed in object domain (\mathcal{O}). The domain \mathcal{O} is divided into N squared cells ($n = 1, 2 \dots N$). The \mathcal{O} is surrounded by data domain (\mathcal{D}) where observation points ($m = 1, 2 \dots M$) are placed.

$$\mathbf{E}^i(\vec{r}) = \mathbf{E}(\vec{r}) + j\omega\mu_0\mathbf{A}(\vec{r}) + \nabla\Phi_e \quad (3.1)$$

For two-dimensional TM polarization in \hat{z} direction the vector potential ($\mathbf{A}(\vec{r})$) and the Green function (\mathbb{G}) are defined as

$$A_z(\vec{r}) = j\omega\epsilon_0 \int_{\Omega} (\epsilon_r - 1) E(\vec{r}') \mathbb{G}(r, r') dr' \quad (3.2)$$

$$\mathbb{G}(r, r') = \frac{1}{4j} H_0^{(2)}(k\rho) \quad (3.3)$$

The two-dimensional electric field integral equation of (3.1) can be written as

$$E^i(\mathbf{r}) = E(\mathbf{r}) - k_0^2 \iint_{\Omega} \frac{1}{4j} \chi(\mathbf{r}') E(\mathbf{r}') H_0^{(2)}(k_0\rho) d\mathbf{r}' \quad (3.4)$$

Where $E^i(\mathbf{r})$, $E(\mathbf{r})$ and $E^s(\mathbf{r})$ are the incident, total and scattered electric fields at \mathbf{r} sequentially, Ω is the cross section of the OI, $\chi = (\epsilon_r - 1)$ is the dielectric contrast, and both coefficients r and r' are position vectors, and $\rho = |r - r'|$.

Equation above represents *domain equation*. The position vector addresses a point at an $\mathcal{O}, (r, r') \in \mathcal{O}$.

Assuming that a dielectric object is immersed in an \mathcal{O} where the \mathcal{O} is divided into N number of cells as seen in Figure 3-1. Then, the electric field in (1) at n^{th} cell where $n = 1, 2 \dots N$ can be defined in a discrete system as

$$E_n^i = E_n + \sum_{n'=1}^N Z_{nn'} \chi_{n'} E_{n'} \quad (3.5)$$

Where $Z_{nn'}$ is the integral operator of (3.4) which represents the interaction of cell n to cell n'

The integral (3.4) is evaluated analytically with the assumption that all cells are circles [9; 120]; thus, the integral of the Hankel function can be approximated using

$$\int_{\phi'=0}^{2\pi} \int_{r'=0}^a H_0^2(k_0 \rho) r' dr' d\phi' = \begin{cases} \frac{2\pi a}{k_0} H_1^2(k_0 a) - \frac{j^4}{k^2} & (\rho < a) \\ \frac{2\pi a}{k} J_1(k_0 a) H_0^2(k_0 \rho) & (\rho > a) \end{cases} \quad (3.6)$$

where a is the radius of a cell. Applying (3.6) to (3.4), the entries of $Z_{nn'}$ are given by

$$Z_{nn'} = \frac{jk_0 \pi a_n}{2} J_1(k_0 a) H_0^2(k_0 \rho); \quad n \neq n' \quad (3.7)$$

$$Z_{nn'} = \frac{jk_0 \pi a}{2} H_1^2(k_0 a) + 1; \quad n = n' \quad (3.8)$$

Assuming that the radius of cells equals to a_n , with $n' = 1, 2 \dots N$, equation (3.5) can be written for $n = 1$ as

$$E_1^i = E_1 + [Z_{1n'}][(\chi_{n'} E_{n'})] \quad (3.9)$$

where $n' = 1, 2 \dots N$ and

$$[Z_{1n'}] = [Z_{11} \quad Z_{12} \quad \dots \quad Z_{1N}]$$

While $[(\chi_{n'} E_{n'})]$ is defined as

$$[(\chi_{n'} E_{n'})] = \begin{bmatrix} \chi_1 & 0 & 0 & 0 \\ 0 & \chi_2 & 0 & 0 \\ 0 & 0 & \ddots & \vdots \\ 0 & 0 & \dots & \chi_N \end{bmatrix} \begin{bmatrix} E_1 \\ E_2 \\ \vdots \\ E_N \end{bmatrix} = [\text{diag}(\chi_{n'})][E_{n'}] \quad (3.10)$$

For simplicity, for the rest of report $[(\chi_{n'} \mathbf{E}_{n'})]$ may be written as $[\text{diag}(\chi_{n'})][\mathbf{E}_{n'}]$ Similar equations can be obtained for $n = 2, 3 \dots N$ so that for this illumination,

$$\begin{aligned} [\mathbf{E}_n^i] &= [\mathbf{E}_n] + [\mathbf{Z}_{nn'}][(\chi_{n'} \mathbf{E}_{n'})] = [\mathbf{E}_n] + [\mathbf{Z}_{nn'}][\text{diag}(\chi_{n'})][\mathbf{E}_{n'}] \\ [\mathbf{E}_n^i] &= [\mathbf{I} + [\mathbf{Z}_{nn'}][\text{diag}(\chi_{n'})]][\mathbf{E}_{n'}] \end{aligned} \quad (3.11)$$

the total electric field $[\mathbf{E}_n]$ can be expressed as

$$[\mathbf{E}_n] = [\mathbf{I} + [\mathbf{Z}_{nn'}][\text{diag}(\chi_{n'})]]^{-1} [\mathbf{E}_n^i] \quad (3.12)$$

where the total field is the addition of the incident and scattered field.

$$E(\mathbf{r}) = E^i(\mathbf{r}) + E^s(\mathbf{r}) \quad (3.13)$$

Therefore, the scattered fields due the present of a dielectric object at imaging domain, at the observations points can be stated in the integral equation as

$$E^s(\mathbf{r}) = k_0^2 \iint_{\Omega} \frac{1}{4j} \chi(\mathbf{r}') E(\mathbf{r}') H_0^{(2)}(k_0 \rho) d\mathbf{r}' \quad (3.14)$$

Assuming that the scattered fields are measured in M observation points where m is index of observation points that is $m = 1, 2 \dots M$, ($n \in \mathcal{D}$), then, equation (3.14) can be stated as matrix equation

$$[\mathbf{E}_m^s] = -[\mathbf{Z}_{mn'}][\text{diag}(\chi_{n'})][\mathbf{E}_{n'}^t] \quad (3.15)$$

Defining that n is the index of the object cell which is $n = 1, 2 \dots N$; ($n \in \mathcal{O}$) and, then, at each projection (t) with $t = 1..T$, a microwave signal illuminates \mathcal{O} . Integral (3.4) can be stated as the matrix equation

$$[\mathbf{E}_n^t]_t = [\mathbf{I} + [\mathbf{Z}_{nn'}][\text{diag}(\chi_{n'})]]^{-1} [\mathbf{E}_n^i]_t \quad (3.16)$$

And the scattered fields can be calculated using

$$\begin{aligned} [\mathbf{E}_m^s]_t &= -[\mathbf{Z}_{mn'}]_t [\text{diag}(\chi_{n'})][\mathbf{E}_{n'}^t]_t \\ [\mathbf{E}_m^s]_t &= -[\mathbf{Z}_{mn'}]_t [\text{diag}(\chi_{n'})][\mathbf{I} + [\mathbf{Z}_{nn'}][\text{diag}(\chi_{n'})]]^{-1} [\mathbf{E}_n^i]_t \end{aligned} \quad (3.17)$$

In MWT application, scattered fields are not measured at transmitter, at $t = 1$ index m which is assigned as the observation points or receiver is $m = 1, 2 \dots M1$. In multiple projections, microwave signals are transmitted from T number of transmitter sequentially. In each transmission, the electric fields are measured at M observation points where $m = 1, 2 \dots M(t)$. $M(t)$ can be dependent on t . The field points can also be at different positions for different t . The antenna arrangement is illustrated in Table 3-1.

Table 3-1: Observation points of scattered field

t (Transmitter No.)	M
t = 1	1, 2, ... M1
t = 2	1, 2, ... M2
⋮	
t = T	1, 2, ... MT

Total data on 1st projection when $t = 1$ is M1 and the total data for all projections will be

$$data = \sum_{t=1}^T M_t \quad (3.18)$$

3.2.2 Solving direct scattering using the method of moment

Following the volume equivalence principle, $j\omega\epsilon_0(\epsilon_r - 1)E(\vec{r}) = J(\vec{r})$, the dielectric material may be replaced by equivalence polarization currents, then, the integral equation can be written as

$$E^i(\mathbf{r}) = \frac{1}{j\omega(\epsilon - \epsilon_0)}J(\mathbf{r}) - jk_0\eta_0 \iint_{\Omega} \frac{1}{4j}J(\mathbf{r}')H_0^{(2)}(k_0\rho)d\mathbf{r}' \quad (3.19)$$

Assuming that the dielectric object is divided into N cells equal in size as described in Figure 3-1, then, a basis function in discrete system can be stated as:

$$P_n(\mathbf{r}) = \begin{cases} 1 & (\mathbf{r}) \in \text{cell}_n \\ 0 & \text{elsewhere} \end{cases} \quad (3.20)$$

The polarization current density in the center of the cell $J(\mathbf{r})$ are approximated as

$$J(\mathbf{r}) = \sum_{n'=1}^N J_{n'} P_{n'} \quad (3.21)$$

Then, integral (3.19) can be expressed in the pulse basis function as

$$E_n^i = \sum_{n'=1}^N J_{n'} \left(\frac{\eta_0 P_{n'}(\mathbf{r})}{jk_0[\epsilon_r(\mathbf{r})-1]} + \frac{k_0 \eta_0}{4} \iint_{\Omega} H_0^{(2)}(k_0 \boldsymbol{\rho}) d\mathbf{r}' \right) \quad (3.22)$$

It can also be expressed in matrix equation as:

$$[\mathbf{E}_n^i] = [\mathbf{Z}_{nn'}][\mathbf{J}_{n'}] \quad (3.23)$$

Evaluating the field at $n = 1, t = 1$, when $n' = 1, 2, \dots, N$, where N is the number of the cells, matrix equation (3.23) can be expressed as

$$[\mathbf{E}_1^i]_t = [\mathbf{Z}_{1n'}][\mathbf{J}_{n'}]_t \quad (3.24)$$

where

$$[\mathbf{Z}_{1n'}] = [Z_{11} \quad Z_{12} \quad \dots \quad Z_{1N}] \quad (3.25)$$

$$[\mathbf{J}_{n'}]_t = \begin{bmatrix} J_1 \\ J_2 \\ \vdots \\ J_N \end{bmatrix} \quad (3.26)$$

However, at each projection, an incident field illuminates all cells of the object, $n = 1, 2 \dots N$, then at $t = 1$ there will be a set of vector and matrix operators

$$[\mathbf{E}_n^i]_{t=1} = \begin{bmatrix} E_{1,1}^i \\ E_{2,1}^i \\ \vdots \\ E_{N,1}^i \end{bmatrix}; [\mathbf{J}_{n'}]_{t=1} = \begin{bmatrix} J_{1,1} \\ J_{2,1} \\ \vdots \\ J_{N,1} \end{bmatrix};$$

$$[\mathbf{Z}_{nn'}] = \begin{bmatrix} Z_{11} & Z_{12} & \dots & Z_{1N} \\ Z_{21} & Z_{22} & \dots & Z_{2N} \\ \vdots & \vdots & \ddots & \vdots \\ Z_{N1} & Z_{N2} & \dots & Z_{NN} \end{bmatrix} \quad (3.27)$$

The $[\mathbf{Z}_{nn'}]$ entries of (3.27) are given by

$$Z_{nn'} = \begin{cases} n \neq n', & \frac{k_0 \eta_0}{4} \iint H_0^{(2)}(k_0 r_m) dx' dy' \\ n = n', & \frac{\eta_0}{jk_0[\varepsilon_r(x,y)-1]} + \frac{k_0 \eta_0}{4} \iint H_0^{(2)}(k_0 r) dx' dy \end{cases} \quad (3.28)$$

By using (3.6) to estimate the integral of Hankel's function in (3.28), the entries are defined as

$$n \neq n' \rightarrow \rho > a; \quad (3.29)$$

$$Z_{nn'} = \frac{\eta_0 \pi a n}{2} J_1(k_0 a) H_0^2(k_0 \rho)$$

$$n = n' \rightarrow \rho < a; \quad (3.30)$$

$$Z_{nn'} = \frac{\eta_0}{jk_0[\varepsilon_r-1]} + \frac{k_0 \eta_0}{4} \left[\frac{2\pi a}{k_0} H_1^2(k_0 a) - \frac{4j}{k_0^2} \right]$$

$$Z_{nn'} = \frac{\eta_0 \pi a}{2} H_1^2(k_0 a) - \frac{j\eta_0}{k_0} \cdot \frac{j[\varepsilon_r-1]}{j[\varepsilon_r-1]} + \frac{\eta}{jk_0[\varepsilon_r-1]}$$

$$Z_{nn'} = \frac{\eta_0 \pi a}{2} H_1^2(k_0 a) + \frac{\eta_0 \varepsilon_r}{jk_0[\varepsilon_r-1]}$$

Solution (3.23) yields $[\mathbf{J}_{n'}]_t$. At each $[\mathbf{E}_n^i]_t$, the equivalent current density is obtained for $n' = 1, 2 \dots N$. Once $[\mathbf{J}_{n'}]_t$ is defined, the scattered field at observation domain can be determined by expanding the integral equation

$$E^s(\mathbf{r}) = jk_0 \eta_0 \iint_{\Omega} \frac{1}{4j} J(\mathbf{r}') H_0^{(2)}(k_0 \rho) d\mathbf{r}' \quad (3.31)$$

Assuming that for a given $[\mathbf{E}_n^i]_t$, $E^s(\mathbf{r})$ is measured at $M(t)$ points of observation which is placed in a data domain ($E^s(\mathbf{r}), \mathbf{r} \in \mathcal{D}$). $[\mathbf{E}_m^s]_t$ due to the presence of a dielectric object and illumination of $[\mathbf{E}_n^i]_t$ can be determined using

$$\begin{aligned} [\mathbf{J}_{n'}]_t &= [\mathbf{Z}_{nn'}]^{-1} [\mathbf{E}_n^i]_t \\ \Rightarrow [\mathbf{E}_m^s]_t &= [\mathbf{Z}_{mn'}]_t [\mathbf{J}_{n'}]_t \end{aligned} \quad (3.32)$$

Nevertheless, equation (3.23) produces zero division at the background when the dielectric contrast is 1 ($\varepsilon_r = 1$). Thus, a new variable is introduced to replace the contrast term in the equation as follows

$$\xi = \frac{k_0[\varepsilon_r-1]}{j\eta_0 \varepsilon_r} \quad (3.33)$$

The dielectric contrast appears in the diagonal of the $[\mathbf{Z}_{nn'}]$ matrix in the object domain, $(n, n') \in \mathcal{O}$, when the cells of the objects interact with themselves ($n = n'$). The ξ replaces ε_r in (3.30) by multiplying (3.23) with ξ as

$$[\text{diag}(\xi_{n'})][\mathbf{E}_n^i]_t = [\text{diag}(\xi_{n'})][\mathbf{Z}_{nn'}][\mathbf{J}_{n'}]_t \quad (3.34)$$

where $[\text{diag}(\xi_{n'})]$ is a diagonal matrix, which can be used to cancel the dielectric contrast in the diagonal of $[\mathbf{Z}_{nn'}]$. The diagonal term of $[\text{diag}(\xi_{n'})][\mathbf{Z}_{nn'}]$ is rearranged. Let us define the first cell of the term that is $n = n' = 1$

$$\begin{aligned} \xi_1 Z_{11} &= \frac{k_0[\varepsilon_{r,1}-1]}{j\eta_0\varepsilon_{r,1}} \left[\frac{\eta_0\pi a}{2} H_1^2(k_0 a) + \frac{\eta_0\varepsilon_{r,1}}{jk_0[\varepsilon_{r,1}-1]} \right] \\ \Rightarrow \xi_1 Z_{11} &= \frac{k_0[\varepsilon_{r,1}-1]}{j\eta_0\varepsilon_{r,1}} \cdot \frac{\eta_0\pi a}{2} H_1^2(k_0 a) - 1 \\ \Rightarrow \xi_1 Z_{11} &= \xi_1 \mathbb{Z}_{11} - 1 \end{aligned} \quad (3.35)$$

where $[\mathbb{Z}_{nn'}]$ is an integral operator of the domain equation with entries

$$[\mathbb{Z}_{nn'}] = \begin{cases} \frac{\eta_0\pi a_n}{2} J_1(k_0 a) H_0^2(k_0 \rho) & \text{if } \rho > a \text{ or } n \neq n' \\ \frac{\eta_0\pi a}{2} H_1^2(k_0 a) & \text{if } \rho \leq a \text{ or } n = n' \end{cases} \quad (3.36)$$

Furthermore, a new domain equation at t projection is written as

$$[\text{diag}(\xi_{n'})][\mathbf{E}_n^i]_t = [[\text{diag}(\xi_{n'})][\mathbb{Z}_{nn'}] - \mathbf{I}][\mathbf{J}_{n'}]_t \quad (3.37)$$

The relation between ξ and χ is

$$\xi = \frac{k_0}{j\eta_0\varepsilon_r} \chi \quad (3.38)$$

Scattered field $[\mathbf{E}_n^s]_t$ at $m = 1, 2 \dots M(t)$ observation points due to the present of a dielectric object and illumination of the microwave signal can be determined by :

$$\begin{aligned} [\mathbf{J}_{n'}]_t &= [[\text{diag}(\xi_{n'})][\mathbb{Z}_{nn'}]_t - \mathbf{I}]^{-1} [\text{diag}(\xi_{n'})][\mathbf{E}_n^i]_t \\ \Rightarrow [\mathbf{E}_m^s]_t &= [\mathbb{Z}_{nn'}]_t [\mathbf{J}_{n'}]_t \end{aligned} \quad (3.39)$$

3.3 Numerical Experiment

3.3.1 Methods

A comparative study is applied to analyze the accuracy of the MM solutions. The MM solutions are compared to exact solutions. A simple cylindrical geometry object with real dielectric contrast is used as it is the only possible geometry that the exact solutions can handle. The OI is defined as an infinite cylindrical object with a_{OI} -radius and real ε_r dielectric. The exact solutions calculate the scattering fields in the observation points using cylindrical harmonic expansions in which it is derived in appendix B.

The MM approaches the cylindrical in squared meshes as seen in Figure 3-2. In 2D view the OI is placed in a square area which is divided in N_A small squared area with a_{cell} -radius equivalent. The radius of the cell is varied by changing the N_A . The dielectric of the cells which is placed inside OI is set as ε_r , others are set as 1. The number of cells inside OI is labeled as N . The size must be small compared to the wave length. Inside the material, the wave length is defined as $\sqrt{|\varepsilon_r|}\lambda_{OI} = \lambda_0$. Peterson [9] recommends that the minimum number of cells for homogeneous dielectric cylindrical cross-section be $100cells/\lambda_{OI}^2$. This is approximately similar to $\approx 0.05\lambda_{OI}$ -cell radius. A set of antennas are placed in a data domain (\mathcal{D}) which is an exterior to \mathcal{O} . The antennas are used as measurement points. An antenna transmits the incident field and the others receive the scattered fields when a dielectric object of interest is given at the \mathcal{O} . In the direct scattering process which is used as the solution of the forward problem of MWT, the MM calculates the scattered fields at the antennas which are assigned as the measurement points.

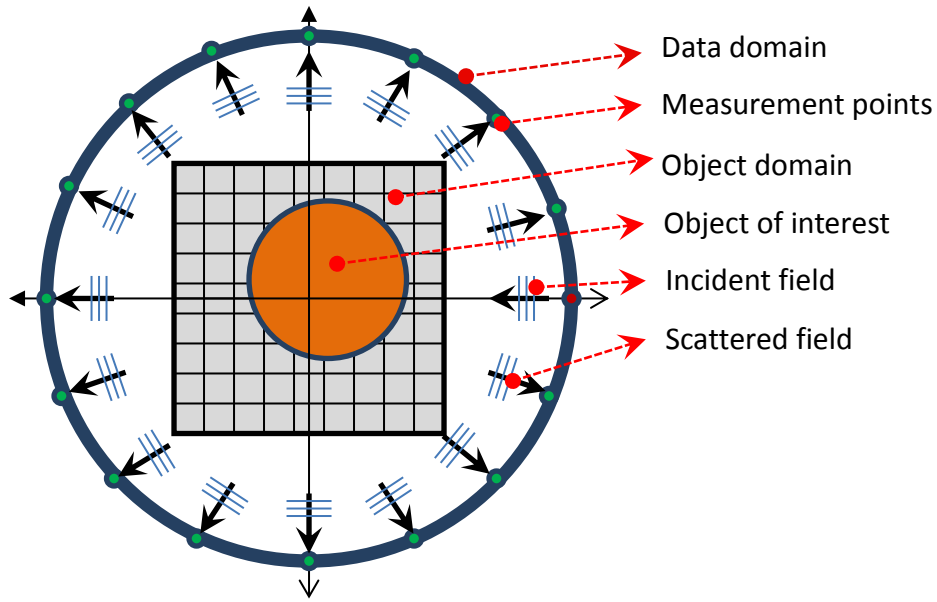


Figure 3-2: Imaging configuration for microwave tomography. The properties of MWT system are object domain (\mathcal{O}), data domain (\mathcal{D}), object of interest (OI) and measurement points

The scattered fields simulated at the measurement points using the MM are evaluated by comparing them against the results of calculation using analytic solution. An absolute mean error is used to measure the quality of MM solutions relative to exact solutions. The quality of the solution is examined in term of cell size and dielectric contrast variations.

3.3.2 Numerical Result

3.3.2.1 The effect of cell size to the accuracy of the results of the method of moment

Microwave signals at 4.5 GHz in the form of plane wave and line source equivalence illuminate an infinitely long dielectric cylinder with dielectric of real 4 and 1 cm or $0.15\lambda_0$ in radius. This OI is placed at the centre of \mathcal{O} in which the domain is divided into N^2 cells. The scattering of the signals at 36 antennas in \mathcal{D} are approximated using the MM with equivalence current density (3.39). Figure 3-3 shows the effect of cell size on the results of MM when the incident field is transmitted from ($\mathcal{D}(\rho = 5, \phi = 0)$).

The plots show that the size of the cell directly affects the accuracy of the solution. The smaller the size, the better the solution is. Nevertheless, decreasing the size means adding the number of cells which will lift up the computational burden. For the case provided in the test, the reasonable result of MM is gained when the radius of cell is equal or less than $0.02\lambda_0$ and good result is obtained from $0.015\lambda_0$ radius of cell. These equal to 64 and 287 cells, respectively. Improving cell size significantly raises the number of cell in which it will increase cost of calculation.

It can be seen from the pattern of the plots at Figure 3-3 that the smallest scattering field is on the same side of transmitting antenna ($\approx 0 \text{ rad}$) and the biggest amplitude lies on the other side of OI . The position of the observation points seems to influence the accuracy of the MM solutions. The MM produces more errors of magnitude on the other side of OI , on the other hand, it gains less errors of phase at $\phi = \pi \text{ rad}$. Figure 3-4 illustrates the change of errors due to variation of the radius of cell at three different observation points. The best result of the MM is produced at $\phi = \pi/2 \text{ rad}$, and the worst result is placed at $\phi = \pi \text{ rad}$. The size of the cells must be relatively small in term of the background medium area. Additionally, one thing that should be put into consideration is the position of the points of observation. Points of observation around $\phi_n = \phi_0 + n.\pi$, where ϕ_0 is the transmitting antenna point, produce bigger errors than other points at \mathcal{D} .

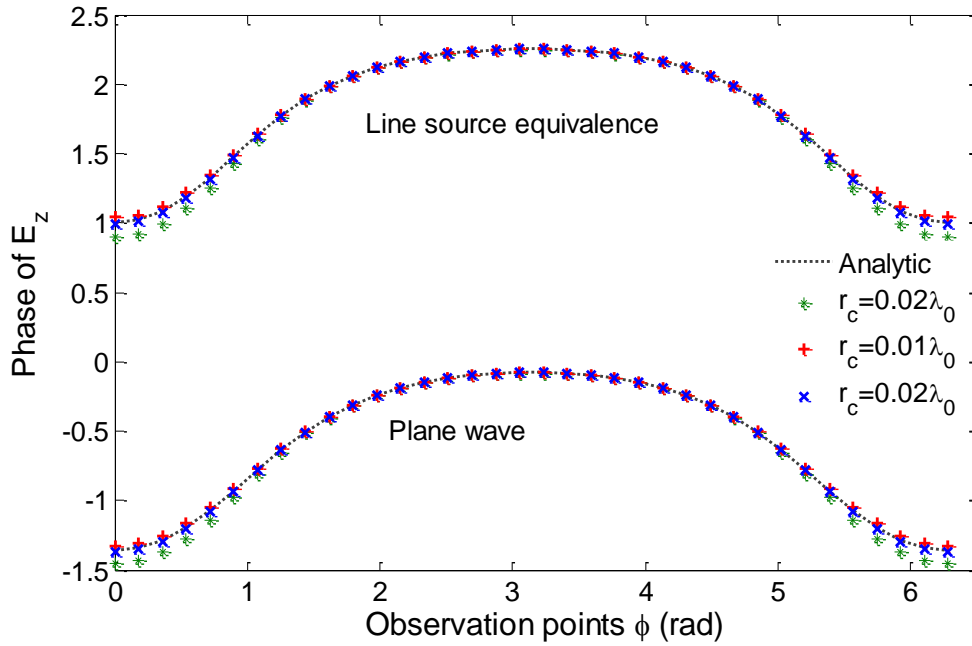
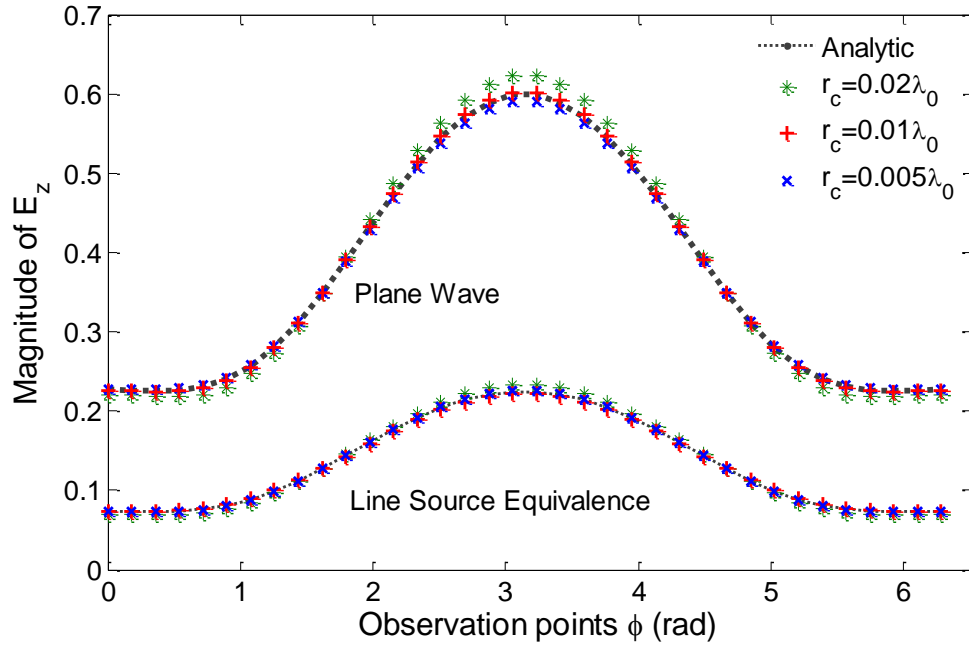
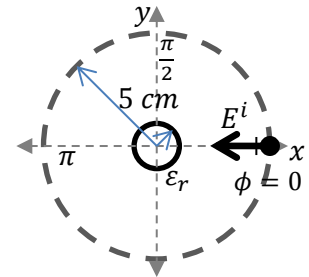


Figure 3-3: The plot of Scattered fields at 36 observation points in object domain ($\mathcal{D}(\rho = 5\text{cm})$). The OI has permittivity $\epsilon_r = 4 + j0$ and radius 1 cm. 4.5 GHz Plane Wave and Line source equivalence illuminate the OI. The scattered field is approximated using the MM. The results are compared with analytic solution.



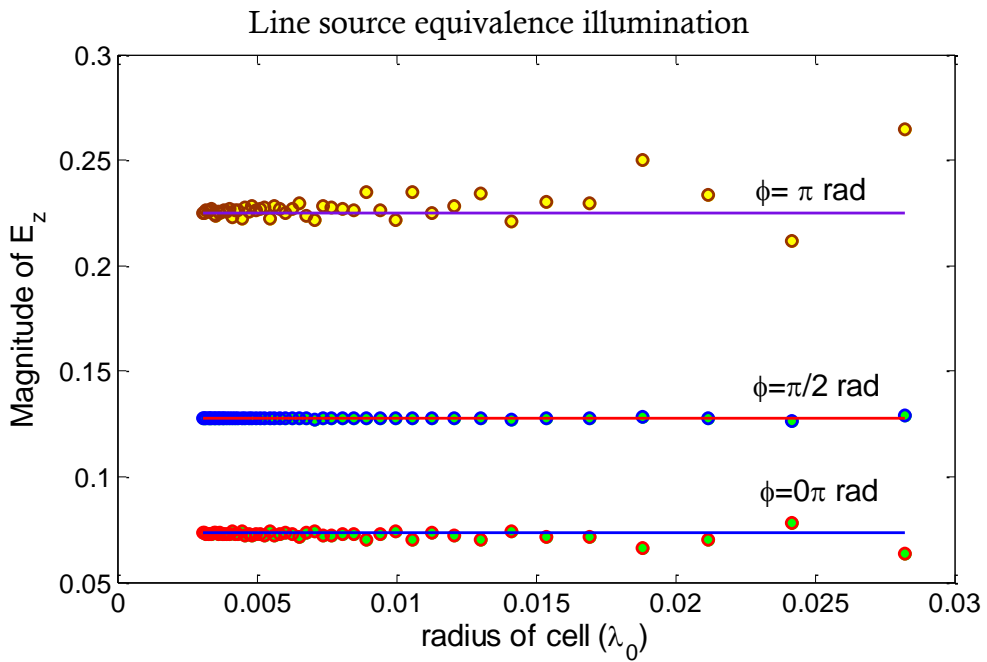
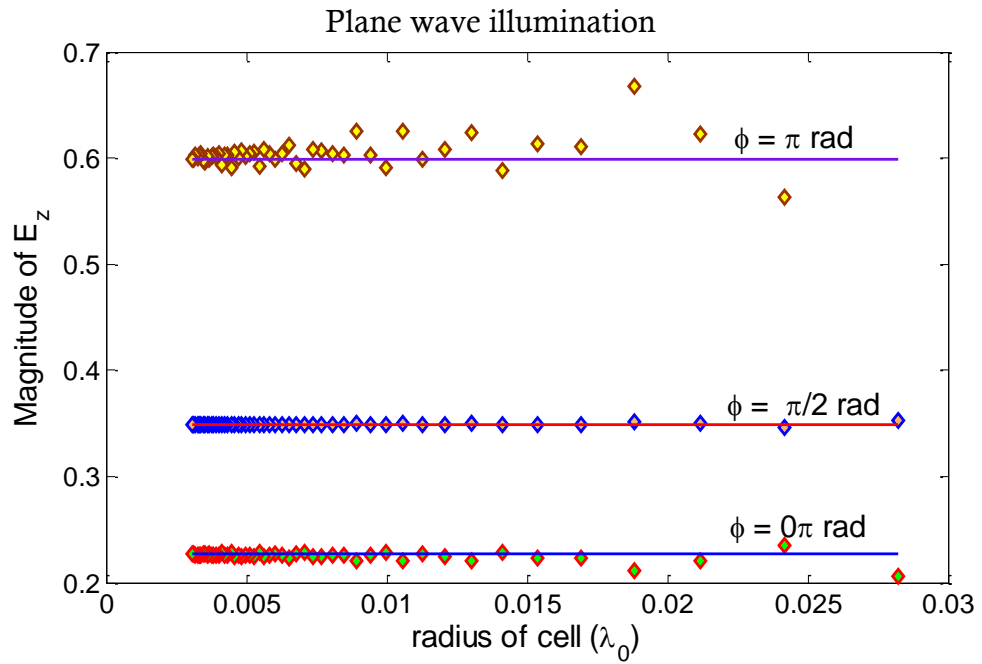
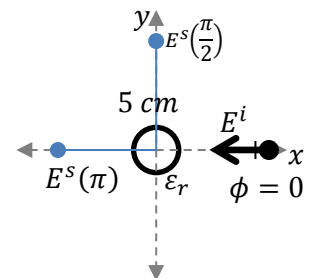


Figure 3-4: The plot of the magnitude of scattered fields at three observation points in object domain ($\mathcal{D}(\rho = 5\text{cm}, \phi = [0, \pi/2, \pi])$) of MM solutions and analytic solution. 4.5 GHz Plane wave (top) and Line source equivalence (bottom) illuminate $\epsilon_r = 4$ a dielectric cylinder with 1 cm in diameter.



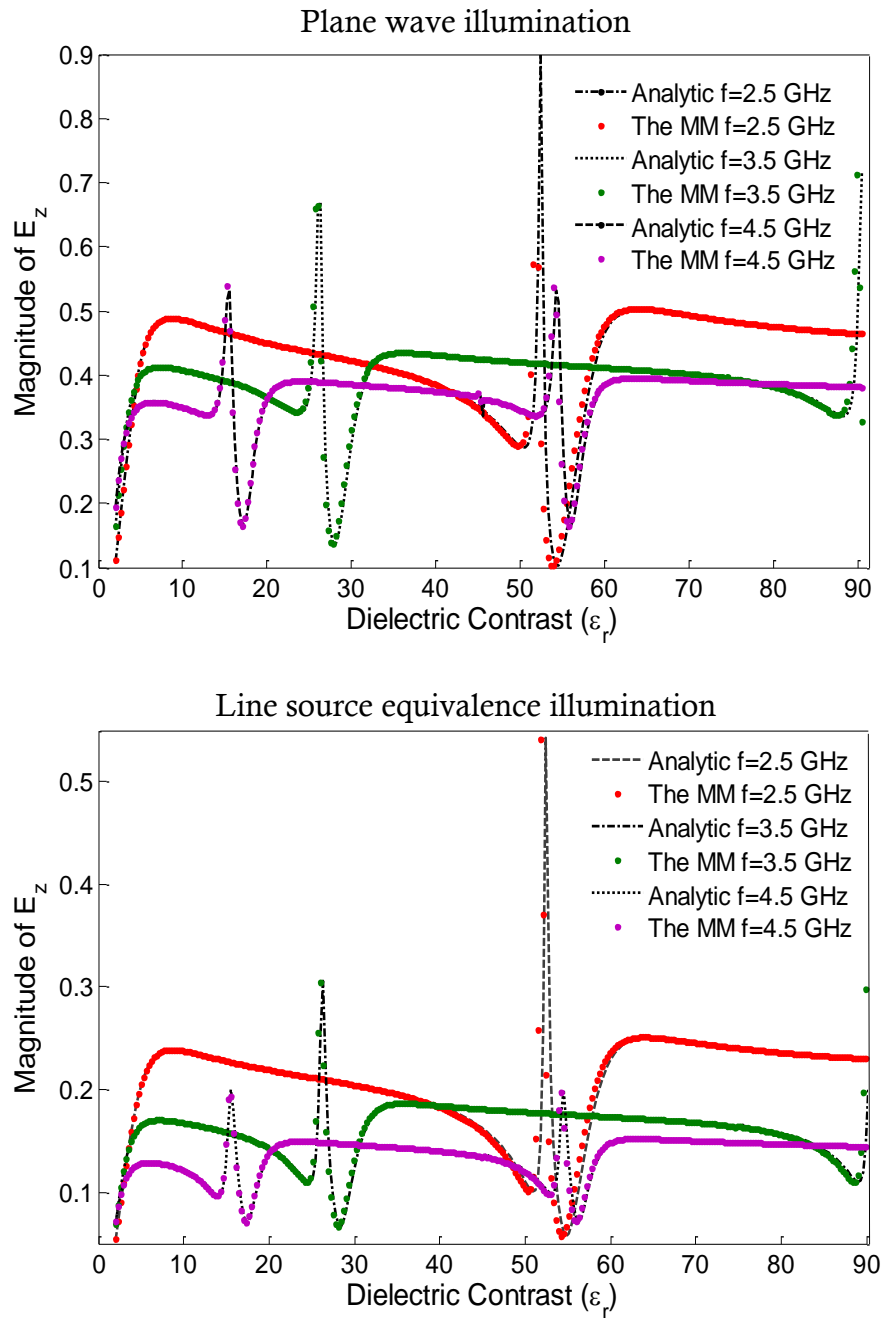
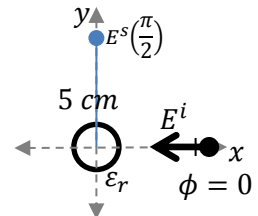


Figure 3-5: The plot of exact solutions and MM solutions of scattering field at a single observation point $\mathcal{D}(\rho = 5\text{cm}, \phi = \pi/2)$. Dielectric contrasts of OI are varied. Three different frequencies of (top) plane wave and (bottom) line source illuminate the OI.



The MM produces less errors for smaller cell size and the size of error is dependent on the position. The source of error might be due to one of the following reasons; firstly, the pulse basis expansion ($\sum_{n'=1}^N J_{n'} P_{n'}$) replaces the equivalence current density ($J(\mathbf{r})$). The definite geometry of OI cross section is divided in cells where the pulse is employed. Thus, finer mesh of OI brings the approximation close to the $J(\mathbf{r})$. Secondly, the enforcement of the integral is done only at the center of the cell, and the integral is solved using series of functions for the circular cell. The error is initiated as a result of point matching and simplification. Third, the numerical error sets off errors to the results of MM due to the round off and truncation of the calculation. These types of errors may appear in the result of MM solutions.

3.3.2.2 *The effect of relative permittivity to the scattered fields*

The evaluation of the accuracy of the MM results is done by illuminating OI which is a cylindrical object with $0.013\lambda_0$ radius and is placed in the center of the object domain. The domain is divided into $N^2 = 900$ cells. Microwave signals at $f = [2.5, 3.5 \text{ and } 4.5 \text{ GHz}]$ illuminate the OI. The scattered field due to each illumination is measured at $\mathcal{D}(\rho = 5, \phi = \pi/2)$. The relative permittivity of the object is varied from $\epsilon_r = 2$ to $\epsilon_r = 90$. The effect of relative permittivity variation to the magnitude of the scattered field is plotted in Figure 3-5.

As mentioned in the previous sections, the radius of cells in the object of interest must be smaller than $0.015\lambda_0$. Moreover, Paterson states that the relative permittivity affects the flexibility the MM solutions [9]. On the contrary, the numerical experiment shows that the absolute value of the scattering field resulted from the MM solutions are close to the exact solutions along the relative permittivity variations. The MM is able to handle high relative permittivity variations. The error gains along the variation are relatively constant.

Thus, the MM can be used to solve forward problems of an inhomogeneous dielectric object at microwave frequency.

3.3.2.3 *Two-dimensional pattern of scattered and total electric fields*

The scattered field at data domain is determined by the quantities which are the relative permittivity of the object, the size of the object and the frequency of microwave signals. The effect of the quantities stated to the patterns is presented in Figure 3-6.

The effect of relative permittivity to the scattered pattern at \mathcal{D} is shown in Figure 3-6. It can be seen that the scattered fields are in line with the direction of the signals. The value of relative permittivity affects on the distribution of the fields. At low contrast, the scattered fields are distributed around the object. A higher contrast object forces the fields further from the source of the signals. The permittivity contrast focuses and reflects the microwave signals. The higher the contrast, the higher the effect on the pattern is.

The pattern of scattered fields due to plane wave and line source equivalence illumination are similar, but the distribution of total fields which are the addition of scattered and incident fields at \mathcal{D} are different as seen in Figure 3-6. The patterns of the incident fields greatly influence the distribution of the total electric fields. The normalized incident of the plane wave that is directed at $-x$, has an equal value along the y axis and has a constant magnitude along the propagation. This results in striped patterns of the total electric fields due to plane wave illumination. The presence of the dielectric object distracts the linear pattern. The fields are bent when they hits the object and they drops on the other side of the object. The magnitude of the fields is dependent on the distance with the source. Thus, the transmitting points should be allocated. The circular pattern of incident field with transmitting antenna as the center of the circle is distracted by the presence of the dielectric material

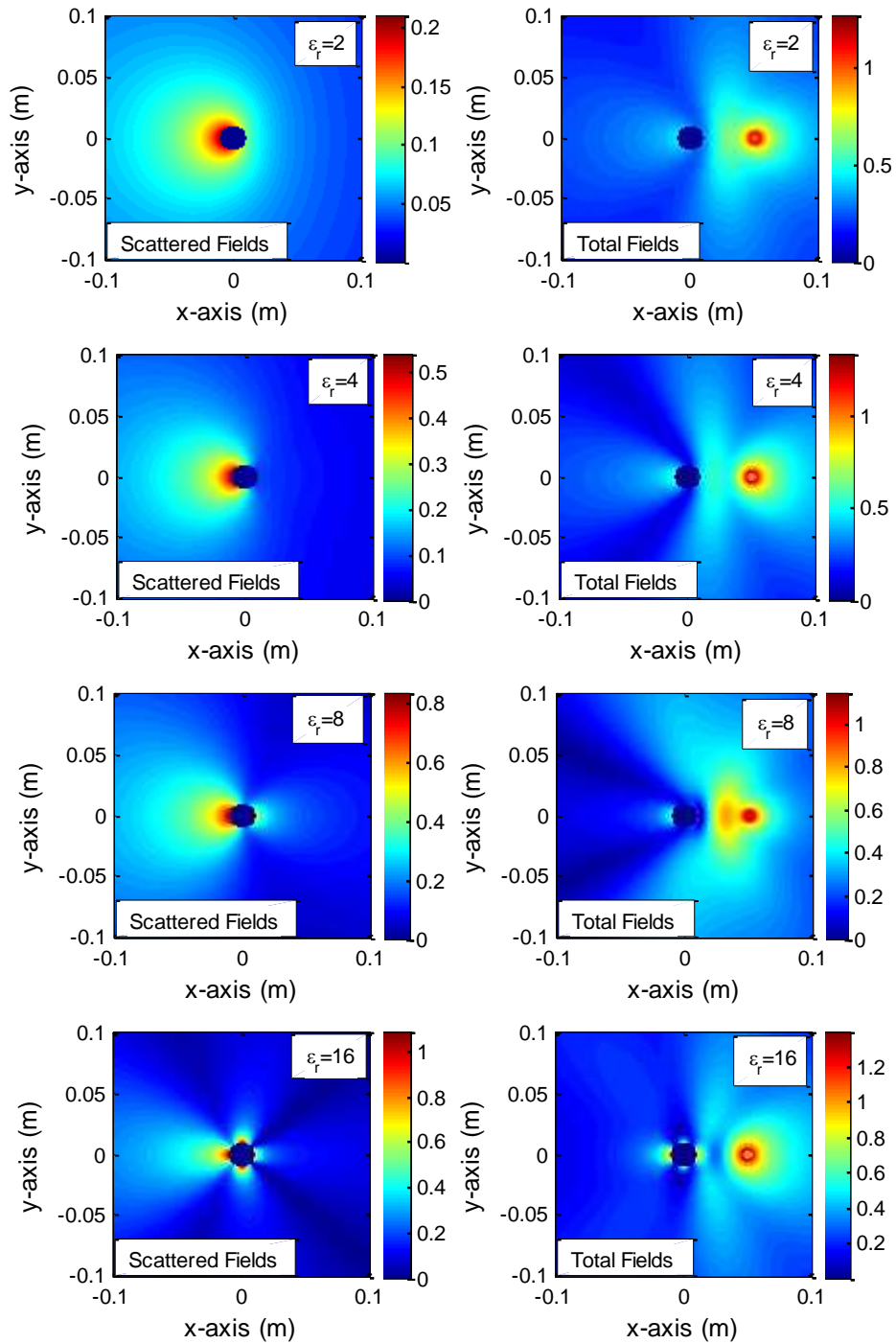


Figure 3-6: The pattern of scattered field and total electric field around a dielectric cylinder with radius 1 cm when 4.5 GHz-TMz microwave signal illuminates the object from +x direction, for three different relative permittivity

In fact the scattered fields cannot be directly measured. The field is determined by measuring the fields before and after the object is introduced. The undisturbed fields are assigned as incident fields and the measured fields after the object is placed in the object domain are the total fields. The addition of scattered fields and incident fields result in total electric fields at observation points. Thus, understanding the pattern of total electric fields is essential, as this variable is the key of the reliability and accuracy of the experimental measurement.

3.4 Conclusion

The direct scattering problem of microwave tomography is defined in term of electric field integral equations (EFIE) for inhomogeneous scatterer. The method of moment (MM) transforms the integral equation into a matrix equation by applying pulse basis function. The solution of matrix equation yields total electric fields $[\mathbf{E}_n]$ or equivalence current density $[\mathbf{J}_{n'}]_t$ coefficients in the centre of N^2 cells of OI. The use of $[\mathbf{J}_{n'}]_t$, replaces $[\mathbf{E}_n]$ in the EFIE based on the volume equivalence principle and vice versa. Once the $[\mathbf{E}_n]$ or $[\mathbf{J}_{n'}]_t$ are obtained, the quantities of scattered fields at \mathcal{D} can be computed for the given relative permittivity.

The direct solution proposed is designed for inhomogeneous dielectric objects, but the study of MM solution is done for homogeneous cylindrical dielectric objects. This geometry can be solved by harmonic expansion which is assigned as an exact solution. The effect of cell size and relative permittivity value are studied to describe the accuracy of the MM solution.

The application of the MM to determine direct scattering of a simple geometry shows that The MM is flexible to the size of the cells. The results of calculations produce good accuracy up to $0.015 \lambda_0$ radius of cells. The MM accuracy endorses flexibility in dividing object of interest into a number of cells. A relatively small number of cells can be used to construct the object.

The value of relative permittivity of OI does not greatly affect the errors of the scattered fields. The errors mainly associated with the approximation, which include errors of modeling. The cylindrical geometry is replaced by a number of cells. The object of interest is divided into N^2 square cells which are equal in size. The relative permittivity $\epsilon_r(\rho)$ is assumed to be constant per cell. The superposition of the cells which are assumed to be circular in shape approximates the original geometry and contrast. The approximation brings modeling errors to the results of calculation. To overcome this limitation, the cells should be sufficiently small. Nevertheless, reducing size will increase the computational burden as the size of the matrix equation rises up.

4

Inverse Problem of Microwave Tomography

4.1 Introduction

The mathematical formulation of Microwave Tomography Inverse Problem (MWT-inverse problem) is presented using Microwave Tomography Objective Function (MWT-objective function). The function is the difference between the value of estimated electric field data and its corresponding measurement data. Therefore, solving the MWT-inverse problem can be done by minimizing the norm of the MWT-objective function, where iterative nonlinear optimizing techniques can be applied. Iteratively, the function is updated by improving the approximation of the estimated data. The MWT-objective function is a set of nonlinear functions, however the iterative update can be determined using linearization techniques, which include Newton Kantorovich method [104; 108], Lavenberg Marquardt method [126], and inexact Newton method [114; 127; 128]. The global solution of MWT inverse problem is defined as if the approximation field equals to the measurement data. This is the same as the norm of the MWT-objective function equals to zero.

The norm of MWT-objective function is an alternative formulation to conventional least squared MWT cost functional to present the MWT-inverse problem. The least squared cost function of MWT-inverse problem is based on the difference between the measured and predicted data for a particular choice of parameters. The problem which is presented in quadratic form of least squared problems is solved by optimization techniques that minimize the cost-functional, for examples Modified Gradient method [64; 67; 129], Gauss Newton inversion[96; 97; 99], and Contrast Source inversion [14; 82; 87].

This chapter covers the presentation of MWT-inverse problem in the form of the norm of MWT objective function. It starts with the description of a two dimensional MWT system, then the reconstruction of data and domain equations of MWT from a direct scattering formulation is explained, and then followed by the formulation of MWT-inverse problem in the form of the MWT objective function and the least squared cost functional as comparison. A numerical experiment is conducted to study the stability of the problems.

4.2 Microwave Tomography System

A two dimensional microwave tomographic system principally is constructed by two basic domains: a bounded object domain $\mathcal{O} \subset \mathbb{R}^2$ and a data domain $\mathcal{D} \subset \mathbb{R}^2$. Both domains are subset of $x - y$ plane (\mathbb{R}^2). The domain \mathcal{O} is denoted as the interior of bound medium. The domain should be large enough to fully contain unknown Object of Interest(OI).

The data domain $\mathcal{D} \subset \mathbb{R}^2$ is the exterior of \mathcal{O} where a set of measurement points is placed. At each incident field radiation, M number of electric field data at \mathcal{D} are measured. Denoting that r and r' are the position vectors and $\rho = |r - r'|$ is the distance between two points at \mathbb{R}^2 , total field at r that is a perturbed field ($E(r)$), is measured when OI is presented. Furthermore, the scattered field due t^{th} incident field illumination at r can be described as the difference between the perturbed and unperturbed fields.

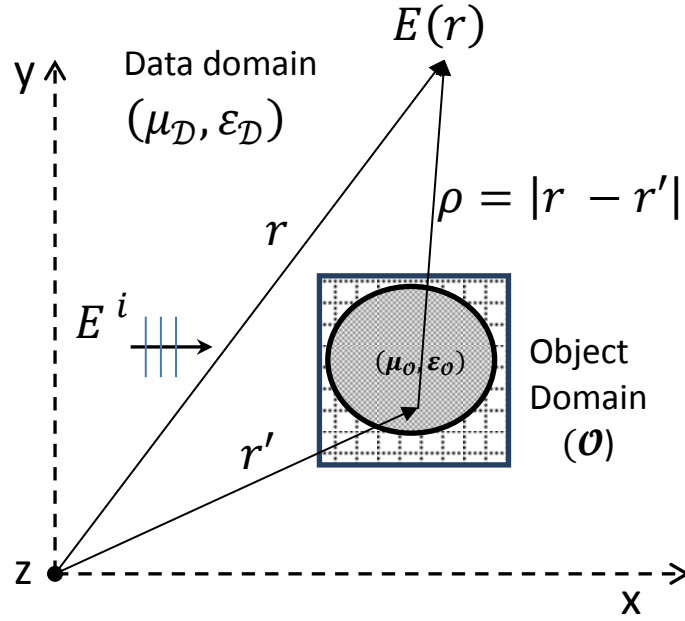


Figure 4-1: Total electric field generated by the microwave plane wave that illuminates a dielectric object

$$E_t^s(\mathbf{r}) = E_t(\mathbf{r}) - E_t^i(\mathbf{r}) \quad (4.1)$$

Microwave tomography works by placing an unknown nonmagnetic OI with permittivity $\epsilon(\mathbf{r})$ inside \mathcal{O} . The object is immersed in a homogeneous nonmagnetic background medium with permittivity ϵ_b which is bound at \mathcal{D} . The OI is illuminated by $t = 1, 2, \dots, T$ number of known incident fields ($[E^i]$). At each radiation of E^i , the scattered fields are measured at M observation points at \mathcal{D} . The scattered fields are generated as a reason of the present of permittivity contrast $\epsilon_r(\mathbf{r})$ at \mathcal{O} . Experimentally, the scattered fields are determined by applying (4.1) to the perturbed and unperturbed fields at observation points. The measured scattered fields are reconstructed to build the image of OI cross section.

Microwave image reconstruction methods determine the distribution of $\epsilon_r(\mathbf{r})$ over OI which represents the image of OI cross section. The methods solve MWT-inverse problem which can be formulated in the set of nonlinear equations or a nonlinear least squares problem. Both formulations are constructed by an object equation and a data equation. The formulation of the equations and the definition of unknown variables in the MWT inverse

problems directly influence the stability of the MWT solutions. Therefore, it is essential to present the formulation of the data and domain equations

4.3 Data and domain equations

The data and domain equations are pairs of nonlinear equations that are used to determine scattered fields from incident fields and dielectric contrast. The equations are presented in integral equations. The mechanism of the scattered process can be described by assuming that the object introduced is a nonmagnetic material. The object only generates equivalent source in term of current density, while the equivalence magnetic density vanishes. Therefore, at each illumination, the electric fields can be stated in object and data integral equations as

$$E^i(\mathbf{r}) = E(\mathbf{r}) - k_0^2 \iint_{\Omega} \frac{1}{4j} \chi(\mathbf{r}') E(\mathbf{r}') H_0^{(2)}(k_0 \rho) d\mathbf{r}' \quad (4.2)$$

$$E^s(\mathbf{r}) = k_0^2 \iint_{\Omega} \frac{1}{4j} \chi(\mathbf{r}') E(\mathbf{r}') H_0^{(2)}(k_0 \rho) d\mathbf{r}' \quad (4.3)$$

where $\chi = (\varepsilon_r - 1)$ is the dielectric contrast, and both coefficients r and r' are position vectors. Equation (4.2) represents the domain equation. The position vectors address a point at \mathcal{O} , $(r, r') \in \mathcal{O}$, while (4.3) expresses the data equation. The vector r defines a data position $r \in \mathcal{D}$ and r' points a cell at \mathcal{O} , $r' \in \mathcal{O}$.

To define the integral equations (4.2) and (4.3) into *the domain* and *data functions*, let us see integral operator $[Z_{nn'}]$ and $[Z_{mn'}]$ which map $L^2(\mathcal{O})$ into $L^2(\mathcal{O})$ and $L^2(\mathcal{O})$ into $L^2(\mathcal{D})$, respectively. The entries are defined by solving (4.2) using the MM which has been described in chapter 2, which are given by

$$Z_{nn'} = \frac{jk_0 \pi a_n}{2} J_1(k_0 a) H_0^2(k_0 \rho); \quad n \neq n' \quad (4.4)$$

$$Z_{nn'} = \frac{jk_0 \pi a}{2} H_1^2(k_0 a) + 1; \quad n = n' \quad (4.5)$$

At $t = 1, 2 \dots T$ incident, the *domain function* and *data function* are written using the integral operators as:

$$[\mathbf{E}_n^i]_t = [\mathbf{I} + [\mathbf{Z}_{nn'}][\text{diag}(\chi_{n'})]][\mathbf{E}_{n'}]_t \quad (4.6)$$

$$[\mathbf{E}_m^s]_t = -[\mathbf{Z}_{mn'}]_t[\text{diag}(\chi_{n'})][\mathbf{E}_{n'}]_t \quad (4.7)$$

Both equations are functions of dielectric contrast $[\chi_{n'}]$ which is assigned as the contrast of the equation and total electric field $[\mathbf{E}_{n'}]$ which is assigned as the source of the equations.

The alternative object and data functions are derived by applying the equivalence volume principle to (4.2) and (4.3). The integral equations are stated as:

$$E^i(\mathbf{r}) = \frac{1}{j\omega(\varepsilon - \varepsilon_0)}J(\mathbf{r}) - jk_0\eta_0 \iint_{\Omega} \frac{1}{4j}J(\mathbf{r}')H_0^{(2)}(k_0\rho)d\mathbf{r}' \quad (4.8)$$

$$E^s(\mathbf{r}) = jk_0\eta_0 \iint_{\Omega} \frac{1}{4j}J(\mathbf{r}')H_0^{(2)}(k_0\rho)d\mathbf{r}' \quad (4.9)$$

In fact (4.8) is not applicable for MWT application as zero division could appear at the background medium and the solution is only valid at OI . Nevertheless, the location of O is determined but the OI is unknown, though the OI is immersed at embedded background medium in O , where $\chi(\mathbf{r}) = 0$. To overcome the limitation, (4.8) is multiplied by the contrast (χ). Furthermore, the *domain equation* and *data equation* with respect to $[\mathbf{J}_{n'}]_t$ can be stated as:

$$[\text{diag}(\chi_{n'})][\mathbf{E}_n^i]_t = \left[[\text{diag}(\chi_{n'})][\mathbf{Z}_{nn'}] - \frac{j\eta_0}{k_0}\mathbf{I} \right] [\mathbf{J}_{n'}]_t \quad (4.10)$$

$$[\mathbf{E}_m^s]_t = -[\mathbf{Z}_{mn'}]_t [\mathbf{J}_{n'}]_t \quad (4.11)$$

This two pairs of equations (4.6)(4.7) and (4.10)(4.11) are used to explain the forward and the inverse scattering problems. Numerically, they are equivalent but they are stated in two different variables; so, whenever both variables in the pair of the functions are updated simultaneously, the stability and the accuracy of the solution could be different.

The forward problem is used to calculate the scattered fields on the observation points. The study of forward problem has been discussed in the previous chapter. Therefore, they are no longer discussed in this chapter. Meanwhile, the inverse problem is used to reconstruct the image of the microwave tomography which is in term of dielectric contrast distribution in domain \mathcal{O} . The inverse problem is constructed using a pair of *domain equation* and *data equation*. The problem is presented in the form of a set of nonlinear system of the objective functional and the least squared of the nonlinear cost-functional.

4.4 Microwave Tomography Inverse Problem

4.4.1 Objective-function of microwave inverse problem

The MWT-objective function in nonlinear system is stated at \mathcal{D} , where the function is the difference of predicted scattered fields and measurement fields. The predicted field is symbolized as a function of dielectric contrast as

$$[\mathbf{E}_m^s]_t([\chi]) = [\mathcal{E}_m^s]_t \quad (4.12)$$

where $[\mathbf{E}_m^s]_t([\chi])$ is the calculated electric field and $[\mathcal{E}_m^s]_t$ is the defined field or measured field. If the approximated $[\chi]$ is close to the exact solution, then, there is a difference between $[\mathbf{E}_m^s]_t([\chi])$ and $[\mathcal{E}_m^s]_t$ which is assigned as the MWT-objective function

Microwave tomography objective function $\mathbf{F}_t([\chi])$

$$\mathbf{F}_t([\chi]) = [\mathbf{E}_m^s]_t([\chi]) - [\mathcal{E}_m^s]_t \quad (4.13)$$

Assuming that at $t = 1$, the scattered fields are measured at $M1$ observation points which are placed in \mathcal{D} outside \mathcal{O} . The entries of the objective function are

$$\mathbf{F}_{t=1}([\chi]) = [\mathbf{E}_m^s]_t([\chi]) - [\boldsymbol{\varepsilon}_m^s]_{t=1} = \begin{bmatrix} E_1^s \\ E_2^s \\ \vdots \\ E_{M1}^s \end{bmatrix}_{t=1} - \begin{bmatrix} \varepsilon_1^s \\ \varepsilon_2^s \\ \vdots \\ \varepsilon_{M1}^s \end{bmatrix}_{t=1} \quad (4.14)$$

Using pairs of the domain (4.6) and data equations (4.7), $[\mathbf{E}_m^s]([\chi])$ can be stated as

$$[\mathbf{E}_m^s]_t([\chi]) = -[\mathbf{Z}_{mn'}]_t[\text{diag}(\chi_{n'})][\mathbf{I} + [\mathbf{Z}_{nn'}]_t[\text{diag}(\chi_{n'})]]^{-1}[\mathbf{E}_n^i]_t \quad (4.15)$$

The MWT-objective function in multiple projection microwave tomography system comprises $t = 1, 2 \dots T$ set of nonlinear functions. It is defined as a column vector

$$\mathbf{F} = \begin{bmatrix} \mathbf{F}_{t=1}([\chi]) \\ \mathbf{F}_{t=2}([\chi]) \\ \vdots \\ \mathbf{F}_{t=T}([\chi]) \end{bmatrix} \quad (4.16)$$

Then, the MWT-inverse problem in term of objective function ($\mathcal{F}([\chi])$) is stated as a normalized norm of MWT-objective function with respect to the measured data

$$\mathcal{F}([\chi]) = \frac{\|\mathbf{F}\|_{\mathcal{D}}^2}{\|\boldsymbol{\varepsilon}^s\|_{\mathcal{D}}^2} \quad (4.17)$$

4.4.2 The Least-Squares data misfit cost-functional of microwave tomography

The microwave inverse problem can be formulated as the optimization problem over the contrast $[\chi]$. The problem minimizes a MWT cost-function which is usually presented in term of least squares data misfit of MWT, that can be written as:

$$\mathcal{C}_t^A([\chi]) = \frac{\|\mathcal{R}_t([\chi])\|_{\mathcal{D}}^2}{\|[\boldsymbol{\varepsilon}_m^s]_t\|_{\mathcal{D}}^2} \quad (4.18)$$

where the norm and the inner product on \mathcal{D} is defined as :

$$\|\mathbf{a}\|_{\mathcal{D}} = \langle \mathbf{a}, \mathbf{a} \rangle_{\mathcal{D}}^{\frac{1}{2}} \quad (4.19)$$

$$\langle \mathbf{a}, \mathbf{a} \rangle_{\mathcal{D}} = \int_{\mathcal{D}} \mathbf{a}^*(r) \mathbf{a}(r) dr$$

$$\|\mathbf{a}\|_{\mathcal{D}}^2 = \langle \mathbf{a}, \mathbf{a} \rangle_{\mathcal{D}} = \begin{bmatrix} a_1^T \\ a_2^T \\ \vdots \\ a_N^T \end{bmatrix} [a_1 \quad a_2 \quad \dots \quad a_N]$$

where a^T is transpose of a

for multiple illumination $t = 1, 2 \dots T$ the cost function is defined as

$$\mathbf{c}^A([\chi]) = \begin{bmatrix} \mathbf{c}_1^A([\chi]) \\ \mathbf{c}_2^A([\chi]) \\ \vdots \\ \mathbf{c}_T^A([\chi]) \end{bmatrix} \quad (4.20)$$

where \mathbf{c}^A is a $T \times 1$ matrix.

The MWT cost function can be also stated in a single equation by summing the cost for all projections.

$$\mathbf{c}_t^B([\chi]) = \frac{\sum_{t=1}^T \|\mathcal{R}_t([\chi])\|_{\mathcal{D}}^2}{\sum_{t=1}^T \|\mathcal{E}_{m,t}^s\|_{\mathcal{D}}^2} \quad (4.21)$$

where \mathbf{c}^B is a scalar, which can be defined for $t = 1, 2 \dots T$ as

$$\mathbf{c}^B([\chi]) = \mathbf{c}_1^B([\chi]) + \mathbf{c}_2^B([\chi]) + \dots + \mathbf{c}_T^B([\chi]) \quad (4.22)$$

The residual error $\mathcal{R}_t([\chi])$ inside the cost-function is defined as the difference between the approximation of scattered fields and the measured data in the observation points at \mathcal{D} .

To illustrate the behavior of both problems: MWT-inverse problem in objective function formulation ($\mathcal{F}([\chi])$) and cost function of MWT-inverse problem $\mathbf{c}^A([\chi])$ and $\mathbf{c}^B([\chi])$, is applied in a contrast inversion problem.

4.5 The solution of objective-function MWT inverse problem of contrast inversion

To describe the solution, the nonlinear MWT inverse problem is presented in an abstract function. Suppose that an objective function f in

convex optimization problem is differentiable so the iteration, $\forall \chi_k \in \mathcal{O}$, follows optimality criterion

$$f(\chi_{k+1}) \geq f(\chi_k) + \nabla f(\chi_k) \cdot \mathcal{s}_k \quad (4.23)$$

The χ_k is optimal if and only if $\chi \in \mathcal{O}$ and

$$\nabla f(\chi_k) \cdot \mathcal{s}_k \geq 0 \quad (4.24)$$

Following the criterion, the function is solved according to iterative Newton scheme

$$\nabla f(\chi_k) \cdot \mathcal{s}_k = -f(\chi_k) \quad (4.25)$$

where the iterative scheme needs derivative of objective function.

Based on the Newton iterative scheme, the derivative of (4.13) is needed to construct the Newton scheme. It can be defined by applying the total deferential to both of the domain and data functions, such that,

$$0 = \Delta[\mathbf{E}_n]_t + [\mathbf{Z}_{nn'}] \Delta([\text{diag}(\chi_{n'})][\mathbf{E}_{n'}]_t) \quad (4.26)$$

$$\Rightarrow \Delta[\mathbf{E}_n]_t = -[\mathbf{Z}_{nn'}] \Delta([\text{diag}(\chi_{n'})][\mathbf{E}_{n'}]_t)$$

$$\Delta[\mathbf{E}_m^s]_t = -[\mathbf{Z}_{mn'}]_t \Delta([\text{diag}(\chi_{n'})][\mathbf{E}_{n'}]_t) \quad (4.27)$$

The variation of the total electric field at (4.26) and (4.27) can be eliminated by introducing the identity of total deferential as

$$\Delta([\chi_{n'}]_{\text{diag}}[\mathbf{E}_{n'}]_t) = [\text{diag}(\chi_{n'})](\Delta[\mathbf{E}_{n'}]_t) + (\Delta[\text{diag}(\chi_{n'})])[\mathbf{E}_{n'}]_t \quad (4.28)$$

Substituting $\Delta[\mathbf{E}_{n'}]_t$ of (4.27) into (4.28)

$$\begin{aligned} & \Delta([\text{diag}(\chi_{n'})][\mathbf{E}_{n'}]_t) = \\ & -[\text{diag}(\chi_{n'})][\mathbf{Z}_{nn'}] \Delta([\text{diag}(\chi_{n'})][\mathbf{E}_{n'}]_t) + \Delta[\text{diag}(\chi_{n'})][\mathbf{E}_{n'}]_t \\ \Rightarrow & [\mathbf{I} + [\text{diag}(\chi_{n'})][\mathbf{Z}_{nn'}]] \Delta([\text{diag}(\chi_{n'})][\mathbf{E}_{n'}]_t) = (\Delta[\text{diag}(\chi_{n'})])[\mathbf{E}_{n'}]_t \quad (4.29) \end{aligned}$$

Defining the equality of diagonal matrix and column vector multiplication as

$$[\text{diag}(\mathbf{a})][\mathbf{b}] = [(\mathbf{ab})] = [(\mathbf{ba})] = [\text{diag}(\mathbf{b})][\mathbf{a}] \quad (4.30)$$

where

$$\begin{bmatrix} a_1 & 0 & 0 \\ 0 & a_2 & 0 \\ 0 & 0 & a_3 \end{bmatrix} \begin{bmatrix} b_1 \\ b_2 \\ b_3 \end{bmatrix} = \begin{bmatrix} a_1 b_1 \\ a_2 b_2 \\ a_3 b_3 \end{bmatrix} = \begin{bmatrix} b_1 a_1 \\ b_2 a_2 \\ b_3 a_3 \end{bmatrix} = \begin{bmatrix} b_1 & 0 & 0 \\ 0 & b_2 & 0 \\ 0 & 0 & b_3 \end{bmatrix} \begin{bmatrix} a_1 \\ a_2 \\ a_3 \end{bmatrix}$$

Using the definition of a small difference, the inner multiplication term in (4.29) is rearranged as

$$[\text{diag}(\chi_{n'})][\mathbf{E}_{n'}]_t = [\text{diag}(\mathbf{E}_{n'})]_t \Delta[\chi_{n'}] \quad (4.31)$$

Substituting (4.31) into (3.29)

$$\Rightarrow \Delta([\text{diag}(\chi_{n'})][\mathbf{E}_{n'}^t]_t) = [\mathbf{I} + [\text{diag}(\chi_{n'})][\mathbf{Z}_{nn'}]]^{-1} [\text{diag}(\mathbf{E}_{n'})]_t \Delta[\chi_{n'}] \quad (4.32)$$

Substituting (4.32) into (3.27)

$$\Delta[\mathbf{E}_m^s]_t = -[\mathbf{Z}_{mn'}]_t [\mathbf{I} + [\text{diag}(\chi_{n'})][\mathbf{Z}_{nn'}]]^{-1} [\text{diag}(\mathbf{E}_{n'})]_t \Delta[\chi_{n'}] \quad (4.33)$$

Assuming that the objective functional is the difference between estimated and measured scattered field, that is

$$\Delta E_t^s = \frac{dF_t(\chi_k)}{d[\chi]} \Delta\chi = F_t(\chi) = E_t(\chi) - \mathcal{E}_t^s \quad (4.34)$$

then, the derivative of $F_t(\chi)$ can be defined as

$$\frac{F_t([\chi])}{d[\chi]} = -[\mathbf{Z}_{mn'}]_t [\mathbf{I} + [\text{diag}(\chi_{n'})][\mathbf{Z}_{nn'}]]^{-1} [\text{diag}(\mathbf{E}_{n'})]_t \quad (4.35)$$

The iterative scheme of the Newton method for all projections can be stated as

$$[\mathbf{D}_k] \cdot [\delta\chi]_k = -\mathbf{F}_k([\chi]_k) \quad (4.36)$$

where

$$[\mathbf{D}_k] = \begin{bmatrix} \frac{F_1([\chi]_k)}{d[\chi]} \\ \frac{F_2([\chi]_k)}{d[\chi]} \\ \vdots \\ \frac{F_T([\chi]_k)}{d[\chi]} \end{bmatrix}; \mathbf{F}_k([\chi]_k) = \begin{bmatrix} [\mathbf{E}_m^s]_1 - [\mathcal{E}_m^s]_1 \\ [\mathbf{E}_m^s]_2 - [\mathcal{E}_m^s]_2 \\ \vdots \\ [\mathbf{E}_m^s]_T - [\mathcal{E}_m^s]_T \end{bmatrix}$$

4.6 The solution of least square cost function of contrast inversion

The cost-function (\mathcal{C}) of contrast inversion is presented in two different least squared problems. The (\mathcal{C}) is a composition of the data and object functions in manner of contrast ($[\chi]$) variable.

$$\mathcal{C}_t^A([\chi]) = \frac{\left\| \left[-[\mathbf{z}_{mn'}]_t [\text{diag}(\chi_{n'})] \left[\mathbf{I} + [\mathbf{z}_{nn'}] [\text{diag}(\chi_{n'})] \right]^{-1} [\mathbf{E}_n^i]_t \right] - [\boldsymbol{\varepsilon}_m^s]_t \right\|_{\mathcal{D}}^2}{\|[\boldsymbol{\varepsilon}_m^s]_t\|_{\mathcal{D}}^2} \quad (4.37)$$

$$\mathcal{C}_t^B([\chi]) = \frac{\sum_{t=1}^T \left\| \left[-[\mathbf{z}_{mn'}]_t [\text{diag}(\chi_{n'})] \left[\mathbf{I} + [\mathbf{z}_{nn'}] [\text{diag}(\chi_{n'})] \right]^{-1} [\mathbf{E}_n^i]_t \right] - [\boldsymbol{\varepsilon}_m^s]_t \right\|_{\mathcal{D}}^2}{\sum_{t=1}^T \|[\boldsymbol{\varepsilon}_m^s]_t\|_{\mathcal{D}}^2} \quad (4.38)$$

The solution of the problems are done by minimizing the cost-function, $\min \mathcal{C}([\chi])$, where $\mathcal{C}: \mathbf{R}^n \rightarrow \mathbf{R}$ is continuously differentiable. Assuming that the cost-function is solvable, then, there exists an optimal point $[\chi]^*$. The optimal value lies at $\mathcal{C}([\chi]) = \mathcal{C}([\chi]^*)$. Since \mathcal{C} is quadratic and differentiable, a necessary and sufficient condition for a point $[\chi]^*$ to be optimal is

$$\nabla \mathcal{C}([\chi]^*) = \nabla \mathcal{C}([\chi]) = 0 \quad (4.39)$$

Minimizing the least-squared problem $\mathcal{C}([\chi])$ is the same as finding the solution of (4.39). Assigning the cost-function as the norm of the residual function, the differential of the cost function $\nabla \mathcal{C}([\chi])$ can be defined as

$$\nabla \mathcal{C}_t([\chi]) = \frac{1}{\|[\boldsymbol{\varepsilon}_m^s]_t\|_{\mathcal{D}}^2} \frac{d\mathcal{R}_t([\chi]^*, [\chi])}{d[\chi]^*} \quad (4.40)$$

The problem must be solved by an iterative algorithm due to the high non-linearity of the functions. The iterative Newton can be used to solve the problems. For all projections, the properties of the schemes can be stated as

Newton properties for ($\mathcal{C}^A([\chi])$)

$$\mathbf{D}_k = \begin{bmatrix} \nabla \mathcal{C}_1([\chi]_k) \\ \nabla \mathcal{C}_2([\chi]_k) \\ \vdots \\ \nabla \mathcal{C}_T([\chi]_k) \end{bmatrix} \quad (4.41)$$

$$\mathbf{F}_k([\boldsymbol{\chi}]_k) = \begin{bmatrix} \mathcal{C}_1^A([\boldsymbol{\chi}]_k) \\ \mathcal{C}_2^A([\boldsymbol{\chi}]_k) \\ \vdots \\ \mathcal{C}_T^A([\boldsymbol{\chi}]_k) \end{bmatrix} \quad (4.42)$$

Newton properties for $(\mathcal{C}^B([\boldsymbol{\chi}]_k))$

$$\mathbf{D}_k = \nabla \mathcal{C}_1([\boldsymbol{\chi}]_k) + \nabla \mathcal{C}_2([\boldsymbol{\chi}]_k) + \cdots + \nabla \mathcal{C}_T([\boldsymbol{\chi}]_k) \quad (4.43)$$

$$\mathbf{F}_k([\boldsymbol{\chi}]_k) = \mathcal{C}^B([\boldsymbol{\chi}]_k) \quad (4.44)$$

The objective and cost functional of CSI is tested in a numerical experiment. The results are discussed in the following section.

4.7 Numerical experiment of contrast inversion

MWT-inverse problem is applied to reconstruct the dielectric value of four cylindrical dielectric objects. The parameter value of OI is $\varepsilon_r = 4$. The diameter of cylinder is 1 cm. The OI is placed randomly inside the object domain. The object domain is immersed in background media with $\varepsilon_{bk} = 1$. Sixteen antennas are placed around the object domain with radius of 7.5 cm. From each antenna, 4.5 GHz microwave signals illuminate data domain sequentially afterwards, the scattered fields at data domain are measured at 8 Rx antennas.

The MWT-inverse problem in three different formulations $\mathcal{F}([\boldsymbol{\chi}]_k)$, $\mathcal{C}^A([\boldsymbol{\chi}]_k)$ and $\mathcal{C}^B([\boldsymbol{\chi}]_k)$ are applied in multiple cylindrical OI. Noiseless numerical data is developed using forward problem. GNI reconstructs the data; for evaluation purposes, the process is terminated after 40 iterations. The characteristics of the iterations are shown in Figure 4-2 and the reconstructed images are presented in Figure 4-3.

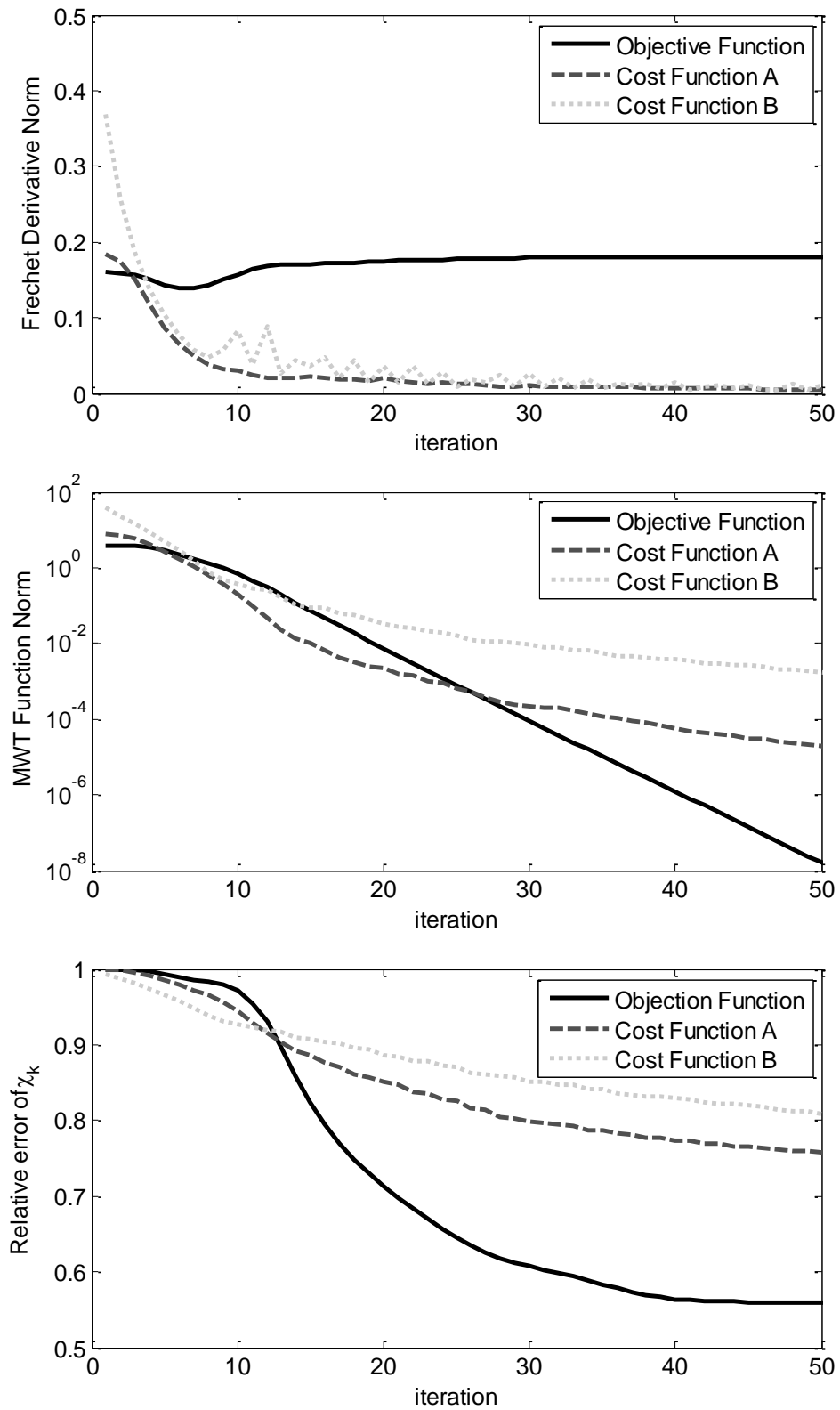


Figure 4-2: The parameter of the solutions of MWT inverse problem in contrast formulation.

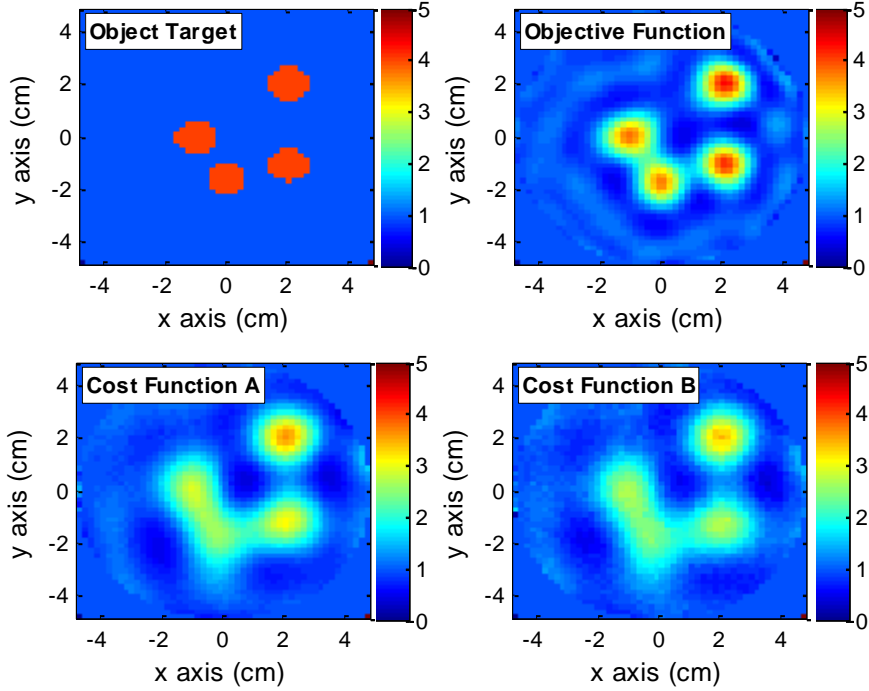


Figure 4-3: Images of four cylindrical cross-section objects. The images are the solution of MWT contrast inversion problem GNI. The MWT inverse problems are presented in three different MWT functions.

It can be seen in Figure 4-3 that the relative errors of the problems for all formulations are decreasing toward zero level. The iteration converges and the output value of MWT-inverse problem functions reaches the tolerance of the functional. If the tolerance of the functional is set similar for all statements which is $F_k([\chi]_k) \leq (\epsilon = \sqrt{e})$; thus, it can be seen that the tolerance is achieved relatively on the same iteration for all problem formulations. Furthermore, the MWT-inverse problem with MWT-objective function formulation works better than the least square function formulation. The relative error of the MWT problem in MWT-objective function is less than 10^{-6} while the other two formulations of relative errors are more than 10^{-5} .

The derivative of least squared cost-functional falls to zero, meaning that the solution of the cost-functional is achieved as, $C^A([\chi]) \leq \epsilon$, where ϵ is a small tolerance number. The direction of iteration reduces along the

iterations. Thus, the error relative of the scattered fields dramatically falls for first few steps; then, it is followed by moderate decrease in errors of scattered graph

The reconstructed images are presented in Figure 4-3. It can be seen that the solution of MWT-inverse problem which is presented using MWT-objective function is better in image quality than that in the solution of MWT-least square cost-function. The location, the number and the shape of the object are clearly distinguished from the background. The quantity of the contrast can be defined. On the other hand, the images reconstructed using inverse problem of cost functional solution is blurred. Furthermore, the quantity of the contrast is affected by the location of the object.

4.8 Conclusions

The MWT-inverse problem is formulated as normalized norm of objective function. This is an alternative MWT-inverse problem formulation of least squared MWT cost functions. The MWT objective function states the MWT inverse problem as the difference of estimated and measured data. This function presents the problem in sets of complex functions. Thus, the high non-linearity of MWT system is clearly exposed. It can be seen that the MWT-inverse problem in objective-function formulation is better than the least squared cost function formulation.

Numerical results show that the MWT-inverse problem can be presented in MWT objective function norm. The parameters of the reconstruction show that the objective function norm and MWT cost function decrease toward zero point. All of the functions reach the tolerance. The stop rule base on the value of MWT-inverse problem output function is satisfied. Meanwhile, the norm of the derivative of MWT-inverse problem with MWT-objective function approaches a constant point, while the norm of derivative of MWT least squared cost function fall down toward zero. The final

destination of the derivative is different, however, they move toward a specific point.

The numerical data is reconstructed using GNI. The solution of the reconstruction is the value of the dielectric contrast on each cell of OI. The plot of dielectric contrast distribution represents the image of OI cross section. The quality of the images of OI from Born approximation problem is relatively similar for all MWT-inverse problem formulations. In contrast, the presentation of the images of contrast inversion shows that the MWT-objective function is better than the least squared cost function for MWT-inverse problem. The detail of the OI is clearly presented using MWT-objective function formulation while the least squared cost function fails to produce sharp images.

5

Linearizing MWT Inverse Problem

An iterative Newton method to solve an MWT inverse problem is presented. The problem which is in the form of a normalized norm of the MWT objective-function is linearized by filtering and transforming the nonlinear MWT inverse problem into a linear system which is assigned as the Newton equation. In this study Levenberg Marquardt (LM) is used to linearize the problem and methods based on pseudo inverse are applied to compute the solution of the linear ill posed problem. The stopping rule for the method is defined and the choice of regularization is studied. The stability of the solution is evaluated in a numerical experiment and tested using noiseless and noisy data.

5.1 Introduction

Let us define the MWT-objective function as a nonlinear abstract function

$$F([\chi]) = \mathbf{b} \quad (5.1)$$

and MWT-inverse problem is an optimization problem, which is defined as minimization of normalized norm of (5.1)

$$\mathcal{F}([\chi]) = \min_{\chi} \frac{1}{\|\mathcal{E}^s\|_{\mathcal{D}}^2} \|F([\chi])\|_{\mathcal{D}}^2 \quad (5.2)$$

where $F([\chi])$ is the MWT-objective function and $([\chi])$ is the dielectric contrast of material in the object domain (\mathcal{O}), which is representing the image of Object of Interest (OI). The measured term \mathbf{b} is the difference between estimated (\mathbf{E}^s) and measured scattered fields ($[\mathcal{E}^s]$) at data domain (\mathcal{D}). Once the unknown variable ($[\chi]$) is determined, the scattered fields in \mathcal{D} can be calculated by solving the forward problem $[\mathbf{E}^s] = f([\chi])|_{\mathcal{D}}$, which is used to define the MWT-objective function.

$$F([\chi]) = \mathbf{b} = [[\mathbf{E}^s] - [\mathcal{E}^s]] \quad (5.3)$$

The MWT-objective function is designed to improve the stability of the solution of MWT inverse problem. The function is an alternative of a cost function of an MWT inverse problem which is commonly presented in a least squared cost function. The norm formulation of MWT is a convex approximation problem. There is an optimal solution for cost function which is gained using various iterative methods, such as Newton iteration [92; 97] and modified gradient [67; 89; 129]. However, the approximate solution could be the local minima of the problem. In addition, the errors of the cost function may not decrease in the errors of the dielectric contrast with respect to the iteration. Therefore, the MWT-objective function is selected in this thesis to construct the MWT-inverse problem. The inverse problem is presented in a set of functions in a complex system in which the inner product of the norm is avoided.

The nonlinear system of the MWT inverse problem is solved using a linearization technique. This technique has been successfully demonstrated in inexact Newton application [114] where the solution is gained using iterative linear regularization method. In this chapter, another Newton class by means of the LM is developed to compute the regularized solution of the MWT inverse problem. The linearizing scheme is done at each iteration using Frechet derivative and pseudo inverse regularization techniques which include truncated singular value decomposition, Landweber Friedman

iteration (LF) [130; 131; 132; 133], and Tikhonov regularization [134], to cure the ill-posed ness and solve the linear problem. The LF iteratively regulates the inversion based on the expansion of the matrix decomposition. The regularization depends on the index of iterations[133]. Tikhonov regularization is a well-known approximation solution which minimizes regularized functional by means of Tikhonov function, where a positive parameter is inserted to (5.1). The method is originally proposed by Tikhonov to solve linear ill-posed problem, and has been developed for solving nonlinear microwave inverse problems [104; 108; 135].

The linearization technique is developed to obtain a stable solution of MWT inverse problem based on the iterative scheme of Gauss Newton Inversion (GNI) as in [93]. The iterative update of GNI is regulated by applying a linear filter which is the version of LM as explained in [136; 137; 138; 139]. The stability and accuracy of the proposed method are studied using numerical experimental.

5.2 Newton Iteration

Iteratively, the MWT inverse problem can be solved using Newton's method. Assuming that the objective function is solvable, where $[\chi]^\dagger$ and $[\chi]_k$ are the solution and the estimated solution, respectively; then, the GNI scheme can be stated based on the Taylor's expansion.

The GNI to solve (5.1) is the approximation solution of the Newton iteration where the Taylor's term is modeled and the remaining term is neglected. The algorithm of the GNI can be summarized as

$$[\chi]_{k+1} = [\chi]_k + d\mathbf{s}_k \quad (5.4)$$

$$\mathbf{s}_k = [\delta\chi]_k = -[\mathbf{J}^*\mathbf{J}]_k^{-1}[\mathbf{J}_k^*\mathbf{F}_k] \quad (5.5)$$

Where

\mathbf{J} is Jacobian matrix of MWT inverse problem

\mathbf{s}_k is the direction of iteration at $[\chi]_k$, and

dis the step size, which is defined to reduce the value of (5.1).

The current iteration of GNI is approximated by solving the objective-function of MWT inverse problem. The Jacobian matrix at current iteration index is approximated by the Fréchet derivative of the operator $F([\mathcal{X}])$ as the \mathbf{J}_k cannot be defined analytically.

Recalling $F([\mathcal{X}])$ of MWT as a multiple projection problem where $t = 1, 2 \dots T$ as

$$F([\mathcal{X}]) = \begin{bmatrix} F_1([\mathcal{X}]) \\ F_2([\mathcal{X}]) \\ \vdots \\ F_T([\mathcal{X}]) \end{bmatrix} \quad (5.6)$$

then the GNI iteration is defined as

$$[\mathbf{D}^* \mathbf{D}]_k \mathbf{s}_k = -[\mathbf{D}_k^* \mathbf{F}_k] \quad (5.7)$$

where \mathbf{D} is multi projection symbol for the Jacobian matrix.

$$[\mathbf{D}]_k = \begin{bmatrix} \frac{F_1([\mathcal{X}]_k)}{d[\mathcal{X}]} \\ \frac{F_2([\mathcal{X}]_k)}{d[\mathcal{X}]} \\ \vdots \\ \frac{F_T([\mathcal{X}]_k)}{d[\mathcal{X}]} \end{bmatrix} \quad (5.8)$$

and the MWT objective function $\mathbf{F}_k([\mathcal{X}]_k)$ is defined as

$$\mathbf{F}_k([\mathcal{X}]_k) = \begin{bmatrix} [\mathbf{E}_m^s]_{1,k} - [\boldsymbol{\epsilon}_m^s]_1 \\ [\mathbf{E}_m^s]_{2,k} - [\boldsymbol{\epsilon}_m^s]_2 \\ \vdots \\ [\mathbf{E}_m^s]_{T,k} - [\boldsymbol{\epsilon}_m^s]_T \end{bmatrix} \quad (5.9)$$

The solution of MWT inverse problem is updated accordingly

$$[\mathcal{X}]_{k+1} = [\mathcal{X}]_k - [\mathbf{D}^* \mathbf{D}]_k^{-1} [\mathbf{D}_k^* \mathbf{F}_k] \quad (5.10)$$

The Newton iteration (5.7) involves the solution of linear ill posed system. There are several techniques to find the regularized solution of the ill posed, which are explained in [140; 141; 142; 143; 144; 145]. In this chapter, a

regularized solution is applied to calculate the search direction of the GNI. However, the problem is highly non-linear, local minima could be hard to be avoided. Thus, an alternative solution based on the linearization of MWT inverse problems is studied. The application of linearization promotes more flexible solutions of the inverse problem.

5.3 Linear filtering technique for non-linear Microwave Inverse Problem

5.3.1 *Linear ill posed problem of microwave tomography inverse problem*

The iterative scheme is developed to solve (5.9) by applying the linear filtering technique to the equation. Parametric approximation as described in [140], is introduced to replace the inverse of the Hessian of the GNI as

$$[\psi([L]_k, \alpha_k)]^{-1} \mathbf{s}_k = -[\mathbf{D}_k^* \mathbf{F}_k] \quad (5.11)$$

where

$$[L]_k = [D^* D]_k$$

The function $\psi([L], \alpha)$ is the inner product of spectral value ($[D^* D]$) and a positive real number(α). Filter (ψ) estimates the inverse of Hessian $[D^* D]^{-1}$. For all regulator parameters α , the limit of regulator towards zero value is equivalent to the inverse of $[L]$. However, the inverse cannot be defined. It is estimated. The functional filter can be stated in an abstract way as:

$$\begin{aligned} \text{for all } L, \lim_{\alpha \rightarrow 0} \psi([L], \alpha) &= \frac{1}{L} \\ \Rightarrow \lim_{\alpha \rightarrow 0} \psi([L], \alpha_k) &= [L]^{-1} \end{aligned} \quad (5.12)$$

The approximation of $[L]^{-1}$ using $\psi([L], \alpha_k)$ should be taken into the consideration to limit the solution inside the intended domain. The iterative scheme of GNI to solve MWT inverse problem can now be stated as

$$[\chi]_{k+1} = [\chi]_k - \psi([L], \alpha_k)[D_k^* F_k] \quad (5.13)$$

Assuming that the parametric functional $\psi([L], \alpha)$ is a good approximation of the inverse of the Hessian, then, the iterative GNI scheme for solving MWT inverse problem in the linear system can be illustrated in Algorithm 5-1. It is applied to calculate the search direction of the Newton step, where the inputs of the algorithm are the measured scattered fields in data domain and known incident fields in the object domain.

Algorithm 5-1 GNI: Gauss Newton Inversion for MWT Inverse Problem

Function GNI $[\mathcal{E}_{mt}^s]_{t=1,2\dots T}, [E^i]_{t=1,2\dots T}$)

Set : $[\chi]_0 = 0; k = 0; SR_k = false$

$$F_0([\chi]_0) = [\mathcal{E}_{mt}^s]_{t=1,2\dots T}$$

Do while $k < max_k \&\¬(SR_k)$

$$[D]_k = \left[\frac{\mathcal{F}_t([\chi]_k)}{d[\chi]} \right]_{t=1,2\dots T}$$

$$s_k = -\psi([L], \alpha_k)[D_k^* F_k]$$

$$d_k = \min_d \|\mathcal{F}([\chi]_k + d_k s_k) - [\mathcal{E}^s]\|^2$$

$$[\chi]_{k+1} = [\chi]_k + d_k \cdot s_k$$

$$k = k + 1$$

$$F_k = E^s([\chi]) - [\mathcal{E}^s]$$

$$SR_k = stoprule([\chi]_k)$$

End do while

Return $([\chi])$

The linearization starts with defining the initial guess of contrast $[\chi]_0$ and MWT objective-function F_0 . The linear system is defined as a normal equation of an MWT-inverse problem. The regulator parameter α_k is used to compute regularized solution of the MWT linear ill posed problem. Various methods can be used as presented in the following section.

5.3.2 Linearizing by means of Levenberg Marquardt method

Introducing a parametric function as

$$\psi([\mathbf{L}], \alpha) = \frac{1}{\alpha + [\mathbf{L}]} \quad (5.14)$$

Functional norm of filtered ψ is stated as

$$\psi([\mathbf{L}], \alpha) = \frac{1}{\left\| \frac{[\mathbf{D}]}{\sqrt{\alpha}} \right\|^2} \quad (5.15)$$

Regulator parameter (α) is a real positive number.

The iterative solution of the MWT inverse problem is derived using a parametric filter. The parametric functional (5.16) acts as the linearizing filter of the nonlinear objective-function. The iterative solution in the regularized linear system can be defined as

$$[\mathbf{X}]_{k+1} = [\mathbf{X}]_k - \left[\frac{1}{\left\| \frac{[\mathbf{D}]_k}{\sqrt{\alpha}} \right\|^2} \right] [\mathbf{D}_k^* \mathbf{F}_k] \quad (5.16)$$

This algorithm is well known as Levenberg and Marquardt method (LM). The LM is convergent and stable if the α_k is selected following

$$\|\mathbf{F}_k - [\mathbf{D}]_k [[\mathbf{X}]_{k+1} - [\mathbf{X}]_k]\| \leq \epsilon \|\mathbf{F}_k\| \quad (5.17)$$

This has been proven by Hanke[144].

Assuming that the direction, $\mathbf{s}_k = [\mathbf{X}]_{k+1} - [\mathbf{X}]_k$, of LM iteration equals to the update value of the solution of the linear ill-posed problem of vector \mathbf{s} . The last term of LM scheme can be written as

$$[\mathbf{L}^\alpha] \mathbf{s} = [\mathbf{D}_k^* \mathbf{F}_k] \quad (5.18)$$

The inverse of the regularized normal equation $[\mathbf{L}^\alpha]^{-1}$ represents linearized operator $\psi([\mathbf{L}], \alpha)$. The variable \mathbf{s} is unknown $N \times 1$ vector which is the direction of iteration. Basically, (5.18) is a regularized normal equation. It is similar to the regularized norm approximation problem.

$$\min_{\mathbf{s}} \left\| [\mathbf{D}] \mathbf{s} - \mathbf{F} \right\|_2^2 + \alpha \|\mathbf{s}\|_2^2 \quad (5.19)$$

This Tikhonov regularization problem can be expressed as

$$\Phi(\mathbf{s}) = \mathbf{s}^* [\mathbf{D}^* \mathbf{D}] \mathbf{s} - 2\mathbf{F}^* [\mathbf{D}] \mathbf{s} + \mathbf{F}^* \mathbf{F} + \alpha \mathbf{s}^* \mathbf{s} \quad (5.20)$$

The vector \mathbf{s} minimizes Φ if and only if the derivative of (5.20) equals to zero, where the optimum point takes place

$$\nabla\Phi(\mathbf{s}) = 2[\mathbf{D}^*\mathbf{D}]\mathbf{s} - 2[[\mathbf{D}]^*\mathbf{F}] + 2\alpha\mathbf{s} \quad (5.21)$$

If \mathbf{s} satisfies the minimization, then, regularized normal equation can be expressed as

$$([\mathbf{D}^*\mathbf{D}] + \alpha I)\mathbf{s} = [[\mathbf{D}]^*\mathbf{F}] \quad (5.22)$$

The regulator is a small positive number $\alpha > 0$, therefore, the regularization does not need the assumption of the rank of matrix $[\mathbf{D}]$.

Assigning matrix $[\mathbf{L}^\alpha]$ represents regularized $([\mathbf{D}^*\mathbf{D}] + \alpha I)$, the solution of (5.22) can be stated as

$$\mathbf{s} = [\mathbf{L}^\alpha]^{-1}[[\mathbf{D}]^*\mathbf{F}] \quad (5.23)$$

However, one step solution usually does not give a good result. Alternatively, an iterative solution is proposed. The iterative method offers a stable solution. Accordingly, it will decrease the sensitivity of the inverse problem, and retain the LM method to produce the expected solution of the MWT inverse problem. At each sequence, the objective-function and its derivative are calculated with respect to the approximated contrast and defined incident field. The system is linearized and transformed into a linear ill posed problem. The linear ill-posed is regulated and solved.

5.4 Numerical experiment

A numerical experiment is aimed to investigate the LM algorithm to solve nonlinear ill posedness of the MWT inverse problem in the sense of linear ill posed problem solution.

5.4.1 Simulated data

The measured field is generated by setting the target OI and calculating the scattered fields at the data domain due to the incident field which illuminates the object domain. Empirically, measured data always contain noise. It is necessary to find the way to work with noise. The noise is generated using a random number in which the signal to noise ratio is defined as

$$SNR_{dB} = 10 \log_{10} \frac{\|\varepsilon_t^s\|^2}{\|N_t^s\|^2} \quad (5.24)$$

The data which belong to the complex number, are measured in data domain. The noise, therefore, is introduced in a complex system, in which the ratio of real and imaginary parts of the complex number are calculated separately to prevent rational over each term of the data component. The magnitude of the signal with and without noise is presented in Figure 5-1.

5.4.1 Object domain and object of interest

The object domain is defined as a square area. It is divided into 50×50 cells equal in size. The number of cell determines the accuracy and computational time. The finer the grid, which means smaller cells, the more accurate the simulation is. However, higher cell number produces large size of unknown vectors. This makes the solution more unstable. The cost of computing the decomposition significantly increases and the higher frequency of singular values, in which the values are very small, rises in number. The cell size can be determined according to the maximum size of the cell that supports the accuracy of the direct scattering problem.

The number of cells corresponds to the size of the cells. It is recommended that the minimum number of the cells be 100 cells per square wave length inside object of interest.

$$N_{min} = \frac{100 \text{ cells}}{\lambda_{\varepsilon_r}^2} \quad (5.25)$$

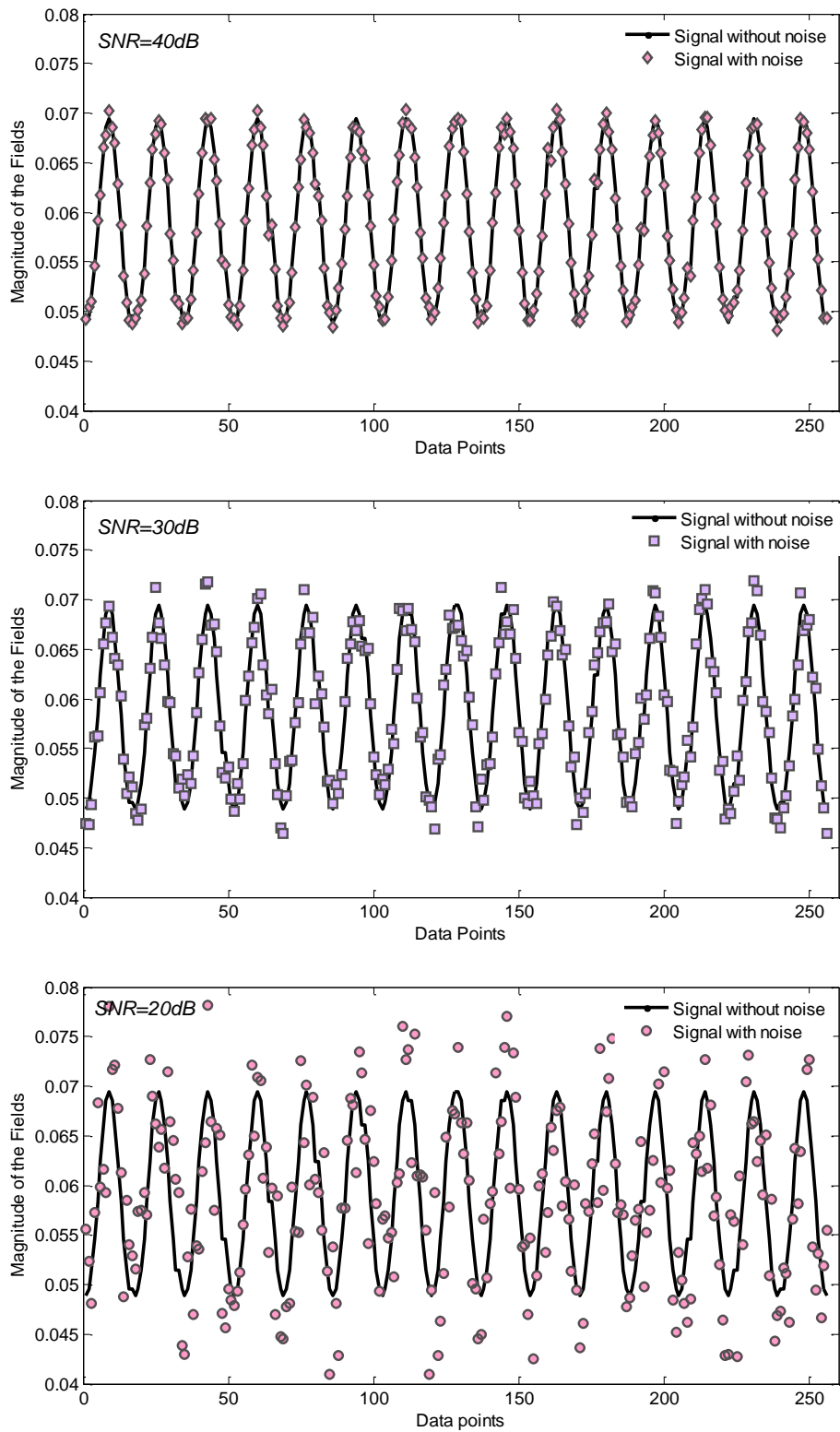


Figure 5-1: The simulation of measured scattered fields at data domain without and with noise of various SNR_{dB}

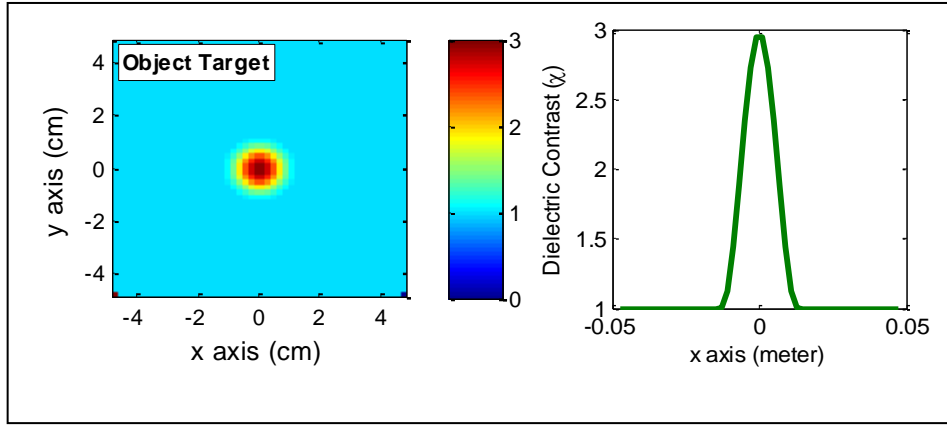


Figure 5-2: The $x - y$ plane distribution and $y = 0$ cross section of object of interest which is immersed in the object domain.

Table 5-1: parameter of the simulated system for the simple test

Parameter	Value
Diameter of Object Domain (\mathcal{O})	9.5 cm
Diameter of Data Domain (\mathcal{D})	13.0 cm
Transmitting Antenna T_x	16 T_x
Receiving Antenna R_x	8 R_x each illumination
Number of cells	$50 \times 50 = 2500$
Object of interest	$1 + (\epsilon_r - 1)\cos^2(\rho)$
Radius of OI	$\frac{\pi\sqrt{x^2 + y^2}}{2r_a}$
Frequency	4.5 GHz

The wave length inside the dielectric object is determined using $\lambda_{\epsilon_r} = \lambda_0/\sqrt{\epsilon_r}$. The object of interest is constructed by the distribution of the dielectric material in which the maximum dielectric contrast is 3 at 4.5 GHz working frequency. Thus, the wave length of the microwave signal at the dielectric material is 3.85 cm and the recommended minimum cell mesh for each 15 cm² is 100 cells. The accuracy of the solution of the direct scattering problem depends on the position of the receiving antenna with respect to the transmitting antenna. The previous chapter shows that the minimum cell number should be larger than the recommended size at the points close to the

transmission antenna. The size of the object domain is 90.25 cm^2 . It is divided into 2500 *cells*, which is more than 4 times of the minimum recommendation.

The measurement set is placed in the background medium which has the dielectric permittivity contrast of 1 as well as the background medium of the object domain. A small object of interest is placed at the center of the domain. It is constructed using $1 + (\epsilon_r - 1)\cos^2(\rho)$ function, where ρ is the radius of the object which is limited at $(\frac{\pi}{2}, 0)$. The cross section of the object at $y = 0$ is presented in the right side of the figure. It can be seen that the peak of the object of interest is 3 which is the maximum contrast of the object. The parameter of Object domain and the *OI* is summarized in Table 5-1.

5.4.2 Error definition

The solution of the MWT inverse problem is done by minimizing the objective function. The function produces a complex vector. To evaluate the descent direction of the MWT objective function, error is defined using normalized an MWT objective function norm (5.2).

$$F_{err}([\mathcal{X}]) = \sqrt{\frac{\|F([\mathcal{X}])\|_D^2}{\|[\mathcal{E}^s]\|^2}} \quad (5.26)$$

The initial guess of the contrast is set equal to the background medium. The functional error will be 100% relative to the measured scattered fields.

The dielectric contrast of the *OI*s is presented in a complex number. However, the object target is defined as a real number where the imaginary part of the contrast is defined as zero. The real part of the dielectric of the *OI* is bigger than the background. If the result of reconstruction is less than 1, then, it is assigned as the background; and the real and imaginary parts of the contrast are set as 1 and 0, respectively. The error of the reconstructed image is defined as the relative error of the contrast.

$$\chi_{err} = \sqrt{\frac{\|[\chi]_{est} - [\chi]_{target}\|^2}{\|[\chi]_{target}\|^2}} \quad (5.27)$$

The norm used as the contrast is a complex number. The imaginary part of the reconstructed image contributes relative errors to the solution.

The iterative solution is updated using the direction and the size of the steps. The direction is calculated using the LM method. To analyze the change in the direction, norm of the direction is defined as

$$norm(\mathbf{s}_k) = \|\mathbf{s}_k\|^2 \quad (5.28)$$

The direction \mathbf{s}_k is a vector with size equals to the cells of the object domain. It is a complex number and updates the value of the contrast of the object domain

5.4.3 Numerical results

The study of LM with linear ill posed regularization is done using OI defined at Figure 5-2. The study is done at noise less data. It is shown that the LM method can be used to reconstruct the OI. Using dynamic Tikhonov regularization, the object can be drawn well. The detailed information can be rebuilt when the approximated solution closes to the exact solution. It is done by decreasing the regulator parameter. Nevertheless, it could not be applied for data with noise. At the point close to the solution, the noise could be larger than the information.

The solution of the linear ill posed problems potentially amplifies the noise as the regulator decreases. The constant of the dynamic regulator 4.52 is set at $r = 0.75$. The iteration starts with zero initial. The scattered field measured equals to the incident field at data domain. The regulator is initially set at $\alpha = 0.1$.

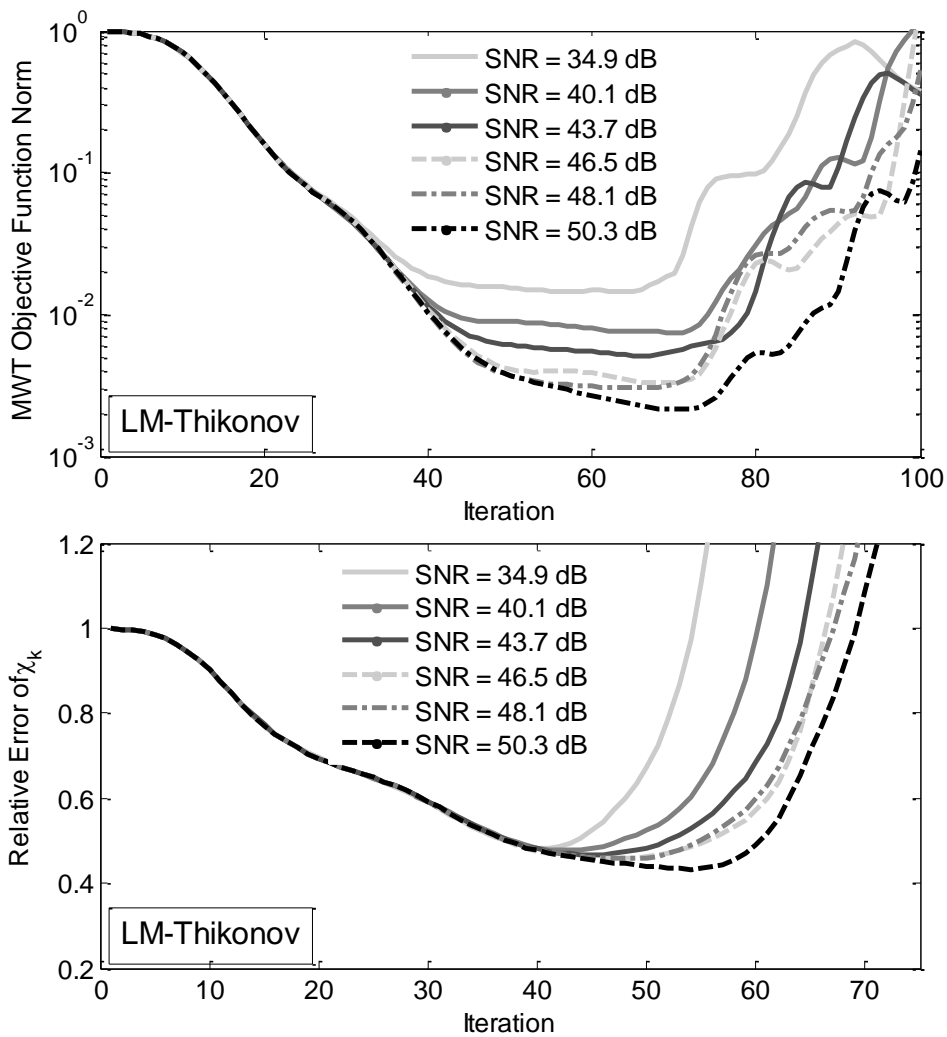


Figure 5-3: The parameter of the solutions of noisy MWT inverse problem of Linearization technique test. The regularization technique is Tikhonov regularization. The regularization is descended

The solution gained can be used to decrease the distance between the initial guess and the exact solution. It can be seen in Figure 5-3 that the relative errors of the contrast slightly decrease at first five iterations. The big value of the regulator flattens the solutions. It can be seen that the revolution of the solution for data with noise is generally similar when the LM method solves the main information. The lines in Figure 5-3 decrease in line with the iteration index up to 40 iterations. Then, the noise starts playing the role.

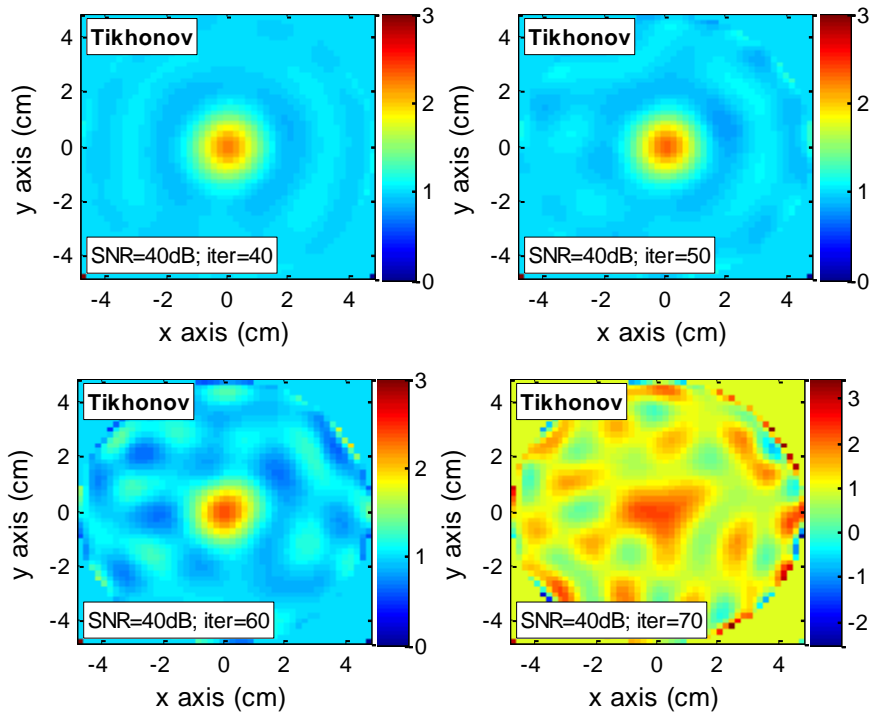
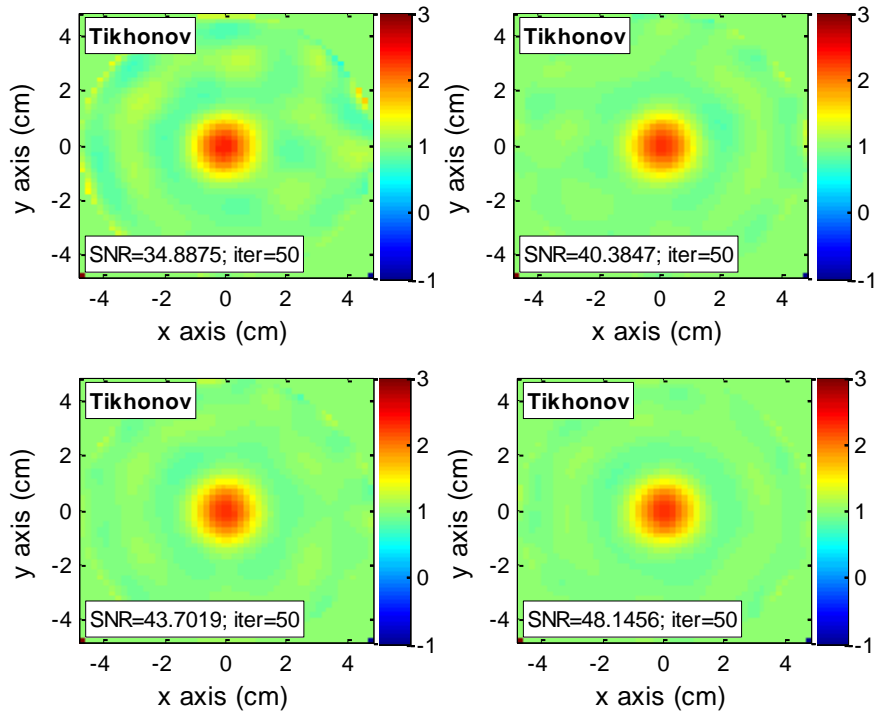


Figure 5-4: The reconstruction of noisy data with SNR 40dB at four different iterations. The images resulted by LM method with Tikhonov regularization. The regularization parameters are descended.

The noise level significantly affects the results of the regulated linear ill posed solutions. The value of the regulator is less than $\alpha = 3e - 5$, while the noise level is comparable to the objective function. It can be seen that the smaller SNR makes the solution easier to be unstable. The lines of relative error of the contrast and functional move to other domains. The iteration is divergence. Therefore, the iteration should be stopped at a proper iteration index based on the noise level introduced.

The reconstructed images at various iterations are presented in Figure 5-4 and Figure 5-5 for SNR = 40 dB and 50 dB. It can be seen that the iteration should be stopped at 60 and 70 iterations for SNR=40dB and SNR=50dB successively. Stopping rule should be set at the desired iterations index.

Iteration = 50



Iteration = 60

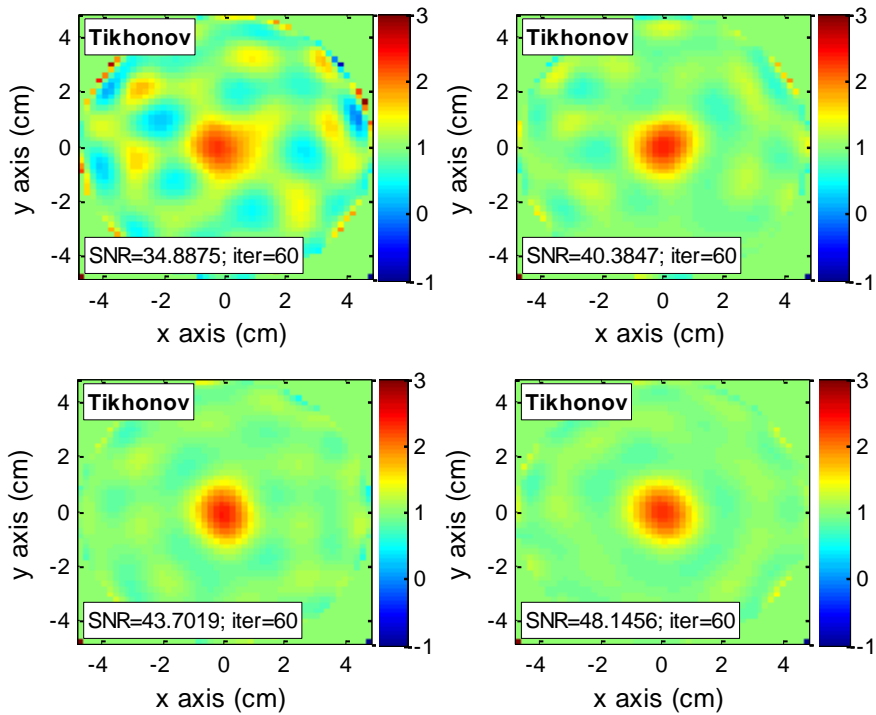


Figure 5-5: The reconstruction of noisy data with various SNR. The images resulted by LM method with Tikhonov regularization. The regularization parameters are descended.

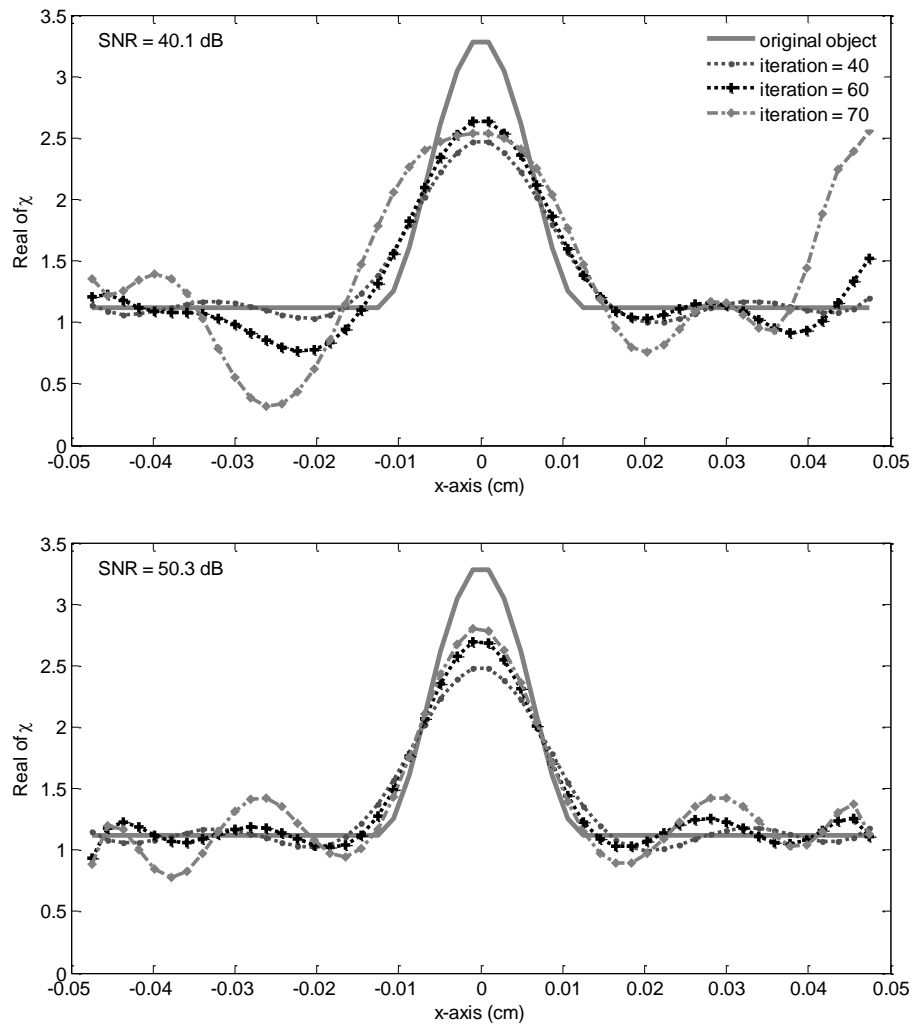


Figure 5-6: the cross section of the contrast (χ) distribution at $y = 0$ of the images resulted by LM when the noise is introduced with SNR 40.1 dB (above) and 50.3 dB (below)

In practice, the object of interest is an unknown variable. Thus, detecting by analyzing the images frame per frame could be hard to do and computationally expensive. The stopping criteria could be defined using the provided parameters. One of the parameters provided is the line of the norm of objective function. It offers essential information of the behavior of the solution, in which the line of SNR=40dB starts to increase at 70 iterations while at 50 dB it remains flat.

In this case the solution misses the appropriate stopping index. The solution starts to fluctuate as the noise is greatly amplified. As it is seen in

Figure 5-6, the cross section of the contrast distribution at 70 iterations of the LM scheme for data with SNR = 40 dB pictures the wrong object. Even by defining prior information that the real part of the dielectric cannot be less than 1, the distribution of the contrast still reflects the effect of the noise. While at SNR = 50 dB, the peak of the object can be clearly seen and discriminated from the background. Filter could be applied if the prior knowledge of the OI is known

5.5 Conclusion

The MWT inverse problem is solved using the LM method. The inverse problem is presented in a nonlinear objective function. The nonlinear system is linearized and formed into a regularized linear ill posed problem. Two different methods to solve the linear ill posed problems are studied. Both methods are used based on pseudo inverse. The linear system is decomposed into singular values and pairs of orthonormal vectors.

The regularization makes the solutions stable. The object can be reconstructed and decided from the background. The position of the object is the same as the original OI . However, both regulator techniques fail to produce detail information of the object. The object is described larger than it should be. The intensity of the contrast is reformed below the exact solution. The behavior of the low pass filter of both regulator methods affects the loss of detailed information. The small singular values are out of calculation. It makes some of the information uncaptured. Therefore, detailed image cannot be described using these techniques..

The regulator parameter of Tikhonov regularization is set to be dynamic. At an initial scheme of the LM algorithm, the regulator is defined relatively large compared to the smallest singular values. Thus, the solution of the LM is guaranteed to be stable and moving toward the exact solution. Then, the regulator is gradually decreased following the power series rule. This is applied to accommodate the detail information which is kept at lower

singular values. It has been shown that the dynamic regulator is able to rebuild the distribution of the dielectric contrast. The norm of the objective function is decreased along with the iteration and the global stopping criterion is achieved.

The noise is introduced to the measured data. The LM method with dynamic Tikhonov regularization is used to reconstruct the distribution of dielectric contrast. It is seen that the global information can be reconstructed at various levels of noise. These are done at a lower index of iterations, where the regulator parameter is relatively big. The noise starts to distract the solution when the approximated solutions are close to the exact solution. At this point, the regulator is small as the objective functional is decreased. Therefore, the levels of noise rise and contribute to the solution. The iteration should be stopped before the noise covers the whole solution and turns the solution to the wrong directions. The stopping rule should be defined to gain an optimum solution. The rule can use the parameter of the iteration like the revolution of objective function and the norm of the Fréchet differential. This rule will be further discussed in the next chapter.

6

Iterative Methods for Solving Microwave Inverse Problem

Newton iterative by means of Inexact Newton Backtracking Method (INBM) has been developed to obtain stable solutions of Microwave Tomography inverse problems. The inverse problem is presented in term of a nonlinear objective function and solved iteratively by minimizing the relative norm of the function. The method proposed is applied to reconstruct numerical noisy data of lossless, lossy and human arm models. The quality of the proposed method is evaluated by comparing the results of INBM with the results of the Lavenberg Marquardt method (LM).

6.1 Introduction

The Multiple illumination of Microwave tomography system (MWT) which is described in (4.3) using a pair of integral equations that describe the data and object equations is stated in an abstract non-linear ill posed problem. For the purpose of INBM application, the MWT inverse problem is written as

$$F(\mathbf{x}) = \mathbf{b} \quad (6-1)$$

where (6.1) has an exact solution at \mathbf{x}^\dagger and the exact data but indefinite measured data is defined as $[\mathcal{E}^s]$ which makes $\mathbf{b} = F(\mathbf{x}^\dagger) = [\mathbf{E}^s(\mathbf{x}^\dagger)] - [\mathcal{E}^s] = 0$.

In the real world, the measured data cannot be separated from noise levels, thus \mathbf{b}_k is undefined due to the unknown exact data and residual errors. The Measured data $[\mathcal{E}^s]$, therefore, is assigned as \mathbf{y}^δ which is the scattered field at data domain with noise ($\mathbf{y}^\delta = [\mathcal{E}^s] + \mathbf{h}(\delta)$) as the exact scattered field ($\mathbf{y} = [\mathcal{E}^s]$) cannot be determined. Assuming that the noise level δ is known, the noisy data \mathbf{y}^δ satisfies

$$\|\mathbf{y} - \mathbf{y}^\delta\| \leq \delta \quad (6-2)$$

Immersing the noise and residual error to \mathbf{b}_k , the perturbed \mathbf{b}_k^ε is defined using the difference of measured data and estimated data

$$\mathbf{b}_k^\varepsilon := \mathbf{y}^\delta - \mathbf{E}^s(\mathbf{x}_k) \quad (6-3)$$

where $\|\mathbf{b}_k - \mathbf{b}_k^\varepsilon\| \leq \delta + \|\mathbf{E}^s(\mathbf{x}^\dagger, \mathbf{x}_k)\|$

The proposed algorithm is based on the Newton method applied to MWT inverse problems. The iterative step of the algorithm involves solving a Newton equation which is linearization of the nonlinear problem (6.1), where the equation is presented as

$$F'(\mathbf{x}_k)\mathbf{s}_k = \mathbf{b}_k^\varepsilon \quad (6-4)$$

Defining \mathbf{D}_k is the derivative of multi projection $F(\mathbf{x})$ at \mathbf{x}_k , then, the Newton equation for multi projection of the MWT inverse problems can be written as

$$\mathbf{D}_k\mathbf{s}_k = \mathbf{b}_k^\varepsilon \quad (6-5)$$

The basic principle in solving the nonlinear MWT inverse problems using iterative Newton class includes inexact Newton that is the correction step of the solution is determined by Newton equation (6.5). The equation is linear, even though the step \mathbf{s}_k is still nonlinear with respect to the objective

function. Beside the equation is commonly underdetermined. For this reason, the INBM is developed to provide a stable solution of MWT inverse problems.

The INBM, an inexact Newton class, is a generalization of Newton method for solving a nonlinear problem like (6.1), in which at the k th iteration, the step \mathbf{s}_k from current approximation solution \mathbf{x}_k is required to satisfy a condition. The step is no longer a direct regularized solution of the Newton equation, but an approximation of the solution which is defined in unspecific manner.

To clarify the proposed algorithm, the iterative scheme of Newton method for solving MWT inverse problem is described.

6.2 Iterative scheme of MWT inverse problem

6.2.1 Regularized solution of linear problem of MWT inverse problem

Iterative step of Newton scheme for solving (6.1) involves the computation of the Newton equation (6.5) that is the linearization of the MWT inverse problem. In the application of parametric function as discussed in chapter 5 reveals that the general solution (\mathbf{s}_k) in LM satisfies

$$\mathbf{s}_k = \psi([\mathbf{L}]_k, \alpha_k)[[\mathbf{D}]_k^*[\mathbf{b}^\varepsilon]_k] \quad (6-6)$$

where $[\mathbf{L}]_k = [\mathbf{D}^* \mathbf{D}]_k$, \mathbf{D}_k is $F'(\mathbf{x}_k)$ of multi projection MWT problem and $[\mathbf{D}]_k^*$ is adjoint of \mathbf{D}_k

Several techniques have been developed to provide regularized \mathbf{s}_k with regularization parameter α . Three regularization techniques are described as follows:

6.2.1.1 Truncated Singular Value Decomposition

It is assumed that the operator $[\mathbf{L}]$ is an invertible complex matrix. It is a squared matrix which has a singular value decomposition

$$[\mathbf{L}] = \mathbf{U} \Sigma \mathbf{V}^T \quad (6-7)$$

The singular value decomposition produces coupled unitary matrix \mathbf{U} and \mathbf{V} which are $\mathbf{U}^T = \mathbf{U}^{-1}$ and $\mathbf{V}^T = \mathbf{V}^{-1}$. The diagonal matrix of Σ is σ_i where $i = 1, 2 \dots N$. If the column vectors of \mathbf{V} is \mathbf{v}_i and the column vectors of \mathbf{U} is \mathbf{u}_i then, the relation can be stated as follows

$$[\mathbf{L}]\mathbf{v}_i = \sigma_i \mathbf{u}_i; [\mathbf{L}]^T \mathbf{u}_i = \sigma_i \mathbf{v}_i \quad (6-8)$$

The solution of (12.1) is stated using the singular value decomposition as

$$\mathbf{s}_k = \left[\sum_{i=1}^N \frac{\bar{u}_i \mathbf{v}_i}{\sigma_i} \right] [[\mathbf{D}]_k^* [\mathbf{b}^\varepsilon]_k] \quad (6-9)$$

The truncated singular value decomposition (TSVD) regularizes the ill-posed problem by truncating the matrix $([\mathbf{L}])$. A small value of singular value (σ_i) is ignored. The ill-conditioned system is regularized as

$$[\mathbf{L}^\alpha]^{-1} = \sum_{i=1}^N \phi_i \frac{\bar{u}_i \mathbf{v}_i}{s_i} \quad (6-10)$$

Where the regularization ϕ_i is defined as

$$\phi_i = \begin{cases} 1; & i = 1, 2 \dots k \\ 0; & i = k + 1 \dots N \end{cases} \quad (6-11)$$

Equation (5.28) is known as the truncated singular value decomposition (TSVD) solution. It solves the linear ill-posed MWT inverse problem. It should be noted that the instability could occur during the computation of \mathbf{s} as some information is omitted.

6.2.1.2 Tikhonov Regularization

The Instability of TSVD can be decreased by applying a parametric filter $\omega(\theta, \alpha)$. One of the well-known filters is the Tikhonov regularization. It is defined as

$$\omega(\sigma_i^2, \alpha) = \frac{\sigma_i^2 + \alpha}{\sigma_i^2} \quad (6-12)$$

where α is the Tikhonov regularization parameter. It addresses the singular decomposition values as

$$\omega(\theta, \alpha)\sigma_i = \frac{\sigma_i^2 + \alpha}{\sigma_i} \quad (6-13)$$

Determining α is essential for the stability and accuracy of the solution. The regulator should be relatively small compared to the largest singular values and relatively big compared to the smallest singular values

For the largest singular values, the regulator contributes small effect while the smallest singular value contributes the biggest inversion values.

$$\omega(\theta, \alpha)\sigma_i = \frac{\sigma_{max}^2 + \alpha}{\sigma_{max}} \approx \sigma_{max} \quad (6-14)$$

The filtered singular value is approximated as

$$\omega(\theta, \alpha)\sigma_i = \frac{\sigma_{min}^2 + \alpha}{\sigma_{min}} \approx \alpha \quad (6-15)$$

Substituting the regularization (6.13) into (6.9) results in Tikhonov regularized ill-posed solution as follows

$$\mathbf{s}_k = \left[\sum_{i=1}^N \frac{\sigma_i}{\sigma_i^2 + \alpha} \bar{u}_i v_i \right] [[\mathbf{D}]_k^* [\mathbf{b}^\varepsilon]_k] \quad (6-16)$$

6.2.1.3 Truncated Landweber method

The solution of the linear system is regulated using the inner iterative index $l = 1, 2, \dots, I$ and guarded with positive nonzero number β .

$$[\mathbf{L}^\alpha]^{-1} = \sum_{j=0}^{l-1} (1 - \beta[\mathbf{L}])^j \quad (6-17)$$

The l^{th} regulative iteration can be expressed in terms of the singular value decomposition system

$$\mathbf{s}_{k,l+1} = \sum_{i=1}^N \frac{1 - (1 - \beta\sigma_i^2)^l}{\sigma_i} \langle [[\mathbf{D}]_k^* [\mathbf{b}^\varepsilon]_k], u_i^T \rangle v_i \quad (6-18)$$

The β is chosen according to the largest singular values. The β lies between

$$0 < \beta < \frac{2}{\sigma_1^2} \quad (6-19)$$

The techniques explained are categorized as direct regularized methods. The direct solution is a predictable number of steps, but it does not support intermediate solutions. The solution is in a specified manner according to the regularization technique used. The accuracy of the solution is dependent on the type of the regulator and the size of the parameter of the regularization in which both parameters are hard to be defined.

6.2.2 Iterative improvement of linear problem

An iterative method is an alternative method to improve the flexibility of the solution. It starts with an approximate answer, and then, the accuracy is improved iteratively, and finally stops once the estimated error is below the tolerance.

Suppose a Newton equation which is a linear system with exact solution \mathbf{s}_k^\dagger satisfies

$$[\psi([\mathbf{L}]_k, \alpha_k)]^{-1} \mathbf{s}_k^\dagger = [[\mathbf{D}]_k^* [\mathbf{b}^\varepsilon]_k] \quad (6-20)$$

The approximated solution is defined as \mathbf{s}_k^\ddagger . It is calculated iteratively, in which its current solution of the system is assigned as $\mathbf{s}_{k,l}^\ddagger$. Initially, it starts with $\mathbf{s}_{k,0}^\ddagger$. Then, at $l = 1, 2 \dots L$ the residue of the solution is defined as

$$\begin{aligned} \mathbf{r}_l &= [[\mathbf{D}]_k^* [\mathbf{b}^\varepsilon]_k] - [\psi([\mathbf{L}]_k, \alpha_k)]^{-1} \mathbf{s}_{k,l}^\ddagger \\ \Rightarrow \mathbf{r}_l &= [[\mathbf{D}]_k^* [\mathbf{b}^\varepsilon]_k] - [\mathbf{L}]_k \mathbf{s}_{k,l}^\ddagger \end{aligned} \quad (6-21)$$

A large residue is caused by an error in the current solution

$$\mathbf{s}_k^\dagger = \mathbf{s}_{k,l}^\ddagger + \mathbf{e}_l \quad (6-22)$$

Multiplying (6.15) with $[\psi([\mathbf{L}]_k, \alpha_k)]^{-1}$

$$\begin{aligned} [\psi([\mathbf{L}]_k, \alpha_k)]^{-1} \mathbf{s}_k^\dagger &= [\psi([\mathbf{L}]_k, \alpha_k)]^{-1} (\mathbf{s}_{k,l}^\ddagger + \mathbf{e}_l) \\ \Rightarrow [\psi([\mathbf{L}]_k, \alpha_k)]^{-1} \mathbf{s}_{k,l}^\ddagger &= [\psi([\mathbf{L}]_k, \alpha_k)]^{-1} \mathbf{s}_k^\dagger - [\psi([\mathbf{L}]_k, \alpha_k)]^{-1} \mathbf{e}_l \\ \Rightarrow [\psi([\mathbf{L}]_k, \alpha_k)]^{-1} \mathbf{s}_{k,l}^\ddagger &= [[\mathbf{D}]_k^* [\mathbf{b}^\varepsilon]_k] - \mathbf{r}_l \end{aligned}$$

$$\begin{aligned}
&\Rightarrow [\psi([\mathbf{L}]_k, \alpha_k)]^{-1}(\mathbf{s}_k^\dagger - \mathbf{e}_l) = [[\mathbf{D}]_k^*[\mathbf{b}^\varepsilon]_k] - \mathbf{r}_l \\
&\Rightarrow [[\mathbf{D}]_k^*[\mathbf{b}^\varepsilon]_k] - [\psi([\mathbf{L}]_k, \alpha_k)]^{-1}\mathbf{e}_l = [[\mathbf{D}]_k^*[\mathbf{b}^\varepsilon]_k] - \mathbf{r}_l \\
&\mathbf{e}_l = [\psi([\mathbf{L}]_k, \alpha_k)]\mathbf{r}_l
\end{aligned} \tag{6-23}$$

The direction of Iterative sequence for improving the linear system is the error \mathbf{e}_l which satisfies (6.16). The iterative solution of the Newton equation is defined as

$$\mathbf{s}_{k,l+1}^\dagger = \mathbf{s}_{k,l}^\dagger + d\mathbf{e}_l \tag{6-24}$$

The step size d is a positive number less than 1. It minimizes the residual norm

$$\min_d \| [[\mathbf{D}]_k^*[\mathbf{b}^\varepsilon]_k] - [\mathbf{L}]_k[\mathbf{s}_{k,l}^\dagger + d\mathbf{e}_l] \|^2 \tag{6-25}$$

Iterative solution $(\mathbf{s}_{k,l}^\dagger)$ represents the approximate solution of the linear ill posed problem (\mathbf{s}_k) at the Newton scheme current solution of MWT inverse problem.

6.3 Inexact Newton Backtracking Method (INBM)

6.3.1 Inexact Newton to solve Newton equations of microwave tomography inverse problem

The objective function of MWT inverse problem is presented as

$$F(\mathbf{x}) = [\mathbf{E}^s(\mathbf{x})] - [\mathcal{E}^s] = 0 \tag{6-26}$$

Generally, it has two main properties of a continuous function, which are: 1) there exists an exact solution $\mathbf{x}^\dagger \in R^n$, where $F(\mathbf{x}^\dagger) = 0$, and 2) F is continuously differentiable in a neighborhood of \mathbf{x}^\dagger . The derivative of multi projection of MWT inverse problem which is assigned as \mathbf{D} is asymmetric. The condition of the normal function of the differential $[\mathbf{D}^*\mathbf{D}]$ is poor. A regularized method is needed to solve the MWT inverse problems.

Newton method is a conventional algorithm for solving well posed nonlinear problems. It starts with initial \mathbf{x}_0 , then, computes a sequence of steps (\mathbf{s}_k) and updates \mathbf{x}_k as

$$\mathbf{x}_{k+1} = \mathbf{x}_k + \mathbf{s}_k \quad (6-27)$$

By introducing a linear filter ψ which regulates the ill-posedness of $[\mathbf{D}^* \mathbf{D}]$, then, Newton equation of the MWT inverse problem can be written as

$$(\psi([\mathbf{D}^* \mathbf{D}]_k, \alpha_k))^{-1} \mathbf{s}_k = -[[\mathbf{D}]_k^* F(\mathbf{x})] \quad (6-28)$$

Then, Newton method algorithm for solving MWT inverse problem can be presented as follows

Algorithm 6-1:NM: Newton Method to solve MWT- Inverse Problem

Function NM(\mathbf{x}_0)

Repeat

$$\mathbf{s}_k = -\psi([\mathbf{D}^* \mathbf{D}]_k, \alpha_k)[[\mathbf{D}]_k^* F(\mathbf{x})]$$

$$\mathbf{x}_{k+1} = \mathbf{x}_k + \mathbf{s}_k$$

$$k = k + 1$$

Until $\frac{\|F(\mathbf{x}_k)\|^2}{\|\mathcal{E}^s\|^2} \leq \epsilon$

Return (\mathbf{x}_k)

In the case of solving well posed system, Newton method is attractive because it converges rapidly from any sufficiently good initial guess. On the other hand, it suffers from noise effect in the case of ill posed problems. It has been shown in the previous chapters that noise and other disturbance greatly affect the regularized Newton method in the form of LM for solving ill posed system of MWT inverse problems.

The other drawback of the regularized Newton scheme is that Newton equation has to be solved at each stage of scheme. The direct regulative solution of Newton method may not be justified if the initial value is far from the exact solution, besides, it can be expensive to handle a large system like the MWT inverse problems. Therefore, an iterative method in which the solution of the linear system is unspecific, approximation is proposed.

An inexact Newton method is applied to compute the regularized MWT inverse problem. The iterative scheme of the method is defined as

$$\mathbf{x}_{k+1} = \mathbf{x}_k + \mathbf{s}_k \quad (6-29)$$

The regularized inexact Newton equation is defined using

$$(\psi([\mathbf{D}^* \mathbf{D}]_k, \alpha_k))^{-1} \mathbf{s}_k = -[[\mathbf{D}]_k^* F(\mathbf{x}_k)] + \mathbf{r}_k \quad (6-30)$$

The residue is given in normal system

$$\mathbf{r}_k = [\mathbf{D}^* \mathbf{D}]_k \mathbf{s}_k + [[\mathbf{D}]_k^* F(\mathbf{x}_k)] \quad (6-31)$$

The addition of residual inexact Newton in (6.24) presents an intermediate solution of Newton equations. Consequently, the method offers a tradeoff between the accuracy with which the regularized Newton equations are computed. The amount of work for solving MWT inverse problems can be decreased as the computation and regularization of Newton equations may not need to be done at each sequence of the inexact Newton scheme.

The accuracy of the computation of Newton equations is determined in unspecific manner. A nonnegative forcing term (η_k) is introduced to control the accuracy. The approximation of the solution of Newton equations is computed based on the relation

$$\frac{\|\mathbf{r}_k\|^2}{\|[\mathbf{D}]_k^* F(\mathbf{x}_k)\|^2} \leq \eta_k \quad (6-32)$$

The Inexact Newton method for the MWT inverse problem replaces the direct regularized solution of Newton equations with its iterative approximation under unspecific manner. The Newton solutions \mathbf{s}_k is determined as such that the following condition is satisfied

$$\|[\mathbf{D}^* \mathbf{D}]_k \mathbf{s}_k\|^2 \leq \eta_k \|[\mathbf{D}]_k^* F(\mathbf{x}_k)\|^2 \quad (6-33)$$

Inexact Newton is applied to solve the Newton equations of the MWT inverse problem. It is conducted iteratively. The regularization and inversion of the problem is computed once. It is defined at the initial step of the inexact Newton. The result of the inexact Newton computation is the direction of

Newton method step for solving the MWT inverse problem. The algorithm of the inexact Newton is presented as follows:

Algorithm 6-2:INM: inexact Newton to solve Newton equations of MMWT Inverse Problem

Function INM($[\mathbf{D}]_k, F(\mathbf{x}_k)$)

Set : $l = 1$

$$\mathbf{s}_{k,0}^\ddagger = 0$$

$$\mathbf{r}_0 = [[\mathbf{D}]_k^* F(\mathbf{x}_k)]$$

$$[\boldsymbol{\psi}] = \boldsymbol{\psi}([\mathbf{D}^* \mathbf{D}]_k, \alpha_k)$$

Repeat

$$\mathbf{e}_l = [\boldsymbol{\psi}] \mathbf{r}_l$$

$$\mathbf{s}_{k,l}^\ddagger = \mathbf{s}_{k,l-1}^\ddagger + d \mathbf{e}_l$$

$$\mathbf{r}_l = [[\mathbf{D}]_k^* F(\mathbf{x}_k)] + [\mathbf{D}^* \mathbf{D}]_k \mathbf{s}_{k,l}^\ddagger$$

$$l = l + 1$$

Until $\|[\mathbf{D}^* \mathbf{D}]_k \mathbf{s}_k\|^2 \leq \eta_k \|[\mathbf{D}]_k^* F(\mathbf{x}_k)\|^2$

Return ($\mathbf{s}_{k,l}^\ddagger$)

6.3.2 Backtracking strategy

The nonlinear MWT-objective function may not actually be reduced by the direction of the solution. The linear model can be directed toward some local minima since the initial point for the inexact Newton method cannot be guaranteed to be near a solution of the nonlinear system. To improve the global convergence, the value of \mathbf{s}_k and η_k is determined to follow some criteria. The global criteria of the inexact Newton are used to ensure the direction of the relative norm of the MWT objective function. The inexact Newton method is globalized by a backtracking strategy. This method is defined as Inexact Newton Backtracking Method (INBM)

$$\|F(\mathbf{x}_k + \mathbf{s}_k)\|^2 \leq [1 - t(1 - \eta_k)] \|F(\mathbf{x}_k)\|^2 \quad (6-34)$$

Equation (6.28) guarantees the reduction of the objective function norm with the direction defined. By given the direction \mathbf{s}_k and force term η_k ,

there, at least, is a fraction of reduction of functional which is guaranteed by founding the term $t \in [0, 1)$.

Backtracking method can be applied to accommodate the selection of \mathbf{s}_k and η_k which are suitable for both (6.27) and (6.28) criteria. The backtracking keeps a not too long step of Newton method. If \mathbf{s}_k is not acceptable by the criteria, then it is shortened until it reaches the criteria. The correction of the parameter follows

$$\begin{aligned}\mathbf{s}_k &= \mathcal{r} \cdot \mathbf{s}_k; \\ \eta_k &= 1 - \mathcal{r} \cdot (1 - \eta_k) \\ \mathcal{r} &\in (\mathcal{r}_{min}, \mathcal{r}_{max}).\end{aligned}\tag{6-35}$$

The fraction of reduction should be selected in the range of $\mathcal{r} \in [0, 1)$. Backtracking is the type of inexact line search. It keeps the step not too long, but does not guard the steps for becoming not too short.

Algorithm 6-3: BK: Backtracking strategy of INM

Function BK($\mathbf{s}_k, F(\mathbf{x}_k)$)

Do While $\|[F(\mathbf{x}_k + \mathbf{s}_k)]\|^2 \leq [1 - t(1 - \eta_k)]\|F(\mathbf{x}_k)\|^2$

$\mathbf{s}_k = \mathcal{r} \cdot \mathbf{s}_k;$

$\eta_k = 1 - \mathcal{r} \cdot (1 - \eta_k)$

End of Do While

Return (\mathbf{s}_k)

6.3.3 Forcing term

Nonnegative forcing term η_k is used to control the levels of accuracy. Finds η_k at $\eta_k \in [0, 1)$ so that any vector \mathbf{s} that satisfies (6.27) where $\eta_k < 1$ is assigned as the stopping criteria of the INM-MWT. The inexact Newton method is locally convergent, if forcing term η_k is uniformly less than 1. Under the present assumptions, if \mathbf{x}_0 is sufficiently close to \mathbf{x}^\dagger , and $0 \leq \eta_k \leq \eta_{max} < 1$ for each k , then, \mathbf{x}_0 converges to \mathbf{x}^* [146; 147; 148]. If η_k is zero for all iterations, then, it is similar to the GNI method. The forcing term is independent on the iteration index(k). The forcing term is applied to

guarantee the decrease of the linear model of the MWT inverse problem. The convergence rate of the method is explained in [149].

The convergence rate of the method is determined by the appropriate choice of the sequence of the forcing term. The term may be determined using the agreement of the MWT objective function and the linear model of the corresponding problem [146]

$$\eta_k = \frac{\|D^*F(x_k)\|^2 - \|[D^*F(x_{k-1})] - [D^*D]_{k-1}s_{k-1}\|^2}{\|D^*F(x_{k-1})\|^2}, \quad k = 1, 2, \quad (6-36)$$

An alternative strategy is explained in [150]. The forcing term is adjusted depending on the ratio of the actual reduction and predicted reduction. The ratio is defined as

$$r_k = \frac{\|D^*F(x_k)\|^2 - \|D^*F(x_k + s_k)\|^2}{\|D^*F(x_k)\|^2 - \|[D^*D]_k s_{k1}\|^2} \quad (6-37)$$

The forcing term is determined according to the ratio r_k

$$\eta_k = \begin{cases} 1 - 2p, & r_{k-1} < p_1 \\ \eta_{k-1}, & p_1 < r_{k-1} < p_2 \\ 0.8\eta_{k-1}, & p_2 < r_{k-1} < p_3 \\ 0.5\eta_{k-1}, & r_{k-1} \geq p_3 \end{cases} \quad (6-38)$$

where $p_1 < p_2 < p_3 < 1$ are prescribed with $p_1 \in (0, \frac{1}{2})$

6.3.4 Inexact Newton Backtracking Method (INBM)

It has been shown that Inexact Newton is sufficiently general as to encompass most exiting method for solving nonlinear inverse problem [147]. In this thesis, inexact Newton is combined with the linearized method in the form of LM. The LM is a type of a regulated Newton method. The Newton equations of the LM for solving the MWT inverse problem is stated as follows

$$[\chi]_{k+1} = [\chi]_k + \psi([D^*D]_k, \alpha_k)[[D]_k^*F([\chi]_k)] \quad (6-39)$$

The linear filter of LM is defined as

$$\psi([\mathbf{D}^* \mathbf{D}]_k, \alpha_k) = \frac{1}{\left\| \frac{[\mathbf{D}]_k}{\sqrt{\alpha}} \right\|^2} \quad (6-40)$$

Linear filter $\psi([\mathcal{X}]_k)$ is an inexact Newton iteration if the filter satisfies

$$\|I - \psi([\mathcal{X}]_k)\|^2 \leq \eta_{max} < 1 \quad (6-41)$$

With the assumption that

$$\begin{aligned} \|\mathbf{r}_k\|^2 &= \|[\mathbf{D}]_k^* [[\mathbf{D}]_k \mathbf{s}_k + F([\mathcal{X}]_k)]\|^2 \ll \|I - \psi([\mathcal{X}]_k)\|^2 \|F([\mathcal{X}]_k)\|^2 \\ &\leq \eta_{max} \|F([\mathcal{X}]_k)\|^2 \end{aligned} \quad (6-42)$$

Rieder describes that any Newton iterative methods which include LM for solving MWT inverse problem can be made to converge with weak order if inner iterations are applied to the Newton equations at k^{th} outer iteration [149]. In this thesis, inexact Newton with backtracking criteria is used to find the solution of Newton equations. It is conducted at the inner loop. The computation generally is terminated according to

$$\begin{aligned} &\|[\mathbf{D}]_k^* [[\mathbf{D}]_k \mathbf{s}_{k,l}^\ddagger + F([\mathcal{X}]_k)]\|^2 \leq \eta_k \|F([\mathcal{X}]_k)\|^2 \\ &\leq \|[\mathbf{D}]_k^* [[\mathbf{D}]_k \mathbf{s}_{k,i}^\ddagger + F([\mathcal{X}]_k)]\|^2; i = 1, 2 \dots l - 1 \end{aligned} \quad (6-43)$$

The Newton iteration is the outer loops of the INBM. It has to be stopped above the noise level to avoid noise amplification. Discrepancy principle can be used to define the stopping rule

$$\|F([\mathcal{X}]_k)\|^2 \leq R\delta \leq \|F([\mathcal{X}]_k)\|^2, \quad k = 1, 2 \dots K - 1 \quad (6-44)$$

where δ is the noise level and $R > 0$ is the real positive number.

The INBM for solving MWT inverse problem is summarized as in algorithm (6.4): Stating the initial solution of the Newton sequence starts the algorithm. Then, the MWT inverse problem is linearized by means on Fréchet derivative. The ill posedness of the system is immersed into the linear system. The approximation of regulated solution is determined iteratively. It is controlled with forcing term. The MWT solution is updated using

approximated regulated solution. The Newton iteration is terminated until stopping rule is satisfied

Algorithm 6-4: INBM: Inexact Newton Method with Backtracking for Microwave Inverse Problem

Function INBM($[\mathbf{y}^\delta]$)

Set : $k = 1$

$$F([\boldsymbol{\chi}]_0) = [\mathbf{b}^\varepsilon]_0 = [\mathbf{y}^\delta] - [\mathbf{E}^s([\boldsymbol{\chi}]_0)]$$

While $\|F([\boldsymbol{\chi}]_k)\|^2 > R\delta$

$$[\mathbf{D}]_k = \left[F'_{ij} = \left(\frac{\partial F_i([\boldsymbol{\chi}]_k)}{\partial [\boldsymbol{\chi}]_j} \right) \right]_{\substack{1 \leq i \leq \sum_{t=1}^T M_t \\ 1 \leq j \leq N}}$$

$$[\mathbf{s}_k] = \text{INM}([\mathbf{D}]_k, F([\boldsymbol{\chi}]_k))$$

$$[\boldsymbol{\delta}\boldsymbol{\chi}]_k = \text{BK}([\mathbf{s}_k, F([\boldsymbol{\chi}]_k)])$$

$$[\boldsymbol{\chi}]_{k+1} = [\boldsymbol{\chi}]_k + [\boldsymbol{\delta}\boldsymbol{\chi}]_k$$

$$k = k + 1$$

$$F([\boldsymbol{\chi}]_k) = [\mathbf{y}^\delta] - [\mathbf{E}^s([\boldsymbol{\chi}]_k)]$$

End of Do While

Return ($[\boldsymbol{\chi}]$)

6.4 Numerical Study of INBM

The INBM algorithm is evaluated using synthetic data. The object of interest is a homogeneous dielectric cylindrical object of interest with relative dielectric parameter $\varepsilon_r = 3$. The radius of the cylinder is 1 cm. Figure 6-1 shows the cross section of OI inside the object domain.

Numerical synthetic data are used to test the algorithm. The simulated data is based on a MWT system. The system consists of 16 antennas which can be used as a microwave signal transmitter and receiver. The data are constructed by assuming that 16 Tx antennas sequentially illuminate 4.5 GHz microwave signal. The source of the signal is approximated as an equivalent infinitive current line.

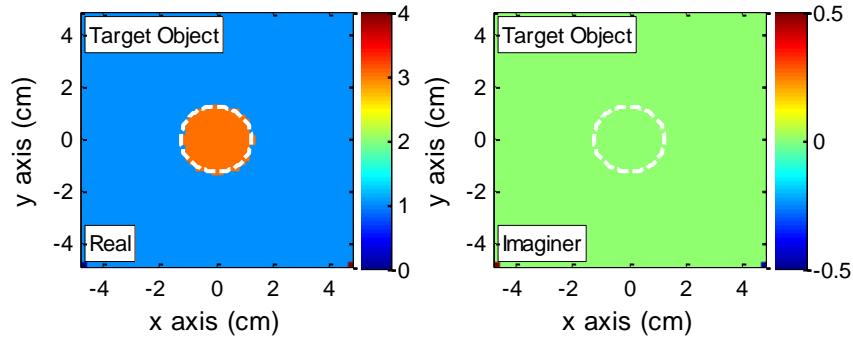


Figure 6-1: The cross section of the object of interest with complex permittivity $\epsilon_r = 3 - j0$. The background of the MWT system is air where the parameter of the dielectric is $\epsilon_r = 1$.

At each illumination, 16 Rx antennas measure the scattered electric field. Positions of Tx antennas are the same as the position of Rx antennas in which it is assumed that the reflection of electric field can be measured. Total of 256 data are collected on each set of MWT measurement. A random number which is assigned as introduced noise and any other additional errors are added to the data. Table 6.1 summarizes the parameter of MWT data measurement.

Table 6-1 the parameter of the simulated system for numerical testing of LM and INBM methods

Parameter	Value
Diameter of Object Domain(\mathcal{O})	9.5 cm
Diameter of Data Domain (\mathcal{D})	13.0 cm
Transmitting Antenna T_x	16 T_x
Receiving Antenna R_x	16 $R_x \times 16 T_x$
Number of data	256
SNR	28.3, 34.2, 40.5 dB
Number of cells	$50 \times 50 = 2500$
ϵ_r	3
Radius of \mathcal{O}	1.5 cm
Frequency	4.5 GHz

INBM reconstructs the numerical synthetic data. The quality of the algorithm in solving MWT inverse problem is compared with the results of LM. Generally, the quality of the algorithm is studied using three parameters, which are

1. *The relative value of the discrepancy.*

Discrepancy defines the termination of the iterative process of the algorithms. The discrepancy is defined using successive norm of the MWT objective function. The iteration is stopped if the relative value of the discrepancy is below the defined tolerance. The ratio is calculated using

$$R(F([\mathcal{X}]_k)) = \frac{\|F([\mathcal{X}]_k)\|^2 - \|F([\mathcal{X}]_{k-1})\|^2}{\|F([\mathcal{X}]_{k-1})\|^2} \quad (6-45)$$

2. *The relative norm of the MWT-objective function*

The process of the iteration is studied using the relative norm of the MWT-objective function. The norm is calculated relative to the measurement. It is defined as

$$\mathcal{F}([\mathcal{X}]_k) = \frac{\|F([\mathcal{X}]_k)\|^2}{\|\varepsilon^s\|^2} \quad (6-46)$$

3. *The relative error of the value of the dielectric contrast of OI*

The quality of the solutions of MWT inverse problem is quantified using the error of the value of dielectric contrast of object domain. Relative errors are computed for all cells inside OI.

$$Err([\mathcal{X}]_k) = \frac{\|[\mathcal{X}]_{target} - [\mathcal{X}]_k\|^2}{\|[\mathcal{X}]_{target}\|^2} \quad (6-47)$$

Several regulator techniques and forcing term selector are studied.

6.4.1 Solving Newton equations using INBM

Newton method is applied to solve the MWT inverse problem. The Newton iteration is composed using a linearization technique. There are two major loops of Newton scheme for solving this inverse problem. The outer is Newton method for solving the nonlinear system of the MWT inverse

problem. It is an iterative method in which the Newton steps are the solution of Newton equations which are the linearization of MWT inverse problem by means Frechet derivative. The inner loop computes the solution of Newton equations. The equations are ill posed. Tikhonov regularization is applied. It is presented in regulated singular value decomposition. Two different methods are used to solve the Newton equations. They are:

1. *Lavenberg Marquardt method (LM)*

$$\mathbf{s}_k = \psi([\mathbf{L}]_k, \alpha_k)[[\mathbf{D}]_k^*[\mathbf{b}^\varepsilon]_k] \quad (6-48)$$

It is categorized as a direct regularization method. The equations are regularized by means of Tikhonov regularization, then, solved using a pseudoinverse problem.

2. *Inexact Newton Backtracking method (INBM)*

$$\mathbf{e}_l = \psi([\mathbf{L}]_k, \alpha_k)[[\mathbf{D}]_k^*[\mathbf{b}^\varepsilon]_k - [\mathbf{L}]_k \mathbf{s}_{k,l}^\ddagger] \quad (6-49)$$

$$\mathbf{s}_{k,l+1}^\ddagger = \mathbf{s}_{k,l}^\ddagger + d\mathbf{e}_l$$

INBM solves the Newton equations in unspecific manner. It replaces the solution of equations by LM which is \mathbf{s}_k with its iterative approximation ($\mathbf{s}_k^\ddagger = \mathbf{s}_{k,l}^\ddagger$). The intermediate solution of the iterative method is selected as the solution if the ratio of the residual norm with the norm of Newton equations output is below a forcing term.

In this study, the iteration of Newton method is not terminated based on the discrepancy stopping rule, but it is conducted at 30 iterations per test. This is conducted to learn the behavior of the MWT objective function before and after the solution of the MWT inverse problem is gained. In practice, the iteration is stopped above the noise level to avoid noise amplification. The ratio of the discrepancy principle can be used to define the stopping rule. As the noise level is unknown, the Newton iteration is stopped accordingly

$$R(F([\boldsymbol{\chi}]_k)) \leq \epsilon \quad (6-50)$$

where ϵ is a nonnegative small number.

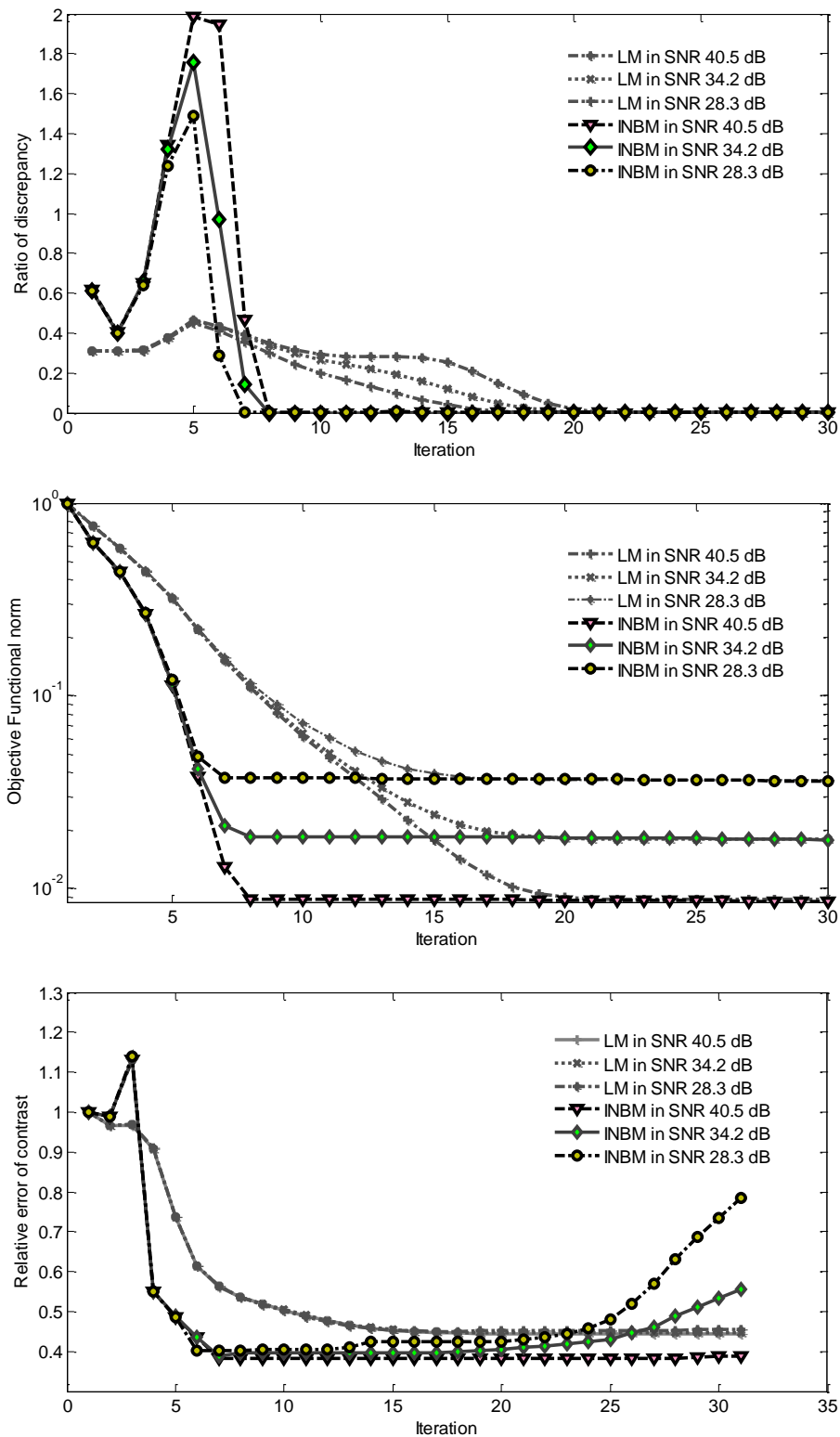


Figure 6-2: The parameters of MWT inverse problem solutions using INBM and LM algorithms. The OI is a cylindrical with complex permittivity $\epsilon_r = 3 - j0$ and radius 1.5 cm.

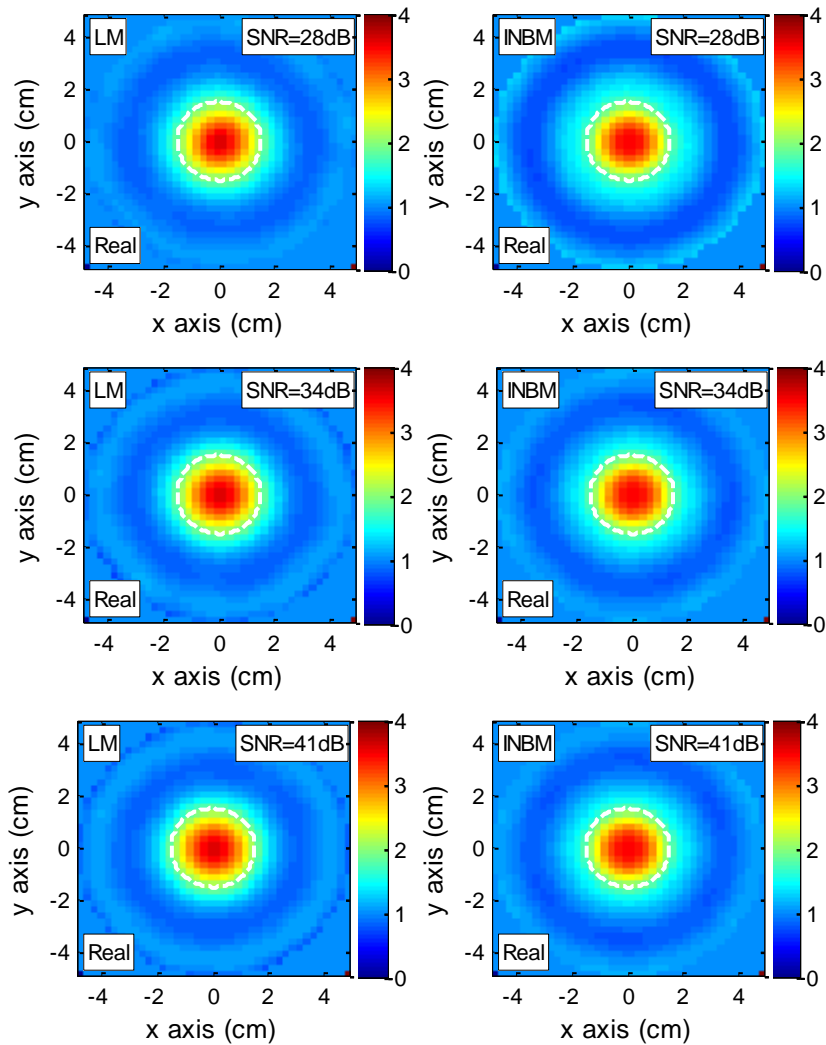


Figure 6-3: The real part of reconstructed Images using INBM and LM algorithms. The OI is a cylindrical object with complex permittivity $\epsilon_r = 3 - j0$ and radius 1.5 cm. The data is taken at 4.5 GHz. White Gaussian noise is introduced with signal to noise ratio 28 dB, 34dB and 41 dB.

Synthetic data are reconstructed using LM and INBM algorithms. The parameter of process of the reconstruction is presented in Figure 6-2 and the reconstructed images are presented in Figure 6-3.

Figure 6-2 shows the parameters of the Newton's iteration when the stopping index of the outer loop is not set. The parameters are the relative value of the discrepancy, the relative norm of MWT objective function and the relative error of the value of the dielectric of the OI.

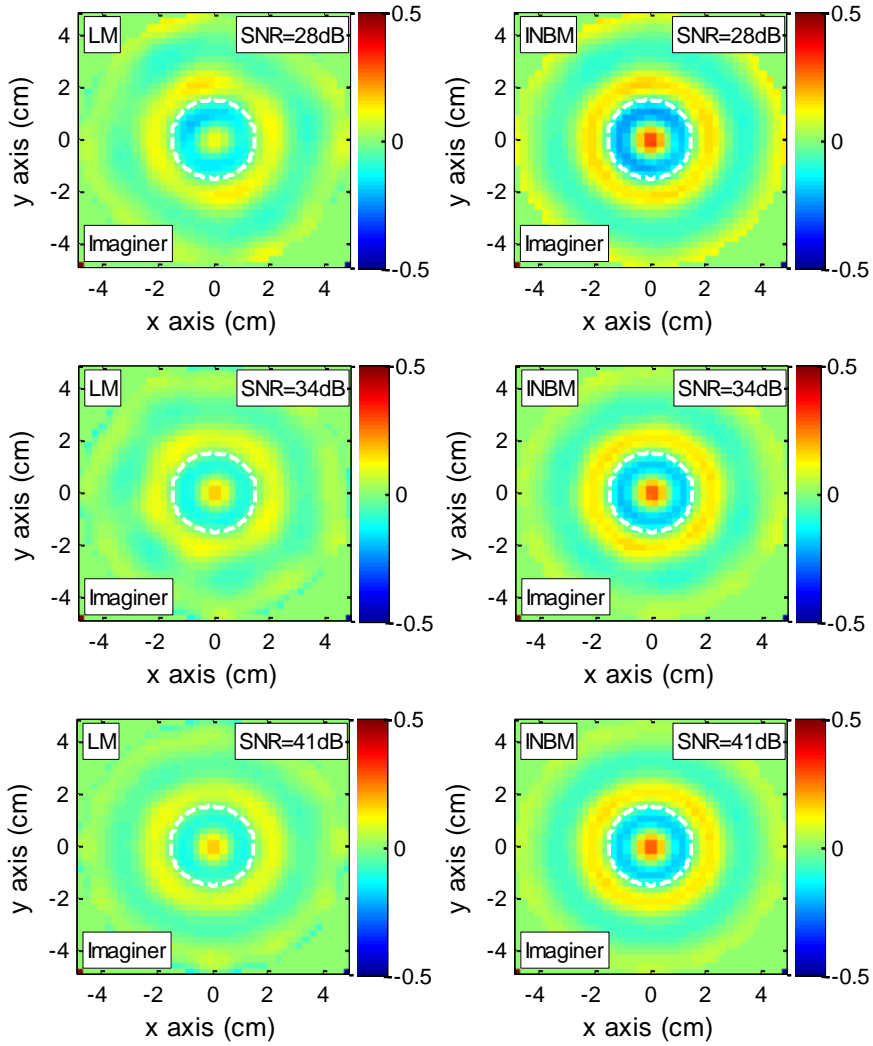


Figure 6-4: The imaginary part of reconstructed Images using INBM and LM algorithms. The OI is a cylindrical object with complex permittivity $\epsilon_r = 3 - j0$ and radius 1.5 cm. The data is taken at 4.5 GHz. White Gaussian noise is introduced with signal to noise ratio 28 dB, 34dB and 41 dB.

It can be seen that the relative values of the discrepancy are relatively similar for all types of data. It can be stated that the value of the relative discrepancy is not affected by the level of noise above SNR 30dB. It has been shown that INBM moves faster than LM for solving the MWT inverse problem. The discrepancy of INBM is relatively big for the first five iterations of Newton method, then, sharply decreases toward a tolerance level. While, the discrepancy value of LM moderately decreases to the level of tolerance.

Table 6-2: The comparison of INBM results to solve MWT inverse problem of cylindrical dielectric OI with complex permittivity $\epsilon_r = 3 - j0$ and radius 1.5 cm and that LM algorithm.

SNR (dB)	LM				INMB			
	k	\mathcal{F}	Err	R	k	\mathcal{F}	Err	R
		(%)	(%)	(%)		(%)	(%)	(%)
40.5	20	0.90	44.4	1.80	8	0.85	38.90	0.00
34.2	18	1.90	44.69	2.61	8	1.85	39.65	0.00
28.3	16	3.80	45.09	2.10	7	3.75	40.30	0.05

Note

1. The iteration is terminated at $(k - 1)^{th}$ iteration when the relative value of the discrepancy is less than a tolerance, which is

$$R(F([\chi]_k)) = \frac{\|F([\chi]_k)\|^2 - \|F([\chi]_{k-1})\|^2}{\|F([\chi]_{k-1})\|^2} < 0.1\%$$

2. The relative norm of MWT objective function and the error of dielectric contrast is calculated at $(k - 1)^{th}$ iteration, which are $\mathcal{F}(F([\chi]_{k-1}))$ and $Err([\chi]_{k-1})$

Following the pattern of relative value of the discrepancy, the relative norms of MWT objective functions resulted by INBM decrease faster than that produced by LM. The flat range of the norms line on INBM is reached after 8 iterations while the norms line of LM flats after 18 iterations.

The line of the objective function norm graphs show that noise level determines the destination level of the objective functions. Decreasing the ratio of signal to noise ratio reduces the level of the norm of objective function value. This follows the idea that the iterations should be stopped above the noise level.

The quality of the results of solving the MWT inverse problem is described using the relative error of the dielectric contrast value. It can be seen in Figure 6-2 that INBM produces better results than LM algorithm. Generally, the error level of INBM solution is lower than that of LM solution. The INBM produces relative errors 40% or less, while the LM produces

relative errors 5% or higher. Moreover, Figure 6-3 shows that the images of OI cross section which are resulted by INBM describe the shape and the value of the dielectric OI accurately while the radius of cylinder on the images resulted by LM is slightly smaller than the original shape of OI. The smoothness of the Tikhonov regularization at LM directly affects the general solution of the Newton method. The quality of the solutions is determined by the parameter of the regulator, which is hard to define. On the contrary, INBM offers flexibility in the accuracy of the Newton equation solutions. Forcing the solutions of the Newton equations improves the quality of global solutions. The quality of MWT inverse problem solutions using INBM algorithm is better than that of LM solutions

In this case, the relative discrepancy is used as the Newton method stopping rule. The iterations are terminated if the discrepancy is $R < 0.001$. The results of reconstructions are summarized in Table 6-2 and the images of the dielectric OI are presented in Figure 6-3. It can be seen that the number of iterations of INBM is less than a halve of the iterations needed by LM algorithm. Within less iterations, INBM produces a better solution than LM algorithm does.

6.4.2 Study of regularization techniques on INBM algorithm

The Newton equations of MWT inverse problem are ill posed and highly nonlinear with respect to the contrast even when it is stated in a linear system. The regularization technique solves the ill posedness of the problem. It has been studied in the previous sections that the intermediate approximation solution, in a specific manner by means of a nonzero forcing term, enforces better solutions of Inexact Newton class algorithm. The approximation is regulated by means of Tikhonov regularization. In this section, the effect of the regularization technique on the solution of the MWT inverse problem using INBM is further studied.

Three different techniques are applied to solve Newton equations under INBM scheme. The regularizations are conducted using pseudo inverse, which are

1. *Tikhonov regularization (Thi)*

$$\psi([\mathbf{L}]_k, \alpha_k) = \left[\sum_{i=1}^N \frac{\sigma_i}{\sigma_i^2 + \alpha} u_i^T v_i \right]; \alpha_k = \frac{\alpha_{(k-1)}}{c} \quad (6-51)$$

2. *Landweber-Friedman iteration (LF)*

$$\psi([\mathbf{L}]_k, \alpha_k) = \left[\sum_{i=1}^N \frac{1 - (1 - \beta \sigma_i^2)^l}{\sigma_i} u_i^T v_i \right]; l_k = l_{(k-1)} + c \quad (6-52)$$

3. *Truncated Singular Value Decomposition (TSVD)*

$$\psi([\mathbf{L}]_k, \alpha_k) = \left[\sum_{i=1}^N \phi_i \frac{u_i^T v_i}{\sigma_i} \right]; \phi_i = \begin{cases} 1; & i = 1, 2, \dots, n \\ 0; & i = n + 1, \dots, N \end{cases} \quad (6-53)$$

The INBM algorithm with three different regulator techniques is applied to reconstruct the MWT synthetic data. The parameter of the reconstruction process which are the relative value of discrepancy criteria, the relative norm of MWT objective function norm and the relative errors of dielectric contrast distribution graphs are presented in Figure 6-5.

Figure 6-5 shows the parameters of the iterative process of INBM with three different regularization techniques in solving the MWT inverse problems. It can be seen that the graphs of the relative value of the discrepancy are relatively similar for all types of the regularization techniques. The discrepancy values are relatively big for first five iterations, then, the values drop toward the zero level. This means that the accuracy of the update values of Newton method is not greatly influenced by the type of the regularization techniques. The accuracy of the Newton equations solution is controlled by the forcing term as the application of INBM offers possibility in evaluating an intermediate solution. It can be seen in Table 6-2 that the defined accuracy is achieved in a different number of inner iterations for different regularization techniques.

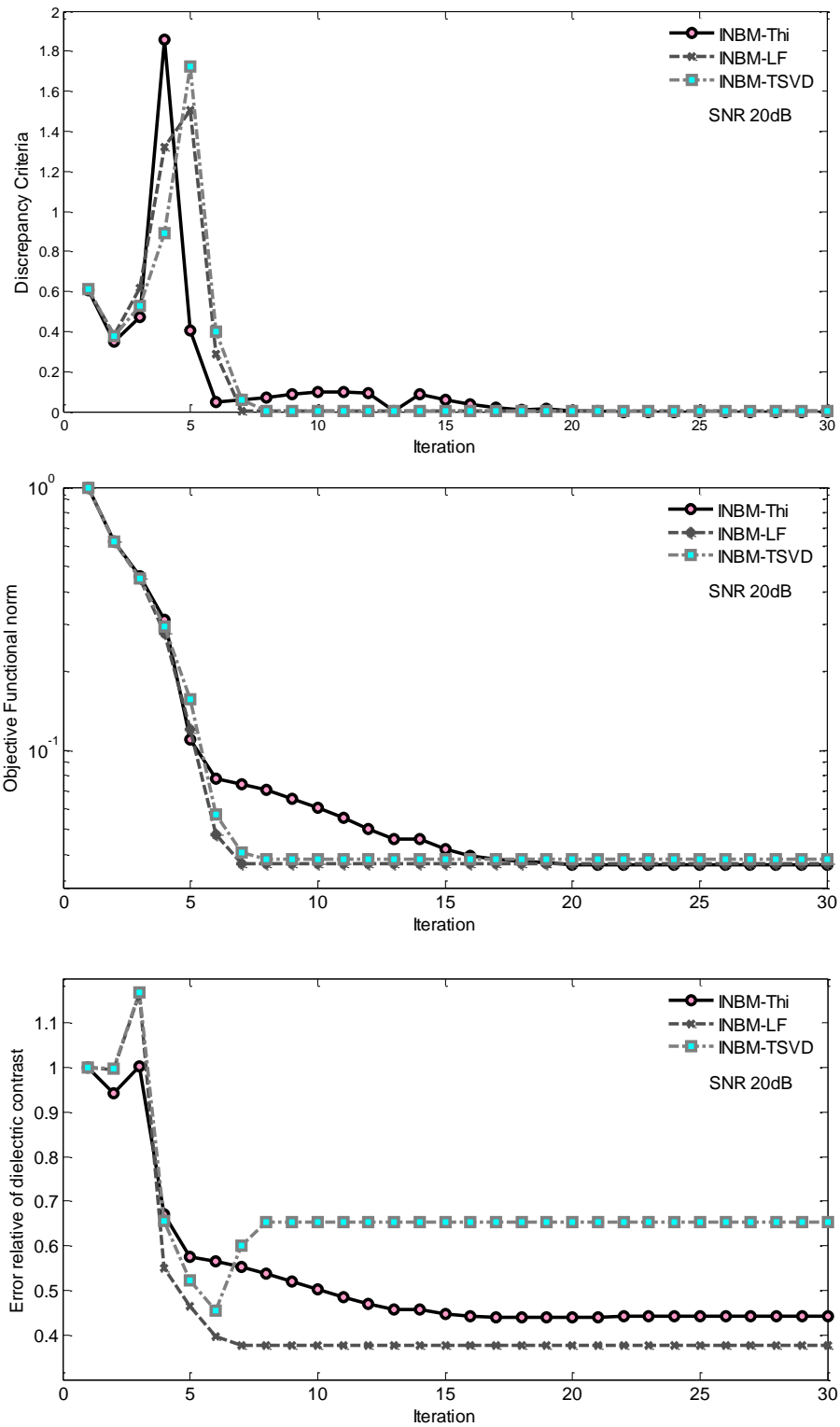


Figure 6-5: The parameters of MWT inverse problem solutions using INBM with Tikhonov regularization (Thi), Landweber-Friedman iteration (LF) and Truncated Singular Value Decomposition (TSVD). The OI is a cylindrical with complex permittivity $\epsilon_r = 3 - j0$ and radius 1.5 cm.

Table 6-3: The comparison of regularization technique for inner loops of Newton iterative (INBM) and direct regularization method by means of Levenberg Marquardt method (LM) as a result of the numerical data reconstruction

	Parameter	INBM			LM
		Tikhonov	Landweber	TSVD	Tikhonov
SNR 40.5 dB	k	8	8	8	20
	$\sum_{k=1}^K l_k$	80	102	69	-
	R	0.00%	0.01%	0.00%	1.80 %
	\mathcal{F}	0.85%	0.87%	0.92%	0.90%
	Err	38.9%	36.99%	45.23%	44.4%
SNR 34.2 dB	k	8	8	8	18
	$\sum_{k=1}^K l_k$	90	86	75	-
	R	0.00%	0.00%	0.00%	2.61%
	\mathcal{F}	1.85%	1.81%	2.01%	1.90%
	Err	39.65%	37.14%	51.93%	44.69%
SNR 28.3 dB	k	7	7	8	16
	$\sum_{k=1}^K l_k$	86	83	91	-
	R	0.05%	0.00%	0.00%	2.10%
	\mathcal{F}	3.75%	3.71%	3.85%	3.80%
	Err	40.30%	37.75%	65.2%	45.09%

Note

1. k is the number of Newton method iteration (outer loop of INBM)
2. l_k is the number of inner iteration
3. R is the discrepancy value at $(k - 1)$. The iteration is terminated when the relative value of the discrepancy is less than a tolerance

$$R(F([\chi]_k)) = \frac{\|F([\chi]_k)\|^2 - \|F([\chi]_{k-1})\|^2}{\|F([\chi]_{k-1})\|^2} < 0.3\%$$

4. \mathcal{F} is the relative norm of the MWT objective function and Err is the error of dielectric contrast calculated at $(k - 1)^{th}$ iteration, namely $\mathcal{F}(F([\chi]_{k-1}))$ and $Err([\chi]_{k-1})$

The graphs of the relative norms of the MWT objective function can be seen in Figure 6-5. It shows the lines of relative norms that move towards the zero level. Initially, the patterns of the lines of the norms of WMT objective function for INBM with three different regularizations are similar; but after the 6th iterations, the line of INBM with Tikhonov regularization is not as sharp as the other lines. The choices of regularization and regulator parameter influence the global solution of the MWT inverse problems. The accuracy of the INBM is set in unspecific manner, then, the path of the iterative solutions are varied, especially when the solution is close to the global solution where the noise level is relatively high compared to the signal.

The quality of the images resulted is evaluated via the revolution of the relative errors of the dielectric contrast. The pattern of the relative errors of the dielectric contrast can be seen in the last figure of Figure 6-5. It is shown that the Tikhonov and LF regularizations produce better quality images than that of TSVD regularization.

The regularization of Newton equations are conducted using pseudo inverse. The basic idea of regularization using this techniques are based on modification of the singular value. The influence of the higher frequency of the singular value is damped or cut. The size of the filter of Tikhonov and LF is loosened along with the iterations. The cutoff frequency of the filter is moved higher by decreasing the size of the regulator. While the cutoff position of the TSVD filter is kept constant along the inner/outer loops, it can be seen in Table 6-3 that the number of outer iterations for INBM is relatively similar. On the other hand, the errors of the dielectric contrast distribution norm produced by TSVD is slightly higher than that produced by the other regularization techniques, nevertheless it is still better than the result of LM algorithm.

It reveals that the intermediate solution which is stated as the approximation solution for the linear ill posed problem of the MWT inverse problem improves the flexibility of the Inexact Newton class method in solving MWT inverse problem. This idea may be boarded by exposing cheaper techniques for solving a large linear ill posed problem for calculating the approximation solution of the inner loop of the INBM.

6.4.3 Choice of forcing terms

The accuracy of the solution is guarded in unspecific manner by means of forcing term η_k . This term is essential to protect the solution from the noise and other disturbances beside it is used to determine accuracy and the rate of the convergence[146]. Three different techniques to determine η_k are applied in INBM algorithm. The techniques are

1. *Eisenstat and Walker [146]*

$$\eta_k = \frac{\|\mathbf{D}^*F(\mathbf{x}_k)\|^2 - \|[\mathbf{D}^*F(\mathbf{x}_{k-1})] - [\mathbf{D}^*\mathbf{D}]_{k-1}\mathbf{s}_{k-1}\|^2}{\|\mathbf{D}^*F(\mathbf{x}_{k-1})\|^2}, \quad k = 1, 2, \quad (6-54)$$

2. *An et al.[151]*

$$\eta_k = \begin{cases} 1 - 2p, & r_{k-1} < 0.4 \\ \eta_{k-1}, & 0.4 \leq r_{k-1} < 0.6 \\ 0.8\eta_{k-1}, & 0.6 \leq r_{k-1} < 0.8 \\ 0.5\eta_{k-1}, & r_{k-1} \geq 0.8 \end{cases} \quad (6-55)$$

$$r_k = \frac{\|\mathbf{D}^*F(\mathbf{x}_k)\|^2 - \|\mathbf{D}^*F(\mathbf{x}_k + \mathbf{s}_k)\|^2}{\|\mathbf{D}^*F(\mathbf{x}_k)\|^2 - \|\mathbf{D}^*F(\mathbf{x}_k) - [\mathbf{D}^*\mathbf{D}]_k\mathbf{s}_{k1}\|^2}$$

3. *Constant forcing term $\eta_k = 0.04$*

The most popular strategy to choose forcing terms is *Eisenstat and Walker*. This strategy reflects the relation of the nonlinear function of the inverse problem $F(\mathbf{x}_k)$ with its solution of Newton equations \mathbf{s}_k . In the MWT inverse problem application, the relation is formulated in the normal system which is between $\mathbf{D}^*F(\mathbf{x}_k)$ and previous Newton solutions $[\mathbf{D}^*\mathbf{D}]_{k-1}\mathbf{s}_{k-1}$ of the Newton scheme. Under suitable and well posed condition, it has been shown that if the initial guess of a nonlinear problem is sufficiently close to

the target, the INBM with this strategy iterates to a global solution. However, this strategy does not prevent the value of the forcing term from becoming too small too quickly.

An et al. improve *Eisenstat and Walker* strategy using a safeguard to prevent the fluctuation of the forcing terms. The change of the forcing terms value is rational to the previous value. The ratio is determined using the relations between the output of the MWT objective function and its Newton equation output. This is the same as the relation between the value of nonlinear problems and its corresponding linear solutions. The ratio is used to determine the rate of change of the forcing term. Thus, the value of the forcing term may be adjusted to prevent overcorrection.

The last strategy sets the forcing term as a constant positive number. Among those three strategies for choosing forcing term, the last one does not refer to the quantity of the MWT objective function. The value of the forcing term of this strategy only reflects the rate of reduction of the MWT objective function. The agreement of the output of the nonlinear problem and its corresponding linear solution is not taken into account.

Three strategies for determining forcing term with different types of relations with the output of the nonlinear problem $F(\mathbf{x})$ are applied in INBM to solve the MWT inverse problems. Three data set of the MWT problems which are summarized in Table 6-1 are used to test the efficiency of the strategies. The iterative Newton method is constructed and the Newton step is determined by solving the Newton equations which are constructed by linearizing the MWT inverse problems. Three different regularization techniques are also applied to regularize the Newton equations. The parameter of the solutions of the MWT inverse problem using INBM algorithm are summarized in Table 6-4 for INBM-Tikhonov, Table 6-5 for INBM-LF, and Table 6-6 for INBM-TSVD implementation.

The INBM is terminated and the solution is gained if one of the following conditions is reached: 1) The value of the discrepancy is less than 0.01 and 2) The value of the relative norm of MWT objective function is less than $\epsilon = 10^{-4}$

Table 6-4: The comparison of three different techniques of choosing the forcing term. The MWT inverse problem is solved using INBM with *Tikhonov regularization*

	Eisenstat& Walker			An et al.			$\eta_k = 0.04$		
dB	40.5	34.2	28.3	40.5	34.2	28.3	40.5	34.2	28.3
k	7	6	6	8	8	7	7	7	7
$\sum_{k=1}^K l_k$	88	86	84	80	86	86	113	143	123
R (%)	0.00	0.00	0.00	0.00	0.00	0.00	0.00	0.00	0.00
\mathcal{F} (%)	0.87	1.84	3.70	0.88	1.81	3.75	0.87	1.82	3.67
Err (%)	39.11	39.96	41.27	38.22	37.14	40.31	34.07	33.15	36.50

Table 6-5: The comparison of three different techniques of choosing the forcing term. The MWT inverse problem is solved using INBM-*Landweber Friedman*.

	Eisenstat& Walker			An et al.			$\eta_k = 0.04$		
dB	40.5	34.2	28.3	40.5	34.2	28.3	40.5	34.2	28.3
k	8	8	7	8	8	7	8	7	7
$\sum_{k=1}^K l_k$	101	84	85	102	86	83	159	143	143
R (%)	0.00	0.00	0.00	0.00	0.00	0.00	0.00	0.00	0.00
\mathcal{F} (%)	0.87	1.81	3.67	0.87	1.81	3.71	0.86	1.82	3.64
Err (%)	40.81	40.99	41.94	36.99	37.14	37.75	33.00	33.15	33.82

Table 6-6: The comparison of three different techniques of choosing the forcing term. The MWT inverse problem is solved using *INBM-TSVD*.

	Eisenstat& Walker			An et al.			$\eta_k = 0.04$		
dB	40.5	34.2	28.3	40.5	34.2	28.3	40.5	34.2	28.3
k	7	7	7	8	8	8	8	7	7
$\sum_{k=1}^K l_k$	87	89	89	69	91	91	87	101	101
R (%)	0.00	0.00	0.00	0.00	0.00	0.00	0.00	0.00	0.00
\mathcal{F} (%)	0.87	2.01	3.95	0.92	2.01	3.85	0.87	1.88	3.81
Err (%)	46.64	52.10	63.68	45.23	51.94	65.2	35.68	36.26	57.90

On the other hand, a failure of INBM to determine a solution is declared if one of the following conditions occurs during the iteration process.

- 1) The number of the outer loop iteration reaches 30
- 2) The backtracking iteration reaches 20, which means that the Newton step (\mathbf{s}_k) is too small due to the small value of r^{20}
- 3) $R(F([\mathbf{x}]_k)) \leq 0$ which means that the Newton method fails.

Table 6-4, Table 6-5 and Table 6-6 show the parameter of the iterative solution of MWT inverse problem using INBM with three different regularization techniques. It can be seen that R drops under 1% after several iterations. The values of R_k at the first five iterations are relatively high. These reflect that the rate of the convergence of the iteration is high. The forcing term accelerates the iteration and directs the solution toward an optimum point. Then, the values of R_k drop after 7th index of outer iterations (k) in which it reaches below the tolerance $R_k < 0.01$. This means that the minimization of MWT inverse problem reaches stationary points. The average number of the iterations for INBM to solve the MWT inverse problem is 7 iterations. The speed of the convergence is similar among the techniques.

The iterative process INBM for solving the MWT inverse problems at early iterations shows the agreement of Newton equations solutions $\|\mathbf{D}^*[F(\mathbf{x}_k) + [\mathbf{D}]_k \mathbf{s}_k]\|^2$ and MWT objective functions $\|\mathbf{D}^*F(\mathbf{x}_k + \mathbf{s}_k)\|^2$. Then, the Eisenstat and Walker technique and An et al. technique increase the value of the forcing terms after the 6th iterations as the disagreement starts to rise among both functional terms. When the forcing term approaches 1 value, the size of \mathbf{s}_k is close to zero. Then, the iteration has to be terminated.

The difference of the nonlinear solution norm and its linear update norm changes η_k . The application of this technique needs the limitation of $\eta_k \in [\min_ \eta, \max_ \eta]$. The technique proposed by An et al. transfers the ratio of a nonlinear solution and its previous nonlinear solution with correspondent linear update into the selection of the forcing term via the classification of the ratio.

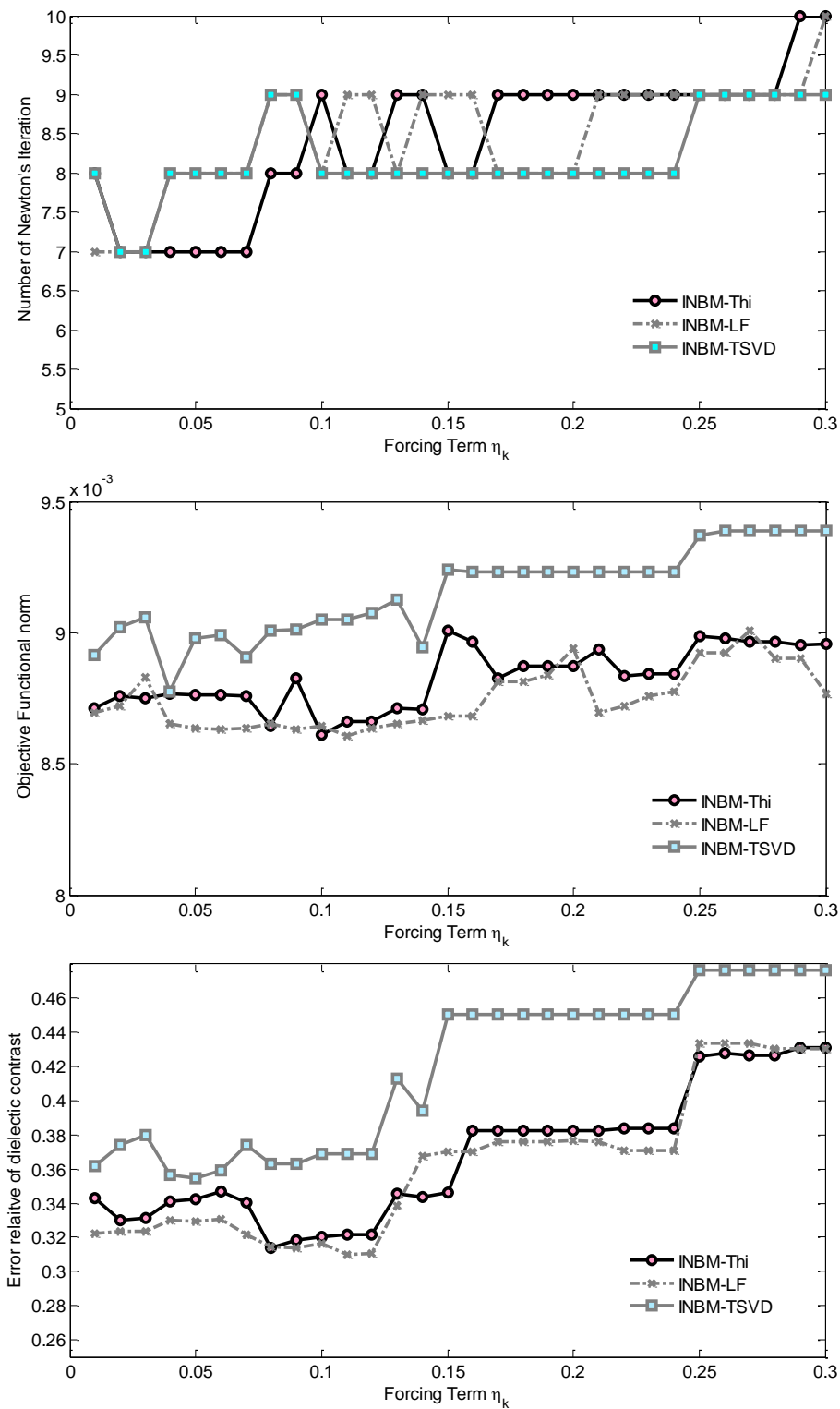


Figure 6-6: The parameters of INBM solutions with respect to forcing term constant. The parameters are number of iteration (k), objective function norm and relative error of $[\chi]_k$. The OI is a cylindrical object with complex permittivity $\epsilon_r = 3 - j0$ and radius 1.5 cm. The working frequency is 4.5 GHz.

The change of η_k is determined by the class of the ratio and a real positive number less than 1. To protect the value of η_k , the minimum class is defined between 0 and $\frac{1}{2}$. Probably, the easiest way to determine the forcing term is an empirical study. The η_k is set as a positive number less than 1. It has been discussed in [151] that this technique produces higher errors than those which apply the agreement of nonlinear and linear solutions.

Tables of the comparison of the parameter of iterative solutions of MWT inverse using *INBM* show that the relative errors of the dielectric contrast reconstructed by *INBM* with constant $\eta_k = 0.04$ is the smallest. Other parameters of the reconstruction results show that the choice of $\eta_k = c$ is flexible and effective to be applied in the *INBM* algorithm. A slight limitation of this selection is that the total inner iteration to solve the Newton equations is the largest among the other choice of forcing terms.

Further test for $\eta_k = c$ is done by scanning the constant c . *INBM* algorithm with constant η_k is used to reconstruct noisy data of the MWT inverse problem with SNR 34.2 dB. The results of the reconstructions in term of the number of iterations, objective function norm and relative error of the dielectric contrast distribution are presented in Figure 6-6.

The graphs show the flexibility of the choice of the forcing terms. The number of iterations needs to terminate outer loop with $R = 0.01$ is between 6 to 9 iterations for $\eta_k = 0.01$ to $\eta_k = 0.25$. The final objective function norm is less than 1%. The relative error of the dielectric contrast is also relatively flat over the span of the forcing terms. The simplicity and the flexibility of setting forcing term as $\eta_k = c$ for MWT inverse problems promote the possibility of applying the technique for further MWT inverse problem applications.

6.5 The application of INBM to Solve MWT- inverse problem of lossy object

6.5.1 Cylindrical homogeneous lossy object

Complex permittivity of lossy material OI is presented as

$$\varepsilon = \text{Re}(\varepsilon) - j\text{Imag}(\varepsilon) \quad (6-56)$$

Where $\text{Re}(\varepsilon)$ and $\text{Imag}(\varepsilon)$ are the real part and imaginary part of complex permittivity, and j is an imaginary sign which equals to $j = \sqrt{-1}$.

The first numerical data for lossy material application is obtained from the solution of the direct MWT scattering problem of two dimensional models of cylindrical homogeneous lossy object. The OI is placed in a free space object domain with radius 4.5 cm. The image of 2D model is shown in Figure 6-7. The domain is placed in a square area which is divided into 50×50 squared cells.

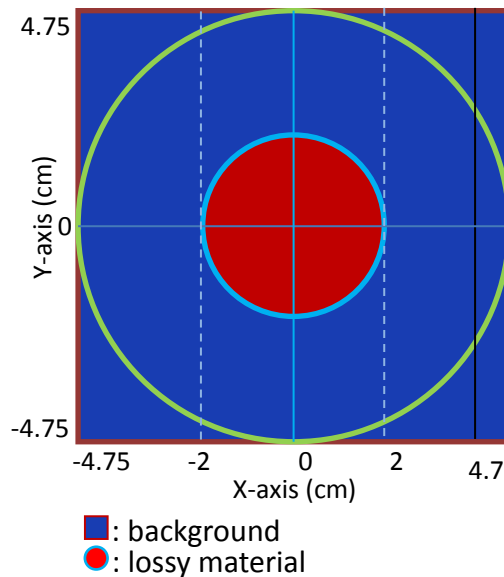


Figure 6-7: a cross sectional view of a homogeneous lossy object of interest. The real part of OI complex permittivity is 3.5. The imaginary part of OI is varied.

In a 2D homogeneous lossy object problem, 16 antennas are used for transmitting and receiving 2.5 GHz microwave signals. The source of the signals is assumed to be an infinite current line source which is computed using Hankel's function. The points of electric field measurement are placed at radius 6.5 cm around the object domain. At each set of measurement, 256 data are generated and 40dB White Gaussian noise is added to the data using *awgn* Matlab function.

The noisy data is reconstructed using INBM and LM algorithms. The initial value of the dielectric contrast is free space $\varepsilon_r = 0$. The tolerance of the discrepancy is set to be $R(F([\chi]_k)) \leq 0.003$, and the solution gained is the relative norm of the MWT objective function $\mathcal{F}(F([\chi]_k)) \leq 10^{-4}$. The reconstructed images of 2D model of homogeneous cylindrical OI using INBM and LM algorithms are presented in Figure 6-8 and Figure 6-9.

The image of OI is presented in real and imaginary parts of complex permittivity. It can be seen that the real parts of LM suffers from a high lossy object. The quantity of $Re(\varepsilon)$ in a lossy object which is $Re(\varepsilon) = 3.5$ cannot be reconstructed. The image is blurred and the value of $Imag(\varepsilon)$ is missed. When the $Imag(\varepsilon)$ of OI equals to -3.8, the value of the real part is a halved of the target value.

The effect of $Imag(\varepsilon)$ on the images resulted by INBM is shown in Figure 6-9. It can be seen that the shape and the value of the complex permittivity of OI is relatively well constructed. INBM solves the MWT inverse problem of a lossy OI with a small value of $Imag(\varepsilon)$ well. The improvement of $Imag(\varepsilon)$ of OI influences the reconstruction of $Re(\varepsilon)$. At a high value of $Imag(\varepsilon)$, the shape of the OI is clearly seen on both real and imaginary images, but the value of $Re(\varepsilon)$ is overdetermined. However, the images of the lossy OI resulted by INBM are still better than those produced by LM algorithm.

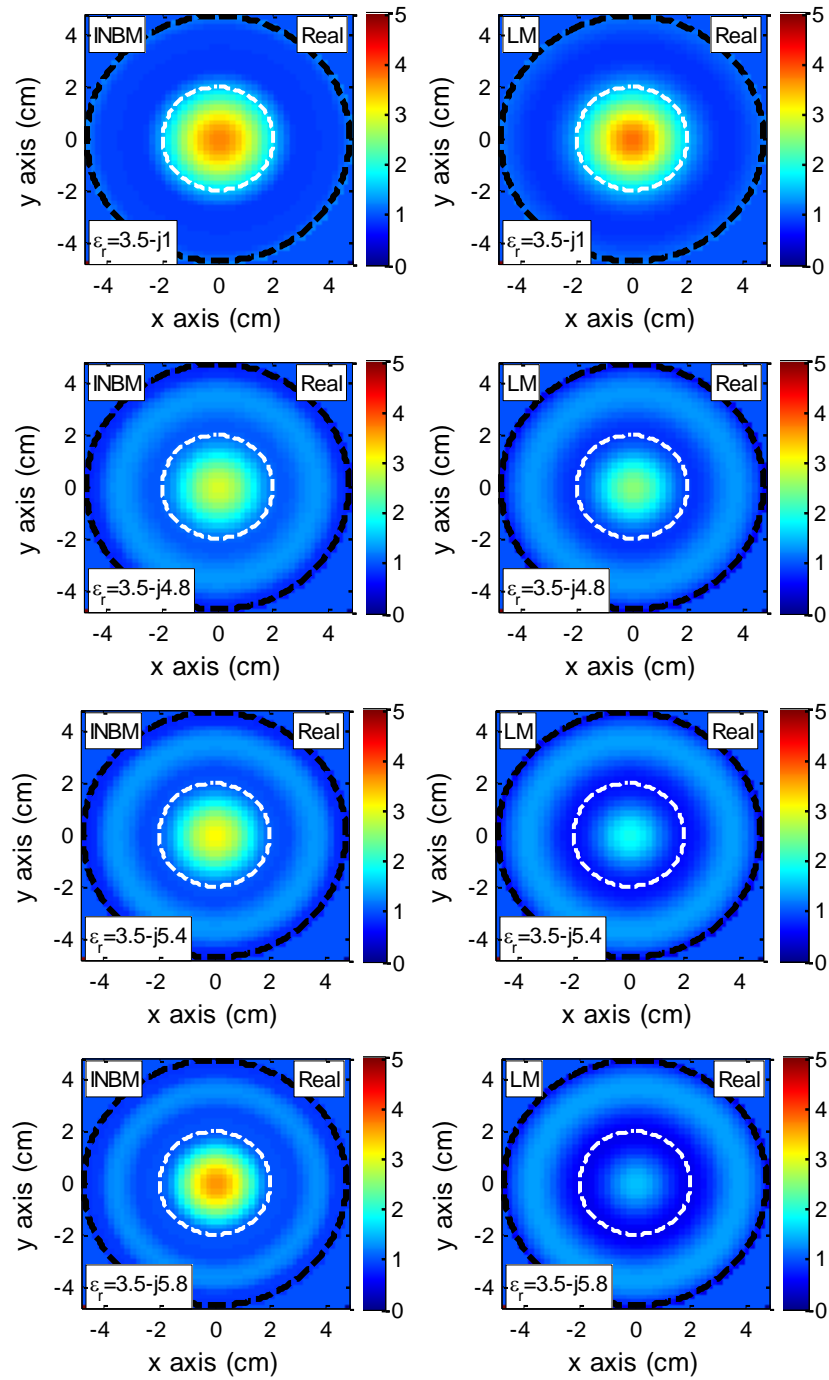


Figure 6-8: The real part of reconstructed images using INBM and LM algorithms. Four different cylindrical OI with radius 2 cm and permittivity $\epsilon = 3.5 - j1$, $\epsilon = 3.5 - j4.8$, $\epsilon = 3.5 - j5.4$ and $\epsilon = 3.5 - j5.8$ are applied. The data are taken at 2.5 GHz. White Gaussian noise is introduced with signal to noise ratio 40 dB

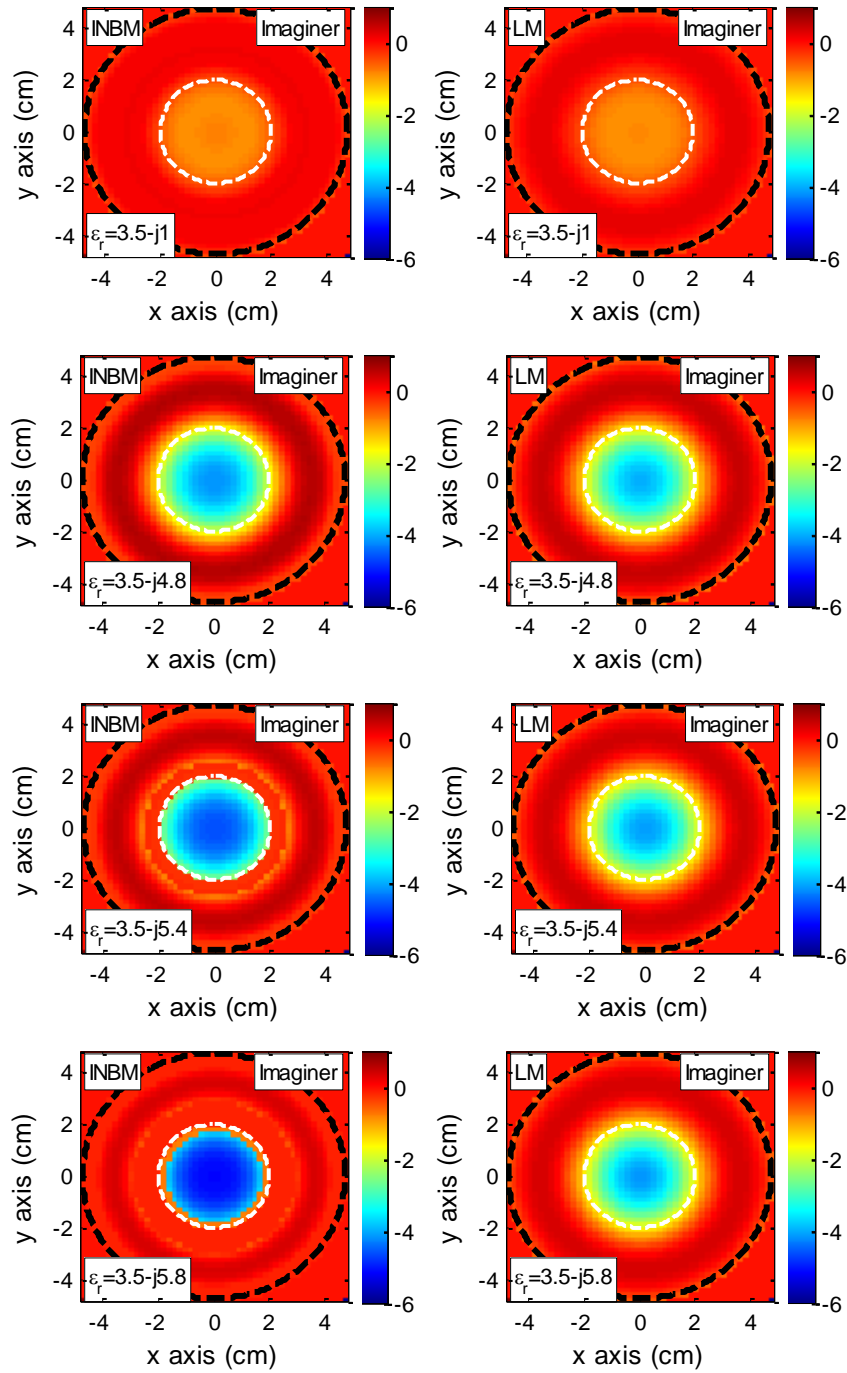


Figure 6-9: The imaginary part of reconstructed images using INBM and LM algorithms. Four different cylindrical OI with radius 2 cm and permittivity $\epsilon = 3.5 - j1$, $\epsilon = 3.5 - j4.8$, $\epsilon = 3.5 - j5.4$ and $\epsilon = 3.5 - j5.8$ are applied. The data are taken at 2.5 GHz. White Gaussian noise is introduced with signal to noise ratio 40 dB

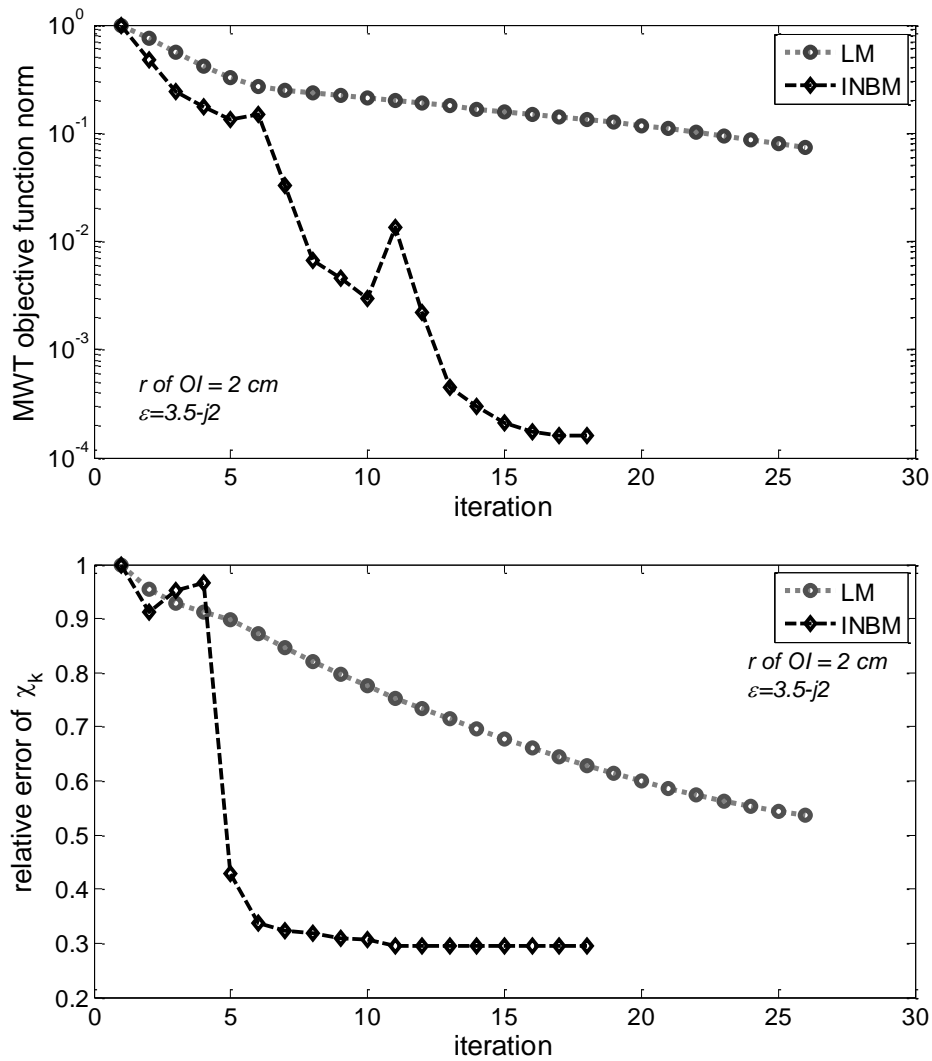


Figure 6-10 The parameter of iterative solutions for INBM and LM algorithms for solving the MWT inverse problem of homogeneous lossy object a) relative norm of objective function b) relative error of the dielectric contrast of OI.

INBM produces better images. The shape and the value of the parameter of INBM result is closer to the target value than that resulted by the LM algorithm. The INBM produces good images of a high lossy cylindrical object. In contrast, the LM suffers from a high imaginary part of OI permittivity. INBM produces a stable solution of MWT inverse problem of lossy material when LM fails.

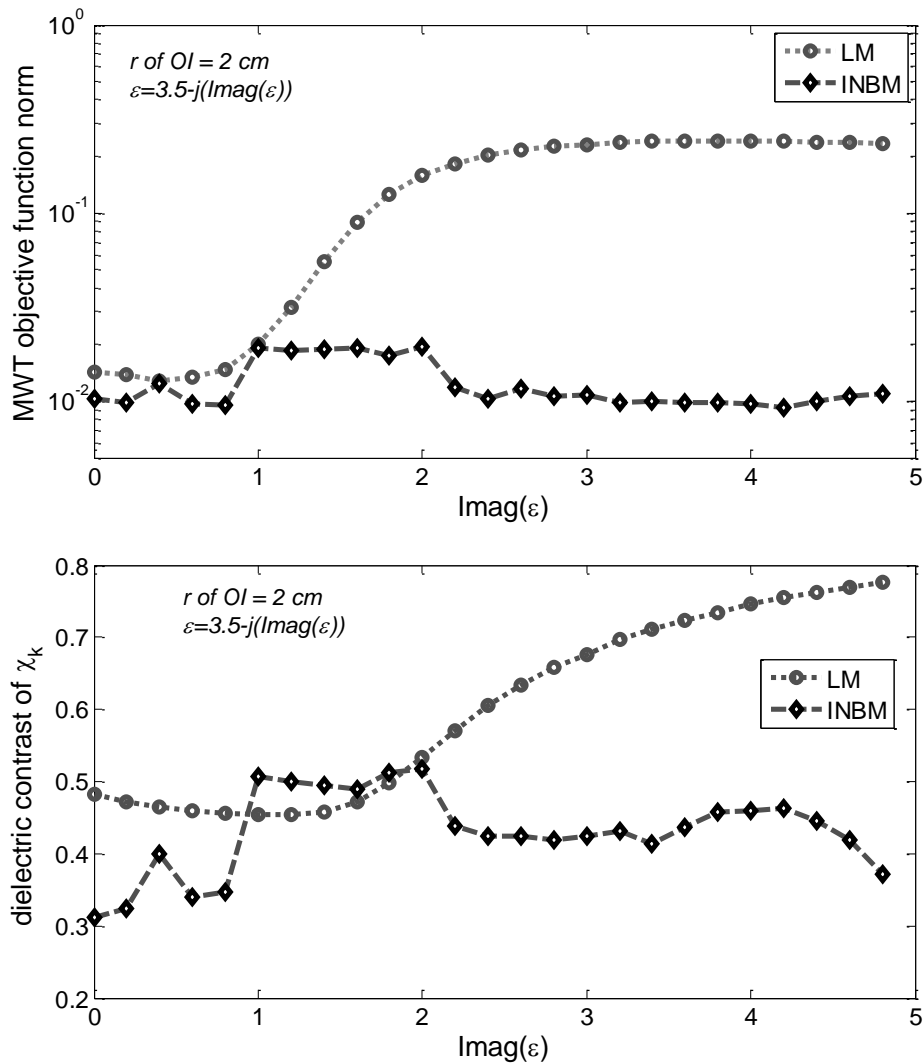


Figure 6-11: The effect of the imaginary part of the complex permittivity to the results of INBM and LM algorithms. The parameters of the solutions are a) MWT objective function norm b) the relative error of the dielectric contrast. The parameters are plotted with respects to the imaginary part of the complex permittivity of OI.

The parameters of iterations are presented in Figure 6-10. It can be seen that the application of INBM offers a tradeoff between the accuracy with which the Newton equations are solved in the amount per work per iterations. The number of the outer iterations to get the global result is reduced by more than a half, besides the accuracy of the result is improved by more than 20%. The graph of the parameters shows that the relative norm of the objective function of INBM declines faster than that of LM algorithm and the line of

the relative errors of INBM is lower than that of the LM. Based on the parameter of the solutions, the INBM for solving the MWT inverse problem is better than the LM algorithm.

The effect of the value of the imaginary part ($Imag(\varepsilon)$) of complex permittivity of the OI is done by reconstructing series of noisy data of the MWT problem of a lossy object. $Imag(\varepsilon)$ varies from 0 to 5 while the real part $Re(\varepsilon)$ of complex permittivity is kept constant $Re(\varepsilon) = 3.5$.

Figure 6-11 shows that the value of $Imag(\varepsilon)$ influences the relative norm of MWT-objective function of LM. The relative norm increases as the value of $Imag(\varepsilon)$ rises. The effect of $Imag(\varepsilon)$ value to LM results is also seen in the relative error of the dielectric contrast graph. The error rises along with the increase of the value of $Imag(\varepsilon)$. On the other hand, the parameters of INBM solutions are relatively unaffected by the high value of $Imag(\varepsilon)$. The lines of the relative norm of the MWT objective function and the relative error of INBM solutions are relatively flat over $Imag(\varepsilon) = 0$ to $Imag(\varepsilon) = 5$. The INBM produces a stable solution of the MWT inverse problem of a simple lossy material

6.5.2 Dielectric tube model for INBM test

The MWT system which is used in the previous sections is applied to generate the MWT data of the dielectric tube model. The MWT data are measured at 16 antennas around the OI. The working frequency is 2.5 GHz. 40 dB white Gaussian noise is added to the data.

The OI is a cylindrical dielectric tube. The inner and outer radiuses of the tube are 3 cm and 4.75 cm, respectively. There are two models of the dielectric tubes, which are a dielectric tube in free space and a tube containing a lossy material. The models are presented in Figure 6-12.

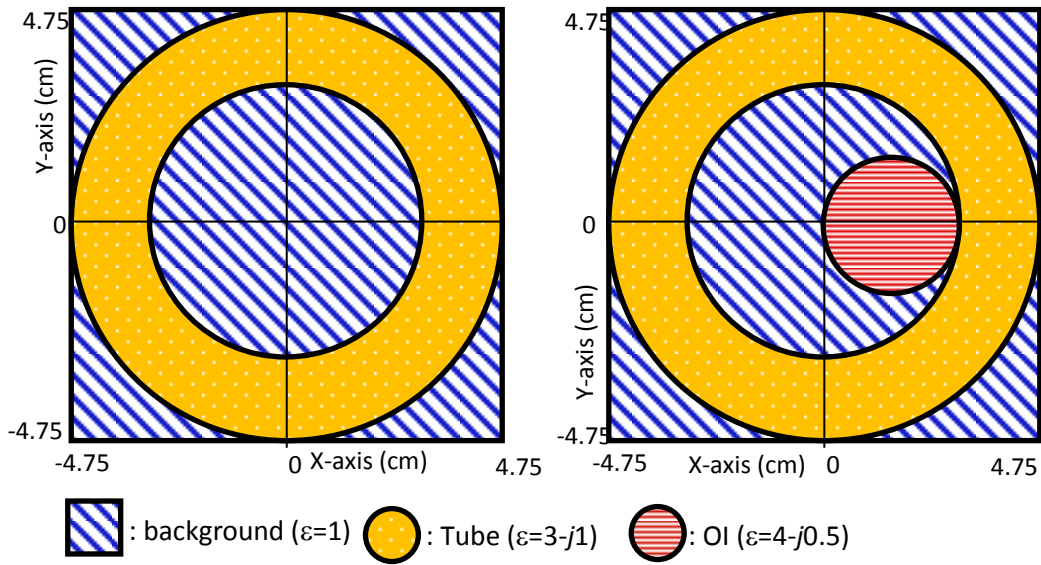


Figure 6-12: the Architecture of a dielectric tube model for INBM test. A) the Dielectric tube is placed in a free space. B) the dielectric cylinder is placed inside dielectric tube.

The data are reconstructed using INBM and LM algorithms. The results of the reconstruction are presented in the images of $Real(\epsilon)$, $Imag(\epsilon)$ and $Abs(\epsilon)$. The reconstructed images of the dielectric tube model A are presented in

Figure:6-13. It can be seen that the INBM produces better images than the LM algorithm. The shape of the tube in the images resulted by INBM are clearly reconstructed. INBM defines the value of the tube complex permittivity closer than LM algorithm does.

The images of the dielectric tube model B resulted using INBM and LM algorithms are presented in Figure:6-14. It can be seen that the introduction of a dielectric lossy material inside the tube influences the reconstructed images. The shape and the dielectric value of the tube are disturbed by the presence of different materials. The accuracy of the images resulted by INBM is better than that resulted by LM algorithm. INBM draws the cylinder lossy material well when LM fails to define the shape and position of the material.

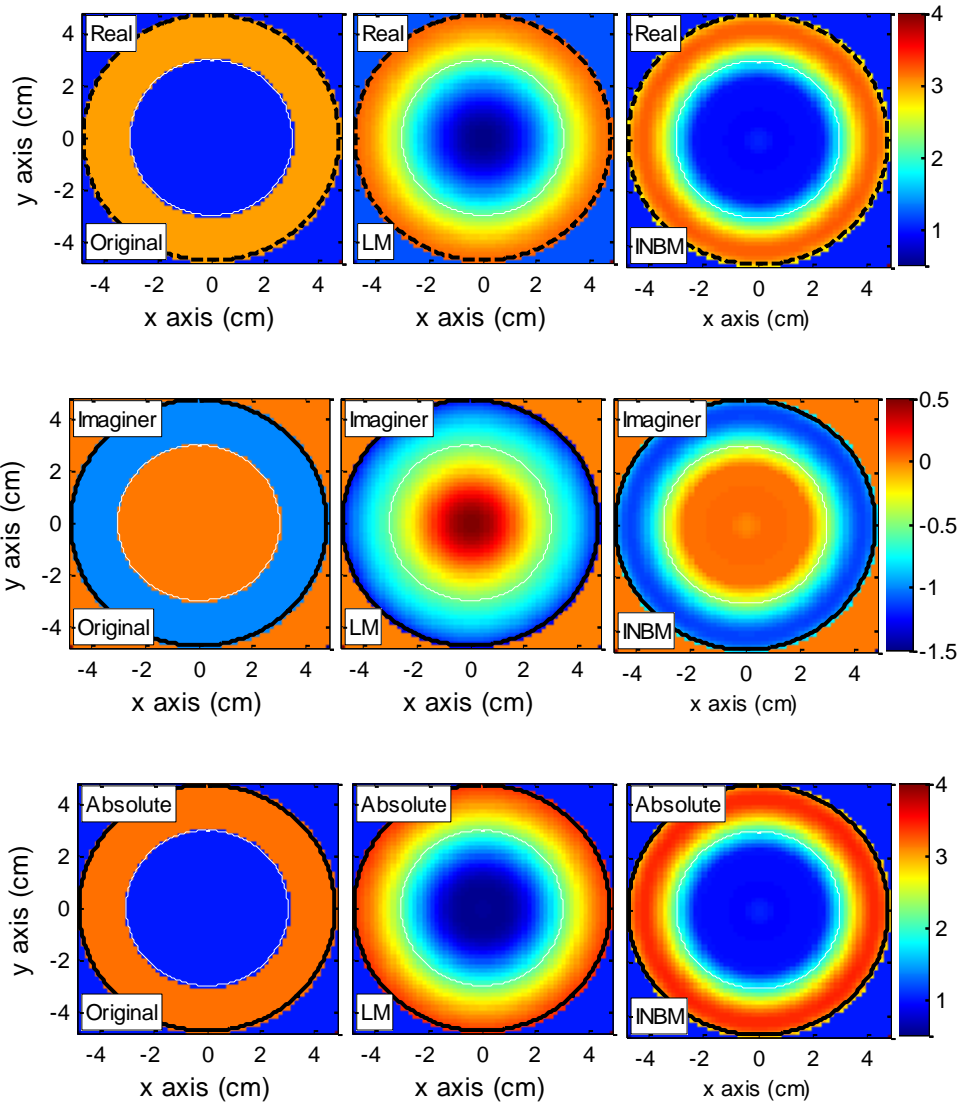


Figure:6-13: The reconstructed images of the dielectric tube model A. The OI is presented in the images of $Real(\epsilon)$, $Imag(\epsilon)$ and $Abs(\epsilon)$. The images are resulted using INBM and LM algorithms.

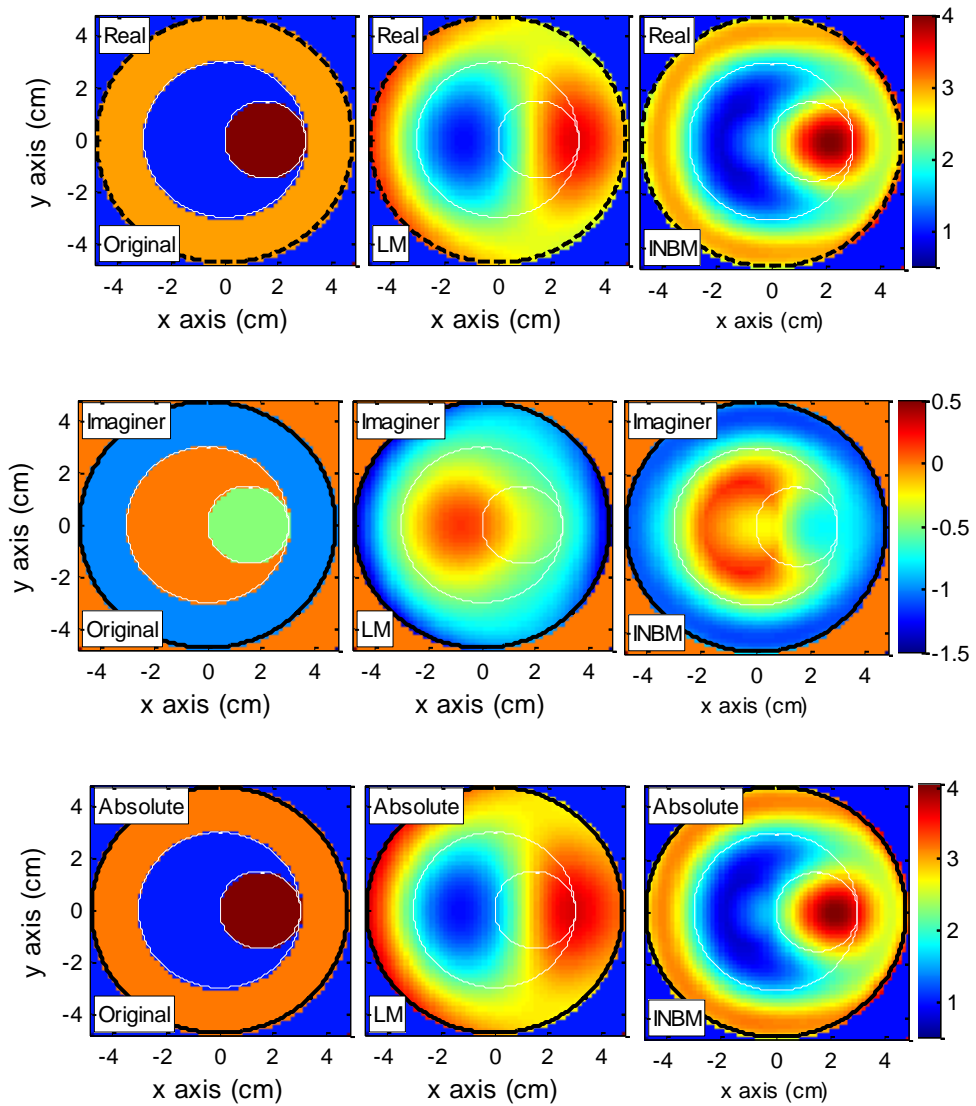


Figure:6-14: the reconstructed images of the dielectric tube model B. The OI is presented in the images of the real part and imaginer part of complex permittivity. The images are resulted using INBM and LM algorithms

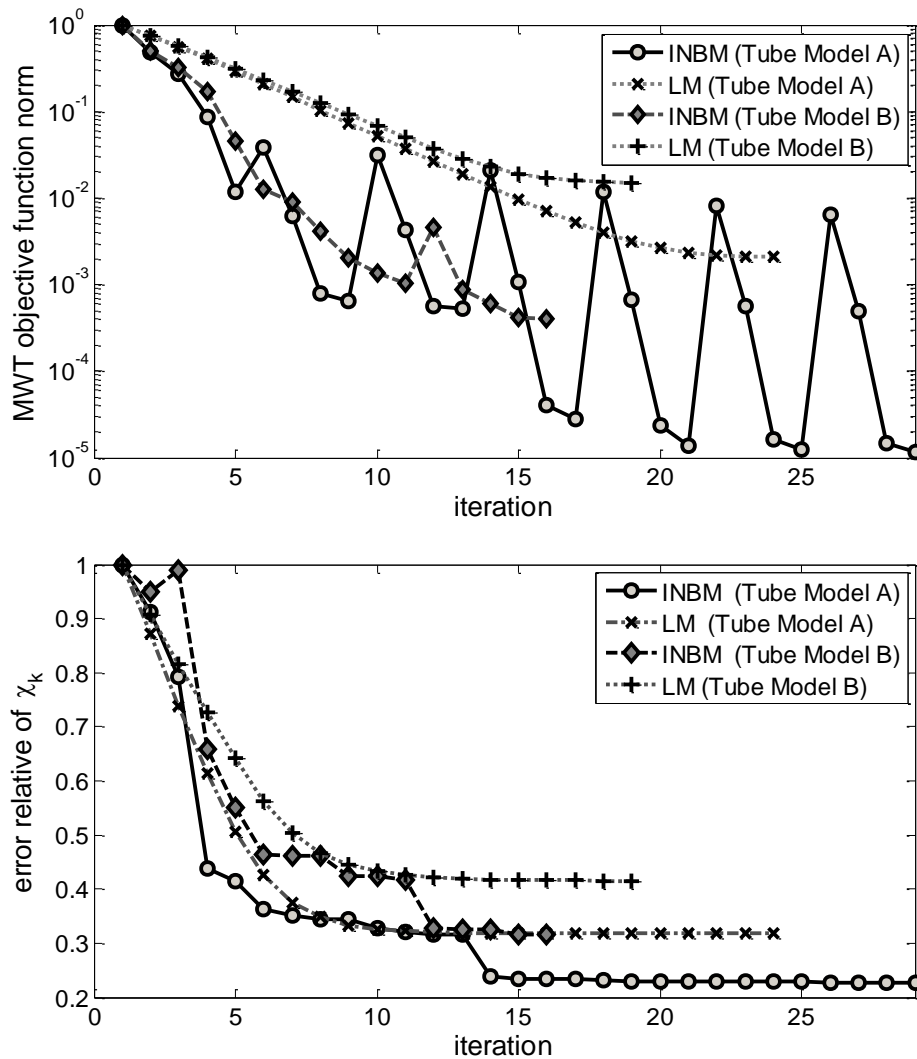


Figure 6-15: The parameter of iterative solutions of INBM and LM algorithm for solving MWT inverse problem of the dielectric tube model a) the relative norm of the objective function b) the relative error of the dielectric contrast of OI.

The unspecific solutions of MWT linear problems in INBM algorithm upgrade the accuracy of the MWT inverse problem solutions. The accuracy of MWT INBM solutions are 22% and 31% for tube model A and model B problems, sequentially. These improve the LM solutions by 10%. The norms of INBM objective function are 1.16×10^{-5} for tube model A and 4.05×10^{-4} for tube model B. These are better than those resulted by the LM algorithms which are bigger than 1×10^{-3} . The application of INBM to

dielectric tube containing different material improves the accuracy and the speed of the LM algorithm.

6.5.3 Human arm model

A synthetic model of human forearm is considered as OI of MWT inverse problem. The model consists of bone, cortical bone, muscle and skin. The complex permittivity of the material is listed in Table 6-7. The images of the 2D arm model are shown in Figure 6-16. There are two types of models, which are centred circular bone and off centre bone. The OI is immersed in the liquid background which has permittivity constant 77.3. The cross section of the object domain is divided into 2500 cells. The domain which is squared in shape is immersed in a liquid background medium. The circular shaped human arm model is placed inside the object domain.

The MWT system which has 16 antennas is considered. The antennas are placed around the object with radius 6.5 cm. Each antenna is arranged to transmit and receive 1.5 GHz microwave signal sequentially in order to create a set of a multi view projection with the OI remaining static. Measured scattered data is developed by solving a direct scattering problem of MWT. The data which is added with 40dB white Gaussian noise is reconstructed using INBM and LM algorithms.

The reconstructed images of a human arm model-A which is bone-centered using INBM and LM algorithms are presented in Figure 6-17. It can be seen that the images of imaginary part of the OI model are better than the real part. The bone is clearly distinguished from the muscle. However, the skin is hard to separate from the muscle, besides the border of cortical bone is fuzzy. The images of the real part are worse than those of the imaginary part. The real part of skin and cortical bone are hard to see. The contrast of $Re(\epsilon)$ of skin with respect to muscle is higher than the contrast of $Imag(\epsilon)$ of the same material, but it still cannot be defined based on the images. It is due to the effect of $Imag(\epsilon)$ to the images of real part of OI complex permittivity.

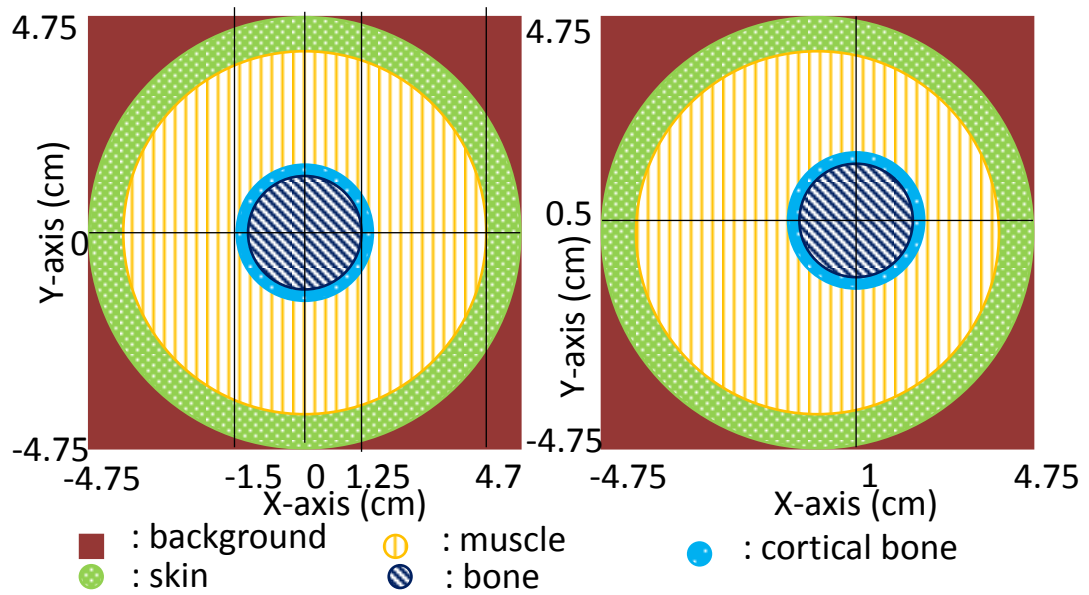


Figure 6-16: Two-dimensional models of human arms a) centered bone (left) b) off center bone (right)

Table 6-7: Complex permittivity materials of a synthetic model of a human forearm

Material	Complex permittivity
Bone	$5.5 - 0.55j$
Cortical Bone	$12.6 - j2.4$
Muscle	$54.8 - j13$
Skin	$39.4 - j12.9$
Background	77.3

INBM produces better solution of MWT inverse problem of a human arm model than LM does. The relative error of the dielectric contrast resulted by the INBM is 23.5% which is lower than that produced by the LM. INBM reconstructs a better image of bone than the LM. The shape and position of bone are clearly defined, while LM fails to define the shape of bone in the real part image.

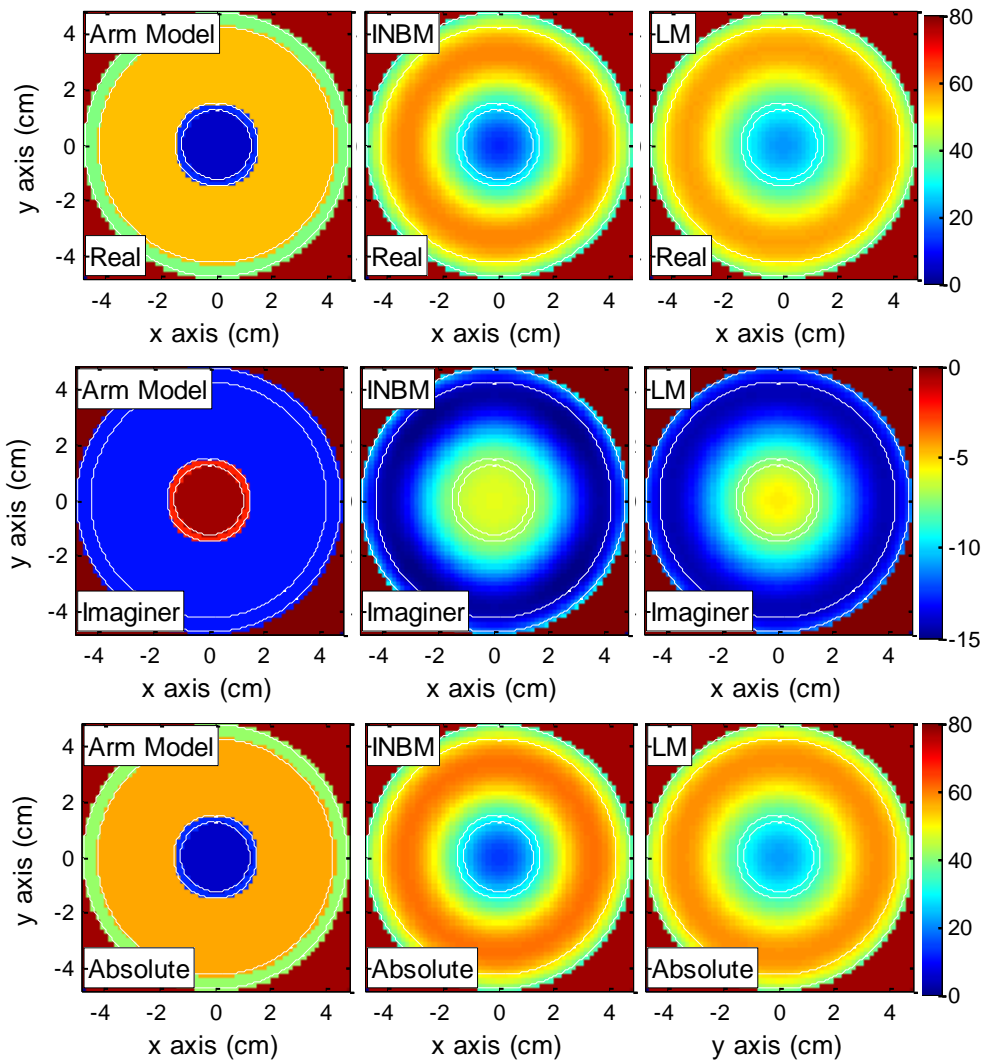


Figure 6-17: The images of a human arm model A (centered bone) resulted using INBM and LM algorithms.

The images of a human arm model-B which is off center bone resulted by INBM and LM algorithm are presented in Figure 6-18. It can be seen that the images of the real part are not as good as those of the imaginary part. In the real part images, the position of the bone is relatively defined, but the size and shape of the bone are missed. On the other hand, the image of the bone is well defined in the images of the imaginary part. The position is well defined and the size is relatively close to the target OI.

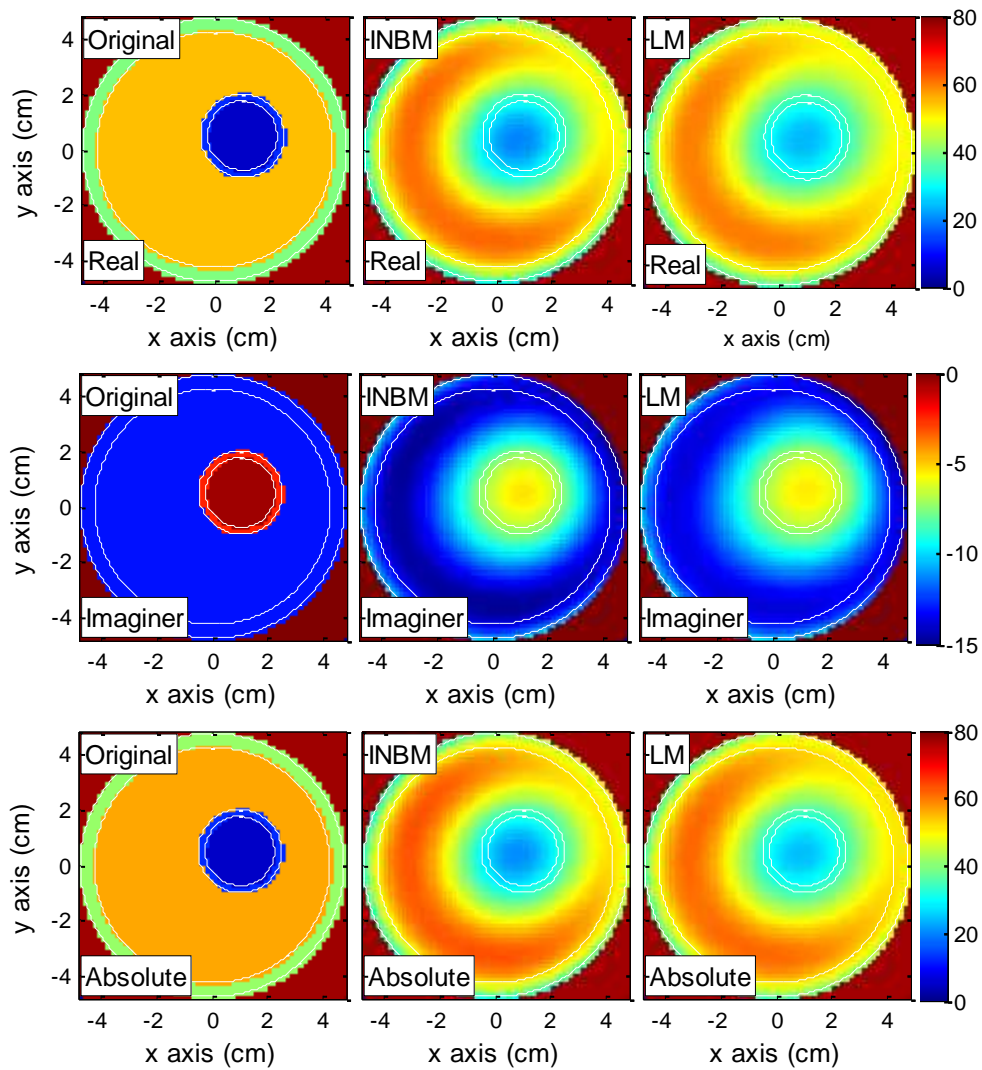


Figure 6-18: the images of a human arm model B (off center bone) resulted using INBM and LM algorithms.

INBM performs better in solving MWT inverse problem of human arm model than LM algorithm. The position and shape of the material of the arm can be defined using INBM, especially the bone and the muscle. The value of permittivity computed using INBM is closer to the target value than that of LM algorithm. The relative error of the dielectric properties of INBM is 27.8% , which is lower than the error s of the LM.

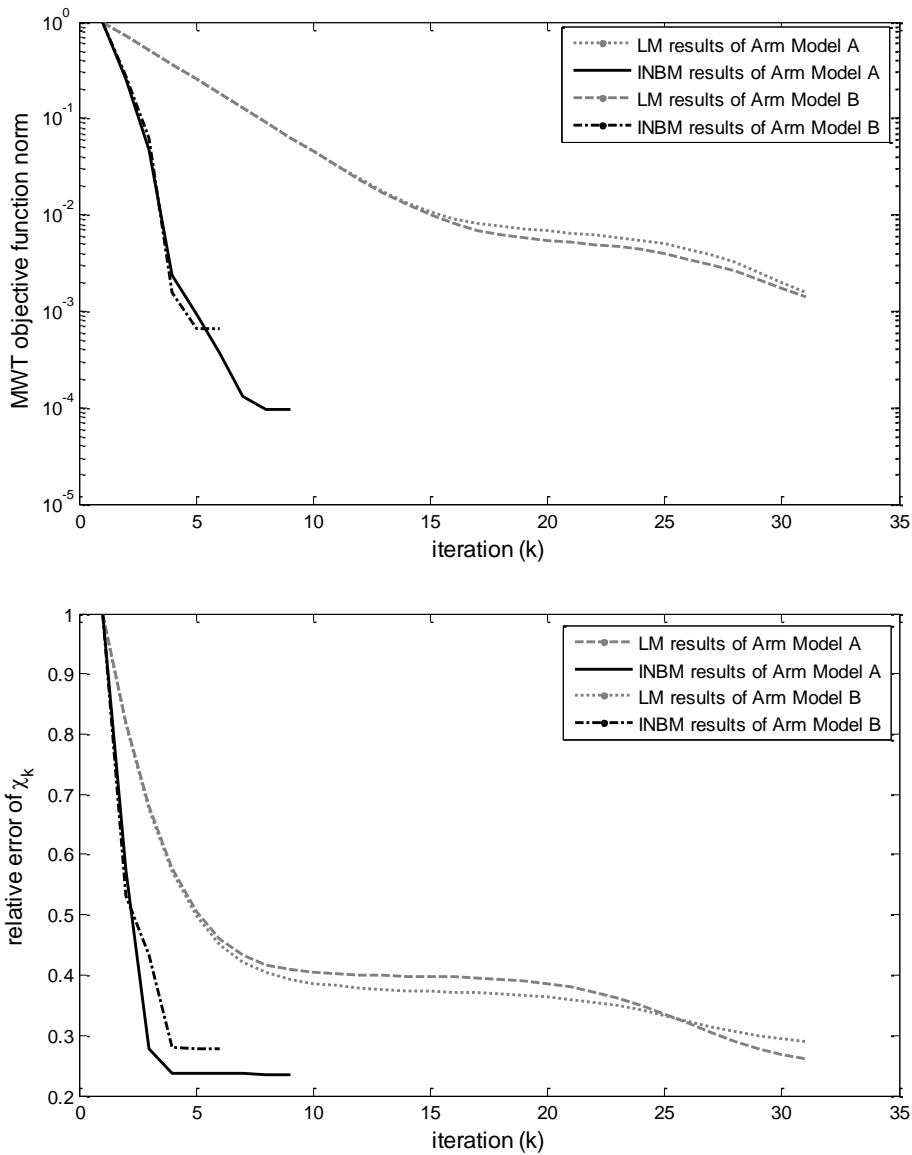


Figure 6-19: The parameter of iterative solutions for INBM and LM algorithms for solving the MWT inverse problem of the human arm model a) the relative norm of the objective function b) the relative error of the dielectric contrast of OI.

6.6 Conclusions

INBM has been developed to solve the MWT inverse problem. It is a Newton Iterative which is done in two stages. 1) linearizing the inverse problem by means of Frecher derivative. This step is the Newton method scheme which is

done at the outer loop; and 2) solving the linear Newton equations which are ill posed. This is the use of iterative method where a nonzero forcing term is applied to control the iteration in unspecific manner.

The INBM has been applied to solve the MWT inverse problem of lossless and lossy objects. The noisy data used is generated by solving the direct scattering problem and added with white Gaussian noise. INBM produces a better solution for the problem of lossless OI than LM. It is also faster than LM. The flexibility of INBM in solving the linear problem of Newton equations is determined by the choice of the forcing terms and the regularization. The level of accuracy of INBM is determined by the choice of forcing terms while the technique of regularization determines the intermediate solution of Newton equations. The accuracy and the amount of work to solve MWT inverse problem is better than that of the LM algorithm. The solution of INBM has a negative effect from the introduction of imaginary part of complex permittivity of OI. However, the quality of INBM in solving lossy object problem is still better than that of the LM algorithm

7

Newton Iterative – Conjugate Gradient on Normal Equation

Newton Iterative-conjugate gradient on normal equation (NI-cgne) is developed for Microwave Tomography application. The method is a Newton method for solving nonlinear problems, which is formulated in the outer and inner loop scheme. The outer loop is a Newton minimization of the problem and the inner loop is the application of conjugate gradient on normal equation for solving Newton equations. The method proposed is tested to solve MWT inverse problems which include the problems of lossless material, lossy material and human arm model. The quality of the proposed method is evaluated by comparing the results of NI-cgne with the results of the direct iterative regularization method by means of Levenberg Marquardt method.

7.1 Newton Iterative

The MWT inverse problem is a nonlinear problem. It can be stated as minimization of the MWT objective function relative norm

$$[\mathcal{X}] = \min_{\mathcal{X}} \|F([\mathcal{X}])\|_{\mathcal{D}}^2 \quad (7.1)$$

The iterative solver proposed is a Newton type algorithm. The iterative solution is updated in the current actual solution ($[\mathcal{X}]_k$) by a correction step which is also known as the direction of Newton (\mathbf{s}_k).

$$[\mathcal{X}]_{k+1} = [\mathcal{X}]_k + \mathbf{s}_k \quad (7.2)$$

The iterative step of Newton method is computed via linear Newton equation. The linear system of Newton equation is constructed using linearization by means of Fréchet derivative. For multiple illuminations of the MWT system, the Newton equation of MWT inverse problem is stated as

$$[\mathbf{D}]_k \mathbf{s}_k = F([\mathcal{X}]_k) \quad (7.3)$$

where Fréchet derivative of the MWT inverse problem which is denoted by $\mathbf{D} = F'$ is defined as

$$\mathbf{D} = \left[F'_{ij} = \left(\frac{\partial F_i(\mathcal{X})}{\partial \mathcal{X}_j} \right) \right]_{\substack{1 \leq i \leq m \\ 1 \leq j \leq n}} \quad (7.4)$$

The stationary point of F which is the optimum solution of (7.1) is a point $[\mathcal{X}]_k \in \mathbb{R}^n$ where \mathbf{s}_k does not exist such that

$$\|[\mathbf{D}]_k^* [F([\mathcal{X}]_k) + \mathbf{D}_k \mathbf{s}_k]\|_{\mathcal{D}}^2 < \|[\mathbf{D}]_k^* F([\mathcal{X}]_k)\|_{\mathcal{D}}^2 \quad (7.5)$$

This includes the local minimizer of $\mathcal{F}([\mathcal{X}])$. This procedure is done in the *outer loop* of Newton iterative.

Assuming that \mathbf{s}_k^δ is the exact solution of the Newton equation which minimizes the residue of the noisy problem

$$\begin{aligned} \|[\mathbf{D}]_k [\mathbf{s}_k^\delta - \mathbf{s}_k]\|^2 &= (\mathbf{s}_k^\delta - \mathbf{s}_k)^* [\mathbf{D}]_k^* [\mathbf{D}]_k (\mathbf{s}_k^\delta - \mathbf{s}_k) \\ &\quad ([\mathbf{D}]_k \mathbf{s}_k^\delta - [\mathbf{D}]_k \mathbf{s}_k)^* (\mathbf{D}_k \mathbf{s}_k^\delta - \mathbf{D}_k \mathbf{s}_k) \\ (F([\mathcal{X}]_k) - [\mathbf{D}]_k \mathbf{s}_k)^* (F([\mathcal{X}]_k) - [\mathbf{D}]_k \mathbf{s}_k) &= \|\mathbf{r}\| \end{aligned} \quad (7.6)$$

Then, the solution of the Newton equation is the minimizer of the residue norm.

$$\mathbf{s}_k = \min_{\mathbf{s}_k} \|F([\boldsymbol{\chi}]_k) - [\mathbf{D}]_k \mathbf{s}_k\|^2 \quad (7.7)$$

which is done in the *inner loop* of NI-cgne.

The iterative scheme of NI-cgne is conducted in the outer and inner loops in which the sequence of the process can be summarized in the following algorithm.

```

Algorithm 7-1NI-cgne: Newton Iterative with Conjugate gradient on
normal equation
Function NI-cgne([\boldsymbol{\chi}]_0)
Repeat NI
     $F([\boldsymbol{\chi}]) = [\mathbf{E}^s([\boldsymbol{\chi}]_0)] - [\boldsymbol{\varepsilon}^s]$ 
     $\mathbf{D} = \left[ \mathbf{F}'_{ij} = \left( \frac{\partial F_i(x)}{\partial x_j} \right) \right]_{\substack{1 \leq i \leq m \\ 1 \leq j \leq n}}$ 
    Repeat cgne
         $\mathbf{s}_k = \min_{\mathbf{s}_k} \|F([\boldsymbol{\chi}]_k) - [\mathbf{D}]_k \mathbf{s}_k\|^2$ 
    Until cgne_stopped(innerloop)
     $[\boldsymbol{\chi}]_{k+1} = [\boldsymbol{\chi}]_k + \mathbf{s}_k$ 
Until NI_stopped(outerloop)
Return ( $\boldsymbol{\chi}$ )

```

The number of the unknowns of the MWT inverse problems is large thus computing the exact solution of the Newton equation using the direct method like the LM can be expensive. Therefore, it seems reasonable to use a cheap and effective iterative method and to find the estimated solution of the Newton equation. The unspecified solution of Newton equation, in which the correction step of the Newton method \mathbf{s}_k follows the forcing term η_k , has been studied in the previous chapter under INBM algorithm. The \mathbf{s}_k is calculated using regularized methods, such as the truncated singular value decomposition, Landweber Friedman method (LF), and Tikhonov regularization. However, the regularizations need singular value decomposition which is expensive for a large scale matrix. In this chapter, conjugate gradient method (CG), as is used in [152; 153], is applied to solve Newton equations of MWT inverse problems. It is a semi regularized method

in which the regularization of the ill posedness is controlled using stopping criteria.

7.2 Conjugate Gradient on Normal Equation

The conjugate gradient on normal equation (cgne) is known as a semi-convergent method for solving asymmetric and ill posed systems as it has been described that the cgne regularizes and solves a non-symmetric positive definite linear system with a normal equation [154].

The cgne is developed to solve Newton equation of the MWT inverse problem which is generally asymmetric in the form of underdetermined and ill posed. It differs from the iterative regularization scheme operator (ψ) described in (6.2.1). The linear operator $\psi((\mathbf{D}_k^* \mathbf{D}_k), \alpha_k)$, which applies regularization, is defined as a normal equation. Then, regularized Newton equation for cgne purposes is transformed in a normal equation.

$$\mathbf{s}_k = \psi((\mathbf{D}_k^* \mathbf{D}_k), \alpha_k) [\mathbf{D}]_k^* F([\boldsymbol{\chi}]_k) \quad (7.8)$$

Where

$$\begin{aligned} \psi^{-1}((\mathbf{D}_k^* \mathbf{D}_k), \alpha_k) &= [\mathbf{D}^* \mathbf{D}]_k = [\mathbf{L}]_k \\ [\mathbf{L}]_k \mathbf{s}_k &= [\mathbf{D}]_k^* F([\boldsymbol{\chi}]_k) \end{aligned}$$

The operator $[\mathbf{L}]_k$ is assumed to be large. The application of singular value decomposition to get regulated solution is expensive. Therefore, conjugate gradient is applied as an alternative method.

The conjugate gradient method iteratively starts with the selection of a guess $\mathbf{s}_{k,0}$. The solution $\mathbf{s}_{k,l}$ at the l^{th} index is corrected according to

$$\mathbf{s}_{k,l+1} = \mathbf{s}_{k,l} + \gamma_l \mathbf{p}_l \quad (7.9)$$

where \mathbf{p}_l is the conjugate direction which is updated based on the gradient of the problem at the current solution q_l . According to the presentation on

normal equation, the gradient which is set as an update direction is defined as $\mathbf{q}_l = ([\mathbf{D}]_k^* F([\boldsymbol{\chi}]_k) - [\mathbf{L}]_k \mathbf{s}_k)$

$$\mathbf{p}_{l+1} = \mathbf{q}_l - \beta_l \mathbf{p}_l \quad (7.10)$$

where γ_l is the solution of scalar optimization problem

$$\gamma_l = \min_{\gamma} \| [\mathbf{D}]_k^* [F([\boldsymbol{\chi}]_k) - [\mathbf{D}]_k (\mathbf{s}_k + \gamma_l \mathbf{p}_l)] \|^2 \quad (7.11)$$

and coefficient (β_l) may be determined using Fletcher-Reeves formula

$$\beta_l = \begin{cases} 0, & l = 0 \\ \frac{\langle \mathbf{q}_l, \mathbf{q}_l \rangle}{\langle \mathbf{q}_{l-1}, \mathbf{q}_{l-1} \rangle}, & l \geq 1 \end{cases} \quad (7.12)$$

where $\langle \mathbf{A}, \mathbf{A} \rangle = \mathbf{A}^T \mathbf{A}$ is the inner product of vector \mathbf{A} . Another formula is Polak-Riniere which is expressed as

$$\beta_l = \begin{cases} 0, & l = 0 \\ \frac{\langle \mathbf{q}_l, \mathbf{q}_l - \mathbf{q}_{l-1} \rangle}{\langle \mathbf{q}_{l-1}, \mathbf{q}_{l-1} \rangle}, & l \geq 1 \end{cases} \quad (7.13)$$

The algorithm of the conjugate gradient on normal equation can be seen in Algorithm 7-2. The iteration starts with initial condition of $\mathbf{p}_0 = \mathbf{q}_0 = [\mathbf{D}]_k^* F([\boldsymbol{\chi}]_k)$ for $l = 0$. Then, the solution is updated according to the conjugate gradient procedure. The step of the conjugate gradient is determined using the minimization of residue norm (7.11). The residue norm is a convex system; thus, the minimization is $\nabla \phi = 0$, that is

$$\frac{d \| [\mathbf{D}]_k^* F([\boldsymbol{\chi}]_k) - [\mathbf{L}]_k (\mathbf{s}_k + \gamma_l \mathbf{p}_l) \|^2}{d\gamma} = 0 \quad (7.14)$$

which can be written as

$$\begin{aligned} \gamma \mathbf{p}_l^* [\mathbf{L}]_k \mathbf{p}_l - \mathbf{p}_l^* [\mathbf{D}]_k^* F([\boldsymbol{\chi}]_k) - \mathbf{p}_l^* [\mathbf{L}]_k \mathbf{s}_{k,l} &= 0 \\ \gamma \mathbf{p}_l^* [\mathbf{L}]_k \mathbf{p}_l &= \mathbf{p}_l^* [[\mathbf{D}]_k^* F([\boldsymbol{\chi}]_k) - [\mathbf{L}]_k \mathbf{s}_{k,l}] \\ \gamma &= \frac{\mathbf{p}_l^* [[\mathbf{D}]_k^* F([\boldsymbol{\chi}]_k) - [\mathbf{L}]_k \mathbf{s}_{k,l}]}{\mathbf{p}_l^* [\mathbf{L}]_k \mathbf{p}_l} \end{aligned} \quad (7.15)$$

This implies that $\gamma = 0$ then $\mathbf{s}_{k,l}$ is the solution of the normal equation. The conjugate gradient step for cgne is presented in the following algorithm.

Algorithm 7-2: CG: Conjugate gradient step
Function cg_step($[\mathbf{L}]_k, [\mathbf{D}]_k^* F([\mathcal{X}]_k), \mathbf{s}_{k,l}$)
If $l = 0$
 $\mathbf{s}_{k,0} = 0$
 $\mathbf{p}_0 = \mathbf{q}_0 = [\mathbf{D}]_k^* F([\mathcal{X}]_k)$
Else if
 $\gamma_l = \frac{\mathbf{p}_l^* [\mathbf{D}]_k^* F([\mathcal{X}]_k) - [\mathbf{L}]_k \mathbf{s}_{k,l}}{\mathbf{p}_l^* [\mathbf{L}]_k \mathbf{p}_l}$
 $\mathbf{s}_{k,l+1} = \mathbf{s}_{k,l} + \gamma_l \mathbf{p}_l$
 $\mathbf{q}_l = ([\mathbf{D}]_k^* F([\mathcal{X}]_k) - [\mathbf{L}]_k \mathbf{s}_k)$
 $\beta_{l+1} = \frac{\langle \mathbf{q}_l, \mathbf{q}_l \rangle}{\langle \mathbf{q}_{l-1}, \mathbf{q}_{l-1} \rangle}$
 $\mathbf{p}_{l+1} = \mathbf{q}_l - \beta_l \mathbf{p}_l$
End if
Return $\mathbf{s}_{k,l+1}$

It is important to check the direction of Newton solution. The evaluation is done by considering.

$$\mathbf{p}^T [\mathbf{L}]_k \mathbf{p} \leq 0 \quad (7.16)$$

where $[\mathbf{L}]_k$ is the approximation of the Hessian of the inverse problem in the form of normal equation. This is similar to the Hessian of the GNI. The failed direction is detected, then, cgne is stopped. The failed condition is avoided, then, the inner iteration proceeds to update the linear solution until a maximum iteration is reached or the stopping rule of the cgne is satisfied. The output of the inner iteration is the direction of the Newton scheme.

In the case of noise level is known

$$\|[\mathbf{D}]_k^* [F^e([\mathcal{X}]_k) - F([\mathcal{X}]_k)]\|^2 \leq \delta, \quad (7.17)$$

where $F^e([\mathcal{X}]_k)$ is an exact objective function containing exact data, and $F([\mathcal{X}]_k)$ is an objective function containing error measurement, noise and other disturbances, then, the most prominent stopping rule of the cgne is the

discrepancy principle. The solution of the linear problem is stopped when the residue of the linear system is comparable with the noise level

$$\|[\mathbf{D}]_k^* F([\boldsymbol{\chi}]_k) - [\mathbf{L}]_k \boldsymbol{s}_k\|^2 \leq C\delta \quad (7.18)$$

where C is a real positive number bigger than 1.

The algorithm of cgne with the discrepancy principle is stated as follows

Algorithm 7-3cgne : Conjugate Gradient on Normal Equation

Function cgne($[\mathbf{D}]_k, F([\boldsymbol{\chi}]_k)$)

Set $[\mathbf{L}]_k = [\mathbf{D}^* \mathbf{D}]_k$

$l = 0; \boldsymbol{s}_{k,0} = 0$

Repeat

$\boldsymbol{s}_{k,l+1} = \text{cg_step}([\mathbf{L}]_k, [\mathbf{D}]_k^* F([\boldsymbol{\chi}]_k), \boldsymbol{s}_{k,l})$

$l = l + 1$

Until $\|[\mathbf{D}]_k^* F([\boldsymbol{\chi}]_k) - [\mathbf{L}]_k \boldsymbol{s}_k\|^2 \leq C\delta$

Return $\boldsymbol{s}_{k,l}$

The cgne is very sensitive to the perturbation of the right hand side of the problem and often the noise enters iteration very quickly. The regularizing efficiency of the cgne depends on the effectiveness of the stopping rule. Nevertheless, the exact objective function is unknown. It is replaced by the noisy objective function. This makes the level of the noise cannot be determined. Therefore, the stopping rule of the cgne has to be determined without considering noise levels.

7.3 Stopping Rule of CGNE

The normal equation in MWT inverse problem is defined in $[\mathbf{D}]_k^* [\mathbf{D}]_k$ where $[\mathbf{D}]_k^*$ is the adjoint of $[\mathbf{D}]_k$ at $[\boldsymbol{\chi}]_k$. The operator $[\mathbf{D}]_k$ is nonsymmetrical. The operator $[\mathbf{D}]_k^* [\mathbf{D}]_k$ is the square but its condition is poor. The difference of the smallest singular value in a higher frequency and the highest singular value at a lower frequency is significantly big. The inverse of operator $[\mathbf{D}]_k^* [\mathbf{D}]_k$ is

unstable due to the higher frequency of the singular value. It has been discussed that by regulating the higher frequency, stable solution is gained. The application of Tikhonov regulator decreases the effect of the higher frequency of the singular value. A stable and accurate solution of the MWT inverse problems is resolved by setting the regulator in accordance with the iteration. Nevertheless, the introduction of noise brings the solution into semi convergence. The error increases when the level of noise is sufficiently big compared to the signal. It appears at the point where the scattered field as the measured signal is comparable to the level of noise. Besides that, the computational cost of the singular value of the system is expensive.

Empirically, the exact function which is written as,

$$[\mathbf{L}]_k \mathbf{s}_{k,l} = [\mathbf{D}]_k^* F([\boldsymbol{\chi}]_k) \quad (7.19)$$

is not defined and the exact solution \mathbf{s}_k^\dagger is not known. Furthermore, the approximated \mathbf{s}_k^* is considered as the solution of (7.17) in which the right hand side contains unknown terms like measurement error, noise and other disturbances. Furthermore, operator $[\mathbf{L}]_k$ is a normalized linear system of the MWT inverse problem, which is a large and ill conditioning matrix. For this reason, \mathbf{s}_k is computed iteratively in term of $\mathbf{s}_{k,l}$.

Iteratively, the solution is computed using a conjugate gradient method on normal equation. The solution of the linear problem at first iteration sequence $l = 1, 2, \dots, l_c$, ($\mathbf{s}_{k,l}$) usually moves toward the solution of the residue norm, which is

$$\mathbf{s}_{k,l} \rightarrow \mathbf{s}_k^* \quad (7.20)$$

where $\|[\mathbf{D}]_k^* F([\boldsymbol{\chi}]_k) - [\mathbf{L}]_k \mathbf{s}_{k,l+1}\|_2^2 < \|[\mathbf{D}]_k^* F([\boldsymbol{\chi}]_k) - [\mathbf{L}]_k \mathbf{s}_{k,l}\|_2^2$

The optimum solution is defined at l_c in which the error of the solution $\|\mathbf{s}_{k,l_c} - \mathbf{s}_k^*\|^2$ is minimum. The error increase for $l > l_c$ due to the influence of noise levels. Therefore, the stopping rule of the iteration needs to be designed to avoid the solution \mathbf{s}_{k,l_c+n} , where n is a real positive number.

The iteration should be stopped at the correct inner iteration index as the method starts to reconstruct the noise. The decreasing of the residue norm may not be similar to the reduction of the errors of the solution. The iteration could exceed the optimum point of the solution. The stopping rule is essential to the regularization of the cgne[155]. Therefore, several stoppings will be discussed in the following section. The rule is developed based on an unknown noise level. The flexibility of the rule is discussed by applying the method to noisy data.

7.3.1 Discrepancy principle

Considering that the MWT objective function suffers from noise, then, the iterative sequence has to be stopped before the noise governs the process of finding the solutions. In the case of the level of noise is known, then, the discrepancy principle can be used to design the stopping rule.

$$\|\mathbf{r}_k\|^2 = \|[\mathbf{D}]_k^* F([\boldsymbol{\chi}]_k) - [\mathbf{L}]_k \boldsymbol{s}_{k,l}\|^2 \leq \delta^2 \quad (7.21)$$

The inner iteration is stopped at the first index where the residue of the linear system is less than the noise level.

$$\frac{\|\mathbf{r}_k\|^2}{\delta} \leq C \quad (7.22)$$

The ratio of residue and noise level C is set to be bigger than 1. It is used to guarantee the reconstruction of the solution above the level of the noise.

The distance of inner solution $\boldsymbol{s}_{k,l}$ to the level of the noise depends on the position of the Newton method solution in the outer iteration. The corresponding Newton method and Newton equation in the inner iteration can be presented in the residue function. The direction of cgne relates to the residue term of the scheme. The residue is updated inside the inner iteration. Thus, the iteration can be monitored and stopped if (7.22) is satisfied.

The simplest rule to choose the stopping criteria sets the residue norm which equals to some upper bound related to δ^2 . Even though δ is not known, the iterative solution step for Newton equation has to be stopped

before the level of noise influences the solution. It can be assumed that there is a confident area in which the level of noise is less than the norm of the residue of the linear problem.

$$\rho = \sqrt{\mathbf{r}_k^T \cdot \mathbf{r}_k} < C\delta^2 \quad (7.23)$$

The solution of the linear problem is gained in the area

$$\rho_l \geq \tau\rho_0 \quad (7.24)$$

where $\tau < 1$.

Stopping rule generally is used at CG method in which the operator is positive definite and exact noise level is known [156]. The stopping rule is applied to the cgne to regularize the linear ill posed problem which suffers from noise. By choosing the correct τ , the linear ill posed problem can be regularized by avoiding the unstable solution. Lower value of τ opens the filter of the linear solution wider. At this set, the solution of $\mathbf{s}_{k,l}$ is closer to the approximated direction \mathbf{s}_k^* . The solution of the MWT inverse problem can be gained faster, but it is unstable. On the other hand, a bigger value of τ will stabilize the solution, but it takes more time than the previous set.

Algorithm 7-4 shows cgne with discrepancy principle for stopping rule. The constant τ is determined empirically.

Algorithm 7-4: cgne- τ : cgne with discrepancy Principle

Function cgne- τ ($[\mathbf{D}]_k, F([\mathcal{X}]_k)$)

Set $l = 0$; $\mathbf{s}_{k,0} = 0$

$$[\mathbf{L}]_k = [\mathbf{D}^* \mathbf{D}]_k$$

$$\rho_0 = \left\| [\mathbf{D}]_k^* F([\mathcal{X}]_k) - [\mathbf{L}]_k \mathbf{s}_{k,0} \right\|^2$$

Repeat

$$\mathbf{s}_{k,l+1} = \text{cg_step}([\mathbf{L}]_k, [\mathbf{D}]_k^* F([\mathcal{X}]_k), \mathbf{s}_{k,l})$$

$$\rho_{l+1} = \left\| [\mathbf{D}]_k^* F([\mathcal{X}]_k) - [\mathbf{L}]_k \mathbf{s}_{k,l} \right\|^2$$

$$l = l + 1$$

Until $\rho_l < \tau\rho_0$

Return $[\mathbf{s}_{k,l}]$

7.3.2 The application of NI-cgne- τ to solve MWT inverse problem

The INBM-CGNE with discrepancy principle as the stopping rule (NI-cgne- τ) is applied to reconstruct the MWT inverse problem. The object of interest is a dielectric disk with parameter $\varepsilon = 3 - j1$ and diameter 4.75 cm. There are two similar holes; which are centered at $(-2,0)$ and $(2,0)$. The radius of the hole is 1 cm. The OI is placed in a background medium with $\varepsilon = 1$.

It is assumed that a MWT system is constructed by 16 antennas which can be used as a microwave signal transmitter and receiver. The data is constructed by assuming that 16 Tx antennas sequentially illuminate 1.5 GHz microwave signal. The source of the signal is approximated as an equivalent infinitive current line. At each illumination, 16 Rx antennas measure the scattered electric field. Positions of Tx antennas are the same as the positions of Rx antenna, in which it is assumed that the reflection of electric field can be measured..

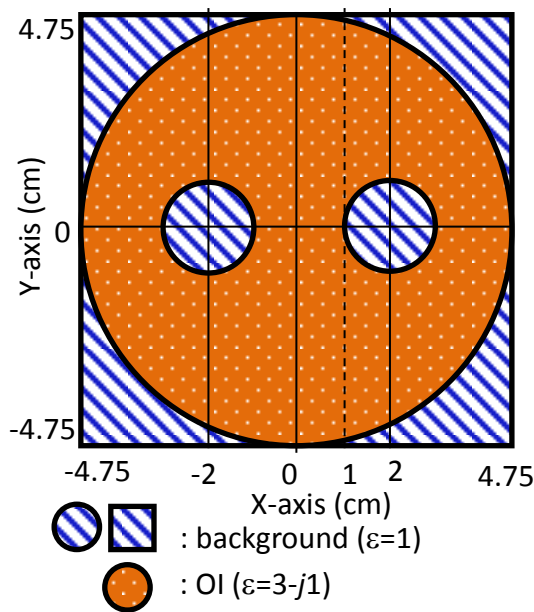


Figure 7-1: the two dimensional cross section of cylindrical dielectric object with two similar holes.

Table 7-1: the parameter of the simulated system for the numerical testing of Ni-cgne- τ method

Parameter	Value
Diameter of Object Domain(\mathcal{O})	9.5 cm
Diameter of Data Domain (\mathcal{D})	13.0 cm
Transmitting Antenna T_x	16 T_x
Receiving Antenna R_x	16 $R_x \times 16 T_x$
Number of data	256
SNR	40 dB
Number of cells	60 \times 60 = 3600
ϵ	3 - j1
Radius of OI	4.75 cm
Frequency	1.5 GHz

Total 256 data are collected on each set of MWT measurement. A random number which is assigned as introduced noise and any other additional errors are added to the data. Table 7-1 summarizes the parameter of MWT data measurement. The Ni-cgne- τ reconstructs the numerical synthetic data which is added with 40dB white Gaussian noise. The solution of the method is compared with the results of LM. The quality of the algorithm is studied using: the relative norm of the MWT-objective function and the relative errors of the value of the dielectric contrast of OI.

Figure 7-2 shows that the parameters of NI-cgne algorithm solution are better than that of LM algorithm. The MWT objective function norm and the dielectric contrast relative error resulted by NI-cgne decreases faster along iterations than the solution of Lm algorithm. The solutions of NI-cgne are better than LM solution. The objective function norm and the relative errors of NI-cgne solutions are lower than those of the LM solution, besides NI-cgne is faster than LM.

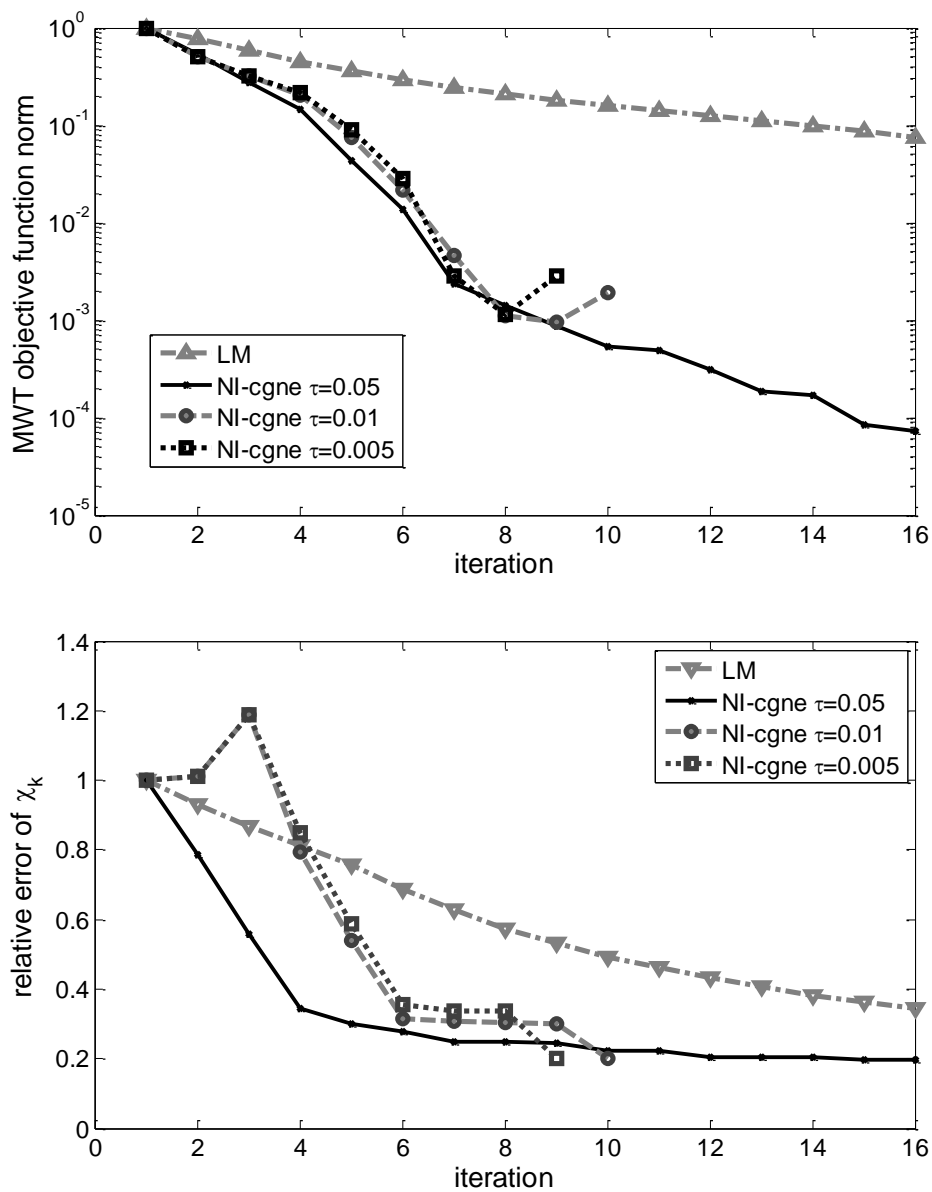


Figure 7-2: The parameters of MWT inverse problem solutions using NI-cgne and LM algorithm. The problem is a dielectric object with two circular holes. NI-cgne with discrepancy τ is applied. Three different discrepancy values $\tau = 0.05$, $\tau = 0.01$ and $\tau = 0.005$ are applied.

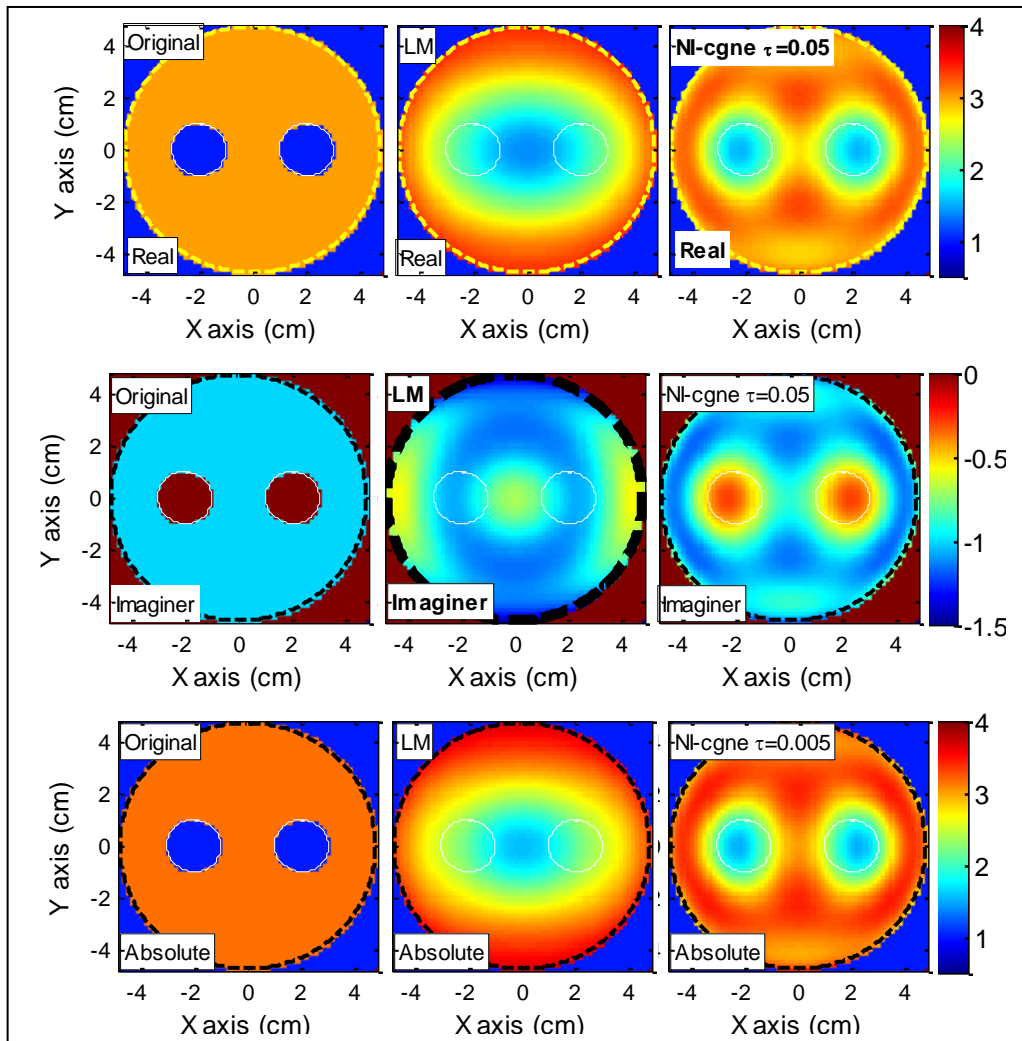


Figure 7-3: The reconstructed images of a dielectric lossy material with two circular holes. The $Real(\epsilon)$, $Imag(\epsilon)$ and $Abs(\epsilon)$ images are resulted using NI-cgne- τ and LM algorithms.

The images of permittivity of OI is presented in the image of $Real(\epsilon)$, $Imag(\epsilon)$ and $Abs(\epsilon)$ as seen in Figure 7-3. It can be seen that NI-cgne produces better images than LM algorithm. NI-cgne with $\tau = 0.005$ solves MWT inverse problem of cylindrical lossy object in 9 iterations with the dielectric contrast error less than 20%. The iteration is half of the iteration of LM method and the errors of solution are 10% less than that of the solution of LM method. The free space holes inside the dielectric cylinder are clearly seen on the images resulted by NI-cgne. On the other hand, LM method fails to describe the holes.

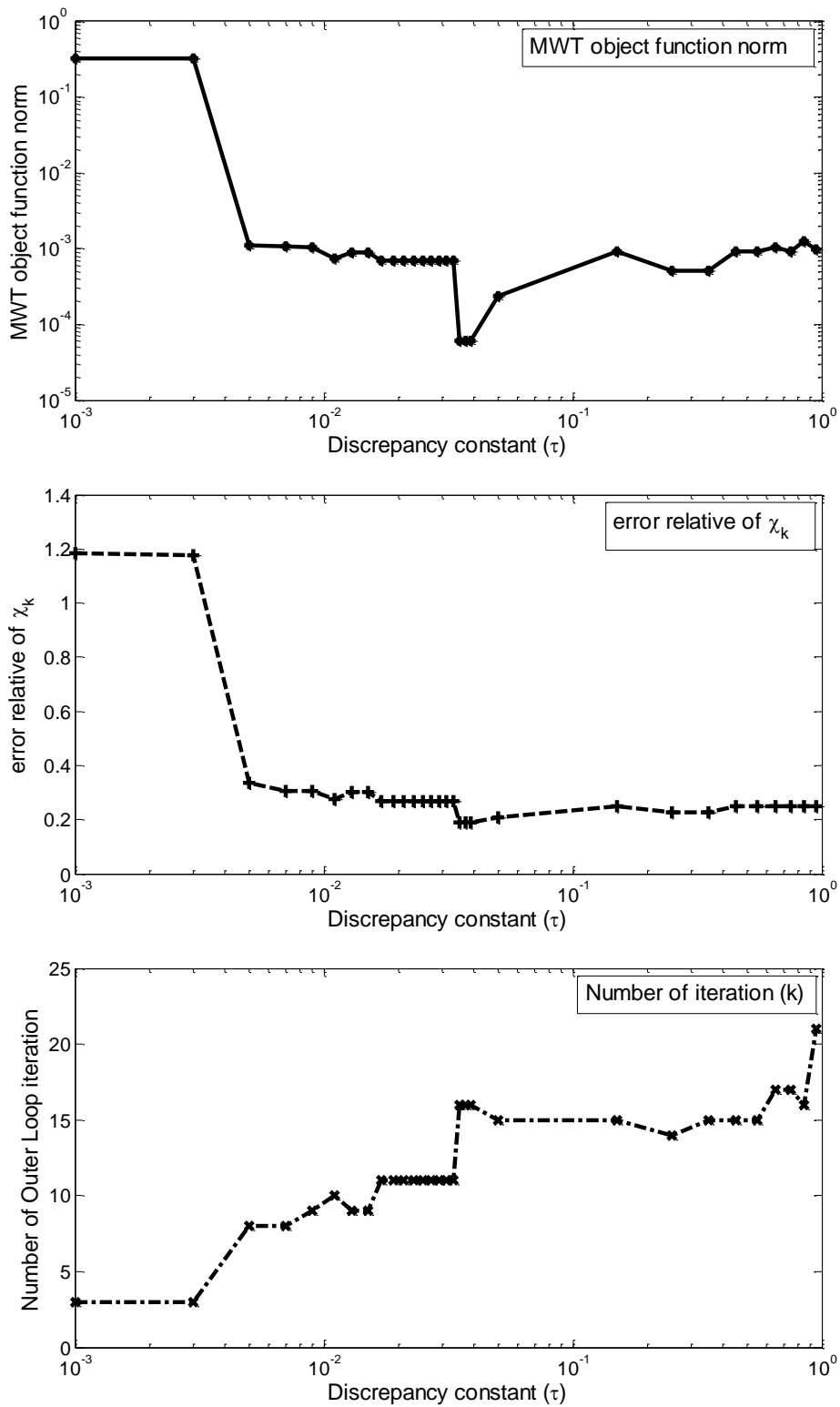


Figure 7-4: The graph or the parameters of solution with respect to discrepancy constant. The parameters are objective function norm, relative error of dielectric contrast and number of iteration k of the results of NI-cgne algorithm with scanning discrepancy criteria τ_k

The regularization of Newton equations is dependent on the proper stopping position of the inner iteration. It can be seen from Figure 7-2 that the selection of τ influences the accuracy and the speed of MWT inverse problem solution. Setting $\tau = 0.005$ for NI-cgne results in fast solution, but the accuracy of the solution is not as good as $\tau = 0.01$ set of NI-cgne. It can be seen that NI-cgne with the lower value of τ is fast, but it is less accurate than NI-cgne with high value of τ .

Further study of $\tau_k = c$ is done by setting a constant value for τ_k of NI-cgne and applying the algorithm to solve MWT inverse problem of cylindrical dielectric OI with free space holes in which the parameter of the problem is summarized in Table 7-1. The quality of the solution is studied through three parameters of the solution which are: the WMT objective function norm, the relative error of the dielectric contrast and the number of Newton method iteration (k). The results of the evaluation are presented in Figure 7-4.

.Figure 7-4 shows that the algorithm generally solves the MWT inverse problem, but it fails if the τ_k are too small ($\tau_k = c < 4^{-3}$). The accuracy of the solution is not affected by the choice of $\tau_k = c$ in which the relative errors of the dielectric contrast are between 20% to 30% and the MWT objective function norm is below 10^{-3} . On the other hand, the speed of the algorithm is influenced by the choice of $\tau_k = c$. Decreasing the value of τ_k improves the speed of the algorithm by more than a halve, however if the value of τ_k is too small, the algorithm fails to solve the problem.

The selection of τ is done empirically. The optimum regularization is hard to define using the discrepancy principle. The range of the ratio of the residue which is used to define the τ is varied among the outer iteration index(k). At a lower outer iteration index, a small value of τ is possible to be reached where it cannot be approached at a higher k . This makes the inner iteration terminated because the maximum number of iterations is reached. Therefore, the stopping rule for the NI-cgne needs to be defined by considering the noise level. One of the popular methods is L-curve technique.

7.3.3 L-curve criterion for regularizing linear ill posed problem

L-curve is a method for determining regularization parameter in solving ill posed problems proposed by Hansen [157; 158]. The choice of the regulator parameter is based on the plot of the residue norm with respect to the solution norm. Usually, the line of the graph is L shaped and the optimum value of the regularization is defined at the corner of the plot. The regularization is defined in a graphical approach. The minimization of the linear ill posed problem is described in the behavior of the least squared minimization problems in the form of normal equation. The regulator is defined by compromising the fitting of the data and the smoothing of the solution. Finding the corner of the L shaped curve can be used as the alternative solution to regulate the ill conditioning of the linear problems.

Let us refresh the application of the direct regularization by means of Tikhonov regularization to the linear ill posed problem of Newton equation (7.3). Regularized parameter α should be found to minimize the residue norm. In a normal system, Newton equation is defined as

$$\mathbf{s}_k, \alpha_k = \min_{\alpha_k, \mathbf{s}_k} \| [\mathbf{D}]_k^* F([\boldsymbol{\chi}]_k) - [\mathbf{D}^* \mathbf{D} + \alpha_k]_k \mathbf{s}_k \|^2 \quad (7.25)$$

which is equivalent to solving Euler equation

$$[\mathbf{D}]_k^* [\mathbf{D}]_k \mathbf{s}_k + \alpha_k \mathbf{s}_k = [\mathbf{D}]_k^* F([\boldsymbol{\chi}]_k) \quad (7.26)$$

where α_k is the regularization parameter which should be chosen, and a regularized solution which is written as \mathbf{s}_k that satisfies (7.23).

The regulated solution of the linear problem is solved using the pseudo inverse. The linear operator is constructed in singular value decomposition and the singular values of the system are filtered by means of Tikhonov regularization.

$$\omega(\sigma_i^2, \alpha^2) = \frac{\sigma_i^2 + \alpha^2}{\sigma_i^2} \quad (7.27)$$

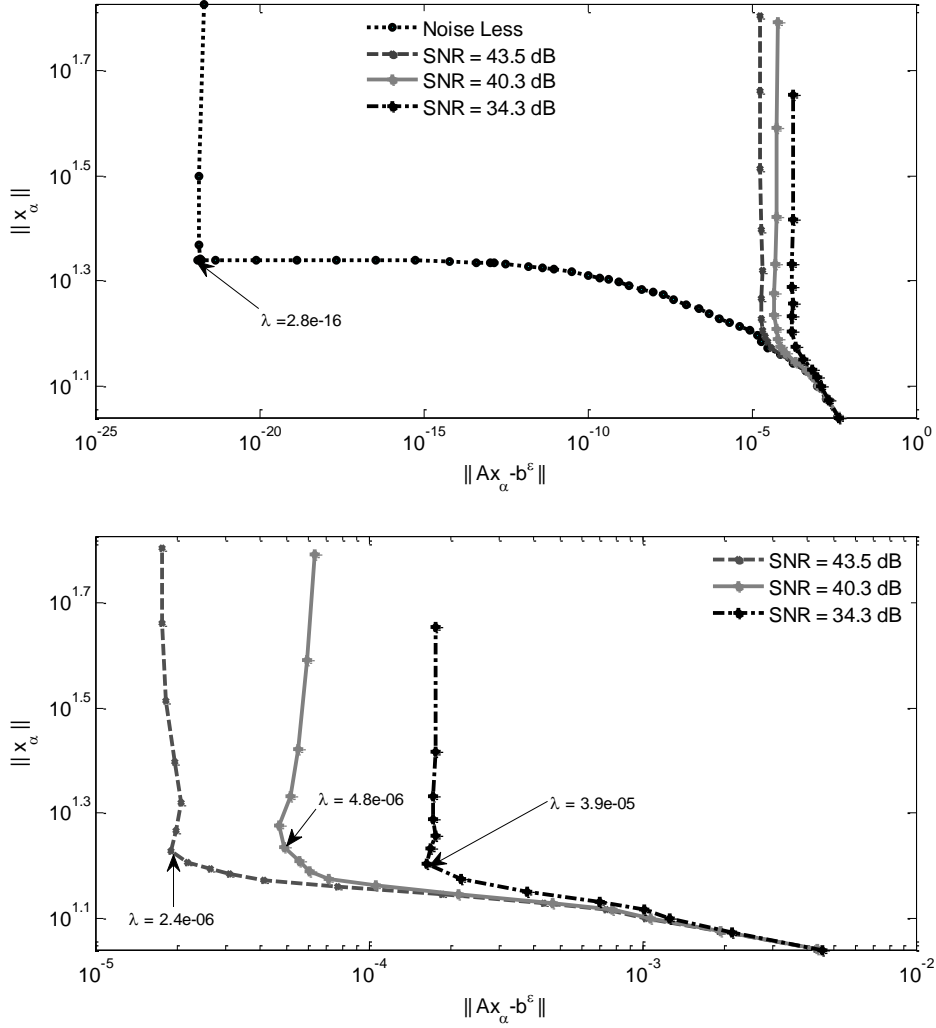


Figure 7-5: L curve criteria for continuous regularization parameter. Top: a discrete L curve for Tikhonov regularization of the linear ill posed problem of the first iteration of the nonlinear MWT inverse. Bottom: the part of the Tikhonov L-curve with noisy data for various SNR.

The function is minimized with Tikhonov regularization. The norm of associated solution is defined as

$$\rho(\alpha_k) = \|F([\mathcal{X}]_k) - [\mathbf{D}]_k \mathbf{s}_k\|^2 \quad (7.28)$$

$$\eta(\alpha_k) = \|\mathbf{s}_k\|^2 \quad (7.29)$$

The L-curve initial is introduced as $plot(\rho(\alpha_k), \eta(\alpha_k))$. There are two main characteristic parts of the curve, which are the flat part and the vertical part. In the flat area, the regularized solution is dominated by regularized errors

while in the vertical part, the solution, it is dominated by noise and other disturbances [158]. The optimum regularization is defined in the corner of flat and vertical parts. To define the corner, a corresponding curvature as a function of the regularization parameter is plotted based on $(\log(\rho), \log(\eta))$ plot. The suggested regularization parameter is the maximum point of the curvature.

The L-curve criterion is defined using log-log plot of the residue norm of the linear problem versus its solution norm. It can be seen in Figure 7-5 that the line of the log-log plot is L shaped for noise less and noisy data. The corner for all lines can be visually distinguished. The optimum regularization at the inner iteration step defined is dependent on the condition of the data. For noise less data, a very low regulator which is $\alpha = 2.8e - 16$, is added to gain the optimum solution. While much larger regulator is needed to get an optimum solution of the linear problem of data with SNR around 34 dB, which is $\alpha = 3.9e - 05$

For different positions of the iterative sequence, the corner of the lines can generally be located. The Tikhonov regulator can be set according to the ill conditioning of the linear system, as the parameter lies in between $\alpha \in (1, 0]$.

Regularizing the linear ill posed problem can be done by applying the iterative cgne. The iterative solution of the normal equation demonstrates semi convergence of the linear problem solution. Initially, the iterations approach the exact solution, then, it moves away from the target. The number of the inner iteration plays regularization for the ill conditioning of the linear ill posed problem. Different from Tikhonov regularization, the regulator parameter of the cgne cannot be adjusted, thus, it leads to a discrete L curve criterion. The number and position of the points on the log-log plot follows the iterative solution by the cgne.

Several algorithms have been reported for locating the corner of an L curve given by a finite set of points. In this section, the solution of the ill posed problem is the approximation of the Newton iterative step,

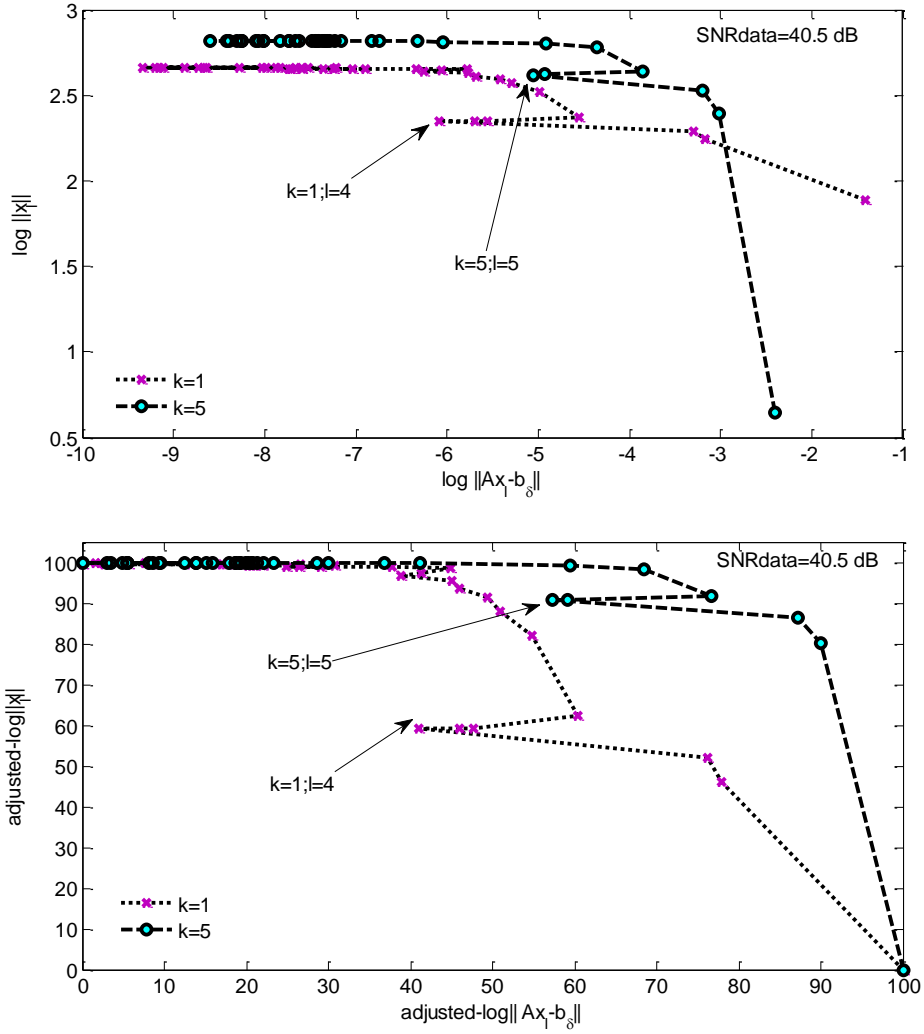


Figure 7-6: L curve criteria for discontinuous regulator parameter by means of CGNE.

Thus, the solution is expected under monotonicity condition on $\|\mathbf{s}_{k,l}\|^2$ which is strictly increasing with l and $\|F([\mathcal{X}]_k) - [\mathbf{D}]_k \mathbf{s}_{k,l}\|^2$ which is strictly decreasing with l is considered, while other points where any of the conditions are not satisfied are discharged.

A Triangle method is an algorithm to determine the corner of discrete L-curve. It is based on the geometrical idea of considering all the triangles formed by two fixing vertices and another scanned vertex. The candidate corner is determined using an angle of the triangle segments and its oriented

area [159]. Adaptive pruning algorithm is proposed in [160]. The basic idea of the algorithm is omitting the right amount of the points from the discrete L-curve which are not categorized as a corner candidate. A corner selector is based on angles between successive points in the line of curve. The selected corner is determined by the global behavior of the angles.

7.3.4 Discrete L-curve criterion

L-curve method has been successfully applied in various inverse problems [161]. However, under certain conditions, the L-curve method is not convergent. This occurs when the solution is rough [162] or with very smooth solutions [163]. The INI-cgne provides discrete regularization points. It is seen in Figure 7-6 that the log-log plot of the residue norm of the linear ill posed and its corresponding solution is fluctuated. The corner of the L curve is hard to define using a triangle or pruned method. An alternative method to define the “corner” of the L shaped graph is developed based on the angle between two vectors which are constructed from three selected points of data. This method is the simplification of the triangle method in which the prospective corner of L shape is based on the angle of the vector.

It is assumed that the points of the data to be examined are A, B and C . Point A is selected to be the most left position of the data points, which means that the data points with minimum residue norm are $\|F([\mathcal{X}]_k) - D_k \mathbf{s}_k\|^2$.

$$[A, N] = \min(\rho_l) ; \quad (7.30)$$

$$\rho_l = \|F([\mathcal{X}]_k) - [D]_k \mathbf{s}_{k,l}\|^2 \quad (7.31)$$

This point is also assigned as the maximum point data (N) to be examined. Point B is the potential corner to be examined, and C is the right vertex of the L curve. Due to the roughness of the data, pattern C is selected only for the first four data that is $C_n, n = 1, 2 \dots 4$, and B is evaluated at $B_m, m = n + 1, n + 2 \dots N - 1$.

Defining the pair of vectors which are \overrightarrow{BA} and \overrightarrow{CB} to be

$$\vec{BA} = X\angle x = \vec{A} - \vec{B} \quad (7.32)$$

$$\vec{CB} = Y\angle y = \vec{B} - \vec{C} \quad (7.33)$$

The angle of the vectors $\angle x$ and $\angle y$ are measured anticlockwise from the real positive axis. The prospected corner is defined from the difference of both angles of the vectors.

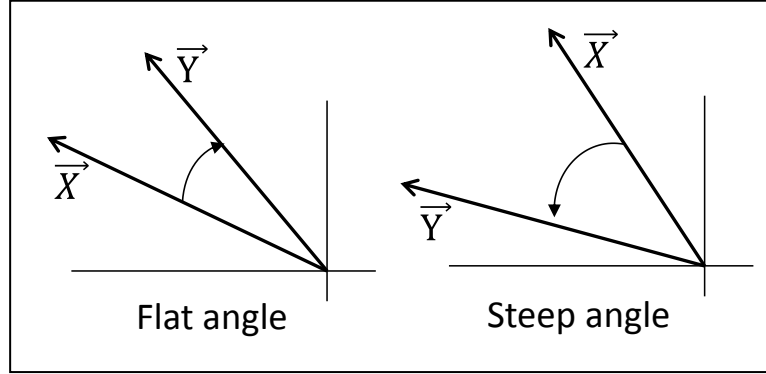


Figure 7-7: Angles between two vectors which construct the vertex of L-curve regularization

$$\theta = \angle y - \angle x \quad (7.34)$$

The point B is assigned as a prospected corner if the angle θ is positive, $\theta > 0$, which is categorized as the steep angle while the other is defined as the flat angle which is eliminated.

Algorithm 7-5: Lcurve : Lcurve regularization for cgne

Function Lcurve ($\rho_l = \|F([\mathcal{X}]_k) - [\mathbf{D}]_k \mathbf{s}_{k,l}\|^2, \eta_l = \|\mathbf{s}_{k,l}\|^2$)

Set

$$[N] = \min(\rho_l); A = (\log(\rho_N), \log(\eta_N)); B^* = 0$$

For $n = 1:4$

$$C = (\log(\rho_n), \log(\eta_n))$$

For $m = n + 1:N - 1$

$$B = (\log(\rho_m), \log(\eta_m))$$

$$X\angle x = \vec{A} - \vec{B}; Y\angle y = \vec{B} - \vec{C}$$

$$\theta = \text{find}((\angle y - \angle x) > 0)$$

$$B^* = \min \left| \theta - \frac{\pi}{2} \right|$$

End for m ; End for n

Return B^*

The algorithm for finding corner of the L-curve of the cgne is stated in Algorithm 7-5. The corner B^* is selected from set of θ which is closest to $\frac{\pi}{2}$ as

$$B^* = \min \left| \theta - \frac{\pi}{2} \right| \quad (7.35)$$

To protect from irregularities of the log-log plot, some considerations are proposed, which include:

1. *Determining of the steep angle of the corner of the curve*

B^* is assigned as steep corner is

$$\left| \theta - \frac{\pi}{2} \right| \leq \frac{\pi}{3} \quad (7.36)$$

2. *Defining regularized solution with Nil solution of angle between two vectors*

In the case of $\theta = []$ and $\forall(\angle y - \angle x) < 0$, then, the corner is defined at N or $B^* = N$. The inner loop reaches a maximum iteration, but it does not stretch the level of noise. The approximated regularized solution is defined in the last index of the inner iteration.

In the case of $\theta = []$ and $\text{not}(\forall(\angle y - \angle x)) < 0$, then, the corner is defined at 1 or $B^* = 1$. The pattern of the log-log plot is too rough or the angle of $Y \angle y$ vectors is too steep that it makes the difference of the vectors unsatisfied (6.100) thus, the corner cannot be defined properly.

3. *Normalizing the point data of the log-log plot*

To avoid the small difference between point data of the log-log plot, data are adjusted into $[0 \dots 100, 0 \dots 100]$ value. The plot is adjusted, thereto, it starts from $C_1 = (100,0)$ to $A = (0,100)$. The rest of the data are projected using an interpolation technique

$$\mathbf{x}_{new} = \frac{100(x_{old} - \min(x))}{\max(x) - \min(x)} \quad (7.37)$$

Projected data are rounded to the nearest integer to decrease the roughness of the curve pattern.

7.4 Numerical experiment

7.4.1 Dielectric tube model of NI-cgne test

MWT measurement setup is designed from 16 sources with 16 antennas which can be used as a transmitter and a receiver. The radius of antennas is 6.5 cm and the frequency of operation is 1.5 GHz. The system is applied in a free space in which the complex permittivity of the background at this frequency of operation is $\varepsilon = 1 - j0$. The object domain is assumed to be a square with 9.5 cm side. The domain is divided into 60×60 cells. The parameter of the MWT system is summarized in Table 7-2.

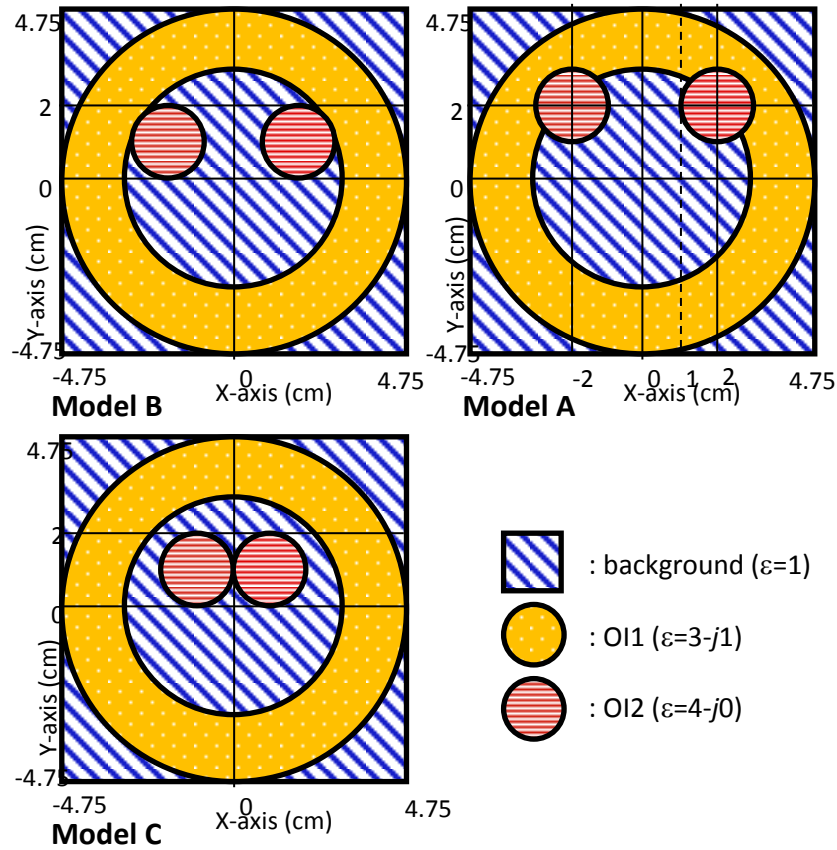


Figure 7-8: Architecture of dielectric tube model for NI-cgne. Two cylindrical dielectric materials are placed in three different positions inside dielectric tube.

Table 7-2 the parameter of the simulated system for the numerical testing of the dielectric tube model

Parameter		Value
Diameter of Object Domain(\mathcal{O})		9.5 cm
Diameter of Data Domain (\mathcal{D})		13.0 cm
Transmitting Antenna T_x		16 T_x
Receiving Antenna R_x		16 $R_x \times 16 T_x$
Number of data		256
SNR		40 dB
Number of cells		60 \times 60 = 3600
ϵ	OI 1	3 - j1
	OI 2	4 - j0
Radius of OI		4.75 cm
Frequency		1.5 GHz

Dielectric tube model consists of a lossy tube with parameter $\epsilon=3-j1$. The outer and inner radius of tube is 4.75 cm and 3 cm, respectively. The tube is placed in a free space. Two identical cylindrical objects with $\epsilon = 4 - j0$ are placed inside the object domain. The architecture and the cross section of the original OI are presented in Figure 7-8.

The data are added with a random noise. The noise is introduced using white Gaussian function with SNR of 40dB. The noisy data are reconstructed using NI-cgne and LM method. Two different stopping rules of CGNE are applied which are discrepancy principle and L-curve criteria. The images of dielectric tube model resulted by the algorithms are presented in Figure 7-9.

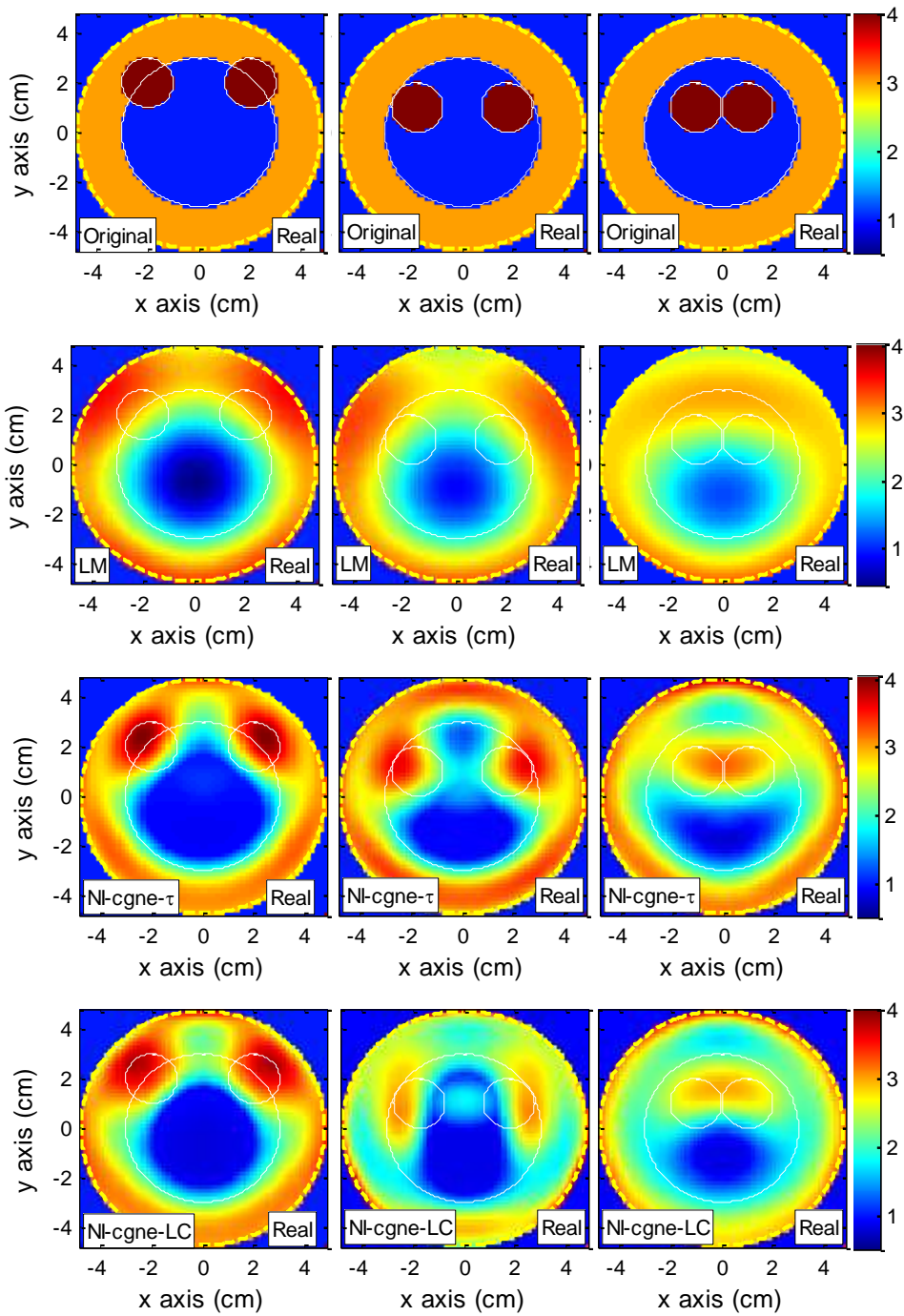


Figure 7-9: The images of $Real(\epsilon)$ of the dielectric tube model for NI-cgne test. The tube contains different materials. The images are resulted using NI-cgne and LM algorithms.

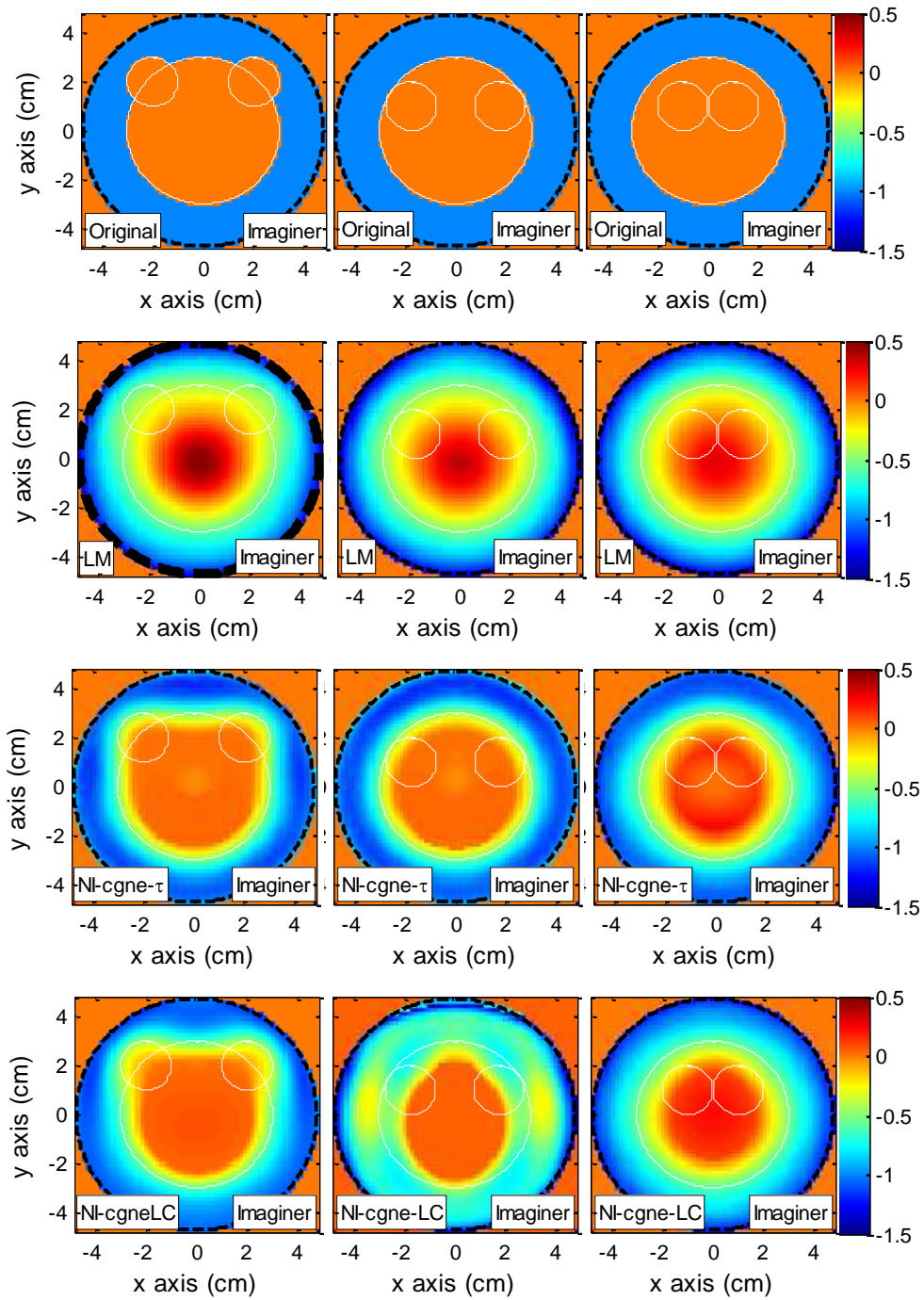


Figure 7-10: The images of $Imag(\epsilon)$ of dielectric tube model for NI-cgne test. The tube contains different materials. The images are resulted using NI-cgne and LM algorithms.

Table 7-3: The results of NI-cgne and LM algorithms in solving the MWT inverse problem of the dielectric tube containing different materials.

Problem	Parameter	Algorithms		
		NI-cgne- τ	NI-cgne-LC	LM
<i>Model A</i>	k	10	8	30
	\mathcal{F}	1.08×10^{-4}	2.74×10^{-4}	6.16×10^{-3}
	Err(χ_k)	28%	31%	37%
<i>Model B</i>	k	30	11	22
	\mathcal{F}	1.07×10^{-4}	1.32×10^{-3}	9.67×10^{-3}
	Err(χ_k)	33%	39%	43%
<i>Model C</i>	k	13	13	21
	\mathcal{F}	7.67×10^{-4}	1.11×10^{-3}	1.46×10^{-2}
	Err(χ_k)	39%	44%	47%

Table 7-3 summarizes the inversion results from TM polarization measurement after 30 outer iterations of Newton method. NI-cgne moves faster than LM method does. After 5 iterations, the MWT objective function norms of NI-cgne- τ and NI-cgne-LC are less than 1×10^{-3} for all dielectric tube models, while the function norms of the LM method are still above 1×10^{-2} . Adding more iterations improves the results of NI-cgne by about a tenth. These are lower than that of the LM method. Generally, the normalized errors of MWT function for all the algorithms tested are very small. The terminal solution of NI-cgne is gained faster than that of LM method.

The solutions of NI-cgne are better than those of LM algorithm. The relative errors of the solutions of the MWT inverse problem using NI-cgne- τ and NI-cgne-LC are generally lower than those of LM method. It can be seen in Figure 7-9 and Figure 7-10 that the dielectric cylinder can be reconstructed using NI-cgne. Although the shape and position of the cylinders are slightly missed, the dielectric contrast of the material can be defined. On the other hand, the LM fails to draw the cylindrical objects.

7.4.2 Human Arm model

The same measurement setup which is summarized in Table 7-2, is still used as the previous numerical test, but now the system is immersed in the water which has a complex permittivity $\epsilon = 77.3 - j0$. A human arm model is contained in the object domain. The model is constructed by skin, muscle bone and cortical bone. The complex permittivities of human arm material are listed in Table 7-4. The model consists of cylindrical muscle surrounded by skin. There are two identical bones which are placed inside the arm. The architecture of the arm is presented in Figure 7-11. The cross section of the complex permittivity images of OI in term of real, imaginary and absolute terms are presented in Figure 7-12.

Table 7-4 complex permittivity materials of a synthetic model of human forearm

Material	Complex permittivity
Bone	$5.5 - j0.55$
Cortical Bone	$12.6 - j2.4$
Muscle	$54.8 - j13$
Skin	$39.4 - j12.9$
Background	77.3

Numerical data is obtained by solving direct scattering problems. The OI is immersed in the background medium which is water. The dielectric contrast of OI is relative to the permittivity of the background. A white Gaussian noise with 40dB is added to the data. The data is reconstructed using NI-cgne and LM algorithms.

The parameter of the solutions obtained from initial estimates which are set in background dielectric contrast $\epsilon_r = 0$, is given in Figure 7-13. The results show that the Newton method moves toward the solution. The objective function norm reduces along with iterations. The NI-cgne moves faster than LM.

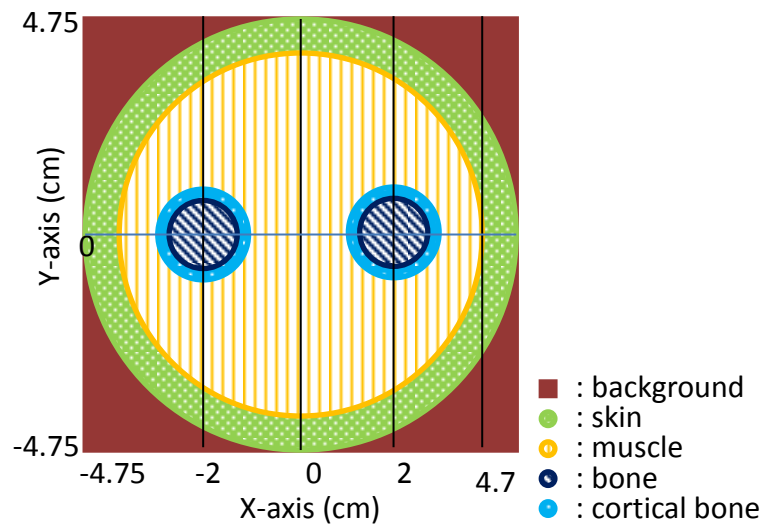


Figure 7-11: The architecture of human arms model for NI-cgne algorithm test

Figure 7-12: Two dimensional cross section of human arm model for NI-cgne test. The model is presented in a) real part b) imaginary part of complex permittivity

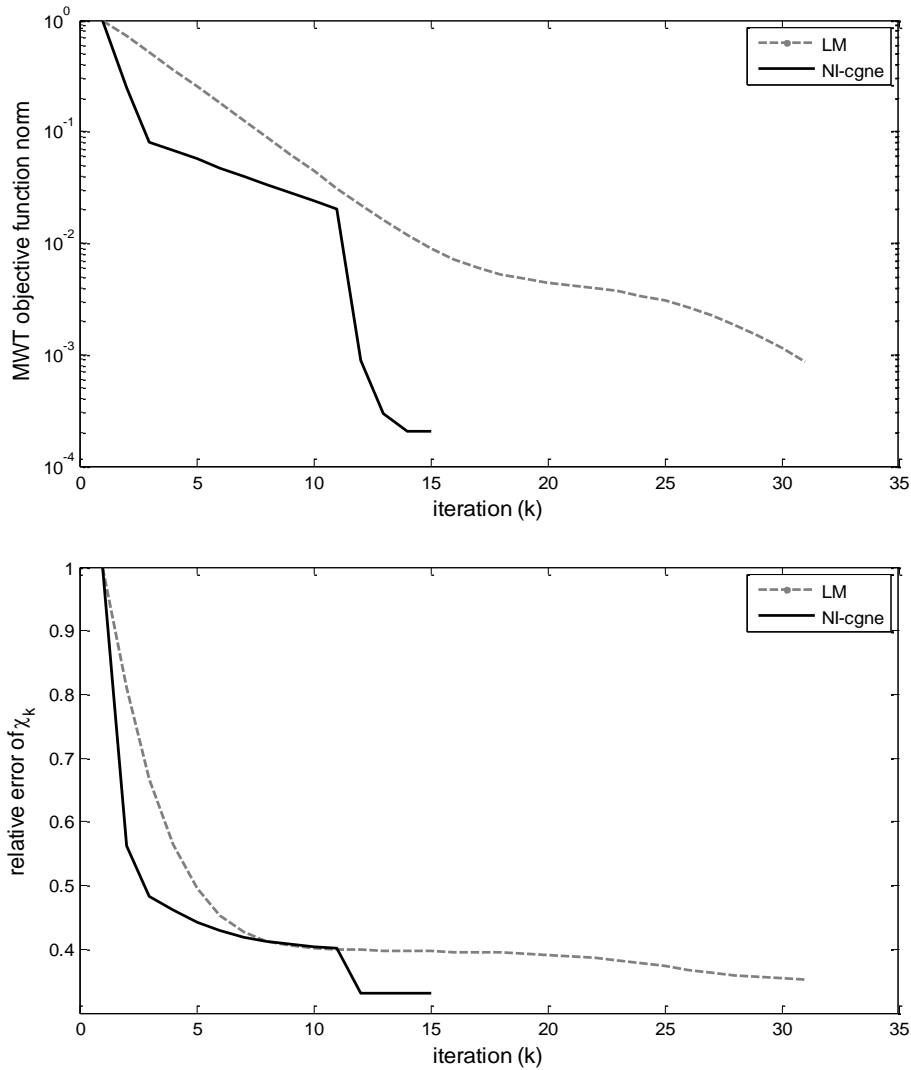


Figure 7-13: The parameter of the iterative solutions of NI-cgne and LM for solving the MWT inverse problem of human arm model a) the relative norm of objective function b) the relative error of the dielectric contrast of OI.

The solution of MWT inverse problem using NI-cgne moves very fast. After 9 iterations, the norm of the NI-cgne objective function reaches 2.05×10^{-4} . This is significantly below the solution of LM which is 8.77×10^{-4} . Generally, the objective functions of MWT inverse problems are relatively small. The solutions are toward global solutions. Contrast to the solution, the relative errors of the dielectric contrast is high. The relative errors of the dielectric contrast are above 30%. This indicates that the solution is lack of information.

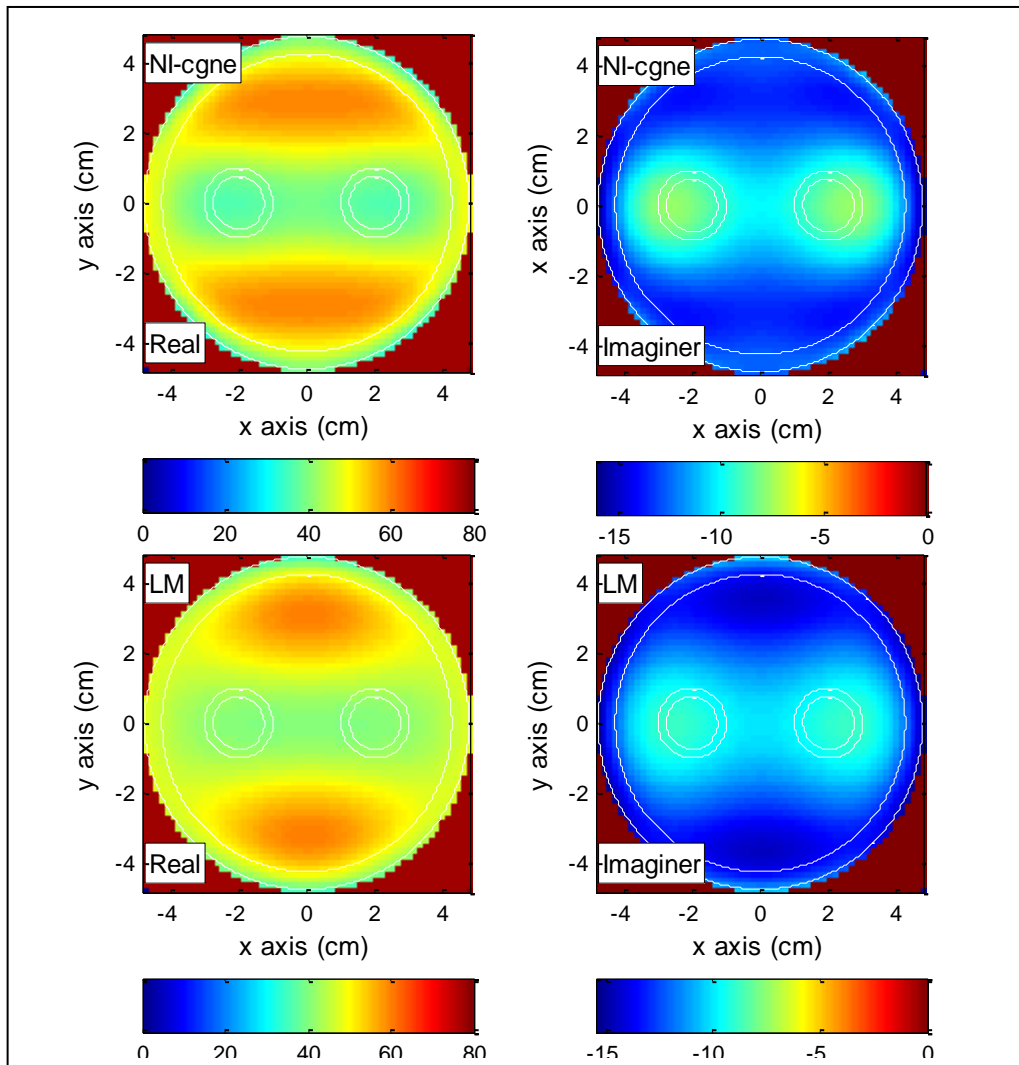


Figure 7-14: Images of human arm model reconstructed by Ni-cgne and LM methods.

The results of MWT inverse problem inversion method by minimizing the MWT objective function are given in Figure 7-14. It can be seen that the bone of the arm can already be observed in the imaginary plot of NI-cgne images, but the indication of the presence of bones in the other images is very poor. The values of the permittivity of the material are fairly defined. On the other hand, LM method fails to reconstruct the arm model. The shape of bones cannot be defined, besides the reconstructed values of the material are completely wrong. LM method needs a priori information like the location of the OI and its approximate permittivity value. Without using this a priori data, the method fails to produce acceptable results [126].

7.5 Conclusions

The numerical experiments using lossy material shows that NI-cgne leads to an effective method for solving MWT inverse problem. The algorithm is fully iterative. It consists of two major loops, the outer loop is used to update the solution of the Newton method and the inner loop is applied to solve Newton equations. The equations are the linearization of the nonlinear MWT inverse problem. The step size of Newton method is determined in unspecific manner the inner iteration which does not involve forward problems. This makes the method suitable for large scale computation.

From the feasibility study results of two dimensional lossy dielectric cylinder simulations, it is observed that the algorithm can be used to determine free space holes inside the lossy OI while the LM method fails. It is also able to describe a dielectric object which is smaller than half of the wave length. The value of permittivity is relatively close to the target, though the shape and location of the target interest is fairly determined.

The numerical study of the syntactic human arm model represents a feasibility study of algorithm in handling heterogeneous lossy objects. The algorithm is not able to reconstruct tissues with the dimension less than the wavelength. The bone of the arm can only be determined at the imaginary images of complex permittivity distributions resulted by NI-cgne. This limitation which is known as Rayleigh criterion may be reduced by increasing the working frequency. However, the nonlinearity of the problem and the complexity of the computation increase due to the diffraction effect. Thus, in order to improve the robustness of the solution using the algorithm, regularization and smoothness can be applied in the inverse problem instead of the procedure of solutions. Multi frequency approach can be introduced to reduce the ill posedness of the problem. This is one of some subject of the future work.

8

Microwave Tomography System

Microwave Tomographic System is developed in The University of Manchester. The system is a circular microwave scanner with the frequency of operation centered as 5 GHz. It consists of a 12.5 cm radius circular array of 16 ground plane antennas. The system is placed in a free space. Each of the array antennas can operate either in transmitting or receiving mode. The measurement procedure records the disturbed electric field which is the field when the object is presented. The scattered electric field data are the difference between disturbed and undisturbed fields. The data are reconstructed using developed methods which are INBM and NI-cgne. The results are compared with the results of LM.

8.1 Introduction

Microwave tomography (MWT) is a promising alternative of industrial and biomedical nondestructive imaging modalities. The advantages of MWT application include: low cost and portability, safe nonionizing radiation, and describing the cross section of the interest through the distribution of electric

properties. In MWT system, the object of interest (*OI*) is irradiated by a known incident field and reconstructs electromagnetic field measurement in a range of a few hundred megahertz up to a few gigahertz into the distribution of electrical properties of *OI* cross section.

Various types of MWT system which provides MWT measured electric field for given incident field has been reported. A few of them include: a microwave scanner operating at 2.33 GHz consists of a 25-cm diameter circular array of 64 water-immersed horn antennas [164; 165], 24 Vivaldi antennas, co-resident antenna elements are connected to a vector network analyser via a 2×24 port matrix switch [166; 167], 6-12 Double Layered Vivaldi Antenna probes vary in Tx-Rx arrangement [168]; 32 identical measurement channels of microwave imaging system [169]; 32 channel monopole antennas [170]; 16 monopole antennas mounted circularly inside a cylindrical Plexiglas tank of 28 cm diameter [171]; and 12 modulated scattered technique antennas of remote field measurement approach [172]. Generally, the system is configured circularly and designed for liquid immersed object domain. A low cost MWT system with free space object domain needs to be developed. In this chapter, the prototype of a designed MWT system is described. The architecture and MWT data collection and calibration are explained. Then, the reconstruction of data by means of Newton iterative methods is applied. The MWT system is studied by evaluating the result of images of object of interest cross section.

8.2 Microwave Tomographic System

A microwave tomography system is developed in the Microwave and Communications (MACS) research group of school of Electrical engineering and Electronics, The University of Manchester. The MWT system is addressed to be low cost as a monopole ground plane antenna array is used. It works in a free space domain, thus, further extension in industrial and biomedical application could be done.

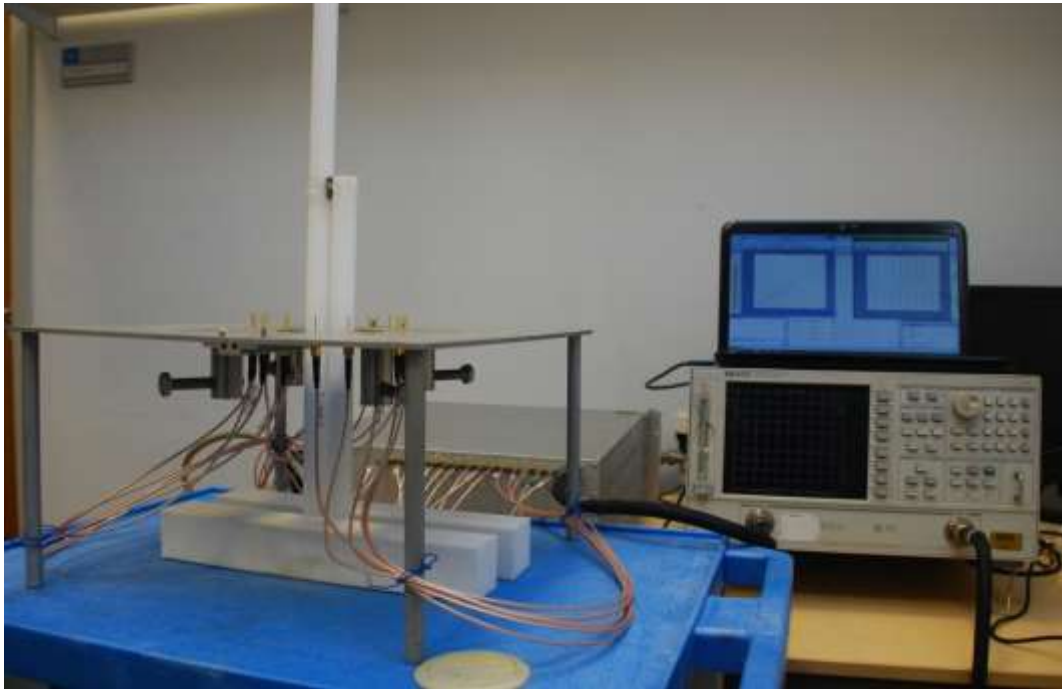


Figure 8-1: The University of Manchester microwave tomography prototype. The 16 ground plane antennas are connected to VNA via Cytec 2x16 matrix switch.

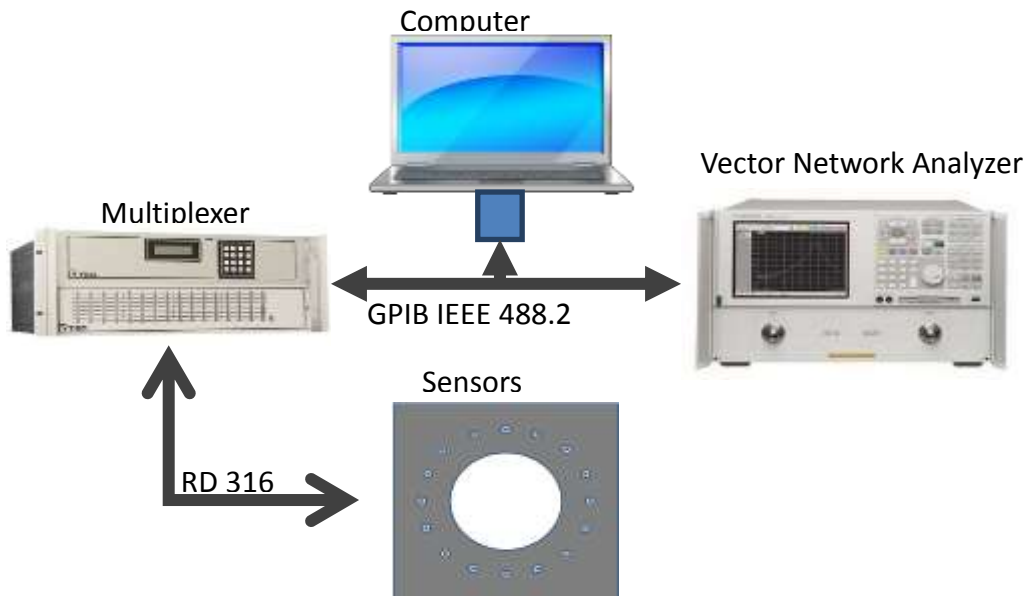


Figure 8-2: The architecture of the University of Manchester-MWT system. The system is computer controlled via GPIB IEEE 488.2. NI GPIB-USB-HS interface is used to connect the system to portable computer.

The prototype of the (the University of Manchester-MWT) system is shown in figure 7-1. It is designed from 16 ground plane antennas which are computer controlled via 2x16 Cytec multiplexer. The antennas are designed to transmit and receive microwave signals. The transmission and measurement of the electric field are conducted by Vector Network Analyzer (VNA)

The background medium of the University of Manchester-MWT system is a free space. OI is immersed in the free space and the scattered field is measured in the data domain which is placed in the free space. The dielectric contrast of the reconstructed image is defined relative to the free space, that is $(\epsilon_r(q) - 1)$. OI is placed inside the object domain. The shape, position and dielectric contrast of OI are unknown. The object domain represents the drawing area of the MWT images. The image is the distribution of the dielectric contrast which represents two dimensional cross sections of OI inside the domain object. The background medium is a free space which permittivity is 1, thus, the value of the image background is zero.

The MWT system of the University of Manchester is modeled works in TM mode at \hat{z} direction, which means that the antennas are orientated at \hat{z} direction and the images are described in (\hat{x}, \hat{y}) plane. The measured scattered field is assumed to be $\mathcal{E}_t^s = E_t^s \hat{z}$ and the incident field is formulated as $E_t^i = E_t^i \hat{z}$. For simplicity, both terms are written as \mathcal{E}_t^s and E_t^i , respectively. Practically, the scattered field cannot be measured directly. It is defined from the difference of undisturbed and disturbed fields. The undisturbed field is similar to the incident field at the data domain, while the disturbed field is measured electric field at the data domain due to the presence of OI. For each set of measurement, microwave signal is transmitted via aTx antenna, then, pairs of undisturbed and disturbed fields are measured at $(M - 1)Rx$ antennas at data domain. Additionally, incident field E_t^i that illuminates $N, N \in \mathcal{O}$ cell of domain object and $(M - 1)Rx, M$ point of antennas are modeled. The modeled fields are used to transform and calibrate the known incident field at the object domain and the measured scattered field at the data domain.

8.3 Architecture of the University of Manchester MWT System

The schematic MWT System is illustrated in Figure 8-2. The system is constructed by four basic instruments, which are portable computers, Vector Network Analyzed (VNA), multiplexer, and ground plane antenna arrays. The system is fully controlled using computer where the interface used is a USB port based National Instrument GPIB-USB-HS. There are two buses in the design, a data bus and a signal bus. National instrument IEEE 488.2 GPIB data cable is used as the data bus between multiplexer (sensor), computer, and VNA. The data bus is used to transfer two types of text data: mnemonic instruction from computer to multiplexer and VNA, and series of numeric data from VNA to computer. An RD 318 coaxial cable is used as the signal bus. The computer transfers transmitting microwave signal from port 1 of the VNA to port In0 of the multiplexer via the signal bus, then, the computer transfers the signal through the bus from port In1 of the multiplexer to port 2 of the VNA.

Algorithm 8-1 MWT: Microwave Tomography Measurement Sequence

```
Function MWT(objVNA, objMul)
    [n, d, s] = getFreq(objVNA)
    f = linspace(s, s + d, n)
    For Tx = 1: MTx
        For Rx = 1: MRx
            setMUL(objMul, Tx, Rx)
            data(Tx, Rx) = getDat(objVNA)
        End For Rx
    End For Tx
    Return [f, data]
```

The measurement is fully controlled using a computer. For example, the computer conducts several activities to measure fields at a point of observation. The computer writes mnemonic text to a Cytex multiplexer asking the multiplexer to connect to desirable pairs of antennas to VNA.

Then, the computer asks VNA to measure $s_{2,1}$ of the pairs. Finally, the computer reads and records the $s_{2,1}$. The procedure for the whole set of measurement is illustrated in algorithm 7-1.

The procedure is described as follows. Initially, the calibration of the VNA is restored. Both VNA and Multiplexer are defined in two instrument object variables which are input to the measurement function. The measurement starts by collecting three parameters of frequency swap which are numbers of point data (POINT), frequency span (SPAN) and start of frequency swap (STAR). The parameters are kept in n, d, s variables, respectively. The parameters are used to define the working frequency. The University of Manchester-MWT system addresses a single frequency, however, for evaluation purposes the frequency is swapped across frequency domains. Function *getFreq(obj)* is used to get the working frequency. Data collected is an electric field which is measured in pairs of T_x and R_x antennas. The transmitting antenna is scanned using outer *for* loop. At each illumination, the field is measured at the rest of the antennas which is done at the nested *for* loop. To handle measurement *setMUL* subroutine is used to set the antenna connection and *getDat* function is used to gain data.

8.4 Antennas Arrangement

Sixteen monopole antennas are applied in the University of Manchester-MWT system. The antennas used are 16 monopole ground planes. The ground plane is connected among the antennas as seen in Figure 8-3 (a). It is specified for the MWT system which is designed for near field application as it is introduced for microwave imaging [169; 173].

The antennas are connected using RD 316 coaxial cable, with SMA Plug Crimp Gold connectors Figure 8-3 (b). The impedance is 50 ohm with attenuation 1.0 dB at 3GHz. Though the maximum frequency of the cable is 3 GHz, it can still be used to transmit microwave signals up to 5 GHz.

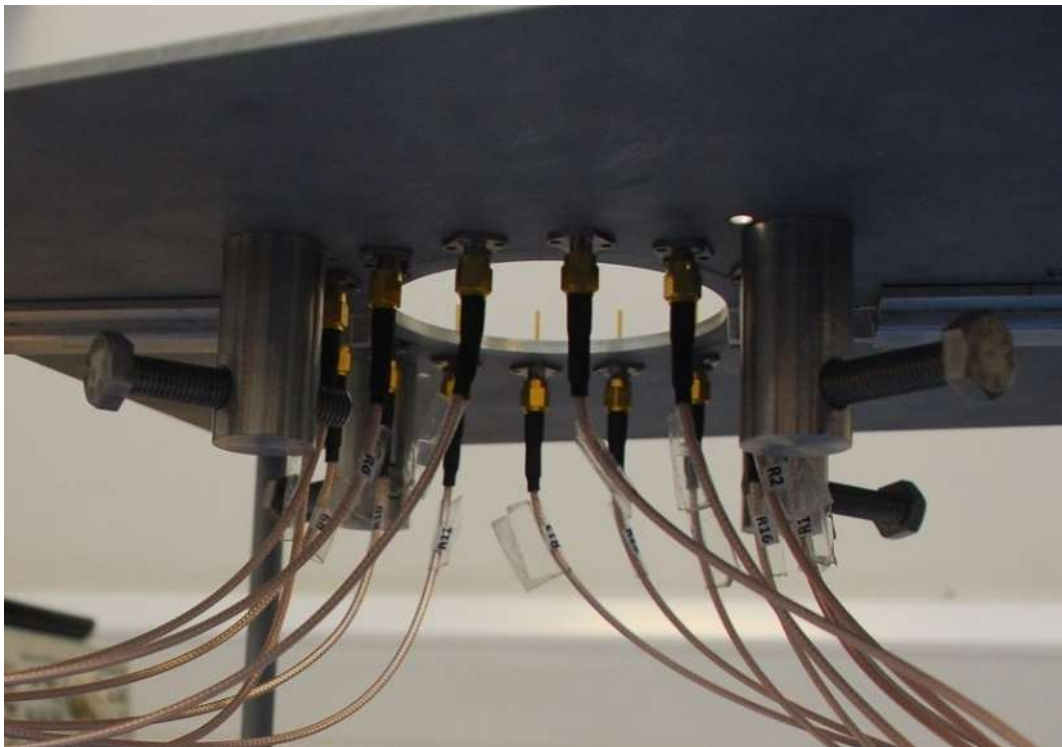
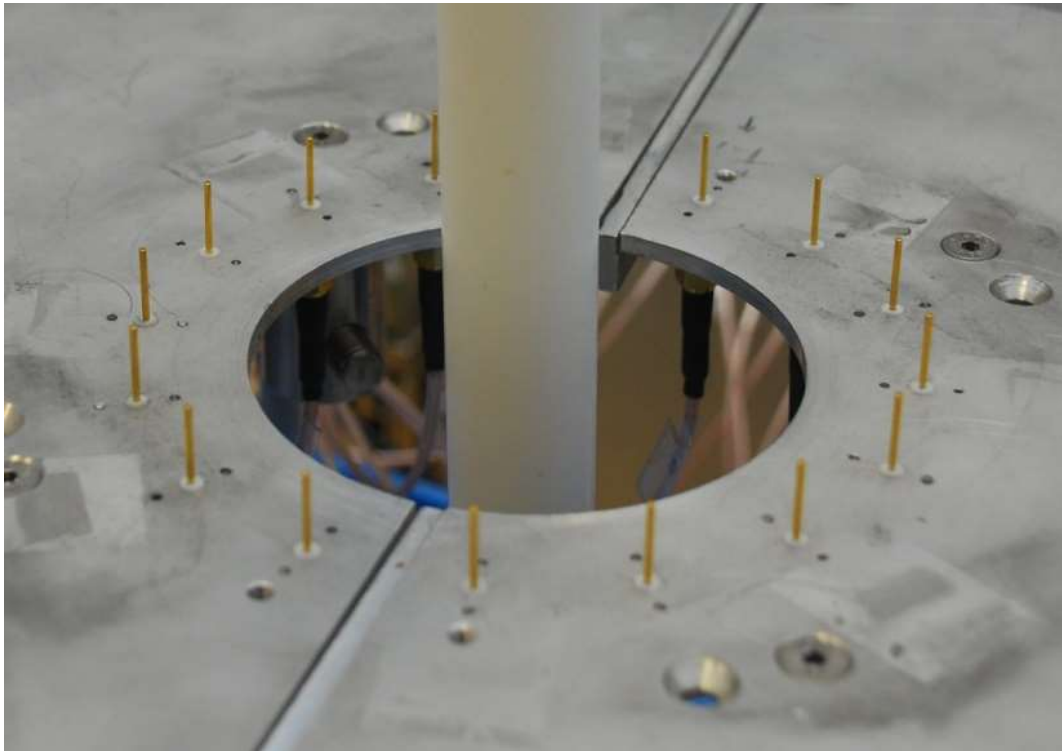


Figure 8-3: The array of antennas of MWT system. a) 16 monopole antennas are placed in a single ground plane. b) the antenna connectors are connected using RD 316 coaxial cable.

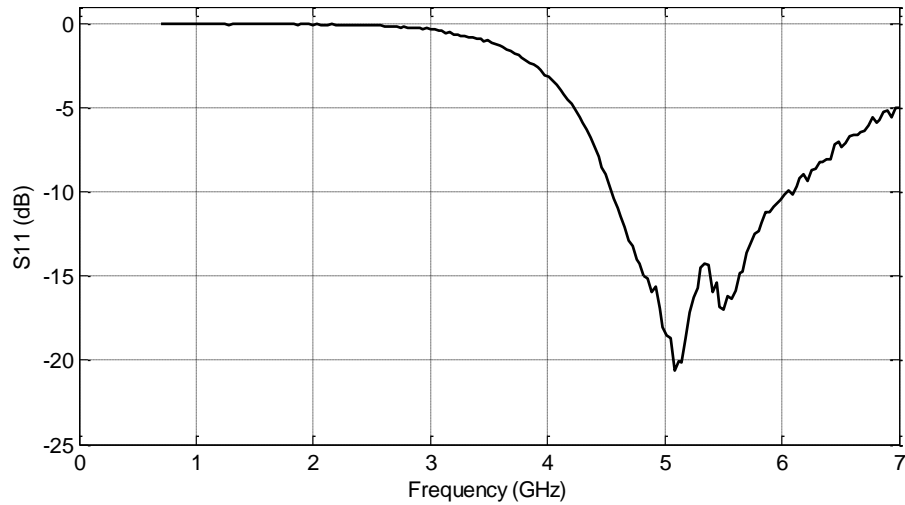


Figure 8-4: s_{11} parameter of the monopole antenna in free space.

The antennas are designed to transmit microwave signals from 2 to 7 GHz, although in the practice it is found that the usable frequency based on the s_{11} characteristic is 4 GHz to 6 GHz as seen in Figure 8-4. The University of Manchester-MWT is a frequency dependent system. The efficiency of the system to adapt frequency is done by evaluating the capability in reconstructing the cross section of interest over the frequency 1GHz up to 5 GHz.

8.5 Object Domain of the University of Manchester-MWT System

The 16 antennas are positioned in a cylindrical array with radius 6.5 cm. This architecture ensures that the entire imaging domains in the form of object domain are evaluated as seen in Figure 8-5 . The antennas are oriented vertically equal in space and radius. A circular hole with radius 5 cm is made in the center of the antenna array to place the object of interest. The decrease of the ground of the antenna may influence the approximation of the antenna model and produce additional errors. However, the OI should cross the ground plane

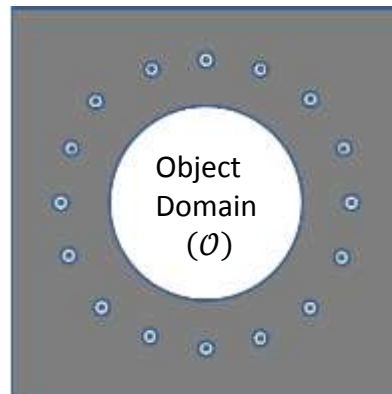


Figure 8-5: the architecture of ground plane antennas. The antennas are arranged circularly around object domain (O) of MWT system

The size of the monopole and the distance between antennas produce cross polarization level of the radiation pattern. Therefore, the measured scattered field near the transmitting antenna suffers from noise more than the other receiving antennas. To reduce the noise effect, the data near the transmitting antenna may not be used. In this experiment, measurements are acquitted for all receiving antennas at each illumination. The effect of the position and the number of antennas are studied with respect to the quality of the image resulted and the time consumed.

8.6 Antenna Multiplexing Using Microwave Switching System

The multiplexer is constructed by 16 bidirectional switch ports with two modules. The antennas from the sensors are connected into the switch ports using RD 318 coaxial cable. The switch can be controlled to connect the port into the modules. Module 1 is assigned as the transmitting antenna. It is connected to the input 1 of the VNA. Module 2 is addressed as the transmitting antenna. It is connected to input 2 of the VNA. For example, as it is seen in Figure 8-6, port 1 and port 2 are addressed as the transmitter and receiver, respectively.

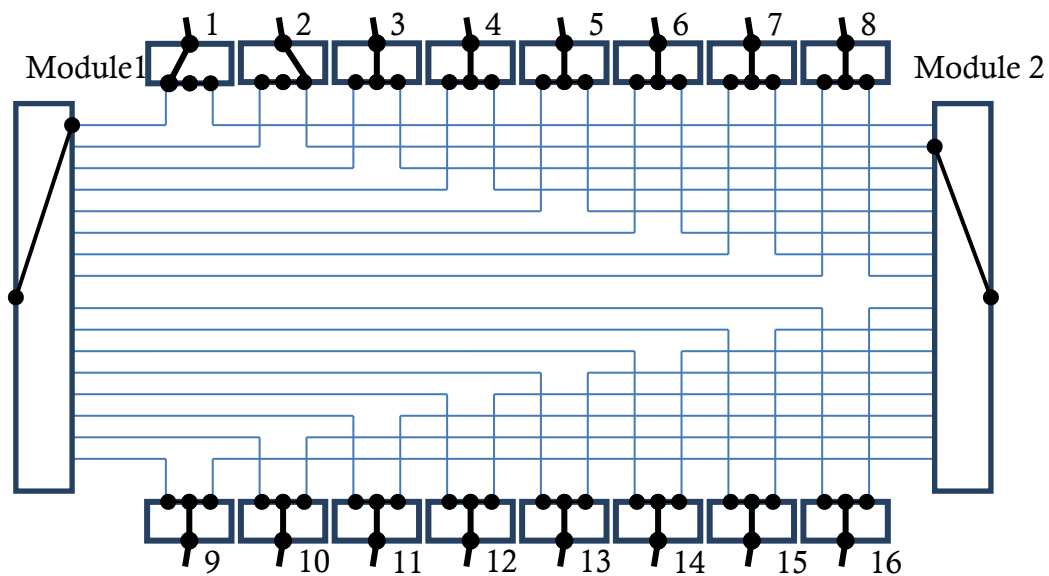


Figure 8-6: the architecture of the matrix switch of Cytec Microwave Multiplexer

Cytec CXM series is used as the multiplexer. This passive bidirectional device switches 50 ohm coaxial microwave signals. It has 16 ports and 2 output points. The ports are controlled by 16 individual switch points, which can be manual or computer controlled. The manual switching can be done using front panel keypad. Basically, the switch is handled using one letter mnemonic function which is mnemonic *L* for latch, meaning closing the specified point while all others are unaffected. Letter *U* for unlatch means opening addressed point while all other points are not affected. Letter *X* for multiplexer means closing the specified points to the desired output and open all other points. The last mnemonic function is usually used to reset the connection to the default assigned.

The multiplexer is commanded by the computer. The command lines are received at the control module, and executed after all of the lines are transmitted. Multiple commands can be sent as long as they do not exceed 36 characters. The commands are cleared using GPIB device clear, like *instrclear* in MATLAB command, for example, *clear all switch* and *module, close module 0 to switch 1*, then, *close module 1 to switch 2*. Instruction is executed by sending following text to the multiplexer

$$X \ 0 \ 1; L \ 1 \ 2 \quad (8.1)$$

The text is sent using *fwrite('text')* command that is

$$fwrite(obj_{Mul}, 'X, 0, 1; L, 1, 2') \quad (8.2)$$

The instruction in the form of text data is written in a multiplexer via GPIB. The multiplexer is addressed as *obj_{Mul}*. The multiplexer object should be defined. The address of multiplexer interface is set manually and it can be automatically detected by the available MATLAB command.

The Cytec multiplexer interface is controlled via IF-4 IEEE 488 bus. The talk/listen addresses are defined using five position DIP switch. The setting is binary, the first switch is the least significant and the fifth is the most significant. In this research, the multiplexer is addressed at 7 decimal or 11100 of the DIP switch. The object address is detected using function *instrfind* of MATLAB function. The visa address is set at 7. The interface of the Cytec multiplexer will be recognized as the GPIB object as

$$Obj_{Mul} = GPIBObjectUsingNIAdaptor : GPIB0 - 7 \quad (8.3)$$

Once the object is detected, the connection is established using an open command *fopen(Obj_{Mul})*.

Algorithm 8-2: setMUL: Setting Multiplexer switch

Subroutine setMUL(*obj_{Mul}*, *Tx*, *Rx*)

fopen(obj_{Mul})

MULinstruction = [*'X, 0, num2str(Tx)'; L, 1, num2str(Rx)*]

fwrite(obj_{Mul}, MULinstruction)

fclose(obj_{VNA})

End of setMUL

The multiplexer is used to connect an appropriate transmitting antenna (*Tx*) to module 0 means port In0 which is connected to Input 1 of VNA, and receiving antenna (*Rx*) to module 1 and connected to Input 2 of VNA. The MATLAB subroutine for handling this instruction can be seen in Algorithm 8-2.

In MATLAB command, the instruction is defined in a string data format. Initially, the data bus is established to communicate computer and multiplexer objects. $fopen(obj_{Mul})$ is used to define the communication line. Then, it is followed by sending instruction to the multiplexer. The Tx and Rx are defined by outer and nested loops which are numeric types of data format. They should be transferred in a string format using $num2str(numeric)$ MATLAB command. Once the instruction is recognized and executed by the multiplexer, the communication line is closed. The data bus can be used to communicate between computer and VNA.

8.7 Read and Write Data from VNA

The scattered field data is measured using Vector Network Analyzer (VNA) HP 8720D. The VNA is communicating with the computer via GPIB data bus. In general, the communication is conducted in the following steps:

1. Create an instrument object
2. Connect to the instrument
3. Configure properties
4. Write and read data
5. Disconnect from the instrument

The VNA is detected as the object in GPIB, it is addressed at 16 decimals. It is assigned using instruction in MATLAB command

$$instrfind('Type','visa','RsrcName',visa_{addr},'Tag','') \quad (8.4)$$

The VNA object is detected using $VGvna$ function which is stated in algorithm 7-3. The address of VNA can be defined using local-instrument state-push button front panel. The address is set at 16, thus the GPIB-VISA instrument is defined at 16, otherwise it is assigned using instrument type ('agilent').

Algorithm 8-3: VGvna: VISA-GPIB object of VNA

Function VGvna(—)

```
instrreset
visa_addr = ' GPIB0 :: 16 :: INSTR'
obj = instrfind('Type', 'visa', 'RsrcName', visa_addr, 'Tag', '')
ifisemty(obj)
    obj_VNA = visa('agilent', visa_addr);
else
    fclose(obj)
    obj_VNA = obj(1)
    end
```

Return (*obj_VNA*)

Algorithm 8-4: getFreq: Acquire Frequency Parameter of VNA

Function getFreq(*obj_VNA*)

```
fopen(obj_VNA)
fwrite(obj_VNA, 'FORM4; OPC?; SING')
fprintf(obj_VNA, 'POIN?')
n = scanstr(obj_VNA)
fprintf(obj_VNA, 'SPAN?')
d = scanstr(obj_VNA)
fprintf(obj_VNA, 'STAR?')
s = scanstr(obj_VNA)
n = cell2mat(n)
d = cell2mat(d)
s = cell2mat(s)
fclose(obj_VNA)
```

Return [*n*, *d*, *s*]

Algorithm 8-5: getDat: Acquire s_{21} signal

Function getDat(*obj_VNA*)

```
fopen(obj_VNA)
set(obj_VNA, 'InputBufferSize', 80050)
fwrite(obj_VNA, 'FORM4; OPC?; SING')
fwrite(obj_VNA, 'OUTPDATA')
data = scanstr(obj_VNA)
fwrite(obj_VNA, 'OPC?; SING')
fwrite(obj_VNA, 'cont')
fclose(obj_VNA)
```

Return (*data*)

The connection of the computer and the instrument is established by opening data bus line to the appropriate object address. The object of VNA is opened using $fopen(obj_{VNA})$ function. Furthermore, the computer communicates with VNA using obj_{VNA} variable.

The data is gained using format type *FORM4* that is an ASCII number with 24 bytes per data value. To express the phase of measured data at each scan of the field, the data is taken at 201 points with a maximum span of 0.5 GHz. The data is transferred using *OUTPDATA* instruction, output the error of the corrected data from the active channel.

The *OUTPDATA* syntax is selected to handle the data acquisition of *FORM4* format. The data gained is the data from the active channel with a suitable display format. The raw data with error-correction is applied. The array represents the currently measured parameter. It is transmitted in real-imaginary pairs. To access appropriate data location, the data is indexed using the array of frequency. The procedure of gaining data using VNA is illustrated in algorithm 7-4 and algorithm 7-5.

8.8 Data Collection and Calibration

8.8.1 Data collection

The measurement data is gathered in undisturbed and disturbed electric fields. The data is scanned from 1 to 5 GHz with 1.5 GHz span, therefore, it is taken at the eight set of calibration. The MWT inverse problem needs scattered field measurement. Practically, the field which can be measured is the total field and the incident field. The former field is the measured data when the *OI* is introduced and the latter is the data when the scatterer is not present. Figure 8-7 illustrates the sample of the raw data of both types of fields. The graphs visualize the absolute value of electric field at R1, Rx 4 and Rx8 when the microwave signal is transmitted from Tx1.

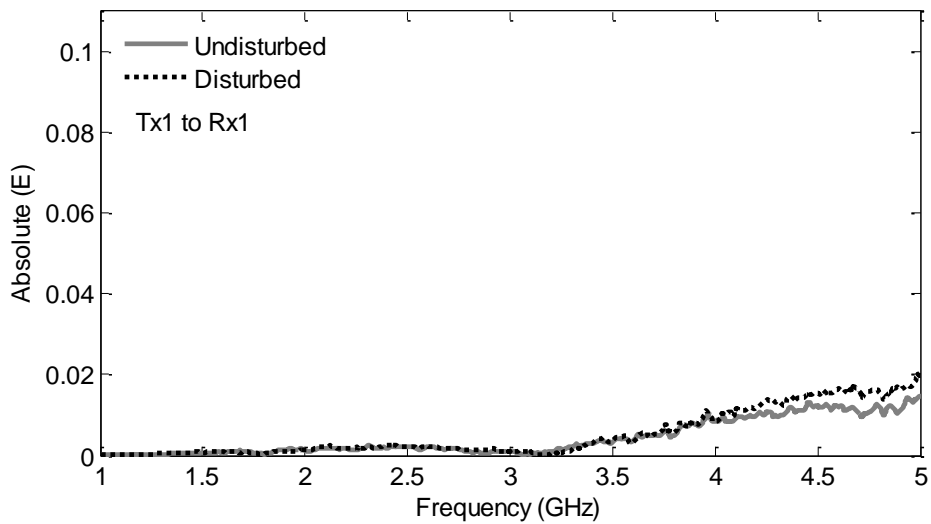
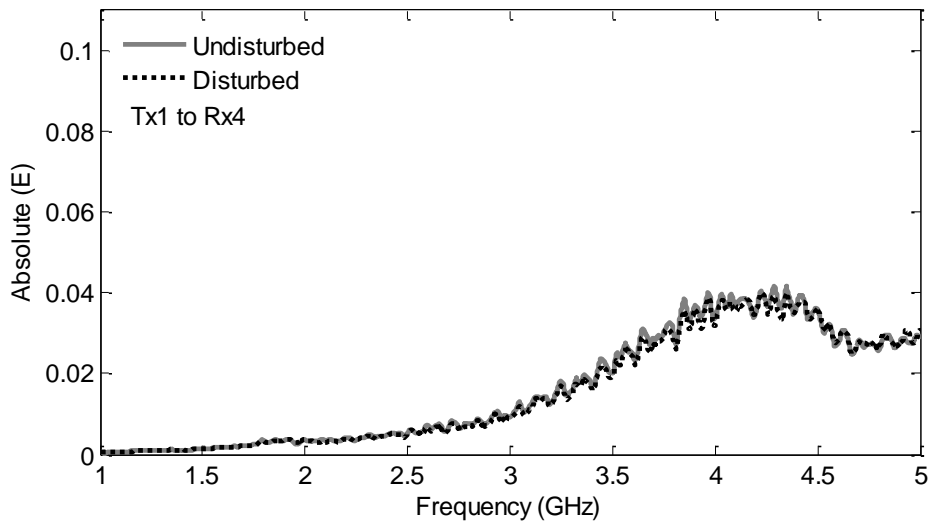
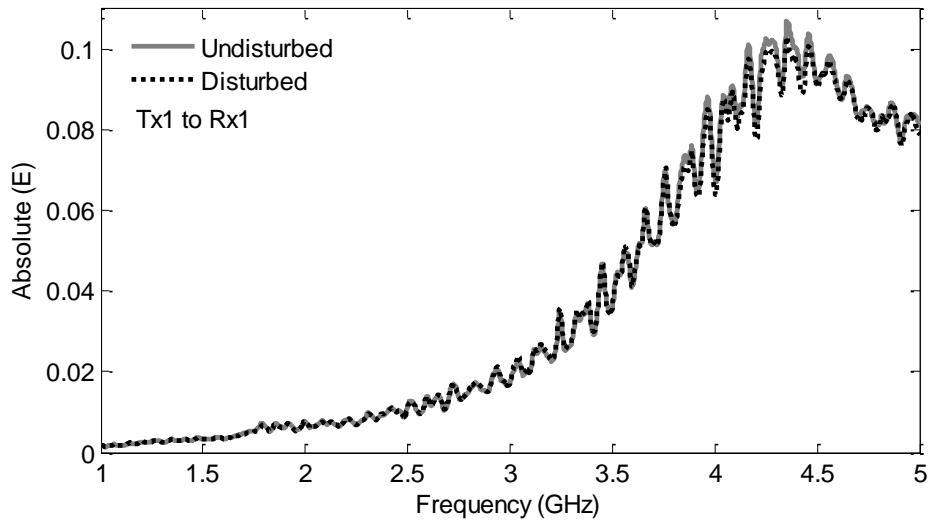


Figure 8-7: Undisturbed and disturbed electric fields measured at Rx2 and Rx9 when microwave signal is transmitted from Tx1

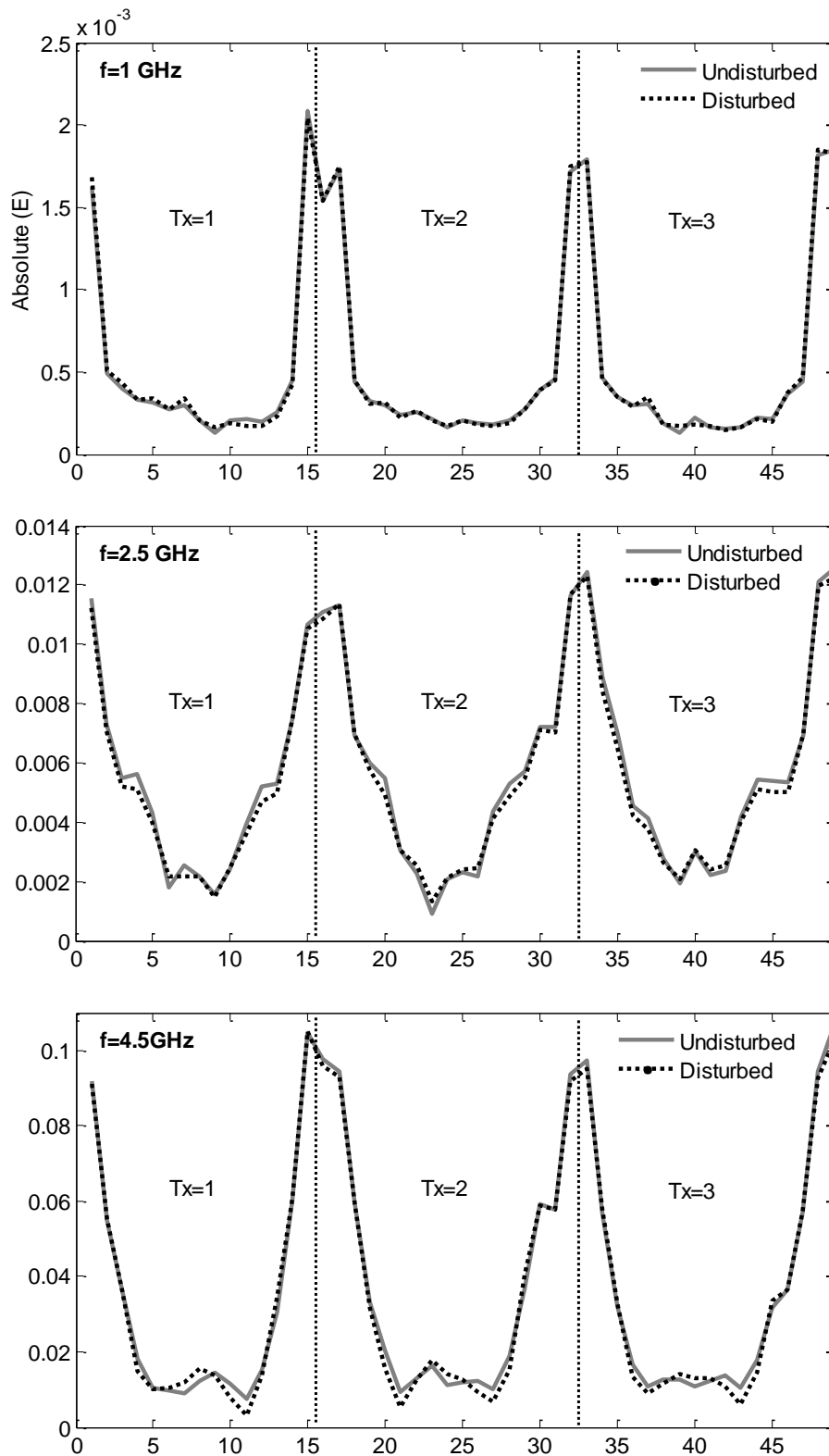


Figure 8-8: Raw data of measured Electric field at Rx antennas around object domain when three different microwave signals are transmitted from first three Tx antennas.

The frequency is scanned from 1 to 5 GHz. Moreover, the difference of both measured electric fields at all data points (all Rx antennas) at three different frequencies are presented at Figure 8-8 it can be seen that the effective frequency of the University of Manchester-MWT system is between 4.5 GHz to 5 GHz. This is in line with the parameters of S11 of the antenna. The reflection coefficient is below -10dB above 4.5 GHz where the difference of undisturbed and disturbed signals is clearly seen. For this reason, the measurement test is concentrated between 4.5 GHz to 5 GHz.

8.8.2 Calibration

The scattered field is the subtraction of the total field with the incident field. The raw data is calibrated. The pairs of real-imaginary of the field measured of $S_{2,1}$ value needs to be transformed into recognized fields term. The calibration is also reasoned to compensate the errors of measurements. This is used to eliminate the data which suffers from errors more than the others.

It is assumed that the unperturbed and perturbed measured fields in $S_{2,1}$ value are defined as E_{mea}^i and E_{mea}^t , respectively. The magnitude and phase of the measured field are varied due to several variables, such as, the position of the antennas, the initial of the magnitude and the phase of the fields and the calibration of the VNA. The complexity of the system and the unknown line length on the multiplexer make the multiplexer allocated at the sensor block, and the calibration of the VNA done before the multiplexer. The measurement procedure creates variations of the data gathered. Therefore, the ratio of the measured value is used instead of the factual value. The ratio eliminates the difference of the magnitude of the data.

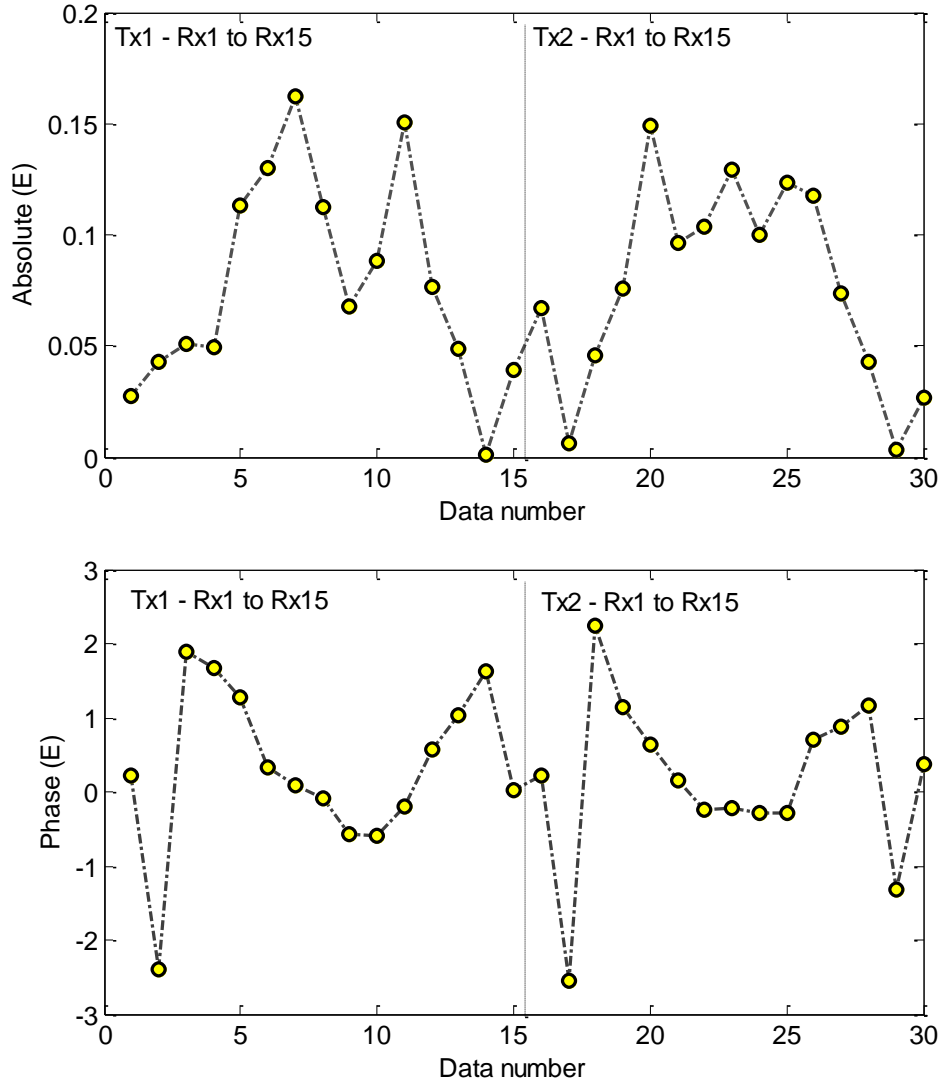


Figure 8-9: The absolute and phase of calibrated scattered field at 4.5 GHz when a plastic rod is introduced

$$R_{mea}^t = \frac{E_{mea}^T}{E_{mea}^i} \quad (8.5)$$

Let us simulate a data measurement. The incident field $E_{simulated}^i$ is transmitted from $T_{x=1}$ using line source equivalent. The incident in object domain produces scattered field at the data domain. Assuming the position of the observation points are equivalent to the position of receiving antennas, then the ratio of measured fields is assumed to be equal to simulated fields.

$$R_{mea}^t = \frac{E_{simulated}^T}{E_{simulated}^i} = \frac{E_{simulated}^s + E_{simulated}^i}{E_{simulated}^i} \quad (8.6)$$

Equation (8.6) produces the simulated scattered field with respect to the ratio of measurement data. The calibration is done by assigning the ratio equals to simulated and measuring data. Then, the desirable scattered field which can be used as the input of inverse problem is done by

$$E_{mea}^s = (R_{mea}^t - 1)E_{simulated}^i \quad (8.7)$$

Applying calibration (8.7) to measure disturbed and undisturbed electric field resulted calibrated electric field at the data domain with known simulated incident field at the object data. The illustration of the calibrated electric field is presented in Figure 8-9.

The disturbance is a cylindrical plastic rod which is made from homogeneous Teflon which utilizes published contrast of contrast of $\chi_r \approx 2.1 + j0.0$ at 3 GHz. The cylinder is placed roughly in the center of the object domain. Referring to the result of the direct scattering numerical experiment (chapter 3), the pattern of scattered field of homogeneous cylindrical object is smooth. However, the pattern of the line in Figure 8-9 is fluctuated. The noise, model error, calibration error and other disturbances influence the quantity of calibrated scattered field.

8.9 The Results of Reconstructing Experimental Data

8.9.1 *The effect of antenna arrangement*

The calibrated scattered field is fluctuated. The noise level is different among measurement points. The number of point data at receiver is essential to the results of reconstruction. The effect of arrangement of working antennas at each microwave illumination is studied. The indexed measurement point which is Rx antennas is illustrated in Figure 8-10 and the arrangement of Rx antennas is described in Table 8-1. The architecture of the mode is similar to all projections of set measurement. The second projection is done by shifting the position of Tx and Rx one index leftward or anticlockwise.

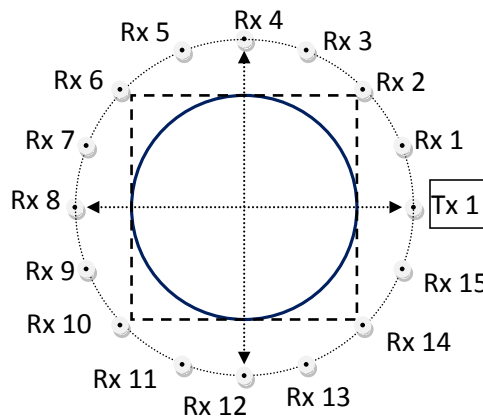


Figure 8-10: The arrangement of antennas. Tx1 is set as a transmitting antenna and Rx1 to Rx15 are defined as receiving antennas

Calibrated electric field with five different antenna arrangements are reconstructed using Inexact Newton and Newton iterative algorithms. The value of functional norm at stopping iterative index at 4.5 to 5 GHz is presented in Figure 8-11. It can be seen that decreasing the number of receiving antenna decreases the terminal value of the functional norm.

Table 8-1: The arrangement of Rx antenna when Tx1 is defined as transmitting antenna.

Transmitter	Receiver	
	Mode	No of Antenna (Rx)
Tx1	A	1, 2, 3, 4, 5, 6, 7, 8, 9, 10, 11, 12, 13, 14, 15.
	B	2, 3, 4, 5, 6, 7, 8, 9, 10, 11, 12, 13, 14.
	C	3, 4, 5, 6, 7, 8, 9, 10, 11, 12, 13.
	D	4, 5, 6, 7, 8, 9, 10, 11, 12.
	E	3, 4, 5, 6, 10, 11, 12, 13

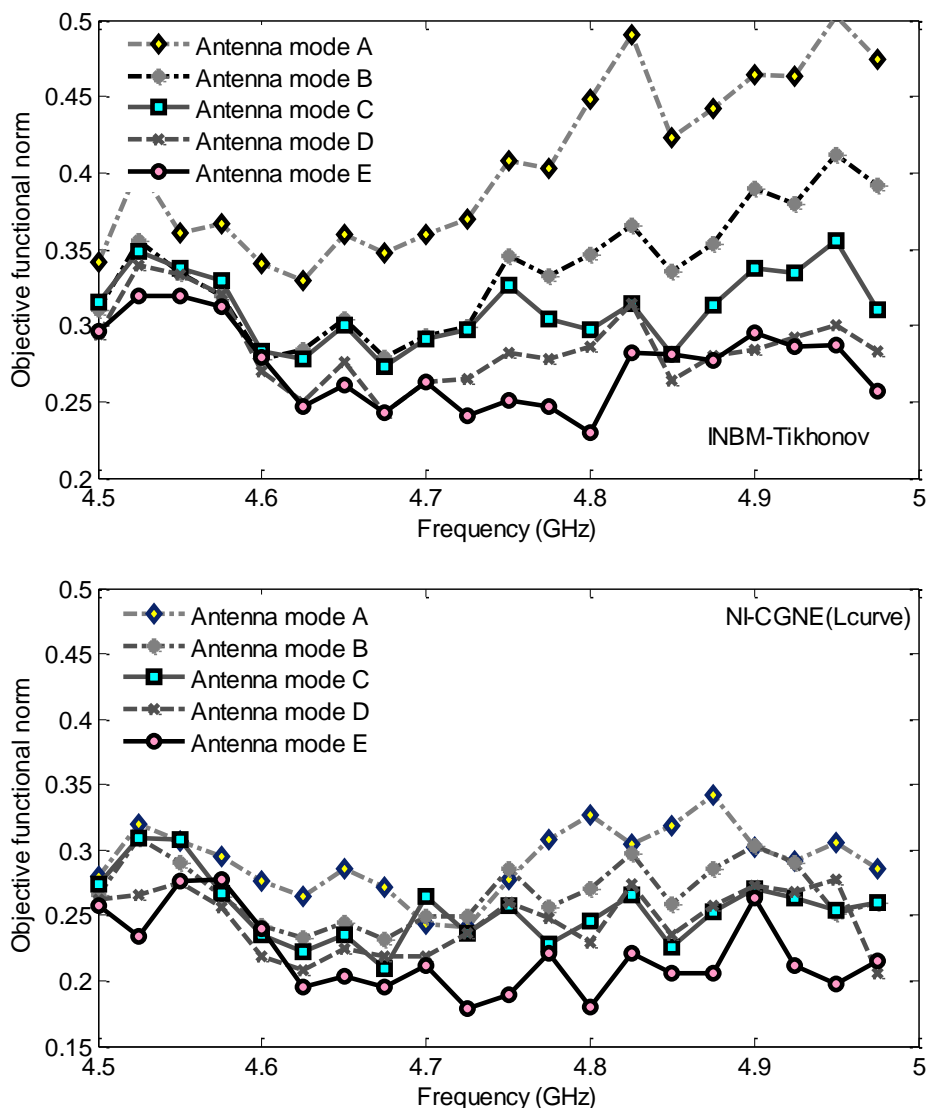


Figure 8-11: The effect of the architecture of the receiver to the pattern of the objective function norms of INBM-Tikhonov and NI-cgne-LC at 4.5 to 5.0 GHz

Mode A uses all the points of measured data while mode E applies half of the data point. The speed of reconstruction of mode E is faster and functional norm is smaller than that of the mode A. Decreasing the number of receiving antennas reduces the number of equation. The complexity of the computational problem is simplified, then, the minimizer results in a smaller functional norm

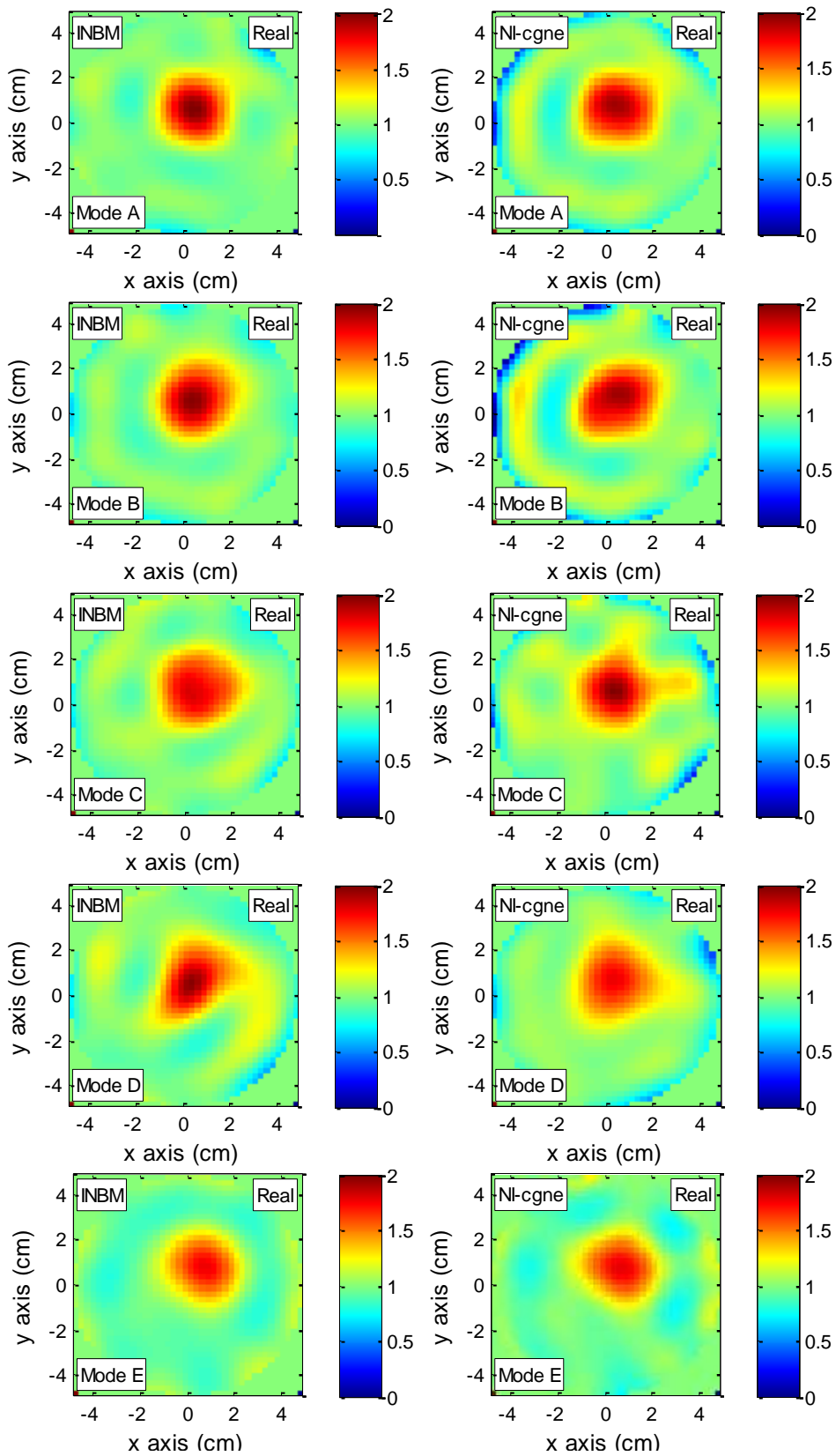


Figure 8-12: The results of antenna arrangement test: Images of plastic rod cross section when receiving antennas are set at five different modes. The working frequency is 4.5 GHz

However, reducing data points may be resulting in the shortfall of additional information. The number of antennas should be selected. Higher number of antennas increases computational burden while lower number of antennas reduces the amount of information. Beside the levels of noise at points data are varied. The position of the points data relative to the transmitting antenna influences the level of the noise. The calibrated scattered field which is varied in number and arrangement of the receiving antenna is studied. The effect of number of receiving antenna to the reconstructed images is presented in Figure 8-12.

In can be seen from the reconstructed images of calibrated scattered field in mode A antenna set where 15 Rx antennas are used that the shape and position of the Teflon cross section is clearly seen, the quantity of dielectric contrast is defined closed to the target value. However, the effect of noise is relatively higher than the reconstructed images of other antenna set modes.

Better images are resulted from the reconstruction of calibrated scattered field of less number of the receiving antennas. In mode C, Eleven out of 15 Rx antennas are used where the Rx antennas which are close to Tx are eliminated. It creates the best images. The shape and position of the object are clearly defined. The value of dielectric contrast is close to the target value and the image is clear from the noise effect. Further decreasing of the number of antennas is done in mode D. It declines the quality of the images. Modifying mode C by eliminating Rx antenna in the opposite side of Tx antenna improves the speed of the reconstruction and the quality of minimizer without losing the information and the quality of the images. Based on this empirical study, mode E is used in the next study.

8.9.2 The application of reconstruction algorithms

The algorithms which are Levenberg Marquardt (LM), Inexact Newton (INBM), and Newton iterative (NI-cgne) are applied to reconstruct the calibrated scattered field due to the introduction of the cylindrical Teflon. The methods are regulated using Tikhonov regularization, Landweber Friedman

iteration and conjugate gradient on normal equation. The results of the reconstruction are summarized in Table 8-2. It can be seen that approximation solution of linear ill posed problems is an alternative of the direct solution which is applied in LM algorithm with Tikhonov regularization. It is faster and more efficient than the direct solution.

The iterative approximation of linear ill posed problem of MWT inverse problem speeds up the process of reconstruction more than 4 times. The LM algorithm needs at least 21 iterations to solve the problem. While, the Newton iterative algorithm solves before the 10th iteration. The quality of iterative solution is also better than the direct solution.

Table 8-2: The number of iterations and objective functional norm of Levenberg Marquardt, Inexact Newton and Newton Iterative algorithms when reconstructing the images of the cross section of cylindrical Teflon

Algorithm	k			\mathcal{F}		
	4.3 GHz	4.6 GHz	5.0 GHz	4.3 GHz	4.6 GHz	5.0 GHz
<i>LM -Tikhonov</i>	21	30	25	0.3152	0.2795	0.2795
<i>INBM-Tikhonov</i>	4	4	4	0.3067	0.2665	0.2465
<i>INBM-Ladweber</i>	4	4	4	0.3167	0.2569	0.2125
<i>NI-CGNE</i>	4	8	5	0.2831	0.2440	0.1925

the objective function norm is calculated using (\mathcal{F})

$$\mathcal{F}([\chi]_k) = \frac{\|F([\chi]_k)\|^2}{\|\mathcal{E}^s\|^2}$$

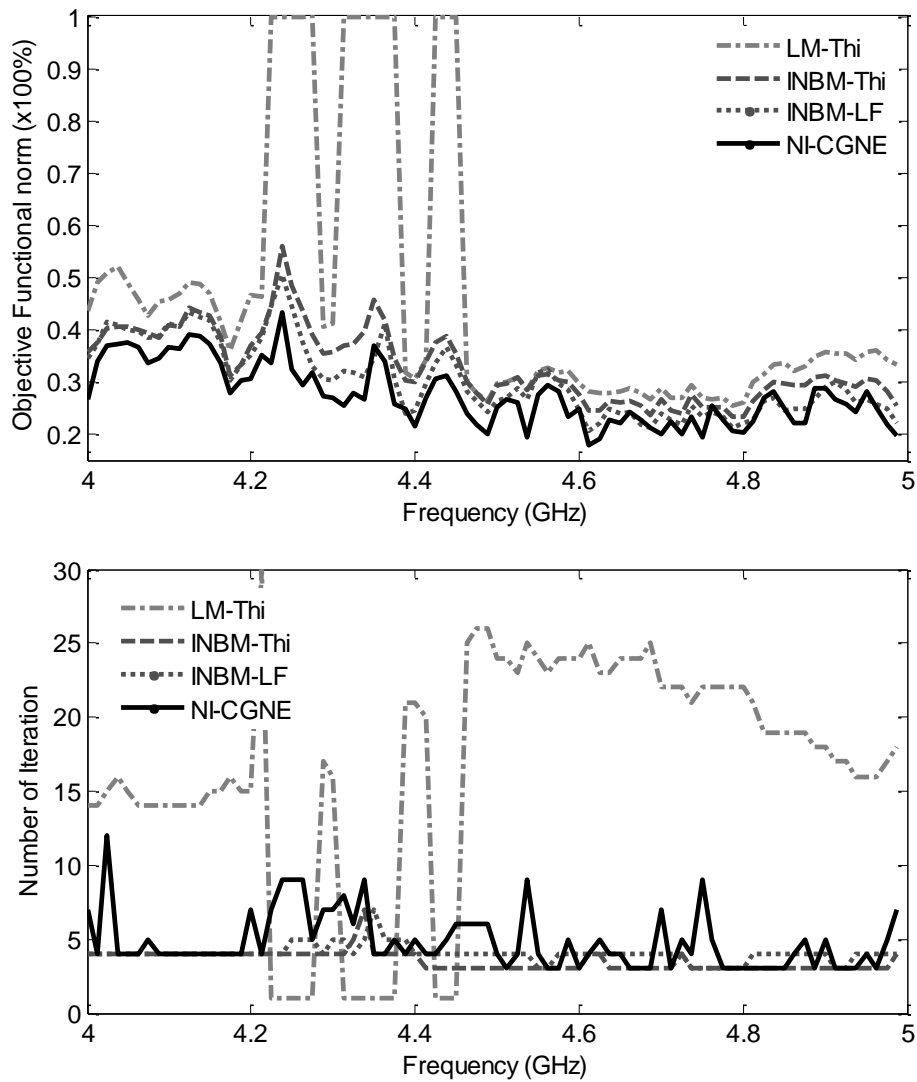


Figure 8-13: The objective functional norm and number of iterations of four different algorithms reconstructing the calibrated scattered field due to the presence of homogeneous dielectric cylinder.

Conjugate gradient provides better regulated approximation solution of the linear ill posed problem. The method is used at Newton iterative algorithm while other iterative regularizations are applied in inexact Newton. It can be seen in Figure 8-13 that the functional norm of the Newton iterative is the best among the other algorithms tested though it needs slightly more iterations to terminate the iteration of Newton method. The images resulted at three different frequencies are presented in Figure 8-14.

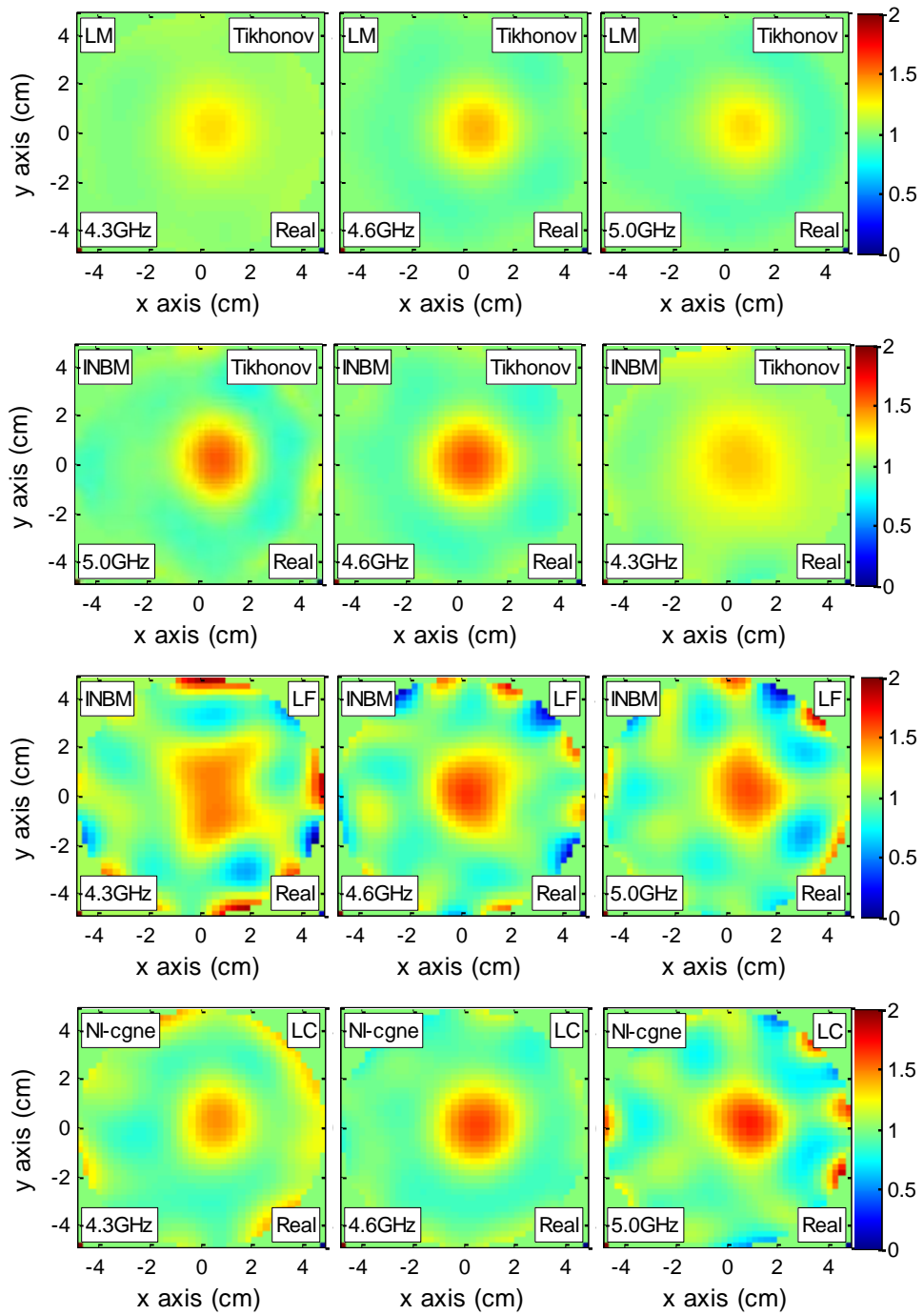


Figure 8-14: Images of plastic rod cross section resulted by various algorithms which are Levenberg Marquardt method, Inexact method and Newton Iterative with conjugate gradient at three different frequencies.

Figure 8-14 illustrates the images of Teflon cross section reconstructed by LM, INBM and NI-cgne algorithms. It can be seen that the images of NI-cgne algorithm are better than those resulted by the algorithms. The shape and the position of the interest are clearly seen, and the contrast of the object is closely determined at 4.6 and 5.0 GHz while the noise can relatively be eliminated.

Generally, the shape of the object can be reconstructed at a low frequency where the coefficient of reflection of the antennas is higher than -10dB. However, the contrast of the object can only be computed at a frequency where the coefficient of the antenna reflection is lower. Except for the Levenberg Marquardt method, the Newton method with various iterative regularized methods determines the contrast value of the dielectric of the object relatively close to the target. Tikhonov regulator shows the capability in delimiting the effect of the noise, while Ladweber Friedman iteration is sensitive to the noise. The conjugate gradient on normal equation which is regularized with L-curve stopping provides the best approximation regularized solution of the linear ill posed problem. The approximation directs the Newton method toward best global minimum point.

8.9.3 Object of interest variation

Inexact Newton with iterative Tikhonov regularization and Newton iterative with conjugate gradient on normal equation methods as regularized linear ill posed solvers are proved to be useful as alternative methods for solving microwave inverse problems. They build images that describe the shape position and contrast value of the object fairly close to the exact object. Further study is done to learn the flexibility of the algorithms in handling the shape and position of several objects.

8.9.3.1 Variation of objects of interest

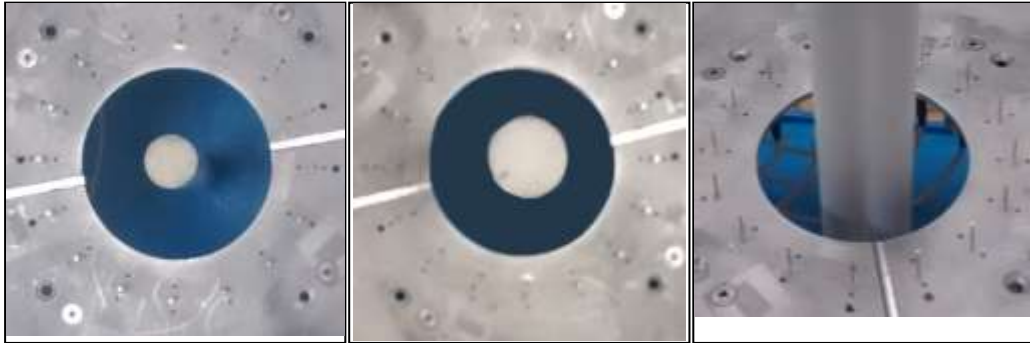


Figure 8-15: three different objects of interest used to test the adaptability of the inexact Newton and Newton iterative algorithms.

Three different objects of interest are introduced in this study. The objects of interest are illustrated in Figure 8-15, which include

- *Object of interest A* (OI A): a small cylindrical Teflon which is placed approximately in the center of the object domain.
- *Object of interest B* (OI B): a medium cylindrical Teflon which is placed approximately in the center of the object domain.
- *Object of interest C* (OI C): two small cylindrical Teflons which are bound and placed in the center of the object domain.

The University of Manchester-MWT system is set to be working at 4.5 GHz. 16 projections are applied at each measurement of undisturbed and disturbed electric fields where the receiver arrangement follows mode E of Table 8-1. Thus, the calibrated scattered field at each illumination consists of 8 data points, and the total number of data to be reconstructed is 128.

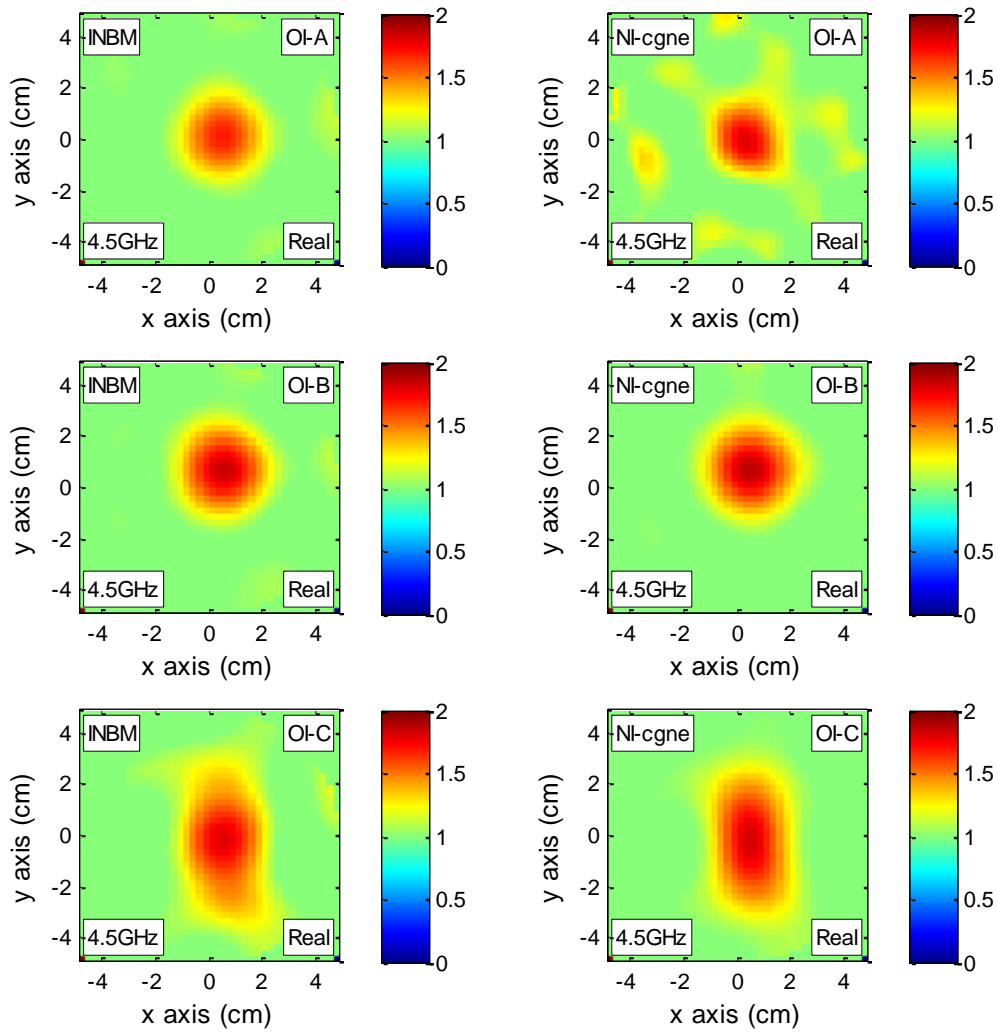


Figure 8-16: Images of three different objects of interest cross section resulted by INBM and NI-cgne at 4.5 GHz

Table 8-3: The result of reconstruction of varied objects of interest cross sectioned by Inexact Newton and Newton iterative algorithms

Algorithm	k			^{a)} \mathcal{F}		
	OIA	OIB	OIC	OIA	OIB	OIC
<i>INBM-Tikhonov</i>	3	4	4	0.3093	0.2665	0.219
<i>NI-CGNE(Lcurve)</i>	5	8	6	0.2380	0.2440	0.1910

The results of the reconstruction of three objects of interest are summarized in Table 8-3.. It can be seen that NI-cgne is 2 to 4 iterations slower than the INBM, however it produces better minimizer for all types of the object. Applied to both algorithms, the Newton iteration is terminated using ratio of the discrepancy of the objective functional norm. The stopping criteria is set to be $R < 0.05$. It can be seen that NI-cgne with L-curve as a regulator provides better Newton step than INBM with Tikhonov regularization. Figure 8-16 shows that NI-cgne describes the value of the contrast of the object better than INBM-Tikhonov. This is in line with the result of the minimizer.

8.9.3.2 Separation of two cylindrical objects of interest

Further adaptive study of the algorithm is done by applying it to distinguish the separation of two objects. Two small cylindrical Teflons are placed at various distance as seen in Figure 8-17

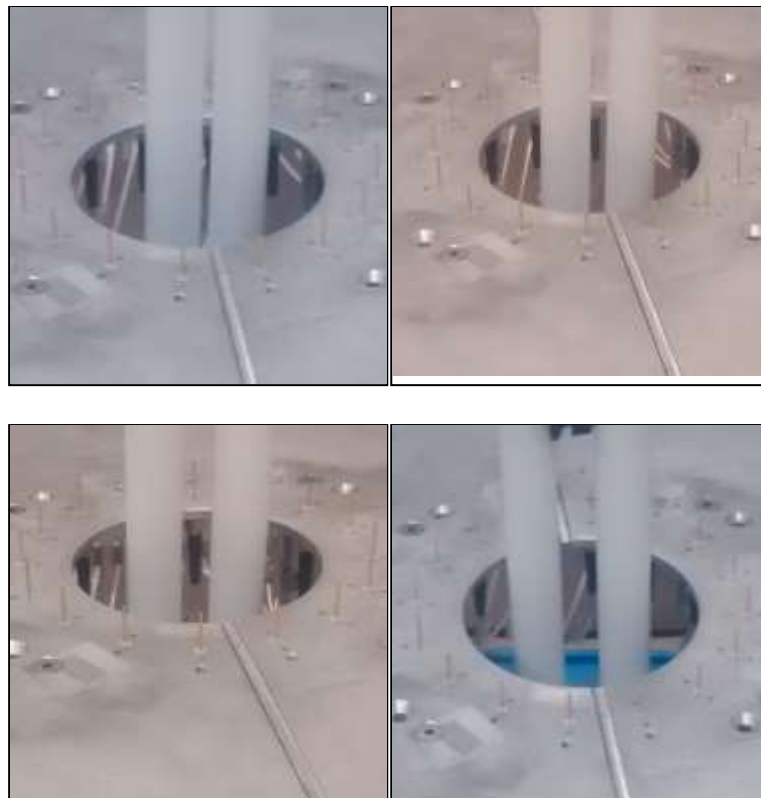


Figure 8-17: Two small cylindrical Teflons which are placed at object domain with four different gaps.

Table 8-4: The result of reconstruction of two small cylindrical Teflons with four different gaps by Inexact Newton and Newton iterative algorithms

Algorithm	k				^{a)} \mathcal{F}			
	^{b)} A	^{c)} B	^{d)} C	^{e)} D	A	B	C	D
<i>INBM-Thi</i>	4	4	4	4	0.2151	0.2134	0.2095	0.2167
<i>NI-CGNE</i>	8	9	9	4	0.1520	0.1487	0.1400	0.1298

^{a)} objective functional norm

^{b)} position A with gap 3 mm

^{c)} position B with gap 6 mm

^{d)} position C with gap 9 mm

^{e)} position D with gap 12 mm

The measurement is done at 4.6 GHz with mode E antenna arrangement. The results of reconstruction are summarized in table 7-4. It can be seen that Newton iterative is slower than the inexact Newton. The INBM with Tikhonov regularization terminates after 4 iterations. On the contrary, the NI generally needs double. However, the objective functional norm of NI is smaller than that of INBM. The minimum functional norm of NI reaches 12% while the minimum functional norm of INBM is more than 20%.

The NI builds better reconstruction images than the INBM as seen in Figure 8-18. The separation of the object of interest can be clearly seen in the images built by Newton iterative with CGNE. The gap of 3 mm can be distinguished. The number of objects can be clearly seen and the contrast of the dielectric is close to the exact value. The effect of the noise appears at the edge of the object domain. This is due to the approximation model of ground plane antenna used. However, the effect of the noise in the image can still be separated from the original object. On the other hand, the INBM is unable to separate 6 mm gap object, and moderately reconstructs contrast of two objects with 9 mm and 12 mm gaps

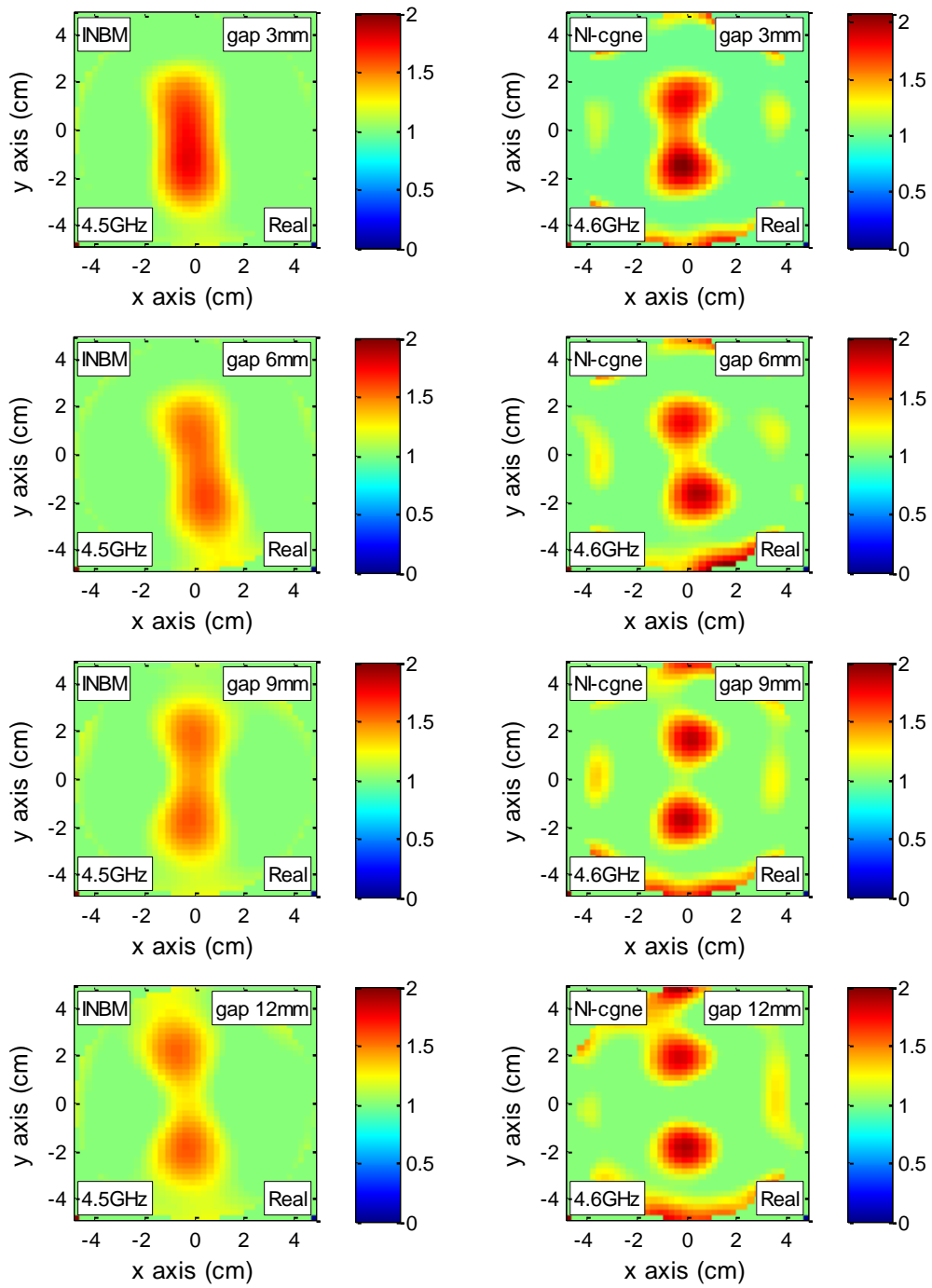


Figure 8-18: Images of two small cylindrical Teflons with four different gaps resulted by INBM and NI-cgne at 4.6 GHz

8.10 Conclusions

Microwave tomography system has been developed. 16 array ground plane antennas are used as a transmitter and a receiver of microwave signal which are generated and measured by a vector network analyzer. The switching is automatically controlled by computer via Cytec multiplexer. The data measured is undisturbed and disturbed electric fields. The scattered field is generated using pairs of measured fields and simulated incident fields at an object domain. The calibrated scattered field is reconstructed using developed algorithms.

The pattern of calibrated scattered field fluctuates due to noise effect, approximation model and other disturbances. To optimize the reconstruction, the arrangement of the set transmitter and receiver is studied. The optimum solution is found if the receiving antenna which is near and directly at the other side of the transmitter is eliminated.

The results of the experiment reveal that the NI-cgne which is the combination of inexact Newton class with iterative regularized linear ill posed problem produces a stable solution for MWT image inverse problem. The conjugate gradient on normal equation is used for iterative regularization. The regularization is determined using L-curve stopping rule. It has been shown that the NI-cgne reconstructs the contrast, shape and gap between objects of the objects of interest well, when other methods studied face several limitations.

9

Conclusions and Future works

9.1 Conclusions

Direct scattering problems of Microwave Tomography (MWT) have been solved using the moment of method with pulse basis function. The problems are solved in two-dimensional TM mode. It has been shown that with respect to the analytical solution, the moment of method provides accurate solution of the direct scattering problem.

The numerical solutions are developed to provide solutions of MWT forward problems which deal with a heterogeneous scatterer. The volume electric field integral equations for scattering from a dielectric cylinder are solved using the moment of method with a pulse basis function and a delta testing function. The numerical investigations reveal that the numerical scattered fields are sensitive to the radius of the cells and dielectric value. A radius $0.03 \lambda_0$ of the cell is the reasonable size for a homogeneous dielectric object of interest with the mean error less than 0.1% while the value of dielectric moderately effects on the error of the field. The increase of the contrast value does not directly change the errors. The numerical errors rise if

the object is too small or too big relative to the object domain. The errors also increase at the place of observation near the transmitter. Therefore, the arrangement of receiver antenna which is the number and position or so called receiver (Rx) is studied to obtain optimum reconstruction results.

The formulation of forward problems is used to derive the inverse problems of MWT. The MWT inverse problems are formulated in non-linear objective function norm instead of a least squared cost function. It has been studied that the solution MWT objective function presents more information than the solution of least squared cost function.

The MWT inverse problems are solved using Newton approach where the linearization is conducted using Fréchet differential. The linear ill posed Newton equations are solved using a direct regularized method. Levenberg Marquardt method (LM) with Tikhonov regularization. Numerical experiments show that LM method can be used to solve MWT inverse problems. The MWT objective function norm decreases and the errors of the images improve. However, the drawback of the LM method is that Newton equations have to be solved at each stage of the scheme which is expensive for MWT system and the solution may not be justified if the initial value is far from exact solution; beside it suffers from the noise effect.

The Inexact Newton Backtracking Method (INBM) is developed to solve MWT inverse problems. It is an inexact Newton class method which applies an implicit solution of the Newton equations by adding a residual of inexact Newton on the equations. The INBM is a nested loops algorithm where the main loop is Newton method to solve nonlinear problems and the nested loop solves the Newton equations which is functioning as the step of the Newton method. The solutions of Newton equations are iteratively determined in unspecific manner with a forcing term. The term defines the speed and accuracy of the MWT inverse problem solutions. The term is determined by the relation of the current nonlinear problem and its linear solution. It has been shown that the forcing term is relatively flexible to be defined. The use of a forcing term reduces the dependence on regulator techniques and its parameter. The solutions of Newton equations are any

intermediate solutions that meet the forcing term criteria. The results of the numerical experiment show that INBM is faster and more adaptive to the lossy material and noise levels than the LM method.

Newton Iterative-conjugate gradient on normal equation (NI-cgne) is a Newton Iterative method where the Newton step is the solutions of the normal form of the Newton equations. The conjugate gradient solves the Newton normal equations. The CGNE iteratively solves the Newton equations by constructing a normal equation of the equations. The method is a semi regulated algorithm. The regularization is done by setting a proper stopping rule. Two different techniques to define stopping rule are studied. They are the discrepancy principle and L-curve criteria. The techniques are modified to adapt with unknown levels of noise and the irregularity of the solutions of the Newton equations. The discrepancy parameter is empirically determined by defining a level of confidence. While the triangle method of L-curve criteria is modified to deal with limited and roughness of discrete number linear solutions. The method is applied to solve MWT inverse problems of lossy material. Numerical experiments with noisy data show that NI-cgne produces more stable solution of MWT inverse problems than LM method. Techniques to define stopping point of the iteration can be used to regulate the Newton equations.

Microwave tomography system is developed in the University of Manchester. The measurement system is constructed by an array of ground plane antennas where the microwave signal is transmitted and measured using vector network analyzer. The system is computerized via Cytec multiplexer. The command is written in MATLAB syntax, in which the mnemonic function of the interface is addressed in a text list via GPIB interface. The measured scattered field is calculated based on the difference of the measurements of undisturbed and disturbed electric field. The difference of the electric field is calibrated toward modeled incident field in object domain and data domain. The incident is assumed to be illuminated from an infinitely long line current source. The calibrated scattered field is reconstructed using LM, INBM and NI-cgne algorithms. The experiments

show that NI-cgne is the most adaptive method. It reconstructs the cross section of the target object better over a wider frequency range. NI-cgne and INBM produce clearly defined shape and location of the OI in which the contrast values are relatively close to the target value while the LM method can only plainly define the shape and location of the object and poorly compute the contrast of the object. . The NI-cgne describes various object shapes and gaps between objects clearly, while the LM fails and INBM can only defines the gap of OI more than 10 mm, besides the contrast of multiple objects is poorly defined.

9.2 Future works

The results of the research promote the idea of developing tomography. The works that will be done include:

- *Investigating higher frequency.* Tomography system may be developed in a higher frequency range. The application of higher frequency such as millimeter and Terahertz waves which have unique characteristics may extend the application of Tomography to the wider application. The interaction of higher frequency signal with object of interest will be studied and the application of time domain method is considered.
- *Investigating the statement of MWT inverse problem and its optimization.* The statement of inverse problem is extended in term of contrast-source variables. The problem will be stated as a multi varied system with contrast and field variables as the unknowns and object function and data function as the systems to be solved. It will also be stated with respect to contrast source variable, in which the unknown contrast distributions of the interest are extracted from the solution of the inverse problem. The investigation involves the development of cheap linear solvers and alternative optimization methods. The goal of reconstruction of tomography is building images of the object of interest accurately and quickly. A cheap solver is essential to support approximation of the linear

ill posed problems. Various linear ill posed solvers will be investigated, which include stochastic methods and other adaptive regulators of ill posed problem solvers.

- *Developing a portable microwave tomography system.* It has been shown that the inverse problem developed could handle the noise level of the experimental measurement system in which monopole antenna is designed as the transmitter and transducer of the electric field. The development of signal generator and acquisition technique will be studied. This research will eliminate the use of expensive and immobile vector network analyzer. Furthermore, the use of Cytex multiplexer is possible to be substituted with digital multiplexer. The microwave tomography system in the portable system can be applied in a wider area of applications and may be connected to other possible devices.

Reference

- 1 Pan, S. X., & Kak, A. C. (1983). A computational study of reconstruction algorithms for diffraction tomography: Interpolation versus filtered-backpropagation. *Acoustics, Speech and Signal Processing, IEEE Transactions on*, 31(5), 1262-1275.
- 2 (!!! INVALID CITATION !!!).
- 3 Slaney, M., Kak, A. C., & Larsen, L. E. (1984). Limitations of imaging with first-order diffraction tomography. *Microwave Theory and Techniques, IEEE Transactions on*, 32(8), 860-874.
- 4 Warsito, W., Marashdeh, Q., & Fan, L.-S. (2007). Electrical capacitance volume tomography. *Sensors Journal, IEEE*, 7(4), 525-535.
- 5 Gwan Soo, P., & Dong Seok, K. (2005). Development of a magnetic inductance tomography system. *Magnetics, IEEE Transactions on*, 41(5), 1932-1935.
- 6 Dobson, D. C., & Santosa, F. (1994). Resolution and stability analysis of an inverse problem in electrical impedance tomography: Dependence on the input current patterns. *SIAM Journal on Applied Mathematics*, 54(6), 1542-1560.
- 7 Gibson, W. C. (2007). *The method of moment in electromagnetics*. Boca Raton: CRC Press.
- 8 Harrington, R. (1993). *Field computation by moment methods* Wiley-IEEE Press
- 9 Peterson, A., Ray, S., & Mittra, R. (1998). *Computational methods for electromagnetics* (Vol. 1): Wiley-IEEE Press
- 10 Kleinman, R. E., & van den Berg, P. M. (1992). A modified gradient method for two dimensional problems in tomography. *Journal of Computational and Applied Mathematics*, 42(1), 17-35.
- 11 van den Berg, P. M., & Kleinman, R. E. (1995). A total variation enhanced modified gradient algorithm for profile reconstruction. *Inverse Probl*, 11(3), L5-L10.
- 12 Hu, J. L., Wu, Z., McCann, H., Davis, L. E., & Xie, C. G. (2006). Bfgs quasi-newton method for solving electromagnetic inverse problems. *IEE Proceedings - Microwaves, Antennas and Propagation*, 153(2), 199.
- 13 van den Berg, P. M., & Abubakar, A. (2001). Contrast source inversion method state of art. *Progress In Electromagnetics Research*, 34, 189–218.
- 14 van den Berg, P. M., & Kleinman, R. E. (1997). A contrast source inversion method. *Inverse Probl*, 13, 1607–1620.

- 15 Olkkonen, M., Mikhnev, V., & Huuskonen, E. (2012, 10-14 Sept. 2012). *Rf moisture measurement of concrete with a resonator sensor*. Paper presented at the Microwave and Telecommunication Technology (CriMiCo), 2012 22nd International Crimean Conference.
- 16 Kemp, I., Peterson, M., Benton, C., & Petkie, D. T. (2009, 21-23 July 2009). *Sub-mm wave imaging techniques for non-destructive aerospace materials evaluation*. Paper presented at the Aerospace & Electronics Conference (NAECON), Proceedings of the IEEE 2009 National.
- 17 Aguilar, S. M., Al-Joumayly, M. A., Burfeindt, M. J., Behdad, N., & Hagness, S. C. (2014). Multiband miniaturized patch antennas for a compact, shielded microwave breast imaging array. *Antennas and Propagation, IEEE Transactions on*, 62(3), 1221-1231.
- 18 Liu, C., & Afsar, M. N. (2012, 1-6 July 2012). *A millimeter wave breast cancer imaging methodology*. Paper presented at the Precision Electromagnetic Measurements (CPEM), 2012 Conference on.
- 19 Zakaria, A., Baran, A., & LoVetri, J. (2012). Estimation and use of prior information in fem-csi for biomedical microwave tomography. *Antennas and Wireless Propagation Letters, IEEE*, 11, 1606-1609.
- 20 Witten, A., & Molyneux, J. E. (1988). Geophysical imaging with arbitrary source illumination. *Geoscience and Remote Sensing, IEEE Transactions on*, 26(4), 409-419.
- 21 Klokov, A., & Sato, M. (2011, 24-29 July 2011). *Application of 3-d migration algorithm to gpr on an irregular ground surface*. Paper presented at the Geoscience and Remote Sensing Symposium (IGARSS), 2011 IEEE International.
- 22 Yilong, Z., Yuehua, L., & Jianfei, C. (2013, 5-8 Nov. 2013). *Detection of concealed objects in passive millimeter wave imaging based on cs theory*. Paper presented at the Microwave Conference Proceedings (APMC), 2013 Asia-Pacific.
- 23 Yi, L., Wuqiang, Y., Zhipeng, W., Tsamakis, D., Chenggang, X., Songming, H., & Lenn, C. (2012, 16-17 July 2012). *Gas/oil/water flow measurement by electrical capacitance tomography*. Paper presented at the Imaging Systems and Techniques (IST), 2012 IEEE International Conference on.
- 24 Bolton, G. T., & Primrose, K. M. (2005). An overview of electrical tomographic measurements in pharmaceutical and related application areas. *AAPS PharmSciTech*, 6(2), E137-E143.
- 25 Hy, W., Yang, C., Ma, L., Ye, Z., Yao, A., & Soleimani, M. (2012, 13-16 May 2012). *Three-dimensional industrial process tomography using electrical and electromagnetic tomography: Recent developments*. Paper presented at the Instrumentation and Measurement Technology Conference (I2MTC), 2012 IEEE International.

- 26 Soleimani, M., Lionheart, W. R. B., & Peyton, A. J. (2007). Image reconstruction for high-contrast conductivity imaging in mutual induction tomography for industrial applications. *Instrumentation and Measurement, IEEE Transactions on*, 56(5), 2024-2032.
- 27 Devaney, A. J. (1982). A filtered backprojection algorithm for diffraction tomography. *Ultrasound Imaging*, 4, 336-360.
- 28 Cui, T. J., Weng Cho, C., Xiao Xing, Y., & Wei, H. (2004). Study of resolution and super resolution in electromagnetic imaging for half-space problems. *Antennas and Propagation, IEEE Transactions on*, 52(6), 1398-1411.
- 29 Shen, Y. C., Gan, L., Stringer, M., Burnett, A., Tych, K., Shen, H., . . . Davies, A. G. (2009). Terahertz pulsed spectroscopic imaging using optimized binary masks. *Applied Physics Letters*, 95(23), 231112-231112-231113.
- 30 Pickwell, E., Cole, B. E., Fitzgerald, A. J., Pepper, M., & Wallace, V. P. (2004). In vivo study of human skin using pulsed terahertz radiation. *Phys Med Biol*, 49(9), 1595.
- 31 Wang, Y., Zhao, Z., Chen, Z., Li, Z., & Kang, K. (2008, 21-24 April 2008). *Investigation of material identification with terahertz pulsed imaging*. Paper presented at the Microwave and Millimeter Wave Technology, 2008. ICMWT 2008. International Conference on.
- 32 Mittleman, D. M., Hunsche, S., Boivin, L., & Nuss, M. C. (1997). T-ray tomography. *Optics Letters*, 22(12), 904-906.
- 33 Yasui, T., Yasuda, T., & Araki, T. (2005, 19-23 Sept. 2005). *Real-time two-dimensional terahertz tomography*. Paper presented at the Infrared and Millimeter Waves and 13th International Conference on Terahertz Electronics, 2005. IRMMW-THz 2005. The Joint 30th International Conference on.
- 34 Yasuda, T., Iwata, T., Araki, T., & Yasui, T. (2007). Improvement of minimum paint film thickness for thz paint meters by multiple-regression analysis. *Applied Optics*, 46(30), 7518-7526.
- 35 Yasui, T., Jewariya, M., Yasuda, T., Schirmer, M., Araki, T., & Abraham, E. (2013). Real-time two-dimensional spatiotemporal terahertz imaging based on noncollinear free-space electrooptic sampling and application to functional terahertz imaging of moving object. *Selected Topics in Quantum Electronics, IEEE Journal of*, 19(1), 8600110-8600110.
- 36 Brahm, A., Pradarutti, B., Kunz, M., Riehemann, S., Notni, G., Nolte, S., & Tunnermann, A. (2009, 21-25 Sept. 2009). *Thz tomography in transmission and reflection*. Paper presented at the Infrared, Millimeter, and Terahertz Waves, 2009. IRMMW-THz 2009. 34th International Conference on.
- 37 Woodward, R. M., Cole, B., Wallace, E. V. P., Pye, R. J., Arnone, D. D., Linfield, E. H., & Pepper, M. (2002). Terahertz pulse imaging in reflection geometry of human skin cancer and skin tissue. *Phys Med Biol*, 47(21), 3853.

- 38 Guillet, J. P., Recur, B., Frederique, L., Bousquet, B., Canioni, L., Manek-Hönninger, I., . . . Mounaix, P. (2014). Review of terahertz tomography techniques. *Journal of Infrared, Millimeter, and Terahertz Waves*, 35(4), 382-411.
- 39 Ferguson, B., Wang, S. H., Abbott, D., & Zhang, X. C. (2002, 2002). *T-ray tomographic imaging*. Paper presented at the Terahertz Electronics Proceedings, 2002. IEEE Tenth International Conference on.
- 40 Brahm, A., Kunz, M., Riehemann, S., Notni, G., & Tünnermann, A. (2010). Volumetric spectral analysis of materials using terahertz-tomography techniques. *Applied Physics B*, 100(1), 151-158.
- 41 Ferguson, B., Wang, S., Gray, D., Abbot, D., & Zhang, X. C. (2002). T-ray computed tomography. *Optics Letters*, 27(5), 1312-1314.
- 42 Ferguson, B., Shaohong, W., Gray, D., Abbott, D., & Zhang, X. C. (2002, 24-24 May 2002). *Three dimensional imaging using t-ray computed tomography*. Paper presented at the Lasers and Electro-Optics, 2002. CLEO '02. Technical Digest. Summaries of Papers Presented at the.
- 43 Jewariya, M., Abraham, E., Kitaguchi, T., Ohgi, Y., Minami, M.-a., Araki, T., & Yasui, T. (2013). Fast three-dimensional terahertz computed tomography using real-time line projection of intense terahertz pulse. *Optics Express*, 21(2), 2423-2433.
- 44 Yin, X. X., Ng, B. W. H., Ferguson, B., Mickan, S. P., & Abbott, D. (2007, 4-7 June 2007). *Terahertz computed tomographic reconstruction and its wavelet-based segmentation by fusion*. Paper presented at the Industrial Electronics, 2007. ISIE 2007. IEEE International Symposium on.
- 45 Liangchao, L., Jianyu, Y., Jianzhong, S., & Changlin, Z. (2011, 2-7 Oct. 2011). *Two-step projection iteration thresholding super resolution for passive millimeter imaging*. Paper presented at the Infrared, Millimeter and Terahertz Waves (IRMMW-THz), 2011 36th International Conference on.
- 46 Ghasr, M. T., Case, J. T., & Zoughi, R. (2014). Novel reflectometer for millimeter-wave 3-d holographic imaging. *Instrumentation and Measurement, IEEE Transactions on*, 63(5), 1328-1336.
- 47 Zeyu, L., Jintao, X., & Jianyu, Y. (2006, 16-19 Oct. 2006). *An image regulation technique for passive millimeter wave focal plane array imaging radar system*. Paper presented at the Radar, 2006. CIE '06. International Conference on.
- 48 Caster, F., Gilreath, L., Shiji, P., Zheng, W., Capolino, F., & Heydari, P. (2014). Design and analysis of a w-band 9-element imaging array receiver using spatial-overlapping super-pixels in silicon. *Solid-State Circuits, IEEE Journal of*, 49(6), 1317-1332.
- 49 Yujiri, L. (2006, 11-16 June 2006). *Passive millimeter wave imaging*. Paper presented at the Microwave Symposium Digest, 2006. IEEE MTT-S International.

- 50 Sheen, D. M., McMakin, D. L., & Hall, T. E. (2001). Three-dimensional millimeter-wave imaging for concealed weapon detection. *Microwave Theory and Techniques, IEEE Transactions on*, 49(9), 1581-1592.
- 51 Hu, Z., Karim, M. F., Ong, L. C., Luo, B., & Chiam, T. M. (2013, 5-8 Nov. 2013). *A simple and efficient method of millimeter-wave image formation using back-projection algorithm*. Paper presented at the Microwave Conference Proceedings (APMC), 2013 Asia-Pacific.
- 52 Kyung Kwon, J., Sang Won, Y., Yeon-Sik, C., & Jin-Koo, R. (2009, 8-13 Feb. 2009). *Development of a passive millimeter-wave imaging system*. Paper presented at the Waveform Diversity and Design Conference, 2009 International.
- 53 Ahmed, S. S., Schiessl, A., & Schmidt, L. (2011, 5-10 June 2011). *Novel fully electronic active real-time millimeter-wave imaging system based on a planar multistatic sparse array*. Paper presented at the Microwave Symposium Digest (MTT), 2011 IEEE MTT-S International.
- 54 Ghasr, M. T., Kharkovsky, S., Bohnert, R., Hirst, B., & Zoughi, R. (2013). 30 ghz linear high-resolution and rapid millimeter wave imaging system for nde. *Antennas and Propagation, IEEE Transactions on*, 61(9), 4733-4740.
- 55 Sheen, D. M., McMakin, D. L., Hall, T. E., & Severtsen, R. H. (2009, 11-12 May 2009). *Active millimeter-wave standoff and portal imaging techniques for personnel screening*. Paper presented at the Technologies for Homeland Security, 2009. HST '09. IEEE Conference on.
- 56 Fujii, Y., Fujiwara, Y., Tanaka, S., Okumura, S., Togo, H., Mochizuki, A., & Kukutsu, N. (2010, 5-10 Sept. 2010). *Feasibility of millimeter wave imaging as tool for nondestructive inspection of wood and wooden structures*. Paper presented at the Infrared Millimeter and Terahertz Waves (IRMMW-THz), 2010 35th International Conference on.
- 57 Ghasr, M. T., Pommerenke, D., Case, J. T., McClanahan, A., Aflaki-Beni, A., Abou-Khousa, M., . . . Zoughi, R. (2011). Rapid rotary scanner and portable coherent wideband q-band transceiver for high-resolution millimeter-wave imaging applications. *Instrumentation and Measurement, IEEE Transactions on*, 60(1), 186-197.
- 58 Case, J. T., Ghasr, M. T., & Zoughi, R. (2011). Optimum two-dimensional uniform spatial sampling for microwave sar-based nde imaging systems. *Instrumentation and Measurement, IEEE Transactions on*, 60(12), 3806-3815.
- 59 Xiaoxiang, L., Leung, H., & Lampropoulos, G. A. (2012). Effect of wall parameters on ultra-wideband synthetic aperture through-the-wall radar imaging. *Aerospace and Electronic Systems, IEEE Transactions on*, 48(4), 3435-3449.

- 60 Narayanan, R. M., Xu, X., & Henning, J. A. (2004). Radar penetration imaging using ultra-wideband (uwb) random noise waveforms. *Radar, Sonar and Navigation, IEE Proceedings -*, 151(3), 143-148.
- 61 Jungang, Y., Xiaotao, H., Thompson, J., Tian, J., & Zhimin, Z. (2011). Low-frequency ultra-wideband synthetic aperture radar ground moving target imaging. *Radar, Sonar & Navigation, IET*, 5(9), 994-1001.
- 62 Fletcher, R., & Reeves, C. M. (1964). Function minimization by conjugate gradients. *Computer Journal*, 7, 149-154.
- 63 Polak, E. (1997). *Optimization: Algorithms and consistent approximations* (Vol. 124). New York: Springer.
- 64 Chaumet, P. C., Belkebir, T., & Sentenac, A. (2009). Experimental microwave imaging of three-dimensional targets with different inversion procedures. *Journal of Applied Physics*, 106(3), 034901-034901-034908.
- 65 Pastorino, M., Caorsi, S., & Massa, A. (2002). A global optimization technique for microwave nondestructive evaluation. *Instrumentation and Measurement, IEEE Transactions on*, 51(4), 666-673.
- 66 Qing Huo, L., Zhong Qing, Z., Wang, T. T., Bryan, J. A., Ybarra, G. A., Nolte, L. W., & Joines, W. T. (2002). Active microwave imaging. I. 2-d forward and inverse scattering methods. *Microwave Theory and Techniques, IEEE Transactions on*, 50(1), 123-133.
- 67 Rubk, T., Meaney, P. M., Meincke, P., & Paulsen, K. D. (2007). Nonlinear microwave imaging for breast-cancer screening using gauss newton's method and the cgls inversion algorithm. *Antennas and Propagation, IEEE Transactions on*, 55(8), 2320-2331.
- 68 Zhong Qing, Z., & Qing Huo, L. (2001, 8-13 July 2001). *Microwave imaging for breast tumor: 2d forward and inverse methods*. Paper presented at the Antennas and Propagation Society International Symposium, 2001. IEEE.
- 69 Semenov, S. Y., Bulyshev, A. E., Souvorov, A. E., Nazarov, A. G., Sizov, Y. E., Svenson, R. H., . . . Tatsis, G. P. (2000). Three-dimensional microwave tomography: Experimental imaging of phantoms and biological objects. *Microwave Theory and Techniques, IEEE Transactions on*, 48(6), 1071-1074.
- 70 Wu, Z. (2001). Tomographic imaging of isolated ground surfaces using radio ground waves and conjugate gradient methods. *Radar, Sonar and Navigation, IEE Proceedings -*, 148(1), 27-34.
- 71 Belkebir, K., Kleinman, R. E., & Pichot, C. (1997). Microwave imaging-location and shape reconstruction from multifrequency scattering data. *Microwave Theory and Techniques, IEEE Transactions on*, 45(4), 469-476.
- 72 Caorsi, S., Donelli, M., Franceschini, D., & Massa, A. (2003). A new methodology based on an iterative multiscaling for microwave imaging. *Microwave Theory and Techniques, IEEE Transactions on*, 51(4), 1162-1173.

- 73 Fhager, A., Voronov, A., Chen, C., & Persson, M. (2007, 11-16 Nov. 2007). *Methods for dielectric reconstruction in microwave tomography*. Paper presented at the Antennas and Propagation, 2007. EuCAP 2007. The Second European Conference on.
- 74 Fhager, A., & Persson, M. (2007). Using a priori data to improve the reconstruction of small objects in microwave tomography. *Microwave Theory and Techniques, IEEE Transactions on*, 55(11), 2454-2462.
- 75 Zhong Qing, Z., & Qing Huo, L. (2004). Three-dimensional nonlinear image reconstruction for microwave biomedical imaging. *Biomedical Engineering, IEEE Transactions on*, 51(3), 544-548.
- 76 Abubakar, A., Semenov, S., Posukh, V. G., & Van den Berg, P. M. (2005, 12-17 June 2005). *Application of the multiplicative regularized contrast source inversion method to real biological data*. Paper presented at the Microwave Symposium Digest, 2005 IEEE MTT-S International.
- 77 Gilmore, C., Abubakar, A., Wenyi, H., Habashy, T. M., & Van den Berg, P. M. (2009). Microwave biomedical data inversion using the finite-difference contrast source inversion method. *Antennas and Propagation, IEEE Transactions on*, 57(5), 1528-1538.
- 78 Gilmore, C., Mojabi, P., & LoVetri, J. (2009). Comparison of an enhanced distorted born iterative method and the multiplicative-regularized contrast source inversion method. *Antennas and Propagation, IEEE Transactions on*, 57(8), 2341-2351.
- 79 Baran, A., Kurrant, D., Zakaria, A., Fear, E., & LoVetri, J. (2014, 6-11 July 2014). *Breast cancer imaging using microwave tomography with radar-derived prior information*. Paper presented at the Radio Science Meeting (Joint with AP-S Symposium), 2014 USNC-URSI.
- 80 Lianlin, L., Hu, Z., & Fang, L. (2009). Two-dimensional contrast source inversion method with phaseless data: Tm case. *Geoscience and Remote Sensing, IEEE Transactions on*, 47(6), 1719-1736.
- 81 Abubakar, A., Hu, W., van den Berg, P. M., & Habashy, T. M. (2008). A finite-difference contrast source inversion method. *Inverse Probl*, 24(6), 065004.
- 82 Abubakar, A., Hu, W., van den Berg, P. M., & Habashy, T. M. (2008, 5-11 July 2008). *A contrast source inversion method for reconstructing objects in an inhomogeneous background medium*. Paper presented at the Antennas and Propagation Society International Symposium, 2008. AP-S 2008. IEEE.
- 83 Abubakar, A., van den Berg, P. M., & Mallorqui, J. J. (2002). Imaging of biomedical data using a multiplicative regularized contrast source inversion method. *Microwave Theory and Techniques, IEEE Transactions on*, 50(7), 1761-1771.
- 84 Semenov, S. Y., Bulyshev, A. E., Abubakar, A., Posukh, V. G., Sizov, Y. E., Souvorov, A. E., . . . Williams, T. C. (2005). Microwave-tomographic imaging of the high dielectric-contrast

- objects using different image-reconstruction approaches. *Microwave Theory and Techniques, IEEE Transactions on*, 53(7), 2284-2294.
- 85 van den Berg, P. M., Kooij, B. J., & Kleinman, R. E. (1997). Image reconstruction from ipswich data. li. *Antennas and Propagation Magazine, IEEE*, 39(2), 29-32.
- 86 van den Berg, P. M., Kooij, B. J., & Kleinman, R. E. (1999). Image reconstruction from ipswich data. lii. *Antennas and Propagation Magazine, IEEE*, 41(2), 27-32.
- 87 Jinghong, M., Changyun, M., & Marklein, R. (2010). Application of contrast source inversion algorithm for reconstructing complicated targets from experimental transverse electric data. 271-274.
- 88 Jinghong, M., Hongqiang, L., Changyun, M., & Marklein, R. (2010, 16-18 Oct. 2010). *Application of the linear and nonlinear inversion algorithms for microwave imaging*. Paper presented at the Image and Signal Processing (CISP), 2010 3rd International Congress on.
- 89 Jinghong, M. (2013). Contrast source inversion algorithm against three dimensional microwave experimental data. *Journal of Information and Computational Science*, 10(5), 1479-1487.
- 90 Abubakar, A., van den Berg, P. M., & Semenov, S. Y. (2003). Two- and three-dimensional algorithms for microwave imaging and inverse scattering. *Journal of Electromagnetic Waves and Applications*, 17(2), 209-231.
- 91 Barrière, P.-A., Idier, J., Laurin, J.-J., & Goussard, Y. (2011). Contrast source inversion method applied to relatively high contrast objects. *Inverse Probl*, 27(7), 075012.
- 92 Kundu, A. K., Bandyopadhyay, B., & Sanyal, S. (2008). *An iterative algorithm for microwave tomography using modified gauss-newton method*. Paper presented at the Biomed 2008.
- 93 Abubakar, A., & Habashy, T. M. (2010, 11-17 July 2010). *Application of the multiplicative-regularized gauss-newton inversion for microwave biomedical imaging applications*. Paper presented at the Antennas and Propagation Society International Symposium (APSURSI), 2010 IEEE.
- 94 De Zaeytjyd, J., Franchois, A., Eyraud, C., & Geffrin, J. M. (2007). Full-wave three-dimensional microwave imaging with a regularized gauss -newton method - theory and experiment. *Antennas and Propagation, IEEE Transactions on*, 55(11), 3279-3292.
- 95 Mojabi, P., & LoVetri, J. (2009). Microwave biomedical imaging using the multiplicative regularized gauss-newton inversion. *Antennas and Wireless Propagation Letters, IEEE*, 8, 645-648.
- 96 Mojabi, P., & LoVetri, J. (2010). Comparison of te and tm inversions in the framework of the gauss-newton method. *Antennas and Propagation, IEEE Transactions on*, 58(4), 1336-1348.
- 97 Abubakar, A., Habashy, T. M., Guangdong, P., & Mao-Kun, L. (2012). Application of the multiplicative regularized gauss-newton

- algorithm for three-dimensional microwave imaging. *Antennas and Propagation, IEEE Transactions on*, 60(5), 2431-2441.
- 98 Fang, Q., Meaney, P. M., Geimer, S. D., Streltsov, A. V., & Paulsen, K. D. (2004). Microwave image reconstruction from 3-d fields coupled to 2-d parameter estimation. *Medical Imaging, IEEE Transactions on*, 23(4), 475-484.
- 99 Meaney, P. M., Yagnamurthy, N. K., Dun, L., Demidenko, E., & Paulsen, K. D. (2001, 8-13 July 2001). A 2-stage gauss-newton reconstruction technique for improved object detection in microwave imaging. Paper presented at the Antennas and Propagation Society International Symposium, 2001. IEEE.
- 100 Fang, Q., Meaney, P. M., & Paulsen, K. D. (2004). Microwave image reconstruction of tissue property dispersion characteristics utilizing multiple-frequency information. *Microwave Theory and Techniques, IEEE Transactions on*, 52(8), 1866-1875.
- 101 Bulyshev, A. E., Souvorov, A. E., Semenov, S. Y., Posukh, V. G., & Sizov, Y. E. (2004). Three-dimensional vector microwave tomography: Theory and computational experiments. *Inverse Probl*, 20(4), 1239.
- 102 Mojabi, P., & LoVetri, J. (2009). Overview and classification of some regularization techniques for the gauss-newton inversion method applied to inverse scattering problems. *Antennas and Propagation, IEEE Transactions on*, 57(9), 2658-2665.
- 103 Roger, A. (1981). Newton-kantorovitch algorithm applied to an electromagnetic inverse problem. *Antennas and Propagation, IEEE Transactions on*, 29(2), 232-238.
- 104 Joachimowicz, N., Pichot, C., & Hugonin, J. P. (1991). Inverse scattering: An iterative numerical method for electromagnetic imaging. *Antennas and Propagation, IEEE Transactions on*, 39(12), 1742-1753.
- 105 Mikhnev, V. A., & Vainikainen, P. (2000). Two-step inverse scattering method for one-dimensional permittivity profiles. *Antennas and Propagation, IEEE Transactions on*, 48(2), 293-298.
- 106 Garnero, L., Franchois, A., Hugonin, J. P., Pichot, C., & Joachimowicz, N. (1991). Microwave imaging-complex permittivity reconstruction-by simulated annealing. *Microwave Theory and Techniques, IEEE Transactions on*, 39(11), 1801-1807.
- 107 Nugroho, A. T., & Wu, Z. (1999). *Microwave imaging of 3d lossy dielectric objects using algebraic reconstruction techniques*. Paper presented at the World Congress on Industrial Process Tomography, Buxton, Manchester.
- 108 Henriksson, T., Joachimowicz, N., Conessa, C., & Bolomey, J. C. (2010). Quantitative microwave imaging for breast cancer detection using a planar 2.45 ghz system. *Instrumentation and Measurement, IEEE Transactions on*, 59(10), 2691-2699.
- 109 Belkebir, K., Elissatt, J. M., Geffrid, J. M., & Pichot, C. (1996). Newton kantorovich and modified gardient inversion algorithms

- apied to ipswich data. *IEEE Antennas and Propagation Magazine*, 38, 41-44.
- 110 Murch, R. D., & Chan, T. K. K. (1996). Improving microwave imaging by enhancing diffraction tomography. *Microwave Theory and Techniques, IEEE Transactions on*, 44(3), 379-388.
- 111 Murch, R. D., & Tan, D. G. H. (1997). Reconstructing objects from the ipswich data set. *Antennas and Propagation Magazine, IEEE*, 39(2), 26-28.
- 112 Bozza, G., Estatico, C., Pastorino, M., & Randazzo, A. (2006). An inexact newton method for microwave reconstruction of strong scatterers. *Antennas and Wireless Propagation Letters, IEEE*, 5(1), 61-64.
- 113 Bozza, G., Estatico, C., Pastorino, M., & Randazzo, A. (2007). Application of an inexact-newton method within the second-order born approximation to buried objects. *Geoscience and Remote Sensing Letters, IEEE*, 4(1), 51-55.
- 114 Bozza, G., Estatico, C., Massa, A., Pastorino, M., & Randazzo, A. (2006, 29 April 2006). *An inexact-newton algorithm for tomographic microwave imaging*. Paper presented at the Imagining Systems and Techniques, 2006. IST 2006. Proceedings of the 2006 IEEE International Workshop on [Imagining read Imaging].
- 115 Estatico, C., Pastorino, M., & Randazzo, A. (2005). An inexact-newton method for short-range microwave imaging within the second-order born approximation. *Geoscience and Remote Sensing, IEEE Transactions on*, 43(11), 2593-2605.
- 116 Bozza, G., & Pastorino, M. (2009). An inexact newton-based approach to microwave imaging within the contrast source formulation. *Antennas and Propagation, IEEE Transactions on*, 57(4), 1122-1132.
- 117 Oliveri, G., Lizzi, L., Pastorino, M., & Massa, A. (2012). A nested multi-scaling inexact-newton iterative approach for microwave imaging. *Antennas and Propagation, IEEE Transactions on*, 60(2), 971-983.
- 118 Estatico, C., Pastorino, M., & Randazzo, A. (2013). Microwave imaging of three-dimensional targets by means of an inexact-newton-based inversion algorithm. *International Journal of Antennas and Propagation*, 10.
- 119 Kosmas, P., Shea, J. D., Van Veen, B. D., & Hagness, S. C. (2008, 5-11 July 2008). *Three-dimensional microwave imaging of realistic breast phantoms via an inexact gauss-newton algorithm*. Paper presented at the Antennas and Propagation Society International Symposium, 2008. AP-S 2008. IEEE.
- 120 Richmond, J. (1965). Scattering by a dielectric cylinder of arbitrary cross section shape. *Antennas and Propagation, IEEE Transactions on*, 13(3), 334-341.
- 121 Kuyucuoglu, F., Cay, Z., & Oguzer, T. (2006, 4-6 April 2006). *Scattering from the pec flat strip by using the method of moments*

- with sinc type basis functions.* Paper presented at the Computational Electromagnetics (CEM), 2006 6th International Conference on.
- 122 Xiaoqiao, D., Changqing, G., Jiade, Y., Zhuo, L., & Yonggang, Z. (2010, 17-20 Sept. 2010). *Electromagnetic scattering by arbitrarily shaped pec targets coated with magnetic anisotropic media using equivalent dipole-moment method.* Paper presented at the Signals Systems and Electronics (ISSSE), 2010 International Symposium on.
- 123 Seran, S., Donohoe, J. P., & Topsakal, E. (2010). A fast method for scattering from a pec strip or pec semicircular cylinder loaded with semicircular dielectric cylinders. *Antennas and Wireless Propagation Letters, IEEE, 9*, 326-329.
- 124 Wu, Z., Boughriet, A. H., McCann, H., Davis, L. E., & Nugroho, A. T. (2001). *Investigation of microwave tomographic imaging techniques for industrial processes.* Paper presented at the Process Imaging for Automatic Control, Boston.
- 125 Boughriet, A. H., Wu, Z., Nugroho, A. T., McCann, H., & Davis, L. E. (2000). *Free-space imaging with an active microwave tomographic system.* Paper presented at the Subsurface Sensing Technologies and Applications II, San Diego.
- 126 Franchois, A., & Pichot, C. (1997). Microwave imaging-complex permittivity reconstruction with a levenberg-marquardt method *IEEE Transactions on Antennas and Propagation, 45(2)*, 203-215.
- 127 Estatico, C., Fedeli, A., Pastorino, M., & Randazzo, A. (2014, 14-17 Oct. 2014). *A numerical analysis concerning microwave imaging in lp banach spaces by using an inexact newton method.* Paper presented at the Imaging Systems and Techniques (IST), 2014 IEEE International Conference on.
- 128 Oliveri, G., Bozza, G., Massa, A., & Pastorino, M. (2010, 11-17 July 2010). *Iterative multi scaling-enhanced inexact newton-method for microwave imaging.* Paper presented at the Antennas and Propagation Society International Symposium (APSURSI), 2010 IEEE.
- 129 van den Berg, P. M., & Kleinman, R. E. (1988). The conjugate gradient spectral iterative technique for planar structures. *Antennas and Propagation, IEEE Transactions on, 36(10)*, 1418-1423.
- 130 Hanke, M. (1997). A regularizing levenberg - marquardt scheme, with applications to inverse groundwater filtration problems. *Inverse Problems and Imaging (IPI), 13(1)*, 79-95.
- 131 Jin, Q. (2012). Inexact newton-landweber iteration for solving nonlinear inverse problems in banach spaces. *Inverse ProblemsEmail, 28(6)*, 065002.
- 132 Wang, W., & Han, B. (2009). An implicit landweber method for nonlinear ill-posed operator equations. *Journal of Computational and Applied Mathematics, 230(2)*, 607-613.

- 133 Xiao, C., & Deng, Y. (2011). A new newton-landweber iteration for nonlinear inverse problems. *Applied Mathematic Computation*, 36, 489-505.
- 134 Seidman, T. I., & Vogel, C. R. (1989). Well posedness and convergence of some regularisation methods for non-linear ill posed problems. *Inverse Probl*, 5(2), 227-238.
- 135 Nugroho, A. T. (2009). Modified newton kantorovich methods for solving microwave inverse scattering problems. *Jurnal ILMU DASAR*, 10(2), 153-159.
- 136 Baumeister, J., Kaltenbacher, B., & Leitao, A. (2010). On levenberg-marquardt-kaczmarz iterative methods for solving systems of nonlinear ill-posed equations. *Inverse Problems and Imaging (IPI)*, 4(3), 335-350.
- 137 Hanke, M. (1997). A regularizing levenberg - marquardt scheme, with applications to inverse groundwater filtration problems. *Inverse Probl*, 13(1), 79-95.
- 138 Marquardt, D. W. (1963). An algorithm for least-squares estimation of nonlinear parameters. *Journal of the Society for Industrial and Applied Mathematics*, 11(2), 431-441.
- 139 Hochbruck, M., & Höning, M. (2009). On the convergence of a regularizing levenberg–marquardt scheme for nonlinear ill-posed problems. *Numerische Mathematik*, 115, 71-79.
- 140 Bakushinsky, A. B., & Kokurin, M. Y. (2004). *Iterative methods for approximate solution of inverse problems,” mathematics and its applications* (Vol. 577). Dordrecht: Springer.
- 141 Engl, H. W., Hanke, M., & Neubauer, A. (1996). *Regularization of inverse problems*. Dordrecht: Kluwer Academic Publishers.
- 142 Kirsch, A. (2011). *An introduction to the mathematical theory of inverse problems* (2 ed. Vol. 120). New York: Springer.
- 143 Vogel, C. R. (2002). *Computational methods for inverse problems*. Philadelphia: Society for Industrial and Applied Mathematics.
- 144 Hanke, M., Neubauer, A., & Scherzer, O. (1995). A convergence analysis of the landweber iteration for nonlinear ill-posed problems. *Numerische Mathematik*, 72(1), 21-37.
- 145 Kaltenbacher, B., Schopfer, F., & Schuster, T. (2009). Iterative methods for nonlinear ill-posed problems in banach spaces: Convergence and applications to parameter identification problems. *Inverse Probl*, 25, 065003 (065019pp).
- 146 Eisenstat, S. C., & Walker, H. F. (1996). Choosing the forcing terms in an inexact newton method. *SIAM Journal on Scientific Computing*, 17(1), 16-32.
- 147 Dembo, R. S., Eisenstat, S. C., & Steihaug, T. (1982). Inexact newton methods. *SIAM Journal on Numerical Analysis*, 19(2), 400-408.
- 148 Zhou, J., Zhang, S., Yang, G., & Tan, J. (2008). A convergence theorem for the inexact newton methods based on hlder continuous

- fréchet derivative. *Applied Mathematics and Computation*, 197(1), 206-211.
- 149 Rieder, A. (2001). On convergence rates of inexact newton regularizations. *Numerische Mathematik*, 88(2), 347-365.
- 150 An, H.-B., Mo, Z.-Y., & Liu, X.-P. (2007). A choice of forcing terms in inexact newton method. *Journal of Computational and Applied Mathematics*, 200(1), 47-60.
- 151 An, H.-B., & Bai, Z.-Z. (2007). A globally convergent newton-gmres method for large sparse systems of nonlinear equations. *Applied Numerical Mathematics*, 57(3), 235-252.
- 152 Favati, P., Lotti, G., Menchi, O., & Romani, F. (2014). An inner-outer regularizing method for ill-posed problems. *Inverse Problems and Imaging (IPI)*, 8(2), 409-420.
- 153 Rieder, A. (2006). Inexact newton regularization using conjugate gradients as inner iteration. *SIAM Journal on Numerical Analysis*, 43(2), 604-622.
- 154 Kelley, C. T. (1995). *Iterative methods for linear and nonlinear equations*. Philadelphia: Society for Industrial and Applied Mathematics (SIAM).
- 155 Hanke, M. (1995). The minimal error conjugate gradient method is a regularized method. *Proceedings of the American mathematical Society*, 123(11), 3487-3497.
- 156 Hamarik, U., & Palm, R. (2005). *Comparison of stopping rules in conjugate gradient type methods for solving ill posed problems*. Paper presented at the Mathematical Modelling and Analysis, Trakai.
- 157 Hansen, P. C. (1992). Analysis of discrete ill-posed problems by means of the l-curve. *SIAM Review*, 34(4), 561-580.
- 158 Hansen, P. C., & O'Leary, D. P. (1993). The use of the l-curve in the regularization of discrete ill-posed problems. *SIAM Journal on Scientific Computing*, 14(6), 1487-1503.
- 159 Castellanos, J. L., Gómez, S., & Guerra, V. (2002). The triangle method for finding the corner of the l-curve. *Applied Numerical Mathematics*, 43(4), 359-373.
- 160 Hansen, P. C., Jensen, T. K., & Rodriguez, G. (2007). An adaptive pruning algorithm for the discrete l-curve criterion. *Journal of Computational and Applied Mathematics*, 198(2), 483-492.
- 161 Hansen, P. C. (2000). The l-curve and its use in the numerical treatment of inverse problem. In P. Johnston (Ed.), *Computational inverse problems in electrocardiology* (pp. 119-142): WIT Press.
- 162 Vogel, C. R. (1996). Non-convergence of the l-curve regularization parameter selection method. *Inverse Probl*, 12(4), 535-547.
- 163 Hanke, M. (1996). Limitations of the l-curve method in ill-posed problems. *BIT Numerical Mathematics*, 36(2), 287-301.
- 164 Jofre, L., Hawley, M. S., Broquetas, A., de los Reyes, E., Ferrando, M., & Elias-Fuste, A. R. (1990). Medical imaging with a microwave

- tomographic scanner. *Biomedical Engineering, IEEE Transactions on*, 37(3), 303-312.
- 165 Joachimowicz, N., Mallorqui, J. J., Bolomey, J. C., & Broquets, A. (1998). Convergence and stability assessment of newton-kantorovich reconstruction algorithms for microwave tomography. *Medical Imaging, IEEE Transactions on*, 17(4), 562-570.
- 166 Gilmore, C., Mojabi, P., Zakaria, A., Ostadrahimi, M., Kaye, C., Noghianian, S., . . . LoVetri, J. (2010). A wideband microwave tomography system with a novel frequency selection procedure. *Biomedical Engineering, IEEE Transactions on*, 57(4), 894-904.
- 167 Gilmore, C., Mojabi, P., Zakaria, A., Pistorius, S., & LoVetri, J. (2010). On super-resolution with an experimental microwave tomography system. *Antennas and Wireless Propagation Letters, IEEE*, 9, 393-396.
- 168 Ostadrahimi, M., Mojabi, P., LoVetri, J., Shafai, L., & Noghianian, S. (2012, 8-14 July 2012). *Enhancement of near-field probing in a microwave tomography system*. Paper presented at the Antennas and Propagation Society International Symposium (APSURSI), 2012 IEEE.
- 169 Zhurbenko, V., Rubæk, T., Krozer, V., & Meincke, P. (2010). Design and realisation of a microwave three-dimensional imaging system with application to breast-cancer detection. *IET Microwaves, Antennas & Propagation*, 4(12), 2200.
- 170 Meaney, P. M., Fanning, M. W., Li, D., Poplack, S. P., & Paulsen, K. D. (2000). A clinical prototype for active microwave imaging of the breast. *Microwave Theory and Techniques, IEEE Transactions on*, 48(11), 1841-1853.
- 171 Attardo, E. A., Borsic, A., Vecchi, G., & Meaney, P. M. (2012). Whole-system electromagnetic modeling for microwave tomography. *Antennas and Wireless Propagation Letters, IEEE*, 11, 1618-1621.
- 172 Ostadrahimi, M., Asefi, M., LoVetri, J., Bridges, G. E., & Shafai, L. (2013, 7-13 July 2013). *An mst-based microwave tomography system using homodyne receiver*. Paper presented at the Antennas and Propagation Society International Symposium (APSURSI), 2013 IEEE.
- 173 Meaney, P. M., Paulsen, K. D., Hartov, A., & Crane, R. K. (1995). An active microwave imaging system for reconstruction of 2-d electrical property distributions. *Biomedical Engineering, IEEE Transactions on*, 42(10), 1017-1026.

Appendix A Integral Equation of Microwave Tomography Inverse Problem

This thesis presents MWT inverse problem in volume integral equations of electromagnetic scattering by a dielectric cylinder [12]. The scattering field is defined in frequency domain where a harmonic wave varying in time is considered as $e^{-j\omega t}$. The symbol j represents the imaginary part $j = \sqrt{-1}$, while ω and t symbolize the radial frequency of the utilized field and the time respectively. Assume that an incident field with an electric field E^i illuminates an inhomogeneous dielectric object (OI) of complex permittivity ε_r and arbitrary shape. The OI with Ω cross section is placed in object domain (\mathcal{O}) and immersed in background medium of complex permittivity ε_b . The scattered field E^s due to the present of the OI are measured in M observation points at data domain (\mathcal{D}). According to the field described, the integral equation of total electric field everywhere inside \mathcal{O} and \mathcal{D} is defined as in [16]

$$E(\mathbf{r}) = E^i(\mathbf{r}) + \int_{\Omega} \mathbb{G}(\mathbf{r}, \mathbf{r}') \chi(\mathbf{r}') E(\mathbf{r}') d\mathbf{r}' \quad (\text{A-1})$$

The volume integral equation is bound in the object domain $\mathcal{O} \in \mathbb{R}^2$ in which a non magnetic OI is immersed, and the measurement domain is defined at $\mathcal{D} \in \mathbb{R}^2$ outside the OI . Vectors p, q, r and r' are position vector of the imaging. Vectors p and q define the points of observation and cells of interests respectively, $p \in \mathcal{D}$ and $q \in \mathcal{O}$, and the position vectors and position vectors r and r' are selected to be arbitrary vectors in \mathbb{R}^2 .

An arbitrary electromagnetic field can be expressed as the sum of a transverse magnetic (TM) and a transverse electric (TE). The kernel or the dyadic Green's function which denotes the point source solution of the electromagnetic wave equation at the background medium, can be stated for 2D-TM (A-2), 2D-TE (A-3) and 3D (A-4) modes as it is defined at [63; 64]

$$\mathbb{G}(\mathbf{r}, \mathbf{r}') = g(\mathbf{r}, \mathbf{r}') \quad (\text{A-2})$$

$$\mathbb{G}(\mathbf{r}, \mathbf{r}') = \left(\mathbb{I} + \frac{1}{k_b^2} \nabla_r \nabla_{r'} \right) g(\mathbf{r}, \mathbf{r}') \quad (\text{A-3})$$

$$\mathbb{G}(\mathbf{r}, \mathbf{r}') = \left(\mathbb{I} + \frac{1}{k_b^2} \nabla_r \nabla_{r'} \right) \frac{e^{jk_b|r-r'|}}{4\pi|r-r'|} \quad (\text{A-4})$$

where k_b is the wave number in background medium with $k_b^2 = \omega^2 \mu_0 \varepsilon_0 \varepsilon_b$. The permeability and permittivity of the free space is assigned as μ_0 and ε_0 respectively. The dyad $g(r, r')$ is the scalar of the Green's function for the homogeneous background. The 2D scalar may be written in Hankel function of zero order of the first kind as $g(r, r') = \frac{j}{4} H_0^{(1)}(k_b|r - r'|)$.

Two dimensional microwave imaging model can be described by defining three forms of electric fields which are total, incident, and scattered field on the MWT system. The total field (E), which is known as the disturbance field, is the electric field in the presence of the OI . The incident field is electric field (E^i) in the absence of the OI . This field is known as non-disturbance field. In the thesis, radiation of line source equivalent is used as the source of the field. Thus, the value of the incident field is defined using Hankel's function. The scattered field (E^s) is electric field due to the presence of the OI . This field is the difference of the total and incident fields. The electric field relation everywhere outside the OI in MWT system is defined as:

$$E(\mathbf{r}) = E^s(\mathbf{r}) + E^i(\mathbf{r}) \quad (\text{A-5})$$

The incident is defined in 2D-TM mode, which is presented in single rectangular component as $E_z^i \hat{z}$. Therefore, the total and scattered fields have only single wave component $E_z \hat{z}$ and $E_z^s \hat{z}$. To simplify the notation of the total, incident and scattered fields in 2D-TM mode are written as E, E^i and E^s respectively for the rest of the thesis.

Microwave tomography inverse problem is defined using a pair of objects and data equations. The integral equation (A-1) speaks for the object equation. The $E(\mathbf{r}')$ represents the field inside \mathcal{O} and $E^i(\mathbf{r}')$ illuminates \mathcal{O} in the present of an unknown $\chi(\mathbf{r}')$. Then, the object equation can be written by following [23]

$$E(\mathbf{r}) = E^i(\mathbf{r}) + \int_{\mathcal{O}} \mathbb{G}(\mathbf{r}, \mathbf{r}') \chi(\mathbf{r}') E(\mathbf{r}') d\mathbf{r}', \mathbf{p} \in \mathcal{O} \quad (\text{A-6})$$

where $\chi(\mathbf{r}')$ is the contrast of the OI with respect to the background. Different formulation of (A-8) in which equivalent current density replaces the dielectric contrast and total fields inside \mathcal{O} can be found in [81].

In MWT application the OI is illuminated with E^i at several transmission points ($t = 1, 2 \dots T$) on which at each illumination the scattered fields are measured at \mathcal{D} . At each illumination (t), the object equation can be stated symbolically in a matrix form as it is introduced in [23]

$$[\mathbf{E}^i]_t = [\mathbf{E}]_t - [\mathbb{G}(\mathbf{r}, \mathbf{r}')] [\chi, [\mathbf{E}]_t] \quad (\text{A-7})$$

Defining inner product of cells in integral equation as

$$[(\mathbf{a}, \mathbf{b})] = \begin{bmatrix} a_1 b_1 \\ a_2 b_2 \\ \vdots \\ a_N b_N \end{bmatrix} = \begin{bmatrix} a_1 & 0 & 0 & 0 \\ 0 & a_2 & 0 & 0 \\ 0 & 0 & \ddots & 0 \\ 0 & 0 & 0 & a_N \end{bmatrix} \begin{bmatrix} b_1 \\ b_2 \\ \vdots \\ b_N \end{bmatrix} = [\text{diag}(\mathbf{a})][\mathbf{b}] \quad (\text{A-8})$$

Applying (A-10) into (A-9)

$$[\mathbf{E}^i]_t = [I - [\mathbb{G}(\mathbf{r}, \mathbf{r}')] [\text{diag}(\chi)]] [\mathbf{E}]_t \quad (\text{A-9})$$

Operator $\mathbb{G}(\mathbf{r}, \mathbf{r}')$ is an integral operator mapping $L^2(\mathcal{O})$ into $L^2(\mathcal{O})$, which means that position vector \mathbf{r} in (A-8) is directing to \mathcal{O} .

The scattered fields in $(\mathcal{D})[\mathbf{E}^s]_t \in \mathcal{O}$ are defined using the following integral equation:

$$E^s(\mathbf{r}) = \int_{\Omega} \mathbb{G}(\mathbf{r}, \mathbf{r}') \chi(\mathbf{r}') E(\mathbf{r}') d\mathbf{r}', \mathbf{p} \in \mathcal{D} \quad (\text{A-10})$$

The position vector \mathbf{r} points \mathcal{D} , where the scattered fields are measured. Equation (A-12) is assigned as the data equation. At each projection(t), it can be symbolized as

$$[\mathbf{E}^s]_t = [\mathbb{G}(\mathbf{r}, \mathbf{r}')_t] [\chi, [\mathbf{E}]_t] = [\mathbb{G}(\mathbf{r}, \mathbf{r}')_t] [\text{diag}(\chi)] [\mathbf{E}]_t \quad (\text{A-11})$$

where operator $[\mathbb{G}(\mathbf{r}, \mathbf{r}')_t]$ is an integral operator mapping $L^2(\mathcal{D})$ into $L^2(\mathcal{D})$. The subscribes t on the operator $[\mathbb{G}(\mathbf{r}, \mathbf{r}')_t]$ is used to make clear the address of position vector \mathbf{r} . On each projection, the position of observation point

could be vary. The position of total field, incident field and contrast are directed to \mathcal{O} , while the position vector of scattered field is pointed at \mathcal{D} .

The scattered fields in M points of observation at \mathcal{D} are the measured data. For each illumination of microwave signal, the MWT data can be defined as

$$[\mathcal{E}^s]_t = [\mathbb{G}(\mathbf{r}, \mathbf{r}')]_t [(\chi, [\mathbf{E}]_t)] \quad \mathbf{p} \in \mathcal{D} \quad (\text{A-12})$$

MWT data $[\mathcal{E}^s]_t$ are gathered at $p \in \mathcal{D}$, where in factual measurement, it contains measurement error, model error, noise and other disturbance parameters.

The calculation of approximated scattered fields from predicted contrast and given incident fields is assigned as *the forward problem*. The approximation of the contrast from the discrepancy of data and approximated scattered field is known as *the inverse problem*.

Appendix B Scattering by a dielectric circular cylinder

Two different incident fields, which are a normalized uniform plane wave and an equivalent line source, are used to derive the analytic solution of scattering by a dielectric circular cylinder.

B.1 Normalized Plane Wave

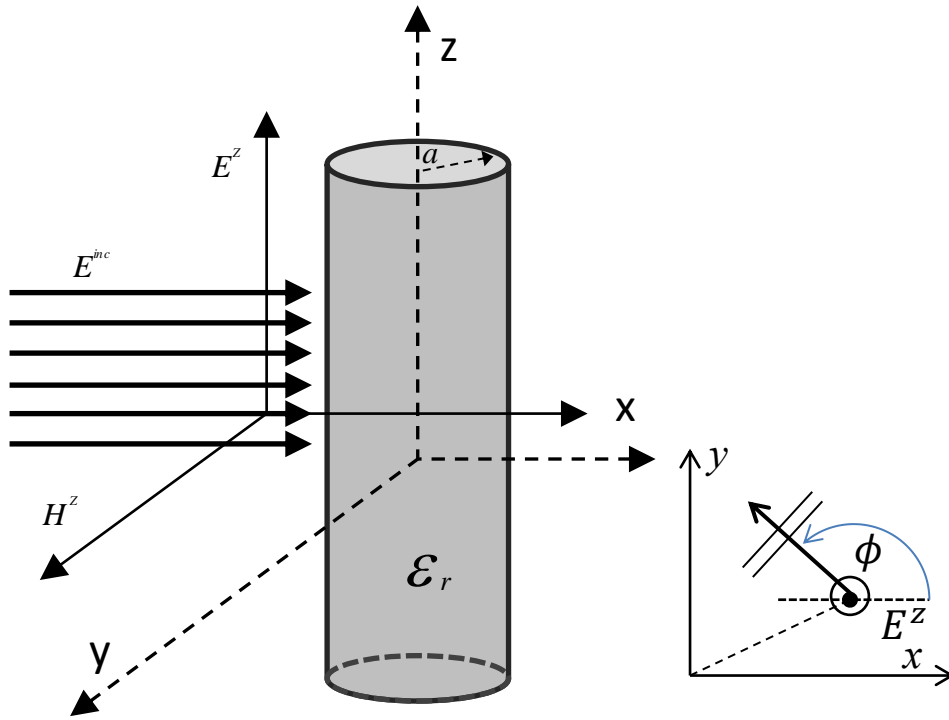


Figure B-1: A TM^z Uniform plane wave incident on a dielectric circular cylinder.

The incident electric field in the form of the normalized plane wave can be written as

$$\hat{a}_z E_0 e^{jk_0(x\cos\phi_i + y\sin\phi_i)} \quad (\text{B-1})$$

Assuming that the wave travels in the $+x$ and $-x$ direction, then the wave can be written respectively as

$$E_z^+ = \hat{a}_z E_0 e^{-jk_0 x} \quad \text{and} \quad E_z^- = \hat{a}_z E_0 e^{+jk_0 x} \quad (\text{B-2})$$

The wave equations in (B-2) can be expressed in cylindrical wave functions as follows

$$E_z^+ = e^{-jkx} = e^{-jk\rho\cos\phi} \sum_{n=-\infty}^{+\infty} j^{-n} J_n(k\rho) e^{jn\phi} \quad (\text{B-3})$$

$$E_z^- = e^{+jkx} = e^{+jk\rho\cos\phi} \sum_{n=-\infty}^{+\infty} j^{+n} J_n(k\rho) e^{jn\phi} \quad (\text{B-4})$$

where J_n is the Bessel function of the first kind.

The scattering by dielectric circular cylinder is defined as

$$E^s = \hat{a}_z E_0 \sum_{n=-\infty}^{+\infty} [a_n H_n^2(k_0\rho) e^{jn\phi}] \rightarrow E^s(\rho \geq a) \in \mathcal{D} \quad (\text{B-5})$$

where the coefficient a_n is determined using

$$a_n = \frac{\eta_0 J_n(k_0 a) J'_n(k_1 a) - \eta_1 J'_n(k_0 a) J_n(k_1 a)}{\eta_1 J_n(k_1 a) H_n^2(k_0 a) - J'_n(k_1 a) H_n^2(k_0 a)} \quad (\text{B-6})$$

B.2 Electric Line Source

The electric line source is a straight line electric current that extends to infinity. Assume that the electric current is directed along z axis. It will radiate nonzero TM^z fields. If an infinity line source of electric current I_0 is located at $(\rho = \rho') \wedge \phi = \phi'$, then, it will produce electric fields which is described in a cylindrical system as

$$E_z(\rho, \phi) = -\frac{k_0^2 I_0}{4\omega\epsilon} H_0^2(k_0 \mathbf{R}) \quad (\text{B-7})$$

The electric field component is proportional to a Hankel's function of the second kind over the distance from source to observation points. Theorem of Hankel's functions expands the line source function by defining \mathbf{R} as radial distance between the source and the observation point $\mathbf{R} = |\rho - \rho'|$.

$$E_z^i = -\frac{\beta^2 I_0}{4\omega\epsilon} \sum_{n=-\infty}^{+\infty} J_n(\beta\rho) H_n^{(2)}(\beta\rho') e^{jn(\phi-\phi')} \quad (\text{B-8})$$

The incidence equation (B-8) is used to illuminate a dielectric circular object. The transmitting antenna is placed near the object.

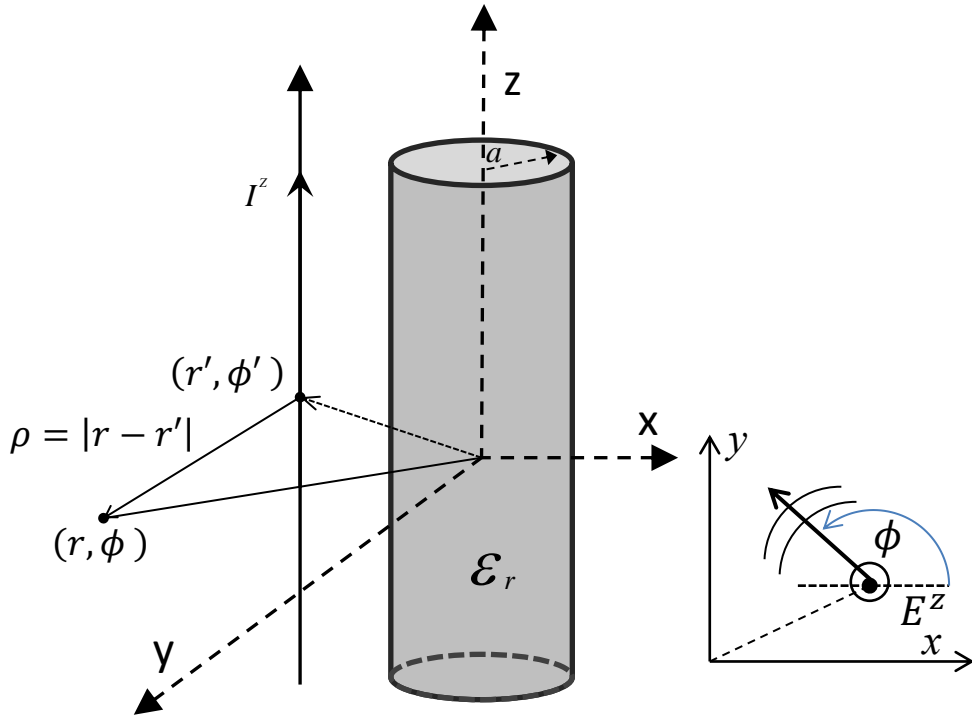


Figure B-2: An infinitely long line source current directed at \hat{z} is placed near a dielectric cylindrical object

As the geometry of the object is simple; thus, the solution of (B-5) can be derived using harmonic expansion. The expansion of scattering field is followed Balanis[183], where The line source scattering by a dielectric circular cylinder is calculated using

$$E_z^S = -\frac{k_0^2 I_0}{4\omega\epsilon} \sum_{n=-\infty}^{+\infty} c_n H_n^{(2)}(k_0 \rho) e^{jn(\phi - \phi')} \quad (\text{B-9})$$

Where the coefficient c_n is determined using

$$c_n = \frac{\frac{\mu_1}{\mu_0} J'_n(k_0 a) J_n(k_1 a) H_n^{(2)}(k_0 \rho') - \frac{k_1}{k_0} J'_n(k_1 a) J_n(k_0 a) H_n^{(2)}(k_0 \rho')}{\frac{k_1}{k_0} H_n^{(2)}(k_0 a) J'_n(k_1 a) - \frac{\mu_1}{\mu_0} H'_n(k_0 a) J_n(k_1 a)} \quad (\text{B-10})$$

Appendix C Regularization of linear ill posed problem

Let us define the operator of the normal equation $[\mathbf{L}]$ is positive definite matrix, \mathbf{b} is a vector measurement and \mathbf{s}^\dagger is the exact solution of the linear system.

$$[\mathbf{L}]\mathbf{s}^\dagger = \mathbf{b} \quad (\text{C-1})$$

The unique solution is hard to be defined. Though the matrix $[\mathbf{L}]$ is symmetrical, but it is ill conditioning. Therefore, an approximation solution \mathbf{s}^\ddagger is computed to estimate the exact solution. It is gained by considering the regulated operator $[\mathbf{L}^\alpha]$. The techniques to calculate the approximation solution is stated in the following section.

C.1 Truncated Singular Value Decomposition

Assuming that operator $[\mathbf{L}]$ is an invertible complex matrix. It is squared matrix and has a singular value decomposition

$$[\mathbf{L}] = U \Sigma V^T \quad (\text{C-2})$$

The singular value decomposition produces coupled unitary matrix U and V which are $U^T = U^{-1}$ and $V^T = V^{-1}$. The diagonal matrix of Σ is σ_i where $i = 1, 2 \dots N$. If the column vectors of V is v_i and the column vectors of U is u_i then, it the relation can be stated as follows

$$[\mathbf{L}]v_i = \sigma_i u_i; [\mathbf{L}]^T u_i = \sigma_i v_i \quad (\text{C-3})$$

The solution of (C-1) is stated using the singular value decomposition as

$$\mathbf{s} = \left[\sum_{i=1}^N \frac{\bar{u}_i v_i}{\sigma_i} \right] \mathbf{b} \quad (\text{C-4})$$

The truncated singular value decomposition (TSVD) regularizes the ill-posed by truncating the matrix $([\mathbf{L}])$. A small value of singular value (σ_i) is ignored. The ill-conditioned system is regularized as

$$[\mathbf{L}^\alpha]^{-1} = \sum_{i=1}^N \phi_i \frac{\bar{u}_i v_i}{s_i} \quad (\text{C-5})$$

Where the regularization ϕ_i is defined as

$$\phi_i = \begin{cases} 1; & i = 1, 2, \dots, k \\ 0; & i = k + 1, \dots, N \end{cases} \quad (\text{C-6})$$

Equation (C-5) is known as the truncated singular value decomposition (TSVD) solution. It solves the linear ill-posed of MWT inverse problem. It should be note that the instability could be occurred during the computation of \mathbf{s} as some information is omitted.

Basically, the inversion of the operator is done by inverting the singular values $(\sigma_i)^{-1}$ of the operator. This is due to the singular vector which is the orthonormal of the Eigen vector. The inversion of the singular vector is represented by its transpose while the singular values matrix is a diagonal matrix in which its cell is constructed by the eigenvalues of the matrix operator. The inversion equals to the division of the singular values $(\sigma_i)^{-1} = 1/\sigma_i$. The instability arises at the high frequency where the division by small singular values appeared. To overcome this problem, the inversion is modified.

The simplest method to modify the inversion is applying a low pass filter ϕ_i to the inversion. The high frequency is cut at a desirable point where desirable information is gained. The filter omits the influence of high frequency It stabilizes the solution, but loss detailed information.

C.2 Tikhonov Regularization

The Instability of (C-5) can be decreased by applying a parametric filter $\omega(\theta, \alpha)$. One of the well-known filters is the Tikhonov regularization. It is defined as

$$\omega(\sigma_i^2, \alpha) = \frac{\sigma_i^2 + \alpha}{\sigma_i^2} \quad \text{C-7}$$

where α is the Tikhonov regularization parameter. It addresses the singular decomposition values as

$$\omega(\theta, \alpha)\sigma_i = \frac{\sigma_i^2 + \alpha}{\sigma_i} \quad (\text{C-8})$$

Determining α is essential to the stability and accuracy of the solution. The regulator should be relatively small compared to the largest singular values and relatively big compared to the smallest singular values. For largest singular values, the regulator contributes small effect while the smallest singular value contributes the biggest inversion values.

$$\omega(\theta, \alpha)\sigma_i = \frac{\sigma_{max}^2 + \alpha}{\sigma_{max}} \approx \sigma_{max} \quad (C-9).$$

The filtered singular value is approximated as

$$\omega(\theta, \alpha)\sigma_i = \frac{\sigma_{min}^2 + \alpha}{\sigma_{min}} \approx \alpha \quad (C-10)$$

Substituting the regularization (C-8) into (C-4) results in Tikhonov regularized ill-posed solution as follows

$$\mathbf{s} = \left[\sum_{i=1}^N \frac{\sigma_i}{\sigma_i^2 + \alpha} \bar{u}_i v_i \right] \mathbf{b} \quad (C-11)$$

Generally, the filter applied is similar to low pass filter in the previous section. The regulator α determines the cut off frequency. When the α is very small, the threshold points decrease and the solution is highly oscillated as the noise could be relatively high compared to the invested values. On the other hand, when the regulator is high, the singular filter is low and the noise components are filtered out, but most information are also cancelled out and the solution is overly smooth.

C.3 Truncated Landweber method

$$[\mathbf{L}^\alpha]^{-1} = \sum_{j=0}^{l-1} (1 - \beta[\mathbf{L}])^j \quad (C-12)$$

The solution of linear system is regulated using the inner iterative index $l = 1, 2, \dots, I$ and guarded with positive nonzero number β . The l^{th} regulative iteration can be expressed in terms of the singular value decomposition system

$$\mathbf{s}_{k,l+1} = \sum_{i=1}^N \frac{1 - (1 - \beta\sigma_i^2)^l}{\sigma_i} \langle b_k^\varepsilon, u_i^T \rangle v_i \quad (C-13)$$

The β is chosen according to the largest singular values. The β lies between

$$0 < \beta < \frac{2}{\sigma_1^2} \quad (\text{C-14})$$

The techniques explained are categorized as direct regularized methods. The direct solution is a predictable number of steps, but it does not support intermediate solution. The solution is in a specified manner according to the regularization technique used. The accuracy of the solution is dependent on the type of regulator and the size of the parameter of the regularization in which both parameters are hard to be defined.

Appendix D The Application of Born Approximation in MWT-Inverse Problem

When the contrast or the size of the object of interest is small, the microwave inverse scattering problem can be simplified by applying the Born Approximation. The Born Approximation estimate the inverse in domain function as

$$[\mathbf{I} + [\mathbf{Z}_{nn'}][\text{diag}(\boldsymbol{\chi}_{n'})]]^{-1} \approx \mathbf{I} \quad (\text{D-1})$$

Considering the assumption (D-1) with respects to domain equation means that the source over domain \mathcal{O} equals to the incident fields inside the imaging domain. This is similar to the undisturbed fields.

D.1 The solution of MWT inverse problem using Born Approximation

Applying the Born approximation, then the MWT objective function $\mathbf{F}_t([\boldsymbol{\chi}])$ can be written as

$$\mathbf{F}_t([\boldsymbol{\chi}]) = [-[\mathbf{Z}_{mn'}]_t[\text{diag}(\boldsymbol{\chi}_{n'})][\mathbf{E}_n^i]_t] - [\boldsymbol{\mathcal{E}}_m^s]_t \quad (\text{D-2})$$

Assigning that the $[\boldsymbol{\mathcal{E}}_m^s]_t$ is the measured scattered fields, then, the distribution of the contrast $[\boldsymbol{\chi}]$ which is representing the image of object cross section is the solution of microwave inverse problem. Although (D-2) is now linear, the system underdetermines these remains and ill-posed problems. The iterative solution is gained by updating the contrast as

$$[\boldsymbol{\chi}]_{k+1} = [\boldsymbol{\chi}]_k + d_k[\boldsymbol{\delta}\boldsymbol{\chi}]_k \quad (\text{D-3})$$

where d_k is an appropriate step length to enforce the reduction of the error of (D-2), $[\boldsymbol{\delta}\boldsymbol{\chi}]$ is the direction of the correction and $k = 1, 2 \dots K$ is the index of iteration.. $[\boldsymbol{\delta}\boldsymbol{\chi}]$ is determined by solving linear system, by means of Fréchet derivative of $\mathbf{b}_t([\boldsymbol{\chi}])$ at $[\boldsymbol{\chi}]$.

$$\frac{d\mathbf{b}_t([\boldsymbol{\chi}])}{d[\boldsymbol{\chi}]} [\boldsymbol{\delta}\boldsymbol{\chi}]_k = -\mathbf{b}_t([\boldsymbol{\chi}]_k) \quad (\text{D-4})$$

Where

$$\frac{db_t([\chi])}{d[\chi]} = \frac{d[\mathbf{E}_m^s]_t}{d[\chi]} = \frac{d(-[\mathbf{Z}_{mn'}]_t[\text{diag}(\chi_{n'})][\mathbf{E}_n^i]_t)}{d[\chi]} = -[\mathbf{Z}_{mn'}]_t[\mathbf{E}_n^i]_t$$

Assuming that the MWT system illuminates $t = 1, 2 \dots T$ incident fields, then, the linear system of (D-4) can be illustrated as

$$\mathbf{D}[\delta\chi]_k = -\mathbf{b}([\chi]_k) \quad (\text{D-5})$$

where

$$\mathbf{D} = \begin{bmatrix} \frac{db_1([\chi])}{d[\chi]} \\ \frac{db_2([\chi])}{d[\chi]} \\ \vdots \\ \frac{db_T([\chi])}{d[\chi]} \end{bmatrix} = \begin{bmatrix} -[\mathbf{Z}_{mn'}]_1[\mathbf{E}_n^i]_1 \\ -[\mathbf{Z}_{mn'}]_2[\mathbf{E}_n^i]_2 \\ \vdots \\ -[\mathbf{Z}_{mn'}]_T[\mathbf{E}_n^i]_T \end{bmatrix}$$

$$\mathbf{b}([\chi]_k) = \begin{bmatrix} [-[\mathbf{Z}_{mn'}]_1[\text{diag}(\chi_{n'})][\mathbf{E}_n^i]_1] - [\mathcal{E}_m^s]_1 \\ [-[\mathbf{Z}_{mn'}]_2[\text{diag}(\chi_{n'})][\mathbf{E}_n^i]_2] - [\mathcal{E}_m^s]_2 \\ \vdots \\ [-[\mathbf{Z}_{mn'}]_T[\text{diag}(\chi_{n'})][\mathbf{E}_n^i]_T] - [\mathcal{E}_m^s]_T \end{bmatrix}$$

The Gauss Newton method is used to solve (D-5). The method approximates the second order derivative as the multiplication of Jacobian of the system.

$$[\mathbf{D}^* \mathbf{D}][\delta\chi]_k = -\mathbf{D}^* \mathbf{b}([\chi]_k) \quad (\text{D-6})$$

Equation (D-6) can be solved explicitly. Nevertheless, the condition of $[\mathbf{D}^* \mathbf{D}]$ is poor. A regulator should be added to reduce the ill-pose of the system.

D.2 Minimising the MWT cost function using Born Approximation

The residual function of MWT under Born approximation is defined as

$$\mathcal{R}_t([\chi]) = \left[[-[\mathbf{Z}_{mn'}]_t[\text{diag}(\chi_{n'})][\mathbf{E}_n^i]_t] - [\mathcal{E}_m^s]_t \right] \quad (\text{D-7})$$

Suppose that $[\chi]_{k-1}$ is known, the updated $[\chi]_k$ is determined using forward problem. The direction $[\delta\chi]_k$ is calculated using the Gauss Newton inversion method. It needs Fréchet derivative of the cost-functional. As the cost-functional is stated in least-squared, it has complex conjugate transpose of the

dielectric contrast ($[\chi]^*$) variable. Thus the Fréchet derivative of $\mathcal{C}^A([\chi])$ and $\mathcal{C}^B([\chi])$ with respect to $[\chi]$ is defined by deriving the derivative of the cost with respect to $[\chi]^*$. The application of the inner product makes the functional $\mathcal{C}([\chi], [\chi]^*)$ become a complex function. According to Wirtinger calculus it is analytic with respect to $[\chi]$ for fixed $[\chi]^*$ and is analytic to $[\chi]^*$ for fixed $[\chi]$. It considers $\mathcal{C}([\chi], [\chi]^*)$ such that $\mathcal{C}([\chi], [\chi]^*) = \mathcal{C}([\chi])$, then, the derivative can be defined as

$$\frac{d\mathcal{C}([\chi])}{d[\chi]} = \mathcal{G}_t([\chi]) = \frac{1}{\|[\mathcal{E}_m^s]_t\|_D^2} [-[\mathbf{E}_n^i]_t^* [\mathbf{Z}_{mn'}]_t^*] \mathcal{R}_t([\chi]) \quad (\text{D-8})$$

Where $[\mathbf{Z}_{mn'}]_t^*$ is the adjoints of $[\mathbf{Z}_{mn'}]_t$ mapping $L_2(\mathcal{D})$ into $L_2(\mathcal{O})$, and over bar denotes complex conjugate. For all projection of MWT, the Fréchet derivative for all incidents fields is stated as

$$\frac{d\mathcal{C}^A([\chi]_k)}{d[\chi]} = \mathbf{D} = \begin{bmatrix} \mathcal{G}_1([\chi]_k) \\ \mathcal{G}_2([\chi]_k) \\ \vdots \\ \mathcal{G}_T([\chi]_k) \end{bmatrix} \quad (\text{D-9})$$

$$\frac{d\mathcal{C}^B([\chi]_k)}{d[\chi]} = \mathbf{D} = \mathcal{G}_1(\chi_k) + \mathcal{G}_2(\chi_k) \dots + \mathcal{G}_T(\chi_k) \quad (\text{D-10})$$

D.3 Numerical experiment of Born Approximation

The MWT-inverse problem is implemented to a simple numerical MWT case. A homogeneous cylindrical object with permittivity 1.4 and radius 1 cm is placed at (-0.02,-0.02) in domain object (\mathcal{O}). The object is illuminated with 4.5 GHz line-source-equivalence microwave signals. The signals sequentially is transmitted from $Tx_{t=1..T}$ where $T = 16$. At each illumination, the scattered fields are received at 8 Rx antenna at data domain. Therefore, for complete scanning total data collected are $16 \times 8 = 128$.

The data are gained by solving the MWT forward problems. Then, it is reconstructed using Gauss Newton inversion method based on three different inverse problem formulations which are $\mathcal{F}([\chi])$, $\mathcal{C}^A([\chi])$ and $\mathcal{C}^B([\chi])$.

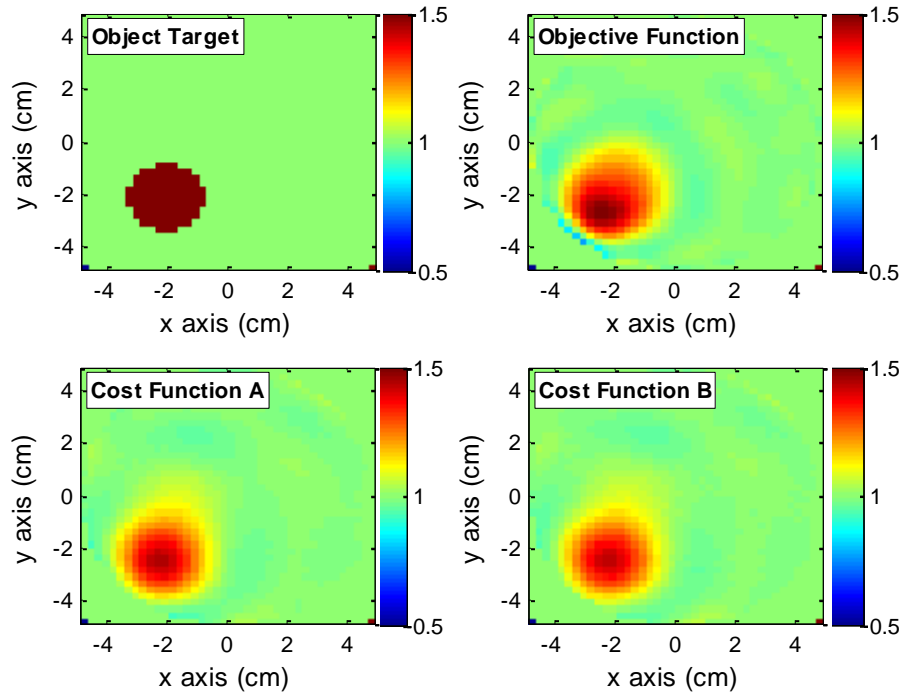


Figure D-3: Image of cylindrical cross-section object under Born Approximation using Gauss Newton Inversion. Three different MWT inverse problems which are MWT objective function, MWT cost function A and B, are formulated and solved using GNI method.

The results of reconstruction are presented in Figure D-1. It can be seen that the Born Approximation problem can be presented in MWT-objective function and least-squared cost functional. Gauss Newton Inversion (GNI) solves MWT problems which are stated in three different functional operators. A first order Newton scheme is formulated using the derivative of the functional of the operator. The direction of GNI steps is the solution of normalized first order Newton method. The step of GNI iteration is defined implicitly using backtrack technique. For evaluation purposes the GNI method is conducted at fixed 25 iterations.

The dielectric contrast distribution over object domain describes the cross section of the OI. The solution of MWT problems using GNI defines the value of the contrast. It is assumed that the OI is divided into N cells and at each cell the dielectric contrast is distributed homogeneously.

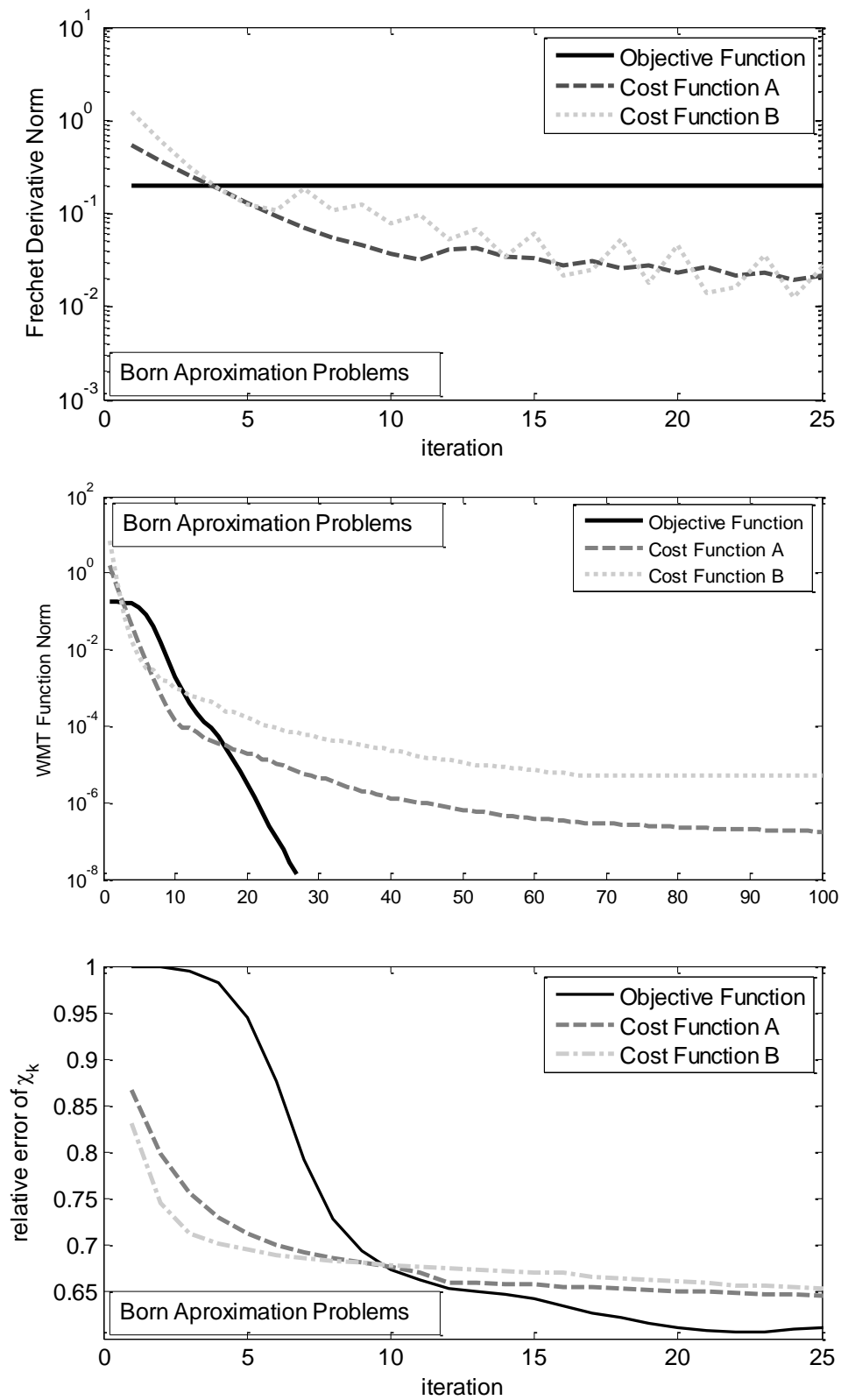


Figure D-4: The parameter of the solutions of Born approximation MWT inverse problem.

GNI updates the estimated dielectric contrast individually on each cell. Therefore, the plot of dielectric contrast value distribution over object domain represents the cross section of OI. It can be seen in Figure D-1 that the reconstructed images describe the shape, the position and the quantities of OI accurately.

The iteration process of Born Approximation can be studied using Figure D-2. The normalized norm of MWT-objective function and least squared cost functional of MWT problem graphs approach zero point. It can be deduced that the estimated solution moves toward exact solution. Moreover, it can be seen that the MWT-objective function formulation for MWT problem is better than the cost functional of MWT problem. It produces error of normalized norm error less than 10^{-7} while the cost functions of MWT produce error about 10^{-4} .

The least-squared cost functional is a convex system, thus the solution is determined whenever the derivative of the functional is zero. It can be seen that the graphs of the Fréchet derivatives of cost functional approach zero. The iteration stops if the value of the cost function is below a small positive tolerance parameter. On the other hand, the line of Fréchet derivative norm of MWT-objective function approaches a non-zero constant along iterations. This is implied that the stop rule for MWT-inverse problem with objective-function formulation should be stated by considering the limit value of derivative. However, the limit value of derivative norm is hard to define. Therefore, the stopping rule may be defined using the norm of the residual error.

The functional operators are derived from the residual error of the scattered fields. The functional respects the dielectric contrast of object under investigation inside domain object. The estimated solution is assigned as the solution of the problems if the functional is less than the determined size of the functional. It can also be illustrated by the relative error of the estimated scattered field with respect to measured scattered field. The relative error graphs, which can be seen at Figure D-2, move toward zero for all functional operators.

E.1 Newton Method for Solving Microwave Inverse Problem; Nugroho, Agung T and Z Wu; The UoM IEEE Electron Devices Poster Conference; 12th june 2013.

The University of Manchester



Newton Method for Solving Microwave Tomography Inverse Problem

NONLINEAR AND ILL-POSED INVERSE PROBLEM in Microwave Tomography?
 Leave such a problem by the implementation of Newton Method to minimize residual error function in reconstructing the distributions of dielectric contrast of an object cross section from measured scattered fields by using a cylindrical object.

ALTERNATIVE SOLUTION
 The residual error function is written as:

$$\mathcal{F}(\chi) = \sum_{p=1}^P \|E_{mea,p}^{scat} - E_{guess,p}^{scat}\|_{\mathcal{M}}$$

The guessed scattered field is determined by solving

$$E^i(x,y) = \frac{1}{j\omega(\epsilon - \epsilon_0)} J_z(x,y) + \frac{k\eta}{4} \iint J_z(x',y') H_0^{(2)}(kr) dx'dy'$$

Applying the method of moment to (2) and substituted at (1) gives

$$\mathcal{F}(\chi) = \sum_{p=1}^P \|Z_{\mathcal{M}} [\chi Z_{\mathcal{N}} - I]^{-1} diag(\chi) E_p^{inc} + E_{mea,p}^{scat}\|_{\mathcal{M}}^2$$

The Newton algorithm minimize residual error function iteratively by solving

$$solve \mathcal{J}(\chi_n)^* \mathcal{F}(\chi_n) = \mathcal{J}(\chi_n)^* \mathcal{J}(\chi_n) \Delta \chi_n; \quad \forall \chi \in \mathbb{N}$$

The Jacobian in (4) is approximated by

$$\nabla \mathcal{F}_p(\chi) \approx \mathcal{J}(\chi)$$

which is determined by applying a small variation to (3). The gradient is stated as follows:

$$\nabla \mathcal{F}_p(\chi) = \frac{d\mathcal{F}(\chi)}{d\chi} = \sum_{p=1}^P [-Z_{\mathcal{M}} [\chi Z_{\mathcal{N}} - I]^{-1} [E_p^{inc} - Z_{\mathcal{N}} J_p]]$$

The algorithm is implemented to reconstruct cylindrical object. The results are presented in figure.

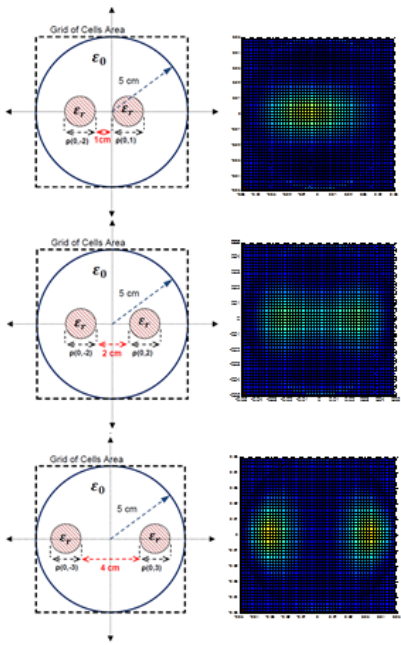


Figure The results of Newton reconstruction. Two similar object inside the object domain. The object are separated in various distance.

CONCLUSION
 Newton method can undoubtedly be used to solve inverse problem for microwave tomography application, due to its flexibility with the cell size and iterative steps. With an appropriate number of iterative steps, high contrast dielectric object can be reconstructed.

Microwave and Communication System Group
School of Electrical and Electronic Engineering
The University of Manchester

For details contact: [Agung T Nugroho](mailto:Agung.T.Nugroho)
 E-Mail: agungtahlo.nugroho@manchester.ac.uk
 Supervisor: **Z Wu**
 E-Mail: zhiqiang.wu@manchester.ac.uk
 Acknowledgements: Directorate General of Higher Education of Republic of Indonesia

E.2 Reconstructing Image of Microwave Tomography Using Contrast Source Inversion Method; Nugroho, Agung T and Z Wu; The UoM, EE E PGR Poster Conference; 20th November 2013

The University of Manchester



Reconstructing Image of Microwave Tomography Using Contrast Source Inversion Method

INTRODUCTION

The Image of Microwave Tomography (MWT) can be produced by measuring scattered fields around the object at each illumination and reconstructing the data using reconstruction algorithms. The reconstructions are completed in two steps: forward and inverse problems. The former step is well posed problem, while the later one is non-linear ill posed problem. In this poster the method proposed is Contrast Source Inversion (CSI) is proposed to solve the non-linear ill posed of MWT inverse problem.

FORWARD PROBLEM

The forward problem is presented in electric field integral equations (EFIE) under TM polarization. The incident fields inside the domain object is stated as

$$E_i^s(x, y) = \frac{J(x, y)}{j\omega\epsilon_0(\epsilon_r - 1)} + \frac{k_0\eta_0}{4} \iint J_i(x', y') H_0^{(2)}(k_0 r) dx' dy'$$

The scattered fields are computed using

$$E_s^s = -\frac{k_0\eta_0}{4} \iint J_s(x', y') H_0^{(2)}(k_0 r) dx' dy'$$

Applying the Method of Moment with Pulse Basis Function, then, the equations can be presented as :

$$\chi Z \mathbf{J} = \left[\chi Z_0 - \frac{\eta_0}{k_0} \mathbf{I} \right] \mathbf{J} \quad \text{and} \quad \mathbf{E}^s = -Z_s \mathbf{J}$$

where Z is the integral operator and $\chi = (\epsilon_r - 1) / \epsilon_r$.

Once χ is given, \mathbf{E}^s can be easily computed. The numerical test of the forward problem are presented in the figure 2.

INVERSE PROBLEM

The MT inverse problem is stated as the operator equation which is continuous and differentiable at $D(F)$ as $F(\chi, J) = y$ where

$$F(\chi, J) = \begin{bmatrix} -Z_s \mathbf{J} \\ \chi Z \mathbf{J} - \frac{\eta_0}{k_0} \mathbf{I} \mathbf{J} \end{bmatrix} \quad \text{and} \quad y = \begin{bmatrix} \mathbf{E}^s \\ 0 \end{bmatrix}$$

Iteratively, the problem is solved using CSI method as:

$$[F'(\chi, J)]^* F'(\chi, J) + \alpha I [\Delta(\chi_{i+1}, J_{i+1})] = F'(\chi, J)^* y$$

Where $F'(\chi, J)$ is Fréchet differential of (F) and α is Tikhonov regularization. The results of numerical experiment of Inverse Problem are presented below

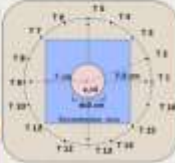


Figure 1: The Architecture of MWT with 16 antennas

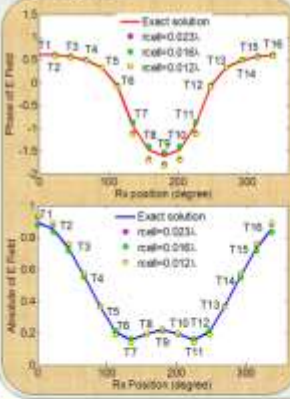


Figure 2: The Measured Scattered Fields at T1-T16.

Note:
Tx = T1, T2 ... T16
Rx = T1, T2 ... T16
Freq = 2.5 GHz
 $\epsilon_0 = \text{air}(1)$; $\epsilon_r = 4$
Radius of OI = 2 cm
Radius of T = 7.5 cm
No of cells = varied

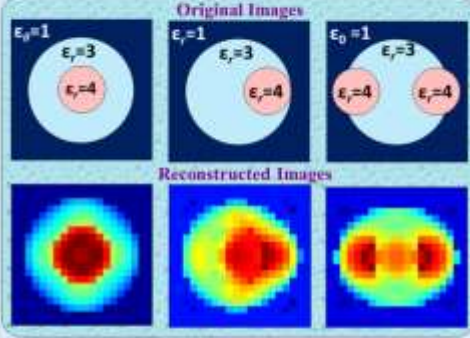


Figure 3: The Original Images and reconstructed images using CSI method.

Note:
Tx = T1, T2 ... T16;
Rx = T1, T2 ... T16
Freq = 2.5 GHz;
 $\epsilon_0 = 1$; $\epsilon_r = 3$ and 4;
No of cells = 30 x 30

CONCLUSIONS

The accuracy of forward problem solution reaches 99 percent, in which the cell's size is determinant of the level of accuracy. The CSI has accurate capability of producing an image but works slowly.

Microwave and Communication Systems

School of Electrical and Electronic Engineering

The University of Manchester

For details contact: AGUNG.TIANJO.NUGROHO

E-Mail: agungtiano.nugroho@manchester.ac.uk

Supervisor: ZHIPENG.WU

E-Mail: zhipeng.wu@manchester.ac.uk

Acknowledgements: Directorate General of Higher Education of Republic of Indonesia

E.3 Inexact Newton Backtracking Method for Solving Microwave Tomography Inverse Problem; Nugroho, Agung T and Z Wu; 2015 IEEE, International Conference on Imaging Systems and Techniques; Macau, China; September 16-18, 2015

Inexact Newton Backtracking Method for Solving Microwave Tomography Inverse Problem

Agung Tjahjo Nugroho
School of Electrical and Electronic Engineering
The University of Manchester
United Kingdom

Zhipeng Wu
School of Electrical and Electronic Engineering
The University of Manchester
United Kingdom

Abstract— An inexact Newton backtracking method (INBM) has been developed to obtain a stable solution of microwave tomography inverse problem. The problem is solved iteratively by linearization. Instead of finding direct regularized solution of linear ill-posed problem, iterative regulated approximation solver in term of INBM is proposed as a new alternative method. The iteration is guarded using a forcing term which is determined on the nonlinear and linearized steps of the microwave inverse problem. The method proposed is tested using numerical examples and experimental data. The quality of proposed method is evaluated by comparing it with the Levenberg Marquardt (LM) method.

Keywords—*Microwave tomography; inverse problem; Inexact Newton backtracking method; Newton iterative method*

I. INTRODUCTION

The image of microwave tomography (MWT) can be produced by illuminating a dielectric object with microwave fields in different directions, and measuring the scattered field around the object at each illumination. The data of the measured scattered fields are processed using image reconstruction algorithms to produce its dielectric property distribution. The reconstruction is completed in two steps, by solving forward and inverse problems.

Numerically, the forward problem which is also known as a direct scattering problem can be solved directly and accurately. On the other hand, the inverse problem, which is usually presented in a least-square problem, is a highly nonlinear system and suffers from illposedness, hence regulated inverse method is needed to solve the problem. Currently, Newton based methods are popular techniques to solve the MWT inverse problem for its speed reason. Newton Kantorovich method [1, 2], Inexact Newton Method [3], Quasi-Newton method [4, 5] and Gauss-Newton inversion [6] had been intensively applied to the MWT inverse problem. The results show that the regulator is essential to stabilize the reconstruction process.

In this paper, a Newton iterative by means of an inexact Newton Backtracking method (INBM) in [7] is used. The MWT inverse problem is presented in a nonlinear system and solved in outer and inner loops. The outer linearizes the MWT inverse problem by means of Fréchet derivative. The ill conditioning of the nonlinear system is transformed into a linear ill-posed problem. The corresponding inner loop solves the linear ill posed problem and finds the approximation that

meets the forcing term of the inexact Newton approach. Thus, the Newton iterative solution is updated by an approximate regularized solution of a linear ill-posed problem instead of a direct regularized solution. The flexibility of the proposed method is tested using synthetic and experimental data. To determine the flexibility of the INBM, the results of reconstruction are compared with the result of LM.

II. FORWARD PROBLEM

The microwave illumination in MWT can be described by a pair of integral equations:

$$E^i(r) = E(r) - k_0^2 \iint_{\Omega} \chi(r') E(r') H_0^2(k_0, \rho) dr' \quad (1)$$

$$E^s(r) = k_0^2 \iint_{\Omega} \frac{1}{4j} \chi(r') E(r') H_0^2(k_0, \rho) dr' \quad (2)$$

Where Ω is cross section of the object, $\chi = (\epsilon - 1)$ is the dielectric contrast, both coefficients r and r' are position vectors, and ρ is the distance between r and r' . Equation (1) represents the domain equation. The position vector addresses a point at object domain $X, (r, r') \in X$, while (2) expresses data equation. Vector r in (2) defines data position at data domain $Y, r \in Y$ and r' point to a cell at domain $X, r' \in X$.

The equations are solved using the Method of Moments. The cross-section of the object of interest is divided into N number of cells with equal size, then $E(r)$ can be approximated by superposition of pulse basis functions. The integrals in (1), (2) are evaluated analytically with the assumption that all cells are circles [8, 9]. With all illuminations of $t = 1, 2, \dots, T$, sequentially the equations can be stated as

$$E_t^i = E_t + Z_X^i(\chi E_t) \quad (3)$$

$$E_t^s = -Z_Y^s(\chi E_t) \quad (4)$$

Both equations are functions of dielectric contrast (χ) and total electric field. The matrix product of contrast (χ) and source (E_t) is related to the product inside the integral equations. Once χ is given in (4), E_t can be easily computed

using (3). Furthermore, the estimated scattered fields E'_s can be determined using the data equations (4), in which the cell size is determinant to the level of accuracy.

III. INVERSE PROBLEM

The integral equations can be stated in abstract as a non-linear ill-posed problem. For the purpose of Newton iterative solver, the MWT problem is written as

$$F(x) = y \quad (5)$$

The goal of the inverse problem is to find the unknown x which is dielectric contrast (y) for a set of measured scattered field data. Assuming that (5) has an exact solution at x^* and the exact, but indefinite measured data is defined as $y = F(x^*)$.

The functional $F: \mathbb{R}^n \rightarrow \mathbb{R}^m$ with $n > m \gg 1$ operates between data domain (Y) and object domain (X). The nonlinear system of MWT is defined with more unknowns than equations, regardless of uniqueness or existence of its solution. The goal of the iterative method for solving the microwave inverse problem is to find stable approximate solution of (5). The iterative solver proposed is a Newton type algorithm. At step k , the iterative solution is updated the current actual solution x_k by a correction step which is also known as the current correction (s_k).

$$x_{k+1} = x_k + s_k \quad (6)$$

Assuming F is Fréchet differentiable with derivative F' , and the direction of Newton step satisfies the first order Taylor series, the linear system of the Newton algorithm is written as

$$F'(x_k) s_k = (y - F(x_k)) - \text{Err}(x^*, x_k) = b_k \quad (7)$$

Error Err arises due to the truncation of the power series at first order term which outlines the linear system of Newton scheme. The error of linear function is the residual of the series which can be stated as

$$\text{Err}(u, v) = (F(u) - F(v)) - F'(v)(u - v) \quad (8)$$

In the real world, the measured data could not be separated from noise, thus b_k is undefined due to the unknown exact data and residual error. The measured data E^s is assigned as y^δ . It is the scattered field at data domain with noise, $y^\delta = E^s + h(\delta)$ as the exact scattered field $y = E^s$ cannot be determined. Assuming that the noise level is known, the noisy data y^δ satisfies

$$\|y - y^\delta\|^2 \leq \delta \quad (9)$$

Immersing the noise and residual error to b_k , the perturbed b_k^ϵ is defined using the difference of measured data and estimated data which is assigned as the objective functional,

$$b_k^\epsilon = y^\delta - F(x_k) \quad (10)$$

The iterative step of (5) is computed via a linear Newton equation

$$F'(x_k) s_k = b_k^\epsilon \quad (11)$$

The basic principle in solving the nonlinear MWT inverse problem using Newton iterative method is that the correction step of the solution is determined by solving linear system. The linearization by means of Fréchet derivative is applied to construct the linear system.

The multiple illuminations of MWT system provide m number of data functions with n unknown dielectric contrast. The Fréchet derivative denoted by $D = F'$ is an $m \times n$ matrix:

$$D = [F'_{ij}] = \left[\left(\frac{\partial F_i(x)}{\partial x_j} \right) \right]_{\substack{1 \leq i \leq m, \\ 1 \leq j \leq n}} \quad (12)$$

The linear system of Newton iterative algorithm is therefore stated as

$$D_k s_k = b_k^\epsilon \quad (13)$$

The stationary point of $\|F\|$ which is the optimum solution of (1) is a point $x_k \in \mathbb{R}^n$ where

$$\|y^\delta - F(x_k) + D_k s_k\|^2 < \|y^\delta - F(x_k)\|^2 \quad (14)$$

This includes local minimizer of $\|y^\delta - F(x_k)\|^2$.

However ill-posedness and asymmetrical of MWT inverse problem (5) due to outnumber of data to the reconstructed cell number are immersed to the linear system of MWT inverse problem. Hence, a regularized linear parameter is presented in the form of least squared minimization problem $\min_x \|y^\delta - F(x_k)\|^2$ and the regularized solution of (13) is stated in regularized linear filter form

$$s_k = \psi \left(D_k^* D_k \right)^{-1} D_k^* b_k^\epsilon \quad (15)$$

where ψ is a regularized linear filter.

A. Levenberg Marquardt method

Several techniques have been developed to provide regularized s_k with regularization parameter α . Tikhonov regularization is probably the most attractive technique. The regularization is defined as

$$\Psi(D, \alpha) = \frac{1}{\alpha + D} \quad (16)$$

This leads to variation of LM. that is $\Psi(D_k^* D_k, \alpha_k) = (D_k^* D_k + \alpha_k I)^{-1}$. Then direct Thikonov regulated solution of (15) can be computed using

$$s_k = \left[\sum_{j=1}^N \frac{\sigma_j}{\sigma_j^2 + \alpha} u_j^T v_j \right] [D_k^* b_k^e] \quad (17)$$

where (u, σ, v^T) are the decomposition matrices of $D_k^* D_k$ and σ is a diagonal matrix of the singular values of $D_k^* D_k$

B. Inexact Newton Backtracking method

Equation (17) is categorized as a direct solution. It is predictable in number of steps, but it does not support intermediate solution. Iterative method is an alternative way to improve the accuracy and speed. It starts with an approximate answer, and then the accuracy is improved iteratively. It stops once the estimated error is below the tolerance.

Define the linear ill-posed problem of MWT in a normal equation as

$$\Psi_k^{-1} s_k = D_k^* b_k^e \quad (18)$$

Suppose the exact solution s_k^* satisfies (18), and current iterative solution is defined as $\bar{s}_{k,l}$, where the initially estimate is $\bar{s}_{k,0}$. A residual of the linear problem in a normal equation is defined as

$$r_l = D_k^* b_k^e - \Psi_k^{-1} \bar{s}_{k,l} \quad (19)$$

The error in current solution is defined as

$$e_l = s_k^* - \bar{s}_{k,l} \quad (20)$$

Multiplying (20) with Ψ_k^{-1} results in iterative linear algorithm

$$e_l = \Psi_k r_l \quad (21)$$

The iterative approximation of Newton correction is updated via

$$\bar{s}_{k,l+1} = \bar{s}_{k,l} + d e_l \quad (22)$$

where e_l is direction of iterative linear solution which is gained by solving (21) and d is the step size which minimizes the residual

$$\min_d \left\| D_k^* (b_k^e - D_k (\bar{s}_{k,l} + d e_l)) \right\|^2 \quad (23)$$

The proposed Newton iterative solution by means of INBM replaces the direct solution in the form of s_k with its iterative approximation $(\bar{s}_{k,l} = \bar{s}_{k,l})$. In this type of method the direction of Newton step is approximated to the following

$$\|b_k^e - D_k \bar{s}_k\|^2 \leq \eta_k \|b_k^e\|^2 \quad (24)$$

where the nonnegative forcing term η_k is used to control the level of accuracy. The term η_k is determined at $\eta_k \in (0,1)$ so that the vector s that satisfies (24) where $\eta_k < 1$ is assigned as the approximate solution of the inexact Newton.

To improve the global convergent, the values of s_k and η_k are guarded to force the reduction of functional. The global criterion of the INBM is used to ensure the direction of objective functional. The inexact Newton method is globalized by

$$\|v^{\delta} - F'(x_k + \bar{s}_k)\|^2 \leq [1 - t(1 - \eta_k)] \|v^{\delta} - F'(x_k)\|^2 \quad (25)$$

Equation (25) guarantees the reduction of the functional with the direction defined. By giving the s_k and η_k , there at least a fraction of reduction of functional which is guaranteed by finding the term $t \in (0,1)$

Backtracking method can be applied to accommodate the selection of s_k and η_k which are suitable for both (24) and (25) criteria. If s_k is not acceptable by the criteria, then it is shortened until it is under the criteria. The correction of parameter follows

$$s_k = r \cdot s_k \quad (26)$$

$$\eta_k = 1 - r(1 - \eta_k) \quad (27)$$

with $r \in (r_{\min}, r_{\max})$. The fraction of reduction should be selected in the range of $r \in (0,1)$. Backtracking is the type of inexact line search. It keeps not too long steps, but it does not guard not too short ones.

The INBM is locally convergent, if forcing term η_k is uniformly less than 1. Under the present assumptions, if x_0 is sufficiently close to x^* , and $0 \leq \eta_k \leq \eta_{\max} < 1$ for each k , then x_n converges to x^* [7]. If $\eta_k = 1$ for all iterations then it is similar to the Gauss Newton method. The forcing term is independent on the iteration index k . The forcing term is applied to guarantee the error decrease of linear model of the MWT inverse problem.

The convergence rate of the method is determined by an appropriate choice of η_k . The term may be determined using the agreement of the functional and the linear model of the corresponding problem. The forcing term is adjusted depending on the ratio of actual reduction and predicted reduction. The ratio is defined as

$$\eta_k = \frac{\left\| \left(y^\delta - F(x_k) \right) \right\|^2 - \left\| \left(y^\delta - F(x_k + \bar{s}_k) \right) \right\|^2}{\left\| y^\delta - F(x_k) \right\|^2 - \left\| \left(y^\delta - F(x_k) \right) - D_k \bar{s}_k \right\|^2} \quad (28)$$

The forcing term is determined according to the ratio η_k

$$\eta_k = \begin{cases} 1 - 2p_1 \leftarrow \eta_{k-1} < p_1 \\ \eta_{k-1} \leftarrow p_1 < \eta_{k-1} < p_2 \\ 0.8\eta_k \leftarrow p_2 < \eta_{k-1} < p_3 \\ 0.5\eta_k \leftarrow \eta_{k-1} \geq p \end{cases} \quad (29)$$

where $p_1 < p_2 < p_3 < 1$ are prescribed with $p_1 \in (0, \frac{1}{2})$

The correction of current solution in Newton scheme is gained iteratively in INBM. The iteration which is the inner loops of global scheme is stopped following

$$\left\| b_k^\delta - D_k \bar{s}_k \right\|^2 \leq \eta_k \left\| b_k^\delta \right\|^2 \leq \left\| b_k^\delta - D_k \bar{s}_{k,j} \right\|^2 \quad (30)$$

where $i=1, 2, \dots, l$

The Newton iteration is the outer loop of the iteration scheme. It has to be stop above the noise level to avoid noise amplification. Discrepancy principle can be used to define the stopping rule

$$\left\| \left(y^\delta - F(x_k) \right) \right\|^2 \leq R\delta \leq \left\| \left(y^\delta - F(x_k) \right) \right\|^2 \quad (31)$$

where $k=1, 2, \dots, (K-1)$, δ is the noise level and $R>0$ is real positive number. As the noise level is unknown, the Newton iteration is stopped when

$$\frac{\left\| \left(y^\delta - F(x_k) \right) \right\|^2 - \left\| \left(y^\delta - F(x_{k+1}) \right) \right\|^2}{\left\| \left(y^\delta - F(x_{k+1}) \right) \right\|^2} \leq R \quad (32)$$

IV. NUMERICAL EXPERIMENT

In the numerical experiment, the measured data are synthetic which are obtained from solving the forward problem in (3) and (4). The images are reconstructed by the Newton iterative method with iterative sequence in (6), where the Newton steps are defined using INBM in (22) and LM in (17). Comparative study is used to analyze the stability of the solutions. The image resulted by Newton iterative method by means INBM is compared to that resulted from the direct regulative solution by means of LM. To analyze the quality of the algorithm, objective functional norm and error relative of the distribution of dielectric contrast are introduced as

$$\alpha(b^\delta) = \frac{\left\| b_k^\delta \right\|^2}{\left\| y^\delta \right\|^2} \quad (33) \quad \text{and} \quad \text{error} = \frac{\left\| x_k - x^* \right\|^2}{\left\| x^* \right\|^2} \quad (34)$$

Both methods are used to reconstruct from the noisy data of MWT inverse problem. A circular rod with $\epsilon_r=3$ is used. The object is illuminated with 4.5 GHz microwave signals from a transmitter antenna. The scattered fields are measured using 16 receiver antennas, including the transmitter antenna itself. The parameters of numerical experiment are summarized in Table I.

The simulation data is added with random numbers which are assigned as introduced noise and any other additional error, with signal to noise ratio set to be SNR 28.3, 34.2 and 40.5 dB. Reconstruction from data with noise is made using both methods. The images obtained at two different iteration indexes can be seen at Fig. 1. The results of reconstruction progress are presented in Fig. 2 and Fig. 3. It can be seen that INBM is faster and produces better images than the LM method. The dielectric contrast and the shape of the dielectric object can be clearly distinguished, while the LM method produces less qualified image. The INBM is capable of eliminating the background material. The error of the solution is lower than the error of the LM method with Thikonov regularization.

TABLE I. PARAMETER OF SIMULATED SYSTEM

Parameter	Value
Diameter of Object Domain (X)	9.5 cm
Diameter of Data Domain (Y)	13.0 cm
Transmitting Antenna T_r	16
Receiving Antenna R_r	16
Number of data (amplitude and phase)	256×2
SNR	28.3, 34.2, 40.5 dB
Number of cells	$50 \times 50 = 2500$
ϵ_r	3
Diameter of object	4 cm
Frequency	4.5 GHz

The iteration of Newton iterative is guarded with discrepancy principle. It is applied in the outer loop of INBM, where the iteration is stopped if the ratio of objective functional difference in successive solutions is less than the defined ratio value. The results of numerical experiment where the outer and inner stopping rule are applied, are summarized in Table II. It can be seen that INBM is superior to the LM method in term of speed and accuracy.

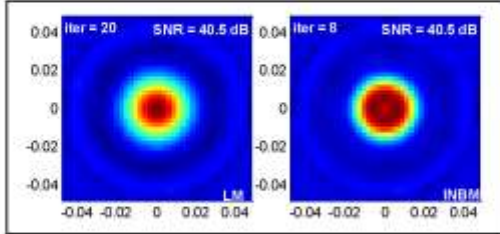


Fig. 1. Images of reconstructed numerical data resulted by Inexact Newton Backtracking method (INBM) and Levenberg Marquardt (LM) method

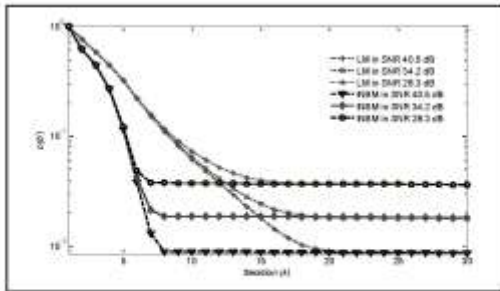


Fig. 2. Progression of objective functional norm of INBM and LM method at various SNR data

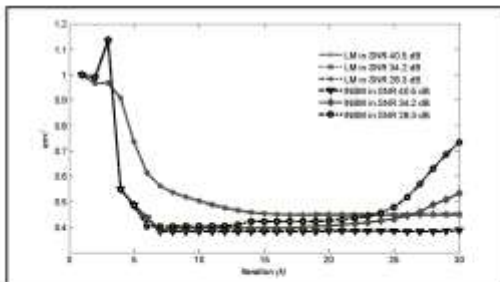


Fig. 3. Progression of relative error of dielectric contrast of INBM and LM method at various SNR data

TABLE II. RESULTS OF NUMERICAL DATA RECONSTRUCTION

SNR (dB)	LM				INBM			
	k	$n(b')$	$err_{x'}$	$R(\%)$	k	$n(b')$	$err_{x'}$	$R(\%)$
40.5	20	0.90	44.4	1.80	8	0.85	38.90	0.00
34.2	18	1.90	44.69	2.61	8	1.85	39.65	0.00
28.3	16	3.80	45.09	2.10	7	3.75	40.30	0.05

V. EXPERIMENTAL TEST

A microwave tomography system has been developed at the School of Electrical and Electronic Engineering, University of Manchester. The MWT system uses 16 monopoles supported by a ground plane. It works in free space domain.

The system is shown in Fig. 4. The parameters used in the measurement are summarized in Table III. The antennas are computer-controlled via a 2x16 Cytec multiplexer.



Fig. 4. Microwave tomography system setup

TABLE III. PARAMETER OF MEASUREMENT SYSTEM

Parameter	Value
Diameter of Object Domain (X)	9.5 cm
Diameter of Data Domain (Y)	13.0 cm
Transmitting Antenna T_x	16
Receiving Antenna R_x	8
Number of data (amplitude and phase)	128×2
Number of cells	$50 \times 50 = 2500$
Object of interest	rod
ϵ_r	2.1
Diameter of object	3 cm
Frequency	4.5 GHz

The transmission and measurement of electric fields are conducted by a Vector Network Analyzer (VNA). Total electric fields are assigned as collected field data. At each illumination, 8 Rx antennas are addressed to measure the total electric fields before and after the object is introduced. The measured scattered fields are defined as the difference of disturbance and non-disturbance fields at receiving antennas. The data are used for reconstruction using both INBM and LM algorithms.

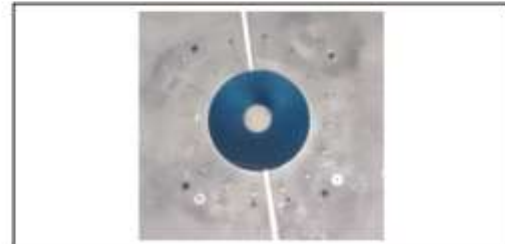


Fig. 5. A long cylindrical rod inside the object domain of the microwave tomography system setup

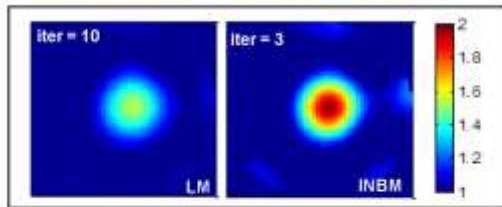


Fig. 6. Images of reconstructed experimental data resulted by INBM and LM method.

The object of interest for experimental test is a cylindrical rod as seen in Fig 5. It has a dielectric constant of 2.1 at 4.5 GHz. The reconstructed images at its cross-section are presented in Fig. 6. It can be seen that both methods draw the shape and position accurately. However the LM method fails to find contrast of the object while the INBM produces an image with a contrast near the exact value. The INBM finishes the reconstruction in 3 iterations with a 28.4% functional error while the LM method converges three times more slowly with a 37.7% error.

VI. CONCLUSIONS

An inexact Newton backtracking method has been presented for solving the MWT inverse problem. The main features of the proposed method include presenting the MWT inverse problem as a nonlinear problem, solving it in outer and inner iteration loops, replacing the direct solution with a more accurate regulated solution, and applying a forcing term to strictly guard the approximated solution. The results of the numerical experiment and experimental tests reveal that the method produces a stable solution for the MWT inverse problem. It improves the image quality and the rate of image reconstruction. Furthermore the experimental test highlights several positive characteristics of the inexact Newton backtracking method, including its capability to reconstruct images from limited data and robustness to unknown noise. Further investigation needs to be made which include the study of the effect of lossy material and heterogeneous materials so that the scope of the application of the algorithm for MWT inverse problem for industrial processes can be extended.

REFERENCES

- [1] Henriksson, T., Joachimowicz, N., Conessa, C., & Bolomey, J. C. (2010). Quantitative microwave imaging for breast cancer detection using a planar 2.45 GHz system. *Instrumentation and Measurement, IEEE Transactions on*, 59(10), 2691-2699.
- [2] Wu, Z. (2003). Effects of noise and system's parameters on the tomographic image reconstruction of ground surfaces. *IEEE Transactions on Antennas and Propagation*, 51(6), 1401-1403.
- [3] Olivari, G., Lizzi, L., Pastorino, M., & Massa, A. (2012). A nested multi-scaling inexact-newton iterative approach for microwave imaging. *Antennas and Propagation, IEEE Transactions on*, 60(2), 971-983.
- [4] Hu, J. L., Wu, Z., McCann, H., Davis, L. E., & Nae, C. G. (2006). BFGS quasi-newton method for solving electromagnetic inverse problems. *IEE Proceedings - Microwaves, Antennas and Propagation*, 153(2), 199.
- [5] Wu, Z., McCann, H., Davis, L. E., Hu, J., Fontex, A., & Nae, C. G. (2009). Microwave-tomographic system for oil- and gas-multiphase-flow imaging. *Measurement Science and Technology*, 20(10), 104026.
- [6] Abubakar, A., Habashy, T. M., Guangdong, P., & Mao-Sam, L. (2012). Application of the multiplicative regularized gauss-newton algorithm for

three-dimensional microwave imaging. *Antennas and Propagation, IEEE Transactions on*, 60(5), 2431-2441.

- [7] Dambo, R. S., Eisenstat, S. C., & Steihaug, T. (1982). Inexact Newton methods. *SIAM Journal on Numerical Analysis*, 19(2), 400-408.
- [8] Jin-Lin, H., Wu, Z., McCann, H., Davis, L. E., & Chang-Gang, X. (2005). Quasi-three-dimensional method of moments for analyzing electromagnetic wave scattering in microwave tomography systems. *Sensors Journal, IEEE*, 5(2), 216-223.
- [9] J. H. Richmond, "Scattering by a dielectric cylinder of arbitrary cross-section shape," *IEEE Trans. Antennas Propagat.*, vol. 13, pp. 334-341, 1965.

E.4 Newton Iterative with Conjugate Gradient on Normal Equations for Reconstruction of Free Space Microwave Imaging ; Nugroho, Agung T and Z Wu; To be submitted to: ; Transactions of the Institute of Measurement and Control Journal

Newton Iterative with Conjugate Gradient on Normal Equations for Reconstruction of Free Space Microwave Imaging.

Agung Tjahjo Nugroho
School of Electrical and Electronic Engineering
The University of Manchester
United Kingdom

Zhipeng Wu
School of Electrical and Electronic Engineering
The University of Manchester
United Kingdom

Abstract— A Newton iterative-conjugate gradient on normal equation is developed for image reconstruction of a dielectric object in free space. In this method an implicit solution of Newton equations is introduced as the step of Newton Iterative (NI). The implicit solution replaces a direct regularized solution. An inexact Newton class is exploited to set the accuracy of the implicit solution and Conjugate Gradient on Normal Equation (CGNE) is considered to solve the Newton equations only approximately and in unspecified manner. Under the natural assumption that the CGNE is a semi regularized method, the results of experiments show that NI-CGNE improves the spatial resolutions and the quality of direct regularization method by means Levenberg Marquardt method results.

Keywords—*Microwave tomography; inverse problem; Newton iterative method; Conjugate gradient on normal equations*

1. INTRODUCTION

Microwave imaging is promising for non-invasive evaluation tools of industrial process. It is an alternative to visible light due to the higher capability in penetrating dielectric object. This method is a better non-ionizing option than X-rays and gamma ray systems. Both modalities produce high quality images in terms of the density contrast within the object, but the radiation hazard and expense of these systems limit for their widespread use. The low frequency tomography system produce images of permittivity and/or conductivity contrast. Recently, this technique is commonly applied in industrial process. However, it is limited with its spatial resolution and the range of electrical properties that can be processes. On the other hand, the physical quantity of the object in microwave domain is stated in complex value of dielectric properties by means of permittivity and conductivity of the material. The complex number enhances the description of the interest. The application of microwave tomography enables to evaluate the object of interest without disturbing the process and produce very good spatial resolution. For those reasons, microwave imaging is an attractive tool for industrial applications. However, the microwave imaging is a nonlinear inverse problem. The problem is difficult to solve due to the ill

poseness of the problem. Therefore, a method to obtain stable solution of microwave tomography inverse problem needs to be developed.

Assuming that object being investigated is placed in an air as it is most convenient to place in industrial applications. The image of object of interest can be produced by illuminating a dielectric object with microwave fields in different directions, and measuring the scattered field around the object at each illumination. The data of the measured scattered fields are processed using image reconstruction algorithms to produce dielectric contrast distribution with respect to air. The reconstruction is completed by solving MWT-inverse problems. The MWT-inverse problem is formulated in an objective function.

MWT-objective function is a highly nonlinear system and suffers from ill-posedness; hence regulated inverse method is needed to solve the problem. Currently, Newton based methods are popular techniques to solve the MWT inverse problem for its speed reason. Newton Kantorovich method [1; 2], Inexact Newton Method [3], Quasi-Newton method [4] and Gauss-Newton inversion [5] had been intensively applied to the MWT inverse problem. The results show that the accuracy of the results is depended on the type of regularization and the size of regulator parameter which are hard to define [6].

Newton Iteration (NI)-Conjugate Gradient on Normal Equation (CGNE) is developed as an alternative to direct regularization techniques, for solving MWT-inverse problem. NI-CGNE is a Newton method for solving nonlinear problem which is formulated in outer and inner loop scheme. The outer loop is a Newton minimization of MWT-objective function norm and the inner loop is the application of CGNE to solve Newton equations. CGNE is a semi regularized method in which regularization techniques are avoided and replaced with a stopping criterion. The method proposed is tested to solve MWT inverse problems of free space applications. The quality of the proposed method is evaluated by comparing the results of NI-CGNE with the result direct iterative regularization method by means of Levenberg Marquardt method (LM).

II. MICROWAVE IMAGING PROBLEM

Let us consider TM polarized microwave signals from M known sources illuminate a cylindrical dielectric object sequentially. The object under test is embedded in a linear homogeneous background. An imaging domain (X) contains the object cross section Ω in which its dielectric properties are described by the contrast function $\chi(\mathbf{r}) = \epsilon(\mathbf{r})/\epsilon_b - 1$, where ϵ_b is the permittivity of the background and $\epsilon(\mathbf{r})$ is the dielectric permittivity at position \mathbf{r} . Each illumination produces incident field $E^i(\mathbf{r})$ at imaging domain $\mathbf{r} \in X$ and results electric scattered fields $E^s(\mathbf{r})$ elsewhere. Assuming no magnetic media are involved, the scattered fields at data domain ($\mathbf{r} \in Y$) outside domain X can be described in the following integral equation:

$$E^s(\mathbf{r}) = -k_b^2 \iint_{\Omega} G(\mathbf{r}, \mathbf{r}') \chi(\mathbf{r}') E(\mathbf{r}') d\mathbf{r}' \quad (1)$$

Equation (1) represents the *data equation* where vector \mathbf{r} in defines data position at data domain (Y), $\mathbf{r} \in Y$ and \mathbf{r}' point to a cell at domain X , $\mathbf{r}' \in X$. The wave number at background media k_b is defined as $k_b = \omega \sqrt{\epsilon_b \mu_0}$, where the harmonic wave varying in time as $e^{-i\omega t}$ and μ_0 is magnetic permeability of vacuum. The Green's function $G(\mathbf{r}, \mathbf{r}')$ is defined for two dimensional Helmholtz equation as $G(\mathbf{r}, \mathbf{r}') = (j/4) H_0^{(2)}(k_b |\mathbf{r} - \mathbf{r}'|)$, where $H_0^{(2)}$ is the Hankel function of second kind and zeroth order.

The total electric fields $E(\mathbf{r})$ everywhere inside and outside imaging domain are the addition of incident fields and electric scattering fields.

$$E(\mathbf{r}) = E^i(\mathbf{r}) + E^s(\mathbf{r}) \quad (2)$$

The total electric fields, $E(\mathbf{r})$, $\mathbf{r} \in Y$, at imaging domain are unknown. It cannot be directly measured. Thus it is worth to express the total electric fields at domain X in *domain equation* as follows:

$$E^i(\mathbf{r}) = E(\mathbf{r}) + k_b^2 \iint_{\Omega} G(\mathbf{r}, \mathbf{r}') \chi(\mathbf{r}') E(\mathbf{r}') d\mathbf{r}' \quad (3)$$

where vectors \mathbf{r} and \mathbf{r}' point to position inside domain X , $\mathbf{r} \in X$, and $\mathbf{r}' \in X$.

Data equation (1) and domain equation (3) express a MWT problem. The problem can be stated as a forward and an inverse problem. A forward problem of MWT defines the scattered fields, $E^s(\mathbf{r})$, $\mathbf{r} \in Y$, form introduction of incident fields and given unknown dielectric contrast at domain X , and an inverse problem determines the unknown $\chi(\mathbf{r})$, $\mathbf{r} \in X$ from electric scattered measurements $\mathbf{y}(\mathbf{r})$, $\mathbf{r} \in Y$. The accuracy and the speed of the MWT solution depend on the accuracy of both forward and inverse MWT problems. Alternatively, the MWT problem is stated in a multivariable system with two unknown variables, which are $\chi(\mathbf{r})$, $\mathbf{r} \in X$ and $E(\mathbf{r})$, $\mathbf{r} \in X$. Both variable are updated simultaneously, thus MWT forward problem is avoided.

The MWT inverse problem can be stated in abstract system. For the purpose of Newton iterative solver, the problem is presented in objective function as

$$F(\mathbf{x}) = \mathbf{y} \quad (4)$$

The nonlinear operator $F(\mathbf{x})$ is a multivariable system, which is defined as

$$F(\mathbf{x}) = \begin{bmatrix} -k_b^2 \iint_{\Omega} G(\mathbf{r}, \mathbf{r}') \chi(\mathbf{r}') E(\mathbf{r}') d\mathbf{r}' \\ E(\mathbf{r}) + k_b^2 \iint_{\Omega} G(\mathbf{r}, \mathbf{r}') \chi(\mathbf{r}') E(\mathbf{r}') d\mathbf{r}' \end{bmatrix} \quad (5)$$

and the right hand known variables are

$$\mathbf{y} = \begin{bmatrix} E^s(\mathbf{r}) \\ E^i(\mathbf{r}) \end{bmatrix} \quad (6)$$

For multiple projections $t = 1, 2, \dots, M$, where M is the number of signal sources, the nonlinear operator and the known variables are define as

$$F(\mathbf{x}) = \begin{bmatrix} F_1(\mathbf{x}) \\ F_2(\mathbf{x}) \\ \vdots \\ F_M(\mathbf{x}) \end{bmatrix}; \mathbf{y} = \begin{bmatrix} \mathbf{y}_1 \\ \mathbf{y}_2 \\ \vdots \\ \mathbf{y}_M \end{bmatrix} \quad (7)$$

The goal of the inverse problem finds the unknown \mathbf{x} in term of $\chi(\mathbf{r})$ and $E(\mathbf{r})$, $\mathbf{r} \in X$ for a set of measured scattered fields data $E^s(\mathbf{r})$, $\mathbf{r} \in Y$ and known incident fields $E^i(\mathbf{r})$, $\mathbf{r} \in X$. The solutions of the problem are gained by solving MWT objective function. For multiple projections the MWT objective function is stated as

$$F(\chi(\mathbf{r}), E_1(\mathbf{r}), E_2(\mathbf{r}), \dots, E_M(\mathbf{r})) = \mathbf{y} \quad (8)$$

Newton method is an attractive method to solve the objective function (8) which is well known as a nonlinear and ill posed problem, because it converges rapidly. However it is sensitive to a prior information and ill-posedness of the system as described in [7: 8]. The NI, therefore, is exploited with an implicit method to produce stable solution of MWT-inverse problem

III. NEWTON ITERATION OF MICROWAVE IMAGING

Assuming that the objective function (8) has an exact solution at \mathbf{x}^1 and the exact but indefinite measured data is defined as $\mathbf{y} = F(\mathbf{x}^1)$ then MWT inverse problem can be stated as minimization of MWT objective function norm

$$[\mathbf{x}] = \min_{\mathbf{x}} \|\mathbf{y} - F([\mathbf{x}])\|_{\mathcal{D}}^2 \quad (9)$$

The iterative solver proposed is a Newton type algorithm. The iterative solution is updated in the current actual solution ($[\mathbf{x}]_k$) by correction step which is also known as the direction of Newton step (\mathbf{s}_k).

$$[\mathbf{x}]_{k+1} = [\mathbf{x}]_k + \mathbf{s}_k \quad (10)$$

The iterative steps of NI are computed via linear Newton equations. The linear system of Newton equations are constructed using linearization by means of Fréchet derivative. For multiple illuminations of MWT system, the Newton equation of MWT inverse problem is stated as

$$[\mathbf{D}]_k \mathbf{s}_k = [\mathbf{y} - F([\mathbf{x}]_k)] \quad (11)$$

Where Fréchet derivative of MWT inverse problem which is denoted by $\mathbf{D} = F'$ is defined as

$$\mathbf{D} = \begin{pmatrix} \left(\frac{\partial F_1(\mathbf{x})}{\partial \chi}\right) & \left(\frac{\partial F_1(\mathbf{x})}{\partial E_1}\right) & \left(\frac{\partial F_1(\mathbf{x})}{\partial E_2}\right) & \dots & \left(\frac{\partial F_1(\mathbf{x})}{\partial E_M}\right) \\ \left(\frac{\partial F_2(\mathbf{x})}{\partial \chi}\right) & \left(\frac{\partial F_2(\mathbf{x})}{\partial E_1}\right) & \left(\frac{\partial F_2(\mathbf{x})}{\partial E_2}\right) & \dots & \left(\frac{\partial F_2(\mathbf{x})}{\partial E_M}\right) \\ \vdots & \vdots & \vdots & \ddots & \vdots \\ \left(\frac{\partial F_M(\mathbf{x})}{\partial \chi}\right) & \left(\frac{\partial F_M(\mathbf{x})}{\partial E_1}\right) & \left(\frac{\partial F_M(\mathbf{x})}{\partial E_2}\right) & \dots & \left(\frac{\partial F_M(\mathbf{x})}{\partial E_M}\right) \end{pmatrix} \quad (12)$$

Where $\left(\frac{\partial F_i(\mathbf{x})}{\partial \chi}\right)$ and $\left(\frac{\partial F_i(\mathbf{x})}{\partial E_j}\right)$ are linear operators such that

$$\left(\frac{\partial F_i(\mathbf{x})}{\partial \chi}\right) h(\mathbf{r}) = \begin{bmatrix} -k_b^2 \iint_{\Omega} G(\mathbf{r}, \mathbf{r}') h(\mathbf{r}') E(\mathbf{r}') d\mathbf{r}'; \mathbf{r} \in Y \\ k_b^2 \iint_{\Omega} G(\mathbf{r}, \mathbf{r}') h(\mathbf{r}') E(\mathbf{r}') d\mathbf{r}'; \mathbf{r} \in X \end{bmatrix} \quad (13)$$

for $i = j = 1, 2, \dots, M$

$$\left(\frac{\partial F_i(\mathbf{x})}{\partial E_j}\right) h(\mathbf{r}) = \begin{bmatrix} -k_b^2 \iint_{\Omega} G(\mathbf{r}, \mathbf{r}') \chi(\mathbf{r}') h(\mathbf{r}') d\mathbf{r}'; \mathbf{r} \in Y \\ j + k_b^2 \iint_{\Omega} G(\mathbf{r}, \mathbf{r}') \chi(\mathbf{r}') h(\mathbf{r}') d\mathbf{r}'; \mathbf{r} \in X \end{bmatrix} \quad (14)$$

for $i = 1, 2, \dots, M; j = 1, 2, \dots, M$ and $i \neq j$

$$\left(\frac{\partial F_i(\mathbf{x})}{\partial E_j}\right) h(\mathbf{r}) = \begin{bmatrix} 0 \\ 0 \end{bmatrix} \quad (15)$$

Newton equations (11) are linear. However they are still nonlinear with respect to the correction step \mathbf{s}_k and ill posed. Therefore regularization is essential to solve the equations. The solution of (11) is stated in regularized linear filter form

$$\mathbf{s}_k = \psi([D^* \mathbf{D}]_k, \alpha_k) [\mathbf{D}]_k [\mathbf{y} - F([\mathbf{x}]_k)] \quad (16)$$

where ψ is a regularized linear filter and α_k is regulator parameter.

The iterative sequence of NI algorithm to solve MWT inverse problem is summarized as follows:

1. Define initial guess $[\mathbf{x}]_0 = \chi_0, E_{1,0}, E_{2,0}, \dots, E_{M,0}$
2. Compose objective function at point $[\mathbf{x}]_k$. The function is formulated as $F([\mathbf{x}]_k) = \mathbf{y}$.
3. Construct Newton equation, which is $[\mathbf{D}]_k \mathbf{s}_k = [\mathbf{y} - F([\mathbf{x}]_k)]$, by linearizing the objective function.
4. Find a regularized solution of Newton equation. $\mathbf{s}_k = \psi([D^* \mathbf{D}]_k, \alpha_k) [\mathbf{D}]_k [\mathbf{y} - F([\mathbf{x}]_k)]$
5. Update the solution $[\mathbf{x}]_{k+1} = [\mathbf{x}]_k + \mathbf{s}_k$

IV. IMPLICIT CALCULATION OF NEWTON SOLUTIONS

Finding a regularized solution of Newton equations is a key stage to solve MWT inverse problem. Direct regularization techniques have been developed [6, 9]. The sequence of regularized steps is computed via

$$\psi_k^{-1} \mathbf{s}_k = [\mathbf{D}]_k [\mathbf{y} - F([\mathbf{x}]_k)] \quad (17)$$

The drawback of regularized Newton scheme is that Newton equations have to be solved at each stage of iteration. Direct regulative solution of Newton method may not be justified if the initial value is far from exact solution, besides, it can be expensive for handling large system like MWT inverse problem. Therefore, an alternative iterative method in which the solutions of Newton equations are defined approximately and in unspecific manner is proposed.

To provide a stable solution of MWT-inverse problem, we develops implicit solution of Newton equations by exploiting the class of inexact Newton method which is initially introduced by Dembo [10]. A residual is added to (17) so that the solutions of Newton equations are implicitly determined using

$$\psi_k^{-1} \mathbf{s}_k = [\mathbf{D}]_k [\mathbf{y} - F([\mathbf{x}]_k)] + \mathbf{r}_k \quad (18)$$

The residual (\mathbf{r}_k) is given

$$\mathbf{r}_k = \psi_k^{-1} \mathbf{s}_k - [\mathbf{D}]_k [\mathbf{y} - F([\mathbf{x}]_k)] \quad (19)$$

The method offers an adjustment of the accuracy of the results. A nonnegative forcing term (η_k) can be introduced to control the accuracy. The approximation of the solution of Newton equations are determined so that the relative value of the residual satisfy

$$\frac{\|\mathbf{r}_k\|^2}{\|[\mathbf{D}]_k [\mathbf{y} - F([\mathbf{x}]_k)]\|^2} \leq \eta_k \quad (20)$$

The addition of residual to the Newton equations presents an intermediate solution of the equations. As consequences, the amount of work for solving MWT inverse problem can be decreased as the computation linear filter ψ may not need to be done at each sequence of the inexact Newton scheme and low cost method like CGNE can be applied.

Suppose the exact solution \mathbf{s}_k^\dagger satisfies (17).

$$\psi_k^{-1} \mathbf{s}_k^\dagger = [\mathbf{D}]_k [\mathbf{y} - F([\mathbf{x}]_k)] \quad (21)$$

and current iterative solution is defined as $\bar{\mathbf{s}}_k$, where the initially estimate is $\bar{\mathbf{s}}_0$. A residual of the Newton equations in a normal equation is defined as

$$\mathbf{r}_k = \psi_k^{-1} \bar{\mathbf{s}}_k - [\mathbf{D}]_k [\mathbf{y} - F([\mathbf{x}]_k)] \quad (22)$$

Assuming that the exact and current solutions are defined, and then an error of the current solution can be stated as

$$\mathbf{e}_k = \mathbf{s}_k^\dagger - \bar{\mathbf{s}}_k \quad (23)$$

Multiplying (26) with ψ_k^{-1} results in iterative linear algorithm

$$\psi_k^{-1} \mathbf{e}_k = \psi_k^{-1} \mathbf{s}_k^\dagger - \psi_k^{-1} \bar{\mathbf{s}}_k \quad (24)$$

$$-\mathbf{r}_k = [\mathbf{D}]_k^* [\mathbf{y} - F([\mathbf{x}]_k)] - \psi_k^{-1} \bar{\mathbf{s}}_k \quad (25)$$

$$\psi_k^{-1} (\mathbf{s}_k^\dagger - \mathbf{e}_k) = [\mathbf{D}]_k^* [\mathbf{y} - F([\mathbf{x}]_k)] + \mathbf{r}_k \quad (26)$$

$$\mathbf{e}_k = -\psi_k \mathbf{r}_k \quad (27)$$

Then the solutions of Newton equations are possibly updated iteratively in the inner loop of NI which is summarized as follows

1. Give an initial guess $\mathbf{s}_{k,0}$; determine forcing term η_k ; and compute linear regulator filter ψ_k
2. Find a regularized solution $\mathbf{e}_{k,l} = -\psi_k \mathbf{r}_{k,l}$
3. Update the solution $\mathbf{s}_{k,l+1} = \mathbf{s}_{k,l} + \mathbf{e}_{k,l}$ and residual $\mathbf{r}_{k,l+1} = \psi_k^{-1} \mathbf{s}_{k,l+1} - [\mathbf{D}]_k^* [\mathbf{y} - F([\mathbf{x}]_k)]$
4. Check stopping criterion (20); if it is satisfied, terminate the inner loop and return $\mathbf{s}_k = \mathbf{s}_{k,l}$; elsewhere, go to 2.

Implicit solutions of Newton equations are determined iteratively in unspecific manner using a forcing term. A vector which satisfies forcing term criterion condition (20) can be assigned as the approximated solution. CGNE which is a cheap iterative method is developed to provide the implicit solutions of Newton equations.

A. Conjugate gradient on normal equation

The CGNE is known as a semi-convergent method for solving asymmetric and ill posed system. It has been described that the CGNE regularizes and solves the non-symmetric positive definite linear system with the normal equations [11]. It differs from direct regularization scheme operator (ψ) described in (17), the operator $\psi([\mathbf{D}^* \mathbf{D}]_k, \alpha_k)$ which applies regularization is defined as a normal equation. Then (27) can be stated as

$$\psi_k^{-1} \mathbf{e}_l = [\mathbf{D}^* \mathbf{D}]_k \mathbf{e}_l = [\mathbf{L}]_k \mathbf{e}_l = \mathbf{r}_{k,l} \quad (28)$$

where the Fréchet derivative \mathbf{D} is only defined in the outer loop of NI and $\mathbf{r}_{k,l}$ is determined using

$$\mathbf{r}_{k,l} = [\mathbf{L}]_k \mathbf{s}_{k,l} - [\mathbf{D}]_k^* [\mathbf{y} - F([\mathbf{x}]_k)] \quad (29)$$

CGNE starts with selection of a guess $\mathbf{s}_{k,0}$. The solution $\mathbf{s}_{k,l}$ at the l^{th} index is corrected according to

$$\mathbf{s}_{k,l+1} = \mathbf{s}_{k,l} + \gamma_l \mathbf{p}_l \quad (30)$$

where the \mathbf{p}_l is the conjugate direction of (29). It is updated based on the gradient of the problem at current solution. The conjugate direction is updated using

$$\mathbf{p}_{l+1} = \mathbf{r}_{k,l} - \beta_l \mathbf{p}_l \quad (31)$$

Coefficient (β_l) may be determined using Fletcher-Reeves formula

$$\beta_l = \begin{cases} 0, & l = 0 \\ \frac{\langle \mathbf{r}_{k,l}, \mathbf{r}_{k,l} \rangle}{\langle \mathbf{r}_{k,l-1}, \mathbf{r}_{k,l-1} \rangle}, & l \geq 1 \end{cases} \quad (32)$$

Where $\langle \mathbf{A}, \mathbf{A} \rangle = \mathbf{A}^T \mathbf{A}$ is inner product of vector \mathbf{A} .

The step of conjugate gradient (γ_l) is determined using minimization of residual norm

$$\gamma_l = \min_{\gamma} \|\mathbf{L}[\mathbf{s}_{k,l} + \gamma_l \mathbf{p}_l] - [\mathbf{D}]_k^* [\mathbf{y} - F([\mathbf{x}]_k)]\|^2 \quad (33)$$

The residual norm is convex system; thus, the minimizer is defined at $\nabla \theta = 0$, that is

$$\gamma_l = \frac{\mathbf{p}_l^T \mathbf{r}_{k,l}}{\mathbf{p}_l^T [\mathbf{L}]_k \mathbf{p}_l} \quad (34)$$

This implies that $\gamma_l = 0$ then $\mathbf{s}_{k,l}$ is the solution of the normal equation.

B. CGNE stopping rule

The solutions of (29) at first iteration sequence $l = 1, 2, \dots, l_c$, ($\mathbf{s}_{k,l}$) usually move toward solution of the residual norm, which is

$$\mathbf{s}_{k,l} \rightarrow \mathbf{s}_k^\dagger \quad (35)$$

where

$$\|\mathbf{r}_{k,l+1}\|_2^2 < \|\mathbf{r}_{k,l}\|_2^2 \quad (36)$$

The optimum solution is defined at l_c in which the error of the solution $\|\mathbf{e}_{k,l_c} = \mathbf{s}_k^\dagger - \mathbf{s}_{k,l_c}\|_2^2$ is minimal. The error increases for $l > l_c$ due to the influence of noise level. Therefore, stopping rule of the iteration needs to be designed to avoid the solution \mathbf{s}_{k,l_c+n} , where n is a real positive number. The iteration should be stopped at the correct inner iteration index as the method starts to reconstruct the noise. The decreasing of the residual norm may not be similar to the reduction the error of the solution. The iteration could exceed the optimum point of the solution [12].

In the case of the level of noise is known, then the discrepancy principle can be used to design the stopping rule.

$$\|\mathbf{r}_{k,l}\|^2 \leq \delta^2 \quad (37)$$

The CGNE is stopped at the first index where the residual of the Newton equations is less than the noise level (δ).

$$\frac{\|\mathbf{r}_k\|^2}{\delta^2} \leq C \quad (38)$$

where C is a ratio of residual and noise level, in which it is set to be bigger than 1, $C > 1$. It is used to guarantee the reconstruction of the solution above the level of the noise.

Setting the residual norm equals to some upper bound related to δ^2 , is the simplest rule to choose the stopping criteria. Even though δ is not known, the iterative solution steps for Newton equations have to be stopped before the level of noise influences the solution. It can be assumed that there is a confident area in which the level of noise is less than the norm of the residual.

$$\|r_k\|^2 > C\delta^2 \quad (39)$$

Then, the solutions of the Newton equations can be determined in the area

$$\|r_{k+1}\|^2 > \|r_{k,j}\|^2 \geq \tau_k \|r_{k,0}\|^2 \quad (40)$$

where $\tau_k < 1$.

Referring to the implicit solution criteria (20), the goal of CGNE implementation is to find, for a given $s_{k,0}$ and τ_k , a vector s_k so that

$$\tau_k \|r_{k,0}\|^2 \leq \|r_{k,j}\|^2 \leq \eta_k \|D_k^T [y - F(x_k)]\|^2 \quad (41)$$

where $0 < \tau_k \leq \eta_k < 1$

When the input is the initial iterate $s_{k,0} = 0$, which is overwritten with the solution, then the right hand side of (42) is the residual $r_{k,0}$.

V. NUMERICAL EXPERIMENT

In this section, we present the reconstruction results of free space synthetic data set and experimental data using developed algorithm. The quality of the algorithm is studied by comparing the reconstruction results of NI-CGNE to the results of Levenberg Marquardt method (LM) which is categorized as a direct regularization technique. We define two quantitative indicators, which are a MWT-objective function norm and a relative error of the dielectric contrast model, to support the comparative study of the algorithms.

MWT-objective function norm

$$f_k = \frac{\|y - F(x_k)\|_2^2}{|y|^2} \quad (42)$$

Relative error of the dielectric model

$$err[x]_k = \frac{\| |x|_k - |x|^* \|^2}{\| |x|^* \|^2} \quad (43)$$

A. Synthetic Data

On the first numerical experiment, we consider two dielectric lossy materials which can be purposed for free space nondestructive evaluations. The first object is a lossy dielectric cylinder of diameter $0.4\lambda_0$ and permittivity $\epsilon = 3 - j1$, with two $0.1\lambda_0$ in diameter holes, the centers of the holes are $(2\text{cm}, 0)$ and $(-2\text{cm}, 0)$ respectively. The second object is a dielectric tube with outer and inner radius are $0.4\lambda_0$ and $0.3\lambda_0$ respectively and a contrast function $\chi = 3 - j1$.

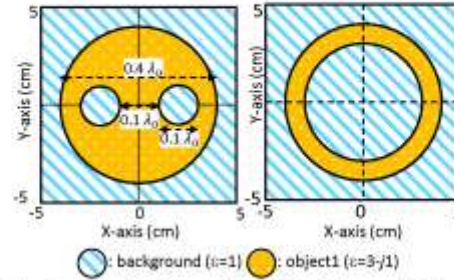


Fig. 1. : Two dimensional cross section of dielectric lossy material models. Numerical Model 1 a cylindrical dielectric object with two identical holes. Numerical Model 2 a dielectric tube. The materials are placed in free space with background permittivity $\epsilon = 1$.

The parameters of MWT system are summarized in Table 1. The object is placed in free space, in which the background permittivity is assumed to be $\epsilon = 1$. To simplify mathematical model, the imaging domain is square which is divided into 3600 equal cells. The dielectric property in each cell is assumed to be homogeneous and evenly distributed. The object is illuminated with 1.5 GHz microwave signal from a transmitter antenna then the measurement of electric fields is conducted at 16 receiver antennas around the object, including the transmitter antenna itself. On each set of measurement, 16 projection data are collected.

TABLE I. PARAMETER OF SIMULATED SYSTEM

Parameter	Value
Object Domain (X)	Square $10 \times 10 \text{ cm}^2$
Data Domain (F)	Circular $r = 13.0 \text{ cm}$
Transmitting Antenna T_x	16
Receiving Antenna R_x	16
Number of data (amplitude and phase)	256×2
SNR	40 dB
Number of cells	$60 \times 60 = 3600$
Frequency	1.5 GHz

The measured data are added with a white Gaussian noise with SNR 40 dB. The data are reconstructed using NI-CGNE and LM algorithms. The reconstructions are terminated if the discrepancy of MWT objective function norm less than 2×10^{-4} or the process exceeds 50 iterations.

The reconstructed images of the numerical model 1 and model 2 are presented in Fig 2 and Fig 3 respectively. We present images of the object in terms of real ($Re(\epsilon)$) and imaginary part ($Imag(\epsilon)$) of the object permittivity. It can be seen from the images of NI-CGNE in Fig 1 that the localization of the dielectric material and the holes are very good, although the shape and the contrast are not very sharp due to the lack of regularization for the ill conditioning of the MWT inverse problem. NI-CGNE improves the spatial resolution of the LM algorithm. The localization of $0.1\lambda_0$ diameter holes is good, although the shape and contrast of the holes are not well defined. In contrast LM fails to identify the holes.

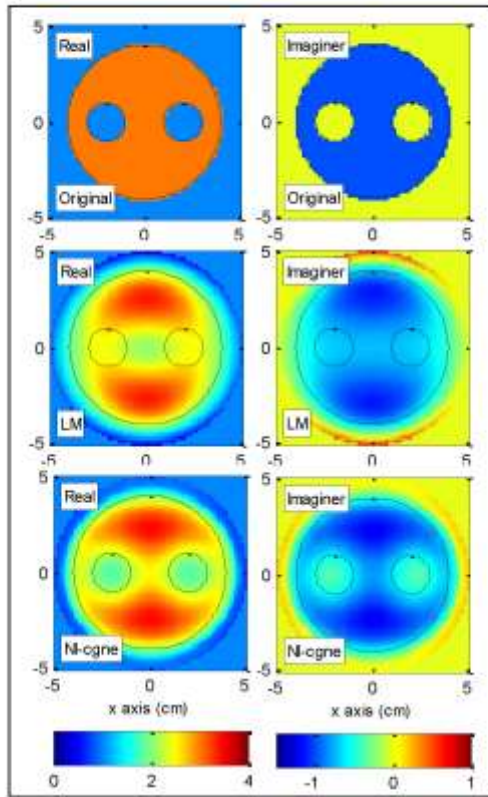


Fig. 2. Images of numerical model 1. The images are the original target and the results of NI-CGNE (NI-cgne) and Levenberg Marquardt (LM) reconstructions. We present the images in terms of $Re(z)$ and $Imag(z)$ distributions.

The dielectric tube is well reconstructed as seen in the real and imaginary part of reconstructed images. We note that the localization of material is well defined. NI-CGNE obtains good reconstructions of the shape and dielectric contrast value while the ill posedness of the system and the present of noise distort the shape and the contrast of LM results.

The NI-CGNE is faster and produces better reconstruction results than that of LM algorithm. The NI-CGNE takes 7 iterations and reduces the objective function norm to 7.6×10^{-3} which is small but produces relatively big model error up to 51%. We observe that adding a few iterations slightly decreases the objective error but does not improve the model error and enlarge the distortion to the shape of the tube. Therefore the NI-CGNE is terminated when the discrepancy of the objective function norm less than a setting tolerance which is a small positive number. In contrast, LM algorithm requires at least 29 iterations to get optimum solutions. We note that extending the iteration raises the objective function norm.

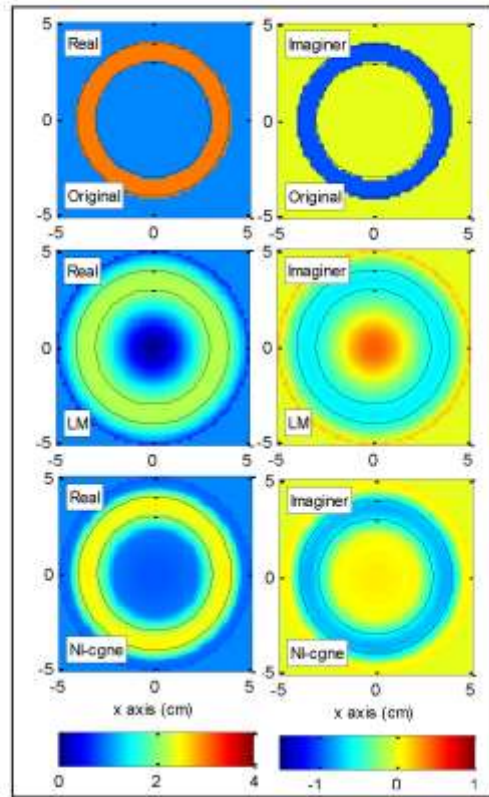


Fig. 3. Images of numerical model 2. The reconstructed images of $Re(z)$ and $Imag(z)$ distribution a dielectric tube. NI-cgne is the images resulted by NI-CGNE algorithm and LM is the results of LM algorithm. The reconstructions are initially started from 0 (background contrast).

TABLE II. RESULTS OF NUMERICAL DATA RECONSTRUCTION

Model	LM			NI-CGNE		
	k	f_k	$err[x]_k$	k	f_k	$err[x]_k$
Model 1	29	2.5×10^{-3}	43%	6	1.0×10^{-4}	36%
Model 2	37	5.0×10^{-4}	65%	7	7.6×10^{-5}	51%

VI. EXPERIMENTAL TEST

The experimental data used are measured using two dimensional microwave tomography system which is developed at the School of Electrical and Electronic Engineering, University of Manchester. The system which can be seen in Fig 4, works in free space domain.



Fig. 4. Microwave tomography system setup

TABLE III. PARAMETER OF MEASUREMENT SYSTEM

Parameter	Value
Diameter of Object Domain (X)	9.5 cm
Diameter of Data Domain (Y)	13.0 cm
Transmitting Antenna T_x	16
Receiving Antenna R_x	8
Number of data (amplitude and phase)	128×2
Number of cells	$60 \times 60 = 3600$
Object of interest	rod
Diameter of object	2 cm
Frequency	4.6 GHz

The data measurements are conducted using 16 monopoles supported by a ground plane. For each set of measurement, 16 transmitters which are positioned equidistant point on a circle with radius 6.5 cm around imaging domain, sequentially transmits 4.6GHz microwave signal. At each illumination, 8 Rx antennas are addressed to measure the total electric fields before and after the object are introduced. The transmission and measurement of electric fields are conducted by a Vector Network Analyzer (VNA).

The objects under investigation are two cylindrical Teflon rods with diameter 2 cm. The rods are placed vertically thereto the object of interest is the cross section of the rods. The rods are placed in imaging domain with distance between rods are 3 mm, 6mm, 9mm and 12 mm which are approximately between $0.05\lambda_0 - 0.18\lambda_0$. The imaging domain is divided into $60 \times 60 = 3600$ cells.

For each set of measurement we measure 16×8 undisturbed electric fields which are the field when the object is not presented, and 16×8 disturbed electric fields. The measured scattered fields are defined as the difference of disturbance and non-disturbance fields at receiving antennas. We first reconstruct the measurement data using LM algorithm. The results are presented in Fig 5 a. The plots show the real part of the relative permittivity in horizontal slices. The localization of the rods is relatively good but the shapes of two rods are hard to define for 3mm and 6 mm gaps and the dielectric contrast is far from target value 2.1.

Then we apply the developed algorithm, NI-CGNE, to reconstruct the data. The results of NI-CGNE reconstructions are presented in Fig 5 b. It can be seen that NI-CGNE improves the spatial resolution of LM algorithm. The rods are well reconstructed and the gaps are clearly seen up to 3 mm.

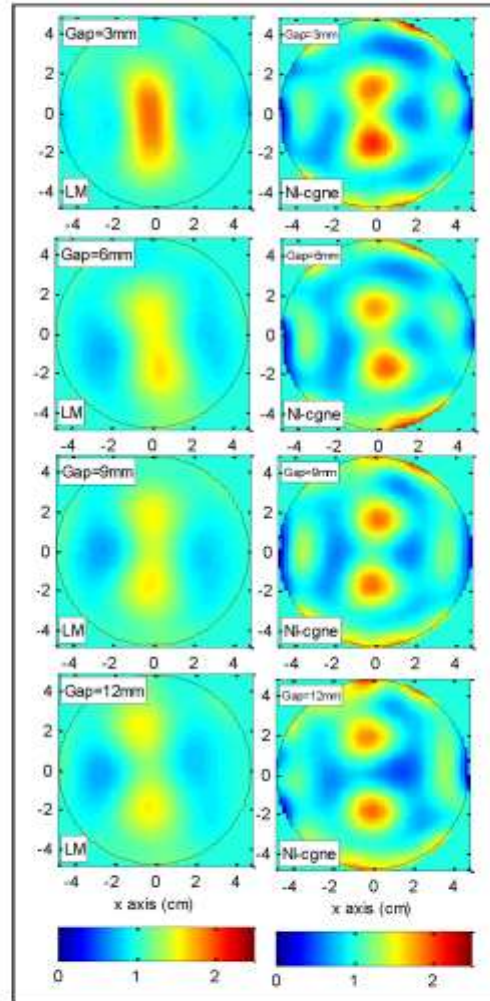


Fig. 5. Images of reconstructed experimental data resulted by INBM and LM method

TABLE IV. RESULTS OF NUMERICAL DATA RECONSTRUCTION

Gap (mm)	LM		NI-CGNE	
	k	f_R	k	$err[\mathbf{x}]_k$
3	18	28%	5	15%
6	22	25%	4	14%
9	19	24%	4	14%
12	24	22%	5	15%

We observe that the locations of both rods are well reconstructed by NI-CGNE. The shape are well defined although the cylindrical boundary are blurred since we are applying semi regularized scheme by means conjugate gradient on normal equations. We also note that positive values less than 1 appears at the background of the NI-CGNE results. These indicate that noise in the data and the ill conditioning of the system influence the results of the reconstruction. Improving the results of NI-CGNE may be done by restarting the iterations using a new initial guess. The initial value is proposed by setting zero value to the cells which have $real(\epsilon) < 1$.

The target is a purely a dielectric material and the result of NI-CGNE reconstructions indicate that the interest is a dielectric because the real part of reconstructed object is about 2 and the imaginary part is close to zero which are close to the target values.

VII. CONCLUSIONS

The Newton Iterative-conjugate gradient on normal equation has been presented for solving the free space MWT inverse problem. The main features of the proposed method include solving the MWT problem as a nonlinear problem in outer and inner iteration loops. The outer loop is the Newton iterative method which regularizes the MWT inverse problem. In this scheme a linear and ill posed Newton equations are constructed. The inner loop provides implicit solutions of the Newton equations. The accuracy of the results is determined using a forcing term which is defined by applying the class of inexact Newton.

As it can be seen in the results, the developed method produces a stable solution of free space MWT inverse problem. The experiments show that NI-CGNE improves the spatial resolution and the quality of the images of the direct regularization method by means LM algorithm. It also reduces the error of the results and iteration time. The experimental test show robustness to unknown noise and capability to reconstruct images from free space MWT data of the developed NI-CGNE method.

REFERENCES

- 1 Joachimowicz, N., Pichot, C., & Hugonin, J. P. (1991). Inverse scattering: An iterative numerical method for electromagnetic imaging. *Antennas and Propagation, IEEE Transactions on*, 39(12), 1742-1753.
- 2 Nngroho, A. T. (2009). Modified newton kantorovich methods for solving microwave inverse scattering problems. *Jurnal ILMU DASAR*, 10(2), 153-159.
- 3 Estatico, C., Pastorino, M., & Randazzo, A. (2005). An inexact-newton method for short-range microwave imaging within the second-order born approximation. *Geoscience and Remote Sensing, IEEE Transactions on*, 43(11), 2593-2605.
- 4 Franchois, A., & Tijhuis, A. G. (2003). A quasi-newton reconstruction algorithm for a complex microwave imaging scanner environment. *Radio Science*, 38(2).
- 5 Kundu, A. K., Bandyopadhyay, B., & Sanyal, S. (2008). *An iterative algorithm for microwave tomography using modified gauss-newton method*. Paper presented at the Biomed 2008.
- 6 Abubakar, A., Habashy, T. M., Guandong, P., & Mao-Kun, L. (2012). Application of the multiplicative regularized gauss-newton algorithm for three-dimensional microwave imaging. *Antennas and Propagation, IEEE Transactions on*, 60(5), 2431-2441.
- 7 Henriksson, T., Joachimowicz, N., Conessa, C., & Bolomey, J. C. (2010). Quantitative microwave imaging for breast cancer detection using a planar 2.45 ghz system. *Instrumentation and Measurement, IEEE Transactions on*, 59(10), 2691-2699.
- 8 Mojabi, P., & LoVetri, J. (2009). Overview and classification of some regularization techniques for the gauss-newton inversion method applied to inverse scattering problems. *Antennas and Propagation, IEEE Transactions on*, 57(9), 2658-2665.
- 9 Rubk, T., Mcaney, P. M., Mcinckc, P., & Paulsen, K. D. (2007). Nonlinear microwave imaging for breast-cancer screening using gauss newton's method and the cgl's inversion algorithm. *Antennas and Propagation, IEEE Transactions on*, 55(8), 2320-2331.
- 10 Dembo, R. S., Eisenstat, S. C., & Steihaug, T. (1982). Inexact newton methods. *SIAM Journal on Numerical Analysis*, 19(2), 400-408.
- 11 Kelley, C. T. (1995). *Iterative methods for linear and nonlinear equations*. Philadelphia: Society for Industrial and Applied Mathematics (SIAM).
- 12 Hanke, M. (1995). The minimal error conjugate gradient method is a regularized method. *Proceedings of the American mathematical Society*, 123(11), 3487-3497.

Microwave Tomography Image Reconstruction Using Inexact Newton Backtracking Method

Agung Tjahjo Nugroho
School of Electrical and Electronic Engineering
The University of Manchester
United Kingdom

Zhipeng Wu
School of Electrical and Electronic Engineering
The University of Manchester
United Kingdom

Abstract—This paper presents an approach to reconstruct an image of Microwave Tomography (MWT). The proposed Inexact Newton Backtracking method (INBM) which is an inexact Newton class algorithm is applied to solve nonlinear and ill posed MWT inverse problems. The method is based on Newton method where the step of the solution is determined by solving a Newton equation which is the linearization of MWT inverse problem. Instead of updating the solution using direct regularized solution of the Newton equation, implicit solution of the Newton equation where a forcing term is used to control the accuracy is applied in each iteration step of the method. The forcing term is determined by considering the agreement between the solution of the Newton equation and its corresponding current nonlinear solution. Numerical examples and experimental results are presented to support the effectiveness of the developed method.

Keywords—*Microwave tomography; inverse problem; Inexact Newton backtracking method; Newton iterative method*

I. INTRODUCTION

The image of Microwave Tomography (MWT) can be produced by illuminating a dielectric object with microwave fields in different directions, and measuring the scattered field around the object at each illumination. The data of the measured scattered fields are processed using image reconstruction algorithms to produce dielectric property distribution. The reconstruction is completed in two steps, by solving forward and inverse problems.

The numerical tool to solve the forward problem is the Moment of Method (MM). Since the MM is a technique used to solve electromagnetic boundary or volume integral equations in the frequency domain and the electromagnetic sources are the MWT quantities of interest, the technique is very useful in solving the forward problem of the MWT. It has been shown numerically that the forward problem which is also known as a direct scattering problem can be solved directly and accurately using the moment of method [1]. On the other hand, the MWT-inverse problem is a nonlinear and ill posed problem. The nonlinearity of the problem is solved by applying different optimising methods to minimize an objective function which can be the difference between measured scattered fields and calculated scattered fields from a forward problem solution. Generally, the methods are iterative where these techniques are computationally complex and expensive because the objective function has to be updated at each

iteration. Various nonlinear algorithms have been developed to solve MWT problems. These include Modified Gradient method [2; 3], Newton-Kantorovich [4], Gauss Newton inversion[5], Quasi Newton method [6], Contrast source inversion [7; 8] and Inexact Newton method [9]. The ill posedness of the problem is handled by employing different regularization techniques which set an appropriate constrain to the solution. Tikhonov regulator for example, which facilitates the inversion of ill conditioning matrix, limits the value of the update solution. However, the weight of the regularization is generally determined by one or more regulator parameters so that the techniques can be application dependent.

In this article, Newton iterative class by means inexact Newton Backtracking method (INBM) in [10] to solve MWT inverse problems via implicit solution is developed in which the algorithm presents an intermediate solution of the problem. Consequently the method offers a tradeoff between the accuracy with which the regularized solution is computed. The algorithm handles the ill posedness of the problem by utilizing a semi regularized method in which any regularization techniques can be applied and controlled with an appropriate criterion. The amount of work for solving MWT inverse problem can be decreased as the computation and regularization do not need to be done at each sequence of the iteration. The stability and robustness of the algorithm is studied under noisy numerical data and experimental data. To determine the flexibility of the INBM, the results of reconstruction are compared with the result of LM.

II. MICROWAVE TOMOGRAPHY PROBLEM

The multiple illumination of MWT is described as a pair of integral equations:

$$E^1(\mathbf{r}) = E(\mathbf{r}) - k_0^2 \iint_{\mathcal{X}} \chi(\mathbf{r}') E(\mathbf{r}') H_0^{(2)}(k_0 \rho) d\mathbf{r}' \quad (1)$$

$$E^s(\mathbf{r}) = k_0^2 \iint_{\mathcal{X}} \chi(\mathbf{r}') E(\mathbf{r}') H_0^{(2)}(k_0 \rho) d\mathbf{r}' \quad (2)$$

where $\chi = (\epsilon_r - 1)$ is the dielectric contrast, and both coefficients r and r' are position vectors, and $\rho = |r - r'|$. Equation (1) represents the domain equation. The position vector addresses a point at object domain $(\mathcal{X}), (r, r') \in \mathcal{X}$, while (2) expresses data equation. Vector r in (2) defines data

position at data domain (\mathbb{Y}), $r \in \mathbb{Y}$ and r' point to a cell at domain \mathbb{X} , $r' \in \mathbb{X}$.

The equations are solved using the Method of Moments (MM). The cross-section of the object of interest is divided into N number of cells with equal size, then $E(r)$ can be approximated by superposition of pulse basis function. The integrals in (1), (2) are evaluated analytically with the assumption that all cells are circles [11].

$$\int_{\vartheta'=0}^{2\pi} \int_{r'=0}^a H_0^2(k_0\rho)r'dr'd\vartheta' = \begin{cases} \frac{2\pi a}{k_0} H_1^2(k_0 a) - \frac{j^4}{k^2} & (\rho < a) \\ \frac{2\pi a}{k} J_1(k_0 a) H_0^2(k_0 \rho) & (\rho > a) \end{cases} \quad (3)$$

where a is radius of the cell. Applying MM and considering (3) to (1) and (2) results

$$E^i(r) = E(r) + Z(\rho)(\chi(r')E(r')) \quad (3)$$

$$E^s(r) = -Z(\rho)(\chi(r')E(r')) \quad (4)$$

where Z is integral operator whose entries are given by

$$Z(\rho) = \frac{j k_0 \pi a_n}{2} J_1(k_0 a) H_0^2(k_0 \rho); \rho > a \quad (5)$$

$$Z(\rho) = \frac{j k_0 \pi a}{2} H_1^2(k_0 a) + 1; \rho < a \quad (6)$$

Defining that n is index of object cell which is $n=1,2,\dots,N$ and m is index of antenna that is $m=1,2,\dots,M$, then with all illumination $t = 1..T$, (3) and (4) can be stated as matrix equation

$$E_t^i = E_t + [Z_{mn}](\chi E_t) \quad (7)$$

$$E_t^s = -[Z_{mn}](\chi E_t) \quad (8)$$

where E_t^i, E_t , and χ are an $1 \times N$ column vector, E_t^s is an $1 \times M$ column vector, $[Z_{mn}]$ is $N \times N$ matrix and $[Z_{mn}]$ is an $M \times N$ matrix. The vector product of (χE_t) is related to the product inside the integral equations. It can be computed using $[diag(\chi)]E_t$ which is equal to

$$(\chi E_t) = \begin{bmatrix} \chi_1 & 0 & 0 & 0 \\ 0 & \chi_2 & 0 & 0 \\ 0 & 0 & \ddots & \vdots \\ 0 & 0 & \dots & \chi_N \end{bmatrix} \begin{bmatrix} E_{t,1} \\ E_{t,2} \\ \vdots \\ E_{t,N} \end{bmatrix} \quad (9)$$

In MWT application scattered field is not measured at transmitter, at $t = 1$ index m which is assigned as observation points or receiver is $m = 2, 3 \dots M$. Let's define the number of antenna is 16. The size $[Z_{mn}]$ in (8) at each illumination is 15×16 where m for all projection follows Table I.

TABLE I. OBSERVATION POINTS OF SCATTERED FIELD

t (Transmitter)	m (Receiver)
$t = 1$	2, 3 ... 16
$t = 2$	1, 3, 4 ... 16
\vdots	\vdots
$t = 16$	1, 2, ... 15

Computing E_t^s at observation points m for given E_t^i and defined χ is called *solving forward problem*. It can be done by substituting (7) into (8).

$$E_t^s = -[Z_{m,n}][diag(\chi)][I + [Z_{n,n}][diag(\chi)]]^{-1}E_t^i \quad (10)$$

On the other hand, determining $\chi \in \mathbb{X}$ from measured $E_t^s \in \mathbb{Y}$ and for given $E_t^i \in \mathbb{X}$ is called *MWT inverse problem*. However the problem is nonlinear and ill posed. It needs image reconstruction methods to solve MWT inverse problem.

III. IMAGE RECONSTRUCTION METHOD

The integral equations of MWT inverse problem can be stated in abstract as a non-linear ill-posed problem. For the purpose of Newton iterative solver, the problem is written as

$$\mathcal{F}(x) = y \quad (11)$$

where

$$x = \begin{bmatrix} \chi_1 \\ \chi_2 \\ \vdots \\ \chi_N \end{bmatrix}; y = \begin{bmatrix} \mathcal{E}_{t=1}^s \\ \mathcal{E}_{t=2}^s \\ \vdots \\ \mathcal{E}_{t=T}^s \end{bmatrix}; \mathcal{F}(x) = \begin{bmatrix} \mathcal{F}_{t=1}(x) \\ \mathcal{F}_{t=2}(x) \\ \vdots \\ \mathcal{F}_{t=T}(x) \end{bmatrix}$$

$\mathcal{E}_{t=1}^s$ is measured field at 1st projection which is an $1 \times M$ column vector and $\mathcal{F}_{t=1}(x)$ is estimated field $E_{t=1}^s$ which is calculated using (10) when a microwave signal is transmitted from $t = 1$.

The goal of the inverse problem finds the unknown x in term of dielectric contrast χ for measured scattered field data. Assuming that (11) has an exact solution at x^\dagger and the exact but indefinite measured data is defined as $y = \mathcal{F}(x^\dagger)$.

The functional $\mathcal{F}: \mathbb{R}^n \rightarrow \mathbb{R}^m$ with $n > m \gg 1$ operates between data domain (\mathbb{Y}) and object domain (\mathbb{X}). The nonlinear system of MWT is defined with more unknowns than equations, regardless of uniqueness or existence of its solution. The goal of the iterative method for solving the microwave inverse problem is to find stable approximate solution of (11). The iterative solver proposed is a Newton type algorithm. The iterative solution is updated the current actual solution (x_k) by correction step which is also known as the correction (s_k).

$$x_{k+1} = x_k + s_k \quad (12)$$

Assuming \mathcal{F} is Fréchet differentiable with derivative \mathcal{F}' , and the direction of Newton step satisfies the first order Taylor series, the linear system of the Newton algorithm is written as

$$\mathcal{F}'(x_k)s_k = (y - \mathcal{F}(x_k)) - Err(x^\dagger, x_k) = b_k \quad (13)$$

Error *Err* arises due to the truncation of the power series at first order term which outlines the linear system of Newton scheme. The error of linear function is the residual of the series which can be stated as

$$Err(u, v) := (\mathcal{F}(u) - \mathcal{F}(v)) - \mathcal{F}'(v)(u - v) \quad (14)$$

In the real world, the measured data could not be separated from noise, thus b_k is undefined due to the unknown exact data and residual error. The measured data E^s is assigned as y^δ . It is the scattered field at data domain with noise, $y^\delta = E^s + h(\delta)$, as the exact scattered field ($y = E^s$) cannot be determined. Assuming that the noise level δ is known, the noisy data y^δ satisfies

$$\|y - y^\delta\|^2 \leq \delta \quad (15)$$

Immersing the noise and residual error to b_k , the perturbed b_k^c is defined using the difference of measured data and estimated data which is assigned as the objective functional:

$$b_k^c = y^\delta - \mathcal{F}(x_k) \quad (16)$$

where $\|b_k - b_k^c\| \leq \delta + \|E(x^t, x_k)\|$. The iterative step of (11) is computed via linear Newton equation

$$\mathcal{F}'(x_k) s_k = b_k^c \quad (17)$$

The basic principle in solving the nonlinear MWT inverse problem using Newton iterative method is that the correction step of the solution is determined by solving linear system. The linearization by means Fréchet derivative is applied to construct the linear system.

The multiple illuminations of MWT system provide $T \cdot m$ number of data functions with n unknown dielectric contrast. The Fréchet derivative of (11) is denoted by D which is a $T \cdot m \times n$ matrix:

$$D = \begin{bmatrix} \mathcal{F}'_{t=1}(x) \\ \mathcal{F}'_{t=2}(x) \\ \vdots \\ \mathcal{F}'_{t=T}(x) \end{bmatrix} \quad (18)$$

where

$$\mathcal{F}'_t(x) \approx -[Z_{m \times n}] [I + \text{diag}(\mathcal{Z}) [Z_{m \times n}]]^{-1} E_t^s$$

The linear system of Newton iterative algorithm is therefore stated as

$$[D_k] s_k = b_k^c \quad (19)$$

The stationary point of $\|\mathcal{F}\|^2$ which is the optimum solution of (1) is a point $x_k \in \mathbb{R}^n$ where there does not exist s_k such that

$$\|(y^\delta - \mathcal{F}(x_k)) + [D_k] s_k\|^2 < \|y^\delta - \mathcal{F}(x_k)\|^2 \quad (20)$$

This includes local minimizer of $\|y^\delta - \mathcal{F}(x_k)\|^2$

However ill posedness and asymmetrical of MWT inverse problem (11) due to outnumber of data to reconstructed cell number are immersed to the linear system of MWT inverse problem. Hence, a regularized linear parameter is presented in the form of least squared minimization problem $\min_{s_k} \|b_k^c -$

$[D_k] s_k\|^2$ and the regularized solution of (19) is stated in regularized linear filter form

$$s_k = [\psi([L_k], \alpha_k)] [D_k^*] b_k^c \quad (21)$$

where $[\psi]$ is regularized linear filter and $[L_k] = [D_k^* D_k]$

A. Levenberg Marquardt method

Several techniques have been developed to provide regularized s_k with regularization parameter α . Tikhonov regularization is probably the most attractive technique. The regularization is defined as

$$\psi(D, \alpha) = \frac{1}{\alpha + D} \quad (22)$$

This leads to variation of LM, that is $\psi([L_k], \alpha_k) = [[L_k] + \alpha_k \cdot I]^{-1}$. Then direct Tikhonov regulated solution of (15) can be computed using

$$s_k = \left[\sum_{i=1}^n \frac{\sigma_i}{\sigma_i^2 + \alpha} u_i^T v_i \right] ([D_k^*] b_k^c) \quad (23)$$

where (u, σ, v^T) is the decomposition of $[L_k]$ and σ is a diagonal matrix of the singular values of $[L_k]$.

The LM is categorized as a classical algorithm for solving MWT inverse problem. Given an initial guess x_0 the LM computes a sequence of regularized steps s_k and iterates x_k according LM algorithm as follows

Function LM(x_0)

Repeat

$$s_k = -\psi([L]_{k+1}, \alpha_k) ([D_k^*] b_k^c)$$

$$x_{k+1} = x_k + s_k$$

$$k = k + 1$$

Until Convergence

Return (x_k)

The method solves and regulates a system of linear equations (the Newton equations of MWT inverse problem) at each stage which is expensive as the number of unknowns is large and may not be justified when x_k is far from a solution. Therefore, implicit solution using the class of inexact Newton methods is considered.

B. Inexact Newton Backtracking method

Equation (23) is categorized a direct solution. It is predictable in number of steps, but it does not support intermediate solution. Iterative method is an alternative to improve the accuracy and speed. It starts with an approximate answer, and then the accuracy is improved iteratively. It stops once the estimated error is below the tolerance.

Defining a linear ill-posed problem of MWT in normal equation as

$$[\psi_k]^{-1} s_k = [D_k^*] b_k^c \quad (24)$$

Suppose the exact solution \mathbf{s}_k^\dagger satisfies (24), and current iterative solution is defined as $\bar{\mathbf{s}}_{k,l}$, where initially estimate is $\bar{\mathbf{s}}_{k,0}$. A residual of the linear problem in normal equation is defined as

$$\mathbf{r}_l = [\mathbf{D}_k^*] \mathbf{b}_k^e - [\boldsymbol{\psi}_k]^{-1} \bar{\mathbf{s}}_{k,l} \quad (25)$$

The error in current solution is defined as

$$\mathbf{e}_l = \mathbf{s}_k^\dagger - \bar{\mathbf{s}}_{k,l} \quad (26)$$

Multiplying (26) with $[\boldsymbol{\psi}_k]^{-1}$, results iterative linear algorithm

$$\mathbf{e}_l = [\boldsymbol{\psi}_k] \mathbf{r}_l \quad (27)$$

Iterative approximation of Newton direction is updated via

$$\bar{\mathbf{s}}_{k,l+1} = \bar{\mathbf{s}}_{k,l} + d \mathbf{e}_l \quad (28)$$

where \mathbf{e}_l is direction of iterative linear solution which is gained by solving (27) and d is the step size which is minimizer the residual

$$\min_d \left\| [\mathbf{D}_k^*] \left(\mathbf{b}_k^e - [\mathbf{D}_k] (\bar{\mathbf{s}}_{k,l} + d \mathbf{e}_l) \right) \right\|^2 \quad (29)$$

The proposed Newton iterative solution by means INBM replaces the direct solution in the form of the direction \mathbf{s}_k with its iterative approximation ($\bar{\mathbf{s}}_k = \bar{\mathbf{s}}_{k,l}$). In this type of method the direction of Newton step is approximated to following

$$\| \mathbf{b}_k^e - [\mathbf{D}_k] \bar{\mathbf{s}}_k \|^2 \leq \eta_k \| \mathbf{b}_k^e \|^2 \quad (30)$$

where the nonnegative forcing term η_k is used to control the level of accuracy. The term η_k is determined at $\eta_k \in [0, 1]$ so that the vector \mathbf{s} that satisfies (30) where $\eta_k < 1$ is assigned as the approximate solution of the inexact Newton.

To improve the global converge, the values of \mathbf{s}_k and η_k are guarded to force the reduction of functional. The global criterion of the INBM is used to ensure the direction of objective functional. The inexact Newton method globalizes by

$$\left\| \left(\mathbf{y}^\delta - \mathcal{F}(\mathbf{x}_k + \mathbf{s}_k) \right) \right\|^2 \leq [1 - t(1 - \eta_k)] \left\| \mathbf{y}^\delta - \mathcal{F}(\mathbf{x}_k) \right\|^2 \quad (31)$$

Equation (31) guarantees the reduction of the functional with the direction defined. By giving the \mathbf{s}_k and η_k , there at least a fraction of reduction of functional which is guaranteed by finding the term $t \in [0, 1]$.

Backtracking method can be applied to accommodate the selection of \mathbf{s}_k and η_k which are suitable for both (30) and (31) criteria. The backtracking will guard the step of the solution for not too long. If \mathbf{s}_k is not acceptable by the criteria, then it is shortened until it is under the criteria. The correction of parameter follows

$$\mathbf{s}_k = r \cdot \mathbf{s}_k; \quad (32)$$

$$\eta_k = 1 - r \cdot (1 - \eta_k) \quad (33)$$

with $r \in (r_{min}, r_{max})$. The fraction of reduction should be selected in the range of $r \in [0, 1]$. Backtracking is type of inexact line search. It keeps the step not too long but does not guard the steps for not too short.

Algorithm of INBM is presented as follows:

Function INBM(\mathbf{x}_0)

Repeat

$$\mathbf{r}_0 = [\mathbf{D}_k^*] \mathbf{b}_k^e; \bar{\mathbf{s}}_{k,l} = 0$$

$$[\boldsymbol{\psi}] = \psi([\mathbf{L}]_k, \alpha_k)$$

Repeat

$$\mathbf{e}_l = [\boldsymbol{\psi}] \mathbf{r}_l$$

$$\bar{\mathbf{s}}_{k,l+1} = \bar{\mathbf{s}}_{k,l} + d \mathbf{e}_l$$

$$\mathbf{r}_l = [\mathbf{D}_k^*] \mathbf{b}_k^e - [\boldsymbol{\psi}_k]^{-1} \bar{\mathbf{s}}_{k,l}$$

$$l = l + 1$$

Until $\| \mathbf{b}_k^e - [\mathbf{D}_k] \bar{\mathbf{s}}_k \|^2 \leq \eta_k \| \mathbf{b}_k^e \|^2$

Do While

$$\left\| \left(\mathbf{y}^\delta - \mathcal{F}(\mathbf{x}_k + \mathbf{s}_k) \right) \right\|^2 > [1 - t(1 - \eta_k)] \left\| \mathbf{y}^\delta - \mathcal{F}(\mathbf{x}_k) \right\|^2$$

$$\mathbf{s}_k = r \cdot \mathbf{s}_k;$$

$$\eta_k = 1 - r \cdot (1 - \eta_k)$$

End of Do While

$$\mathbf{x}_{k+1} = \mathbf{x}_k + \mathbf{s}_k$$

$$k = k + 1$$

Until Convergence

Return (\mathbf{x}_k)

The INBM is locally convergent, if forcing term η_k is uniformly less than 1. Under the present assumptions, if \mathbf{x}_0 is sufficiently close to \mathbf{x}^\dagger , and $0 \leq \eta_k \leq \eta_{max} < 1$ for each k , then \mathbf{x}_0 converges to \mathbf{x}^\dagger [7]. If $\eta_k = 1$ for all iterations then it is similar to the Gauss Newton method. The forcing term is independent to the iteration index k . The forcing term is applied to guarantee the decrease of the error of linear model of the MWT inverse problem.

The convergence rate of the method is determined by an appropriate choice of η_k . The term may be determined using the agreement of the functional and the linear model of the corresponding problem. The forcing term is adjusted depending on the ratio of actual reduction and predicted reduction. The ratio is defined as

$$r_k = \frac{\| \mathbf{y}^\delta - \mathcal{F}(\mathbf{x}_k) \|^2 - \left\| \left(\mathbf{y}^\delta - \mathcal{F}(\mathbf{x}_k + \bar{\mathbf{s}}_k) \right) \right\|^2}{\| \mathbf{y}^\delta - \mathcal{F}(\mathbf{x}_k) \|^2 - \| \mathbf{y}^\delta - \mathcal{F}(\mathbf{x}_k) - [\mathbf{D}_k] \bar{\mathbf{s}}_k \|^2} \quad (34)$$

The forcing term is determined according to the ratio r_k

$$\eta_k = \begin{cases} 1 - 2p_1, & r_{k-1} < p_1 \\ \eta_{k-1}, & p_1 < r_{k-1} < p_2 \\ 0.8\eta_{k-1}, & p_2 < r_{k-1} < p_3 \\ 0.5\eta_{k-1}, & r_{k-1} \geq p_3 \end{cases} \quad (35)$$

where $p_1 < p_2 < p_3 < 1$ are prescribed with $p_1 \in (0, \frac{1}{2})$

The correction of current solution in Newton scheme is gained iteratively in INBM. The iteration which is the inner loops of global scheme is stopped following

$$\|b_k^i - [D_k] \delta_{k,l}\|^2 < \eta_k \|b_k^i\|^2 \leq \|b_k^i - [D_k] \delta_{k,l}\|^2 \quad (36)$$

where $l = 1, 2 \dots l-1$

The Newton iteration is the outer loop of the iteration scheme. It has to be stop above the noise level to avoid noise amplification. Discrepancy principle can be used to define the stopping rule

$$\|y^\delta - \mathcal{F}(x_k)\|^2 \leq R\delta \leq \|y^\delta - \mathcal{F}(x_k)\|^2 \quad (37)$$

where $k = 1, 2 \dots K-1$, δ is the noise level and $R > 0$ is real positive number. As the noise level is unknown, the Newton iteration is stopped when

$$\frac{\|y^\delta - \mathcal{F}(x_k)\|^2 - \|y^\delta - \mathcal{F}(x_{k+1})\|^2}{\|y^\delta - \mathcal{F}(x_{k+1})\|^2} \leq R \quad (38)$$

IV. NUMERICAL EXPERIMENT

In the numerical experiment, the measured data are synthetic which are obtained from solving the forward problem (10). The images are reconstructed by the Newton iterative method with iterative sequence (12), where the Newton steps are defined using INBM (28) and LM (23). Comparative study is used to analyze the stability of the solutions. The image resulted by Newton iterative method by means INBM is compared to that resulted from the direct regulative solution by means LM.

The process of the iteration is studied using the relative norm of the MWT-objective function. The norm is calculated relative to the measurement. It is defined as

$$\text{norm}(\mathcal{F}(\mathcal{X}_k)) = \frac{\|\mathcal{F}(\mathcal{X}_k)\|^2}{\|e^r\|^2} \quad (39)$$

The quality of the solutions of MWT inverse problem is quantified using the error of the value of dielectric contrast of object domain. Relative errors are computed for all cells inside OI.

$$\text{Err}(\mathcal{X}_k) = \frac{\|\mathcal{X}_{\text{target}} - \mathcal{X}_k\|^2}{\|\mathcal{X}_{\text{target}}\|^2} \quad (40)$$

A. Cylindrical Rod Model

In a 2D homogeneous lossy object problem as cylindrical rod model is introduced and 16 antennas are used for transmitting and receiving 2.5 GHz microwave signals. The source of the signals is assumed to be an infinite current line source which is computed using Hankel's function. The points of electric field measurement are placed at radius 6.5 cm around the object domain. At each set of measurement, 256 data are generated and 40dB White Gaussian noise is added to the data using `awgn` Matlab function.

TABLE II. PARAMETER OF SIMULATED SYSTEM

Parameter	Value
Diameter of Object Domain (\mathcal{X})	9.5 cm
Diameter of Data Domain (\mathcal{Y})	13.0 cm
Transmitting Antenna T_x	16
Receiving Antenna R_x	16
Number of data (amplitude and phase)	256
SNR	40 dB
Number of cells	$50 \times 50 = 2500$
ϵ_r	$3.5 - j5.8$
Diameter of object	4 cm
Frequency	2.5 GHz

The data are reconstructed using both INBM and LM algorithms where the parameters of numerical experiment are summarized in Table II. The initial value of the dielectric contrast is free space $\epsilon_r = 0$. The tolerance of the discrepancy is set to be $R(\mathcal{F}(\mathcal{X}_k)) \leq 0.003$, and the solution gained is the relative norm of the MWT objective function $\text{norm}(\mathcal{F}(\mathcal{X}_k)) \leq 10^{-4}$. The reconstructed images of 2D model of homogeneous cylindrical OI using INBM and LM algorithms are presented in Fig 1.

The image of OI is presented in real and imaginary parts of complex permittivity. It can be seen that the real parts of LM method suffers from a high lossy object. The quantity of $\text{Real}(\epsilon)$ in a lossy object which is $\text{Real}(\epsilon) = 3.5$ cannot be reconstructed. The image is blurred and the value of $\text{Imaginary}(\epsilon)$ is missed. On the other hand it can be seen that the shape and the value of the complex permittivity of OI is relatively well constructed. INBM solves the MWT inverse problem of a lossy OI with a small well. The shapes of the OI are clearly seen on both real and imaginary images, but the value of $\text{Real}(\epsilon)$ are overdetermined. However, the images of the lossy OI resulted by INBM are still better than those produced by LM algorithm.

INBM produces better images. The shape and the value of the parameter of INBM result is closer to the target value than that resulted by the LM algorithm. The INBM produces good images of a high lossy cylindrical object. In contrast, the LM method suffers from a high imaginary part of OI permittivity. INBM produces a stable solution of MWT inverse problem of lossy material when LM method fails.

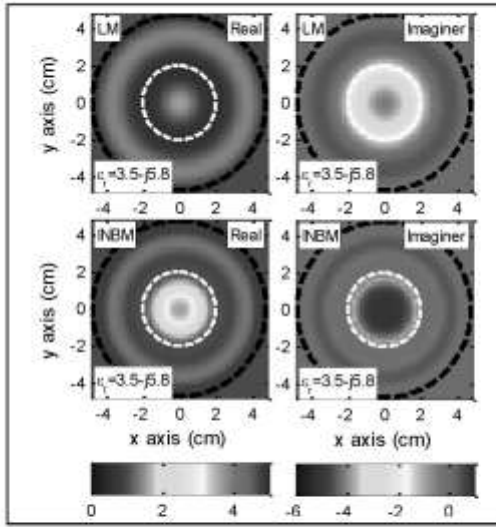


Fig. 1. The real and imaginary part of reconstructed images using INBM and LM algorithms. The data are taken at 2.5 GHz where white Gaussian noise is introduced with signal to noise ratio 40 dB

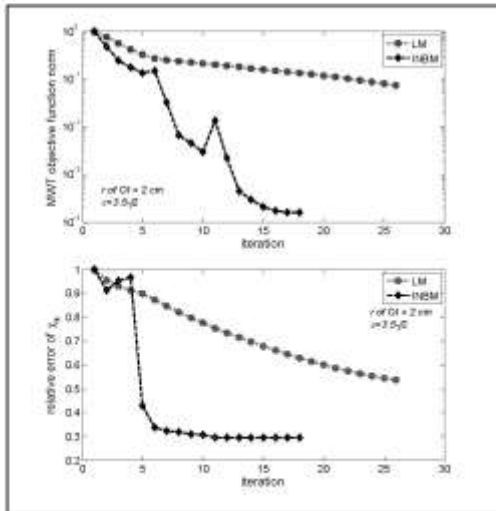


Fig. 2. The parameter of iterative solutions for INBM and LM algorithms for solving the MWT inverse problem of homogeneous lossy object a) relative norm of objective function b) relative error of the dielectric contrast of ϵ_0 .

The parameters of iterations are presented in Fig 2. It can be seen that the application of INBM offers a tradeoff between the accuracy with which the Newton equations are solved in the amount per work per iterations. The number of the outer iterations to get the global result is reduced by more than a half,

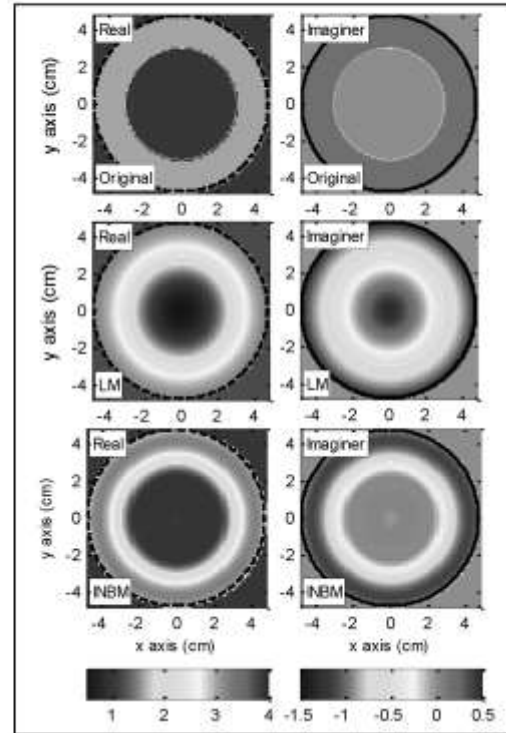


Fig. 3. The reconstructed images of the dielectric tube model.

besides the accuracy of the result is improved by more than 20%. The graph of the parameters shows that the relative norm of the objective function of INBM declines faster than that of LM algorithm and the line of the relative errors of INBM is lower than that of the LM. Based on the parameter of the solutions, the INBM for solving the MWT inverse problem is better than the LM algorithm.

B. Dielectric Tube Model

The MWT system which is used in the previous sections is applied to generate the MWT data of the dielectric tube model. The OI is a cylindrical dielectric tube. The inner and outer radiuses of the tube are 3 cm and 4.75 cm, respectively. There are two models of the dielectric tubes, which are a dielectric tube in free space and a tube containing a lossy material.

The data are reconstructed using INBM and LM algorithms. The results of the reconstruction are presented in the images of $Real(\epsilon)$ and $Imag(\epsilon)$. The reconstructed images of the dielectric tube model are presented in Fig 3. It can be seen that the INBM produces better images than the LM algorithm. The shape of the tube in the images resulted by INBM are clearly reconstructed. INBM defines the value of the tube complex permittivity closer than LM algorithm does.

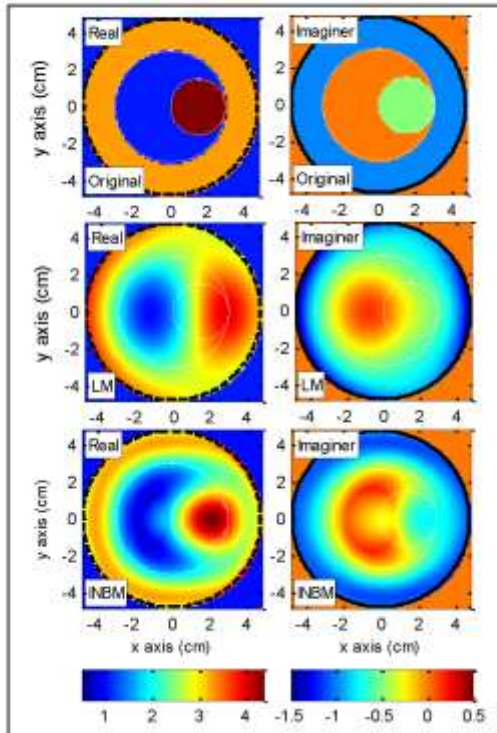


Fig. 4. the reconstructed images of the dielectric tube containing dielectric material model.

The images of the dielectric tube containing dielectric material model resulted using INBM and LM algorithms are presented in Fig 4. It can be seen that the introduction of a dielectric lossy material inside the tube influences the reconstructed images. The shape and the dielectric value of the tube are disturbed by the presence of different materials. The accuracy of the images resulted by INBM is better than that resulted by LM algorithm. INBM draws the cylinder lossy material well when LM method fails to define the shape and position of the material.

The unspecific solutions of MWT-Newton equations in INBM algorithm upgrade the accuracy of the MWT inverse problem solutions. The accuracy of INBM solutions are 22% and 31% for tube model and tube containing dielectric material problems, sequentially. These improve the LM solutions by 10%. The norms of INBM objective function are 1.16×10^{-5} for tube model and 4.05×10^{-4} for the other tube model. These are better than those resulted by the LM algorithms which are bigger than 1×10^{-3} . The application of INBM to dielectric tube containing different material improves the accuracy and the speed of the LM algorithm.

V. EXPERIMENTAL TEST

A microwave tomography system has been developed at School of Electrical and Electronic Engineering, University of Manchester. The MWT system uses 16 monopoles supported by a ground plane. It works in free space domain. The system is shown in Fig 4. The parameters used in the measurement are summarized in Table IV. The antennas are computer controlled via a 2x16 Cytec multiplexer. 16 antennas are used as transmitter. At each illumination 8 antennas are used as receiver where the arrangement of the receiver is presented in Table V.



Fig. 5. Microwave tomography system setup

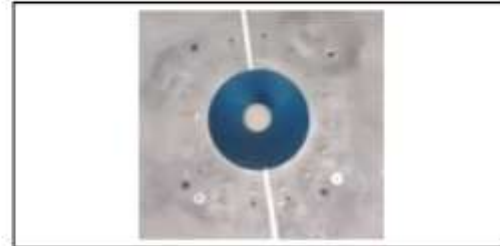


Fig. 6. a cylindrical long rod inside object domain of MACS Microwave Tomography system

TABLE III. PARAMETER OF MEASUREMENT SYSTEM

Parameter	Value
Diameter of Object Domain (X)	9.5 cm
Diameter of Data Domain (Y)	13.0 cm
Transmitting Antenna T_x	16
Receiving Antenna R_x	8
Number of data	128×2
Number of cells	$50 \times 50 = 2500$
Object of interest	rod
ϵ_r	2.1
Diameter of object	3 cm
Frequency	4.3, 4.6 and 5.0 GHz

TABLE IV. OBSERVATION POINTS OF SCATTERED FIELD

t (Transmitter)	m (Receiver)
$t = 1$	4, 5, 6, 7, 11, 12, 13, 14
$t = 2$	5, 6, 7, 8, 12, 13, 14, 15
\vdots	\vdots
$t = 16$	3, 4, 5, 6, 10, 11, 12, 13

The transmission and measurement of electric fields are conducted by Vector Network Analyzer (VNA). Total electric fields are assigned as collected field data. At each illumination, 8 Rx antennas are addressed to measure the total electric fields before and after the object are introduced. The measured scattered fields are defined as the difference of disturbance and non-disturbance fields at receiving antennas. The data is reconstructed using INBM and LM algorithm.

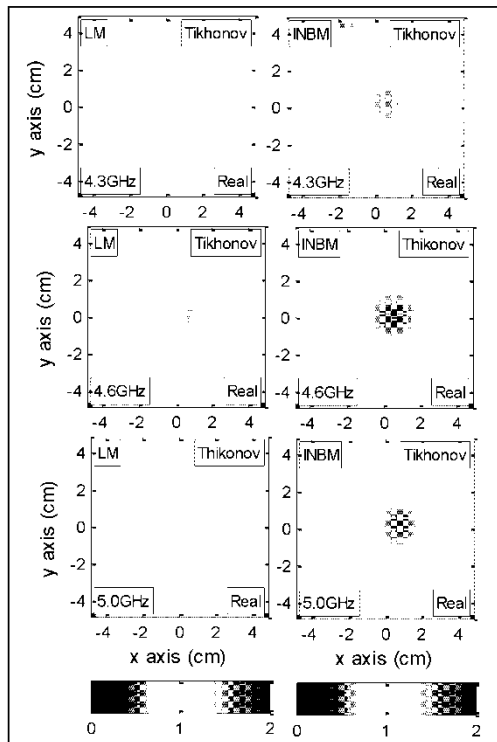


Fig. 7. Images of plastic rod cross section resulted by LM algorithm and INBM algorithm at three different frequencies.

The object of interest for experimental test is cylindrical rod which has dielectric constant 2.1 at 4.5 GHz. Fig 7. illustrates the images of Teflon cross section reconstructed by LM and INBM algorithms. It can be seen that the images of INBM algorithm are better than those resulted by the LM algorithm. The shape and the position of the interest are clearly seen, and the contrast of the object is closely determined at 4.6 and 5.0 GHz while the noise can relatively be eliminated. Generally, the shape of the object can be reconstructed at a frequency where the coefficient of reflection of the antennas is higher than -10dB. However, the contrast of the object can only be computed at a frequency where the coefficient of the antenna reflection is lower.

VI. CONCLUSIONS

An inexact Newton backtracking method has been proposed and studied to solve MWT inverse problem. The main features of the proposed method include: present MWT problem as a nonlinear problem; solve the inverse problem in outer-inner loops; replace the direct solution of linearization with its regulated approximation; and strictly guard the approximation with a forcing term. The application of this inexact class improves the quality of the reconstruction. The two loops technique reduces the number of global loop significantly. It reduces the time of computation as the linearization and inversion are computed once at each outer loop of INBM. Furthermore experimental data test highlights several positive characteristic of INBM, which are capability to reconstruct limited data, robustness to unknown noise and other disturbance; and capability to deal with nonlinear objective functional.

The results of the numerical experiment and experimental test reveal that the Newton iterative method which is inexact Newton class, combined with iterative regularized linear ill posed problem produce stable the solution for MWT image inverse problem. The optimal solution are gain when the forcing term is applied according the ratio of nonlinear functional and linear current update. The forcing term is used to determine the stopping rule of inner iteration while the stopping rule of Newton iteration is determined using simple discrepancy principle.

REFERENCES

- Harrington, R. (1993). *Field computation by moment methods* Wiley-IEEE Press
- Kleinman, R. E., & van den Berg, P. M. (1992). A modified gradient method for two dimensional problems in tomography. *Journal of Computational and Applied Mathematics*, 42(1), 17-35.
- van den Berg, P. M., & Kleinman, R. E. (1995). A total variation enhanced modified gradient algorithm for profile reconstruction. *Inverse Probl*, 11(3), L5-L10.
- Joachimowicz, N., Mallorqui, J. J., Bolomey, J. C., & Broquets, A. (1998). Convergence and stability assessment of newton-kantorovich reconstruction algorithms for microwavc tomography. *Medical Imaging, IEEE Transactions on*, 17(4), 562-570.
- Kundu, A. K., Bandyopadhyay, B., & Sanyal, S. (2008). *An iterative algorithm for microwave tomography using modified gauss-newton method*. Paper presented at the Biomed 2008.
- Hu, J. L., Wu, Z., McCann, H., Davis, L. E., & Xie, C. G. (2006). Bfgs quasi-newton method for solving electromagnetic inverse problems. *IEE Proceedings - Microwaves, Antennas and Propagation*, 153(2), 199.
- van den Berg, P. M., & Abubakar, A. (2001). Contrast source inversion method state of art. *Progress In Electromagnetics Research*, 34, 189-218.
- van den Berg, P. M., & Kleinman, R. E. (1997). A contrast source inversion method. *Inverse Probl*, 13, 1607-1620.

- 9 Bozza, G., Estatico, C., Pastorino, M., & Randazzo, A. (2006). An inexact newton method for microwave reconstruction of strong scatterers. *Antennas and Wireless Propagation Letters, IEEE*, 5(1), 61-64.
- 10 Dembo, R. S., Eisenstat, S. C., & Steihaug, T. (1982). Inexact newton methods. *SIAM Journal on Numerical Analysis*, 19(2), 400-408.
- 11 Jin-Lin, H., Zhipeng, W., McCann, H., Davis, L. E., & Cheng-Gang, X. (2005). Quasi-three-dimensional method of moments for analyzing electromagnetic wave scattering in microwave tomography systems. *Sensors Journal, IEEE*, 5(2), 216-223.